

POLITECNICO DI TORINO

Collegio di Ingegneria Chimica e dei Materiali

**Master of Science Course
in Materials Engineering**

Master of Science Thesis

**Synthesis and characterization of MoS₂-
PANI composite materials for
electrochemical applications**



Tutor

Prof. Silvia Bodoardo

Candidate

Irene Canale

July 202

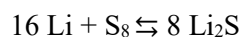
RIASSUNTO

Introduzione ed obiettivi del lavoro

Negli ultimi duecento anni, la storia umana è risultata profondamente connessa allo sviluppo e all'introduzione delle fonti energetiche. Il carbone, il petrolio e altri combustibili fossili hanno infatti reso possibile l'evoluzione della società come la conosciamo oggi. Tuttavia, l'uso sfrenato di queste risorse non rinnovabili e altamente inquinanti ha spinto la comunità scientifica a cercare altre soluzioni. Sono state così introdotte sul mercato le energie rinnovabili (in particolare l'energia eolica e solare), supportate dallo sviluppo delle batterie: dispositivi essenziali in grado di immagazzinare e trasportare l'energia anche in periodi e luoghi in cui tali risorse non sono disponibili.

Con il seguente lavoro di tesi, svolto grazie a una collaborazione tra il Politecnico di Torino e l'università FCT di Lisbona, si è cercato di approfondire lo stato dell'arte di una delle classi di batterie più recenti e promettenti, quelle Litio-Zolfo ed affrontare una delle maggiori limitazioni che ancora affliggono questi dispositivi: il fenomeno dello *Shuttle* dei polisolfuri.

Le batterie Litio-Zolfo (Li-S) sono costituite da un catodo a base di Zolfo e un anodo di Litio metallico separati da un elettrolita organico. La batteria Li-S presenta un'elevata capacità di 1675 mAh g⁻¹ e un'alta energia specifica teorica pari a 2600 Wh Kg⁻¹, circa cinque volte quella delle celle litio ione. A queste caratteristiche si sommano un minor impatto ambientale e una notevole riduzione dei costi essendo lo Zolfo un elemento poco costoso e molto diffuso. L'insieme di queste proprietà rendono le batterie Litio-Zolfo promettenti tecnologie nel campo dell'elettronica, dei dispositivi portatili e dello storage elettrico. Tuttavia, la chimica di processo, basata sulla conversione reversibile dello zolfo (S₈) in solfuro di litio (Li₂S) presenta ancora diverse criticità che limitano la diffusione di questa tecnologia su larga scala. La reazione di conversione, che complessivamente può essere espressa come:



comprende, infatti, anche una serie di reazioni di natura non elettrochimica (come reazioni di disproporzione) che rendono l'intero processo molto complesso e ancora in parte sconosciuto. Da questo insieme di reazioni vengono generate specie intermedie formate da anioni di Litio, note come polisolfuri.

Durante la fase di carica si formano al catodo polisolfuri a catena lunga Li₂S_x (4 < x ≤ 8) che grazie alla loro elevata solubilità all'interno di solventi organici e ai gradienti di concentrazione che si formano all'interno dell'elettrolita, tendono a migrare verso l'anodo. Una volta giunti all'anodo, i polisolfuri ad "alto ordine" vengono ridotti con il Litio metallico a polisolfuri a catena corta Li₂S_x (1 < x ≤ 2). Dopodiché, sebbene questi polisolfuri presentino una solubilità minore rispetto ai precedenti, riescono comunque a raggiungere il catodo dove vengono ossidati nuovamente.

Quando la migrazione dei polisolfuri all'interno dell'elettrolita e le conseguenti reazioni di ossido-riduzione che li coinvolgono, si sviluppano in modo ciclico e ripetuto nel tempo, questi danno origine a quello che viene comunemente definito l'effetto Shuttle dei polisolfuri.

Questo fenomeno porta con sé una serie di pesanti criticità, tra cui, le principali prevedono:

- l'instaurarsi di una corrente parassita che contrasta e riduce la corrente di carica e l'efficienza Columbica;
- un aumento di temperatura (connessa alla formazione di una corrente parassita) con conseguenti problemi a livello di sicurezza e di funzionamento;
- importanti e improvvise cadute di potenziale e di C-rate;
- un minore utilizzo dei materiali attivi contenuti nella cella, a seguito delle reazioni parassite che si instaurano tra questi e i polisolfuri, con conseguente diminuzione di capacità e una ridotta vita utile;
- infine, una maggiore propensione all'auto-scarica della cella, quando questa viene lasciata carica in condizioni di riposo, con riduzione del valore di OCV (Open Circuit Voltage) e della capacità di scarica.

Appare evidente quindi che ridurre la portata dell'effetto Shuttle all'interno delle batterie Litio-Zolfo sia una questione di primaria importanza.

In letteratura si trovano numerosi esempi di strategie che sono state adottate nel corso degli ultimi anni per cercare di limitare la severità di questo fenomeno, come: l'uso di elettroliti alternativi, l'aggiunta di additivi o materiali carboniosi porosi capaci di bloccare i polisolfuri al loro interno, l'adozione di membrane e separatori ioni-selettivi, sistemi di protezioni dell'anodo o l'utilizzo di anodi alternativi al Litio e infine funzionalizzazione della superficie catodica o rivestimento di questa attraverso polimeri di varia natura.

In questo lavoro di tesi è stato utilizzato un approccio che richiama l'ultimo punto sopra elencato. Si è deciso infatti di creare un Double-Layer da applicare sul catodo con l'obiettivo di andare a bloccare sia da un punto di vista chimico che fisico i polisolfuri. Per farlo è stato realizzato un composito costituito da un polimero conduttore, la PANI (Polianilina) e un dicalcogenuro metallico, il Disolfuro di Molibdeno (MoS_2).

Per la realizzazione del composito sono stati scelti questi materiali poiché:

- PANI: presenta unità ripetitive di fenilendiammina e chinone-diimina che le conferiscono una conduttività elettrica specifica e un comportamento redox unici capaci di promuovere elettrocataliticamente le reazioni di conversione delle specie contenenti Zolfo. Inoltre, la Polianilina presenta siti multi-ancoranti tra cui il gruppo quinonoidico dell'immina che rappresenta un sito di ancoraggio preferenziale per i polisolfuri.
- MoS_2 : instaura forti legami chimici e interazioni dipolari con i polisolfuri inibendone la dissoluzione all'interno dell'elettrolita. Inoltre, per le sue forti interazioni con i polisolfuri e la sua elevata conduttività elettronica l' MoS_2 è considerato cataliticamente attivo per la conversione di questi. Può agire infine anche come conduttore di Litio.

Parte sperimentale: sintesi dei campioni

Durante la prima fase del lavoro sperimentale, stati messi a punto diversi metodi di sintesi per la PANI (nel seguito indicata come Italiana e Portoghese) seguendo i protocolli forniti nei due rispettivi paesi. Le principali differenze nei processi di sintesi hanno interessato:

- La quantità e la tipologia dei reagenti (in particolare l'acido utilizzato per il processo di doping durante la sintesi del polimero: HCl nel caso della PANI Italiana e H_2SO_4 per la PANI Portoghese);

- La presenza, per quanto riguarda la PANI Portoghese, di un agente surfattante e co-dopante (CSA, Camphor-10-sulfonic acid), probabilmente responsabile della sua morfologia allungata e tubolare;
- La presenza, sempre per quanto riguarda la PANI Portoghese, di un bagno di ghiaccio usato per favorire la reazione di polimerizzazione e aumentare la conduttività del prodotto finale.

Su questi materiali sono state poi eseguite analisi FESEM, XRD e RAMAN. Attraverso la Field Emission Scanning Electron Microscopy (Figura 1) è stato possibile evidenziare, tra le due tipologie di PANI, grosse differenze a livello morfologico. Infatti, mentre la PANI Italiana mostra una struttura poco definite e compatta, la PANI Portoghese mostra invece una morfologia marcatamente tubolare e aperta.

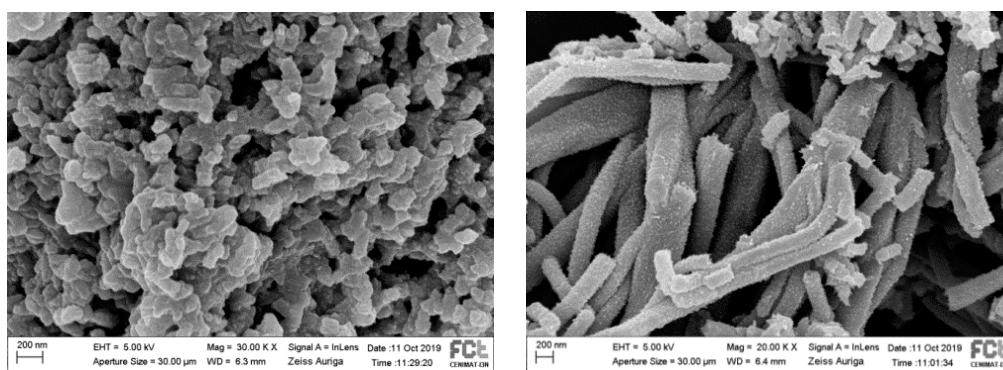


Figura 1: Analisi FESEM di PANI Italiana (a sinistra) e PANI Portoghese (a destra).

Attraverso le analisi XRD è stato possibile inoltre evidenziare la natura semicristallina di questi materiali, mentre con le analisi RAMAN (Figura 2) è stato possibile e mettere in luce, per entrambi i campioni, i picchi caratteristici della forma dopata della PANI ovvero dell'unica forma (emeraldina) conduttiva di questo polimero.

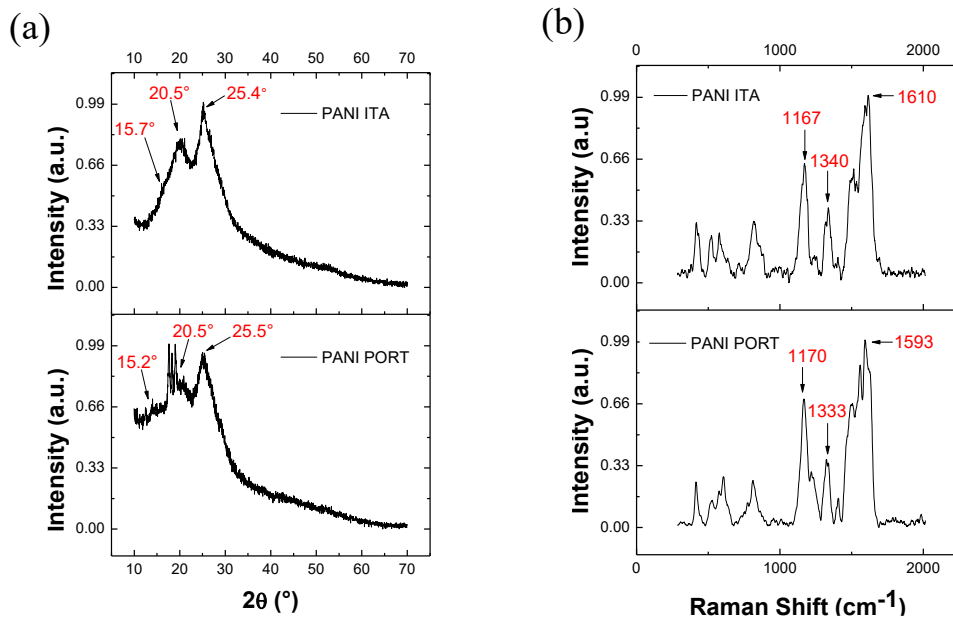


Figura 2: (a) Analisi XRD, (b) Analisi Raman per i due campioni di PANI.

Sono stati poi analizzati due diverse tipologie di MoS_2 : nella forma commerciale e MoS_2 ottenuto tramite un processo idrotermale. Per la sintesi di questo secondo materiale è stata utilizzata una soluzione di Molibdato di sodio e Tiourea, fatta reagire a elevate temperature (200°C) e pressioni (280 Pa) in un reattore a microonde. Su questi campioni sono state poi svolte delle analisi di caratterizzazione.

Dalle analisi FESEM (Figura 3), in particolare, è emerso che l' MoS_2 commerciale presenta una forma bulk composta da numerosi layers fortemente adesi uno con l'altro. L' MoS_2 idrotermale invece mostra una struttura a nanoflower in cui i nanosheets non risultano più impilati l'uno sull'altro, bensì disposti a formare delle strutture tondeggianti che possono ricordare una rosa.

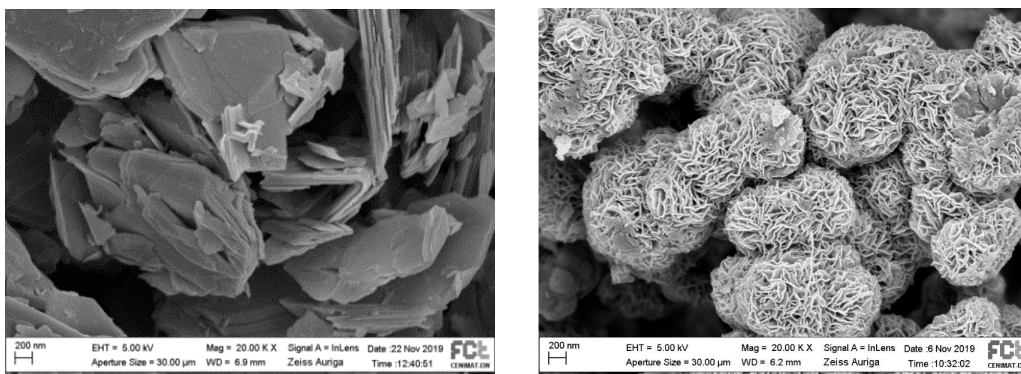


Figura 3: Confronto analisi FESEM tra due campioni di MoS_2 : commerciale (a sinistra), idrotermale (a destra)

Le analisi RAMAN (Figura 4) invece hanno permesso, nel primo caso, di riconoscere i phonon mode caratteristici della forma bulk di questo materiale, mentre nel secondo caso, di evidenziare la natura

amorfa del MoS₂ idrotermale. Sebbene questo materiale, presenti una struttura interessante, non è stato adottato nella realizzazione dei materiali composite a causa della limitatissima quantità ottenibile da ciascun processo di sintesi (0.0035 g).

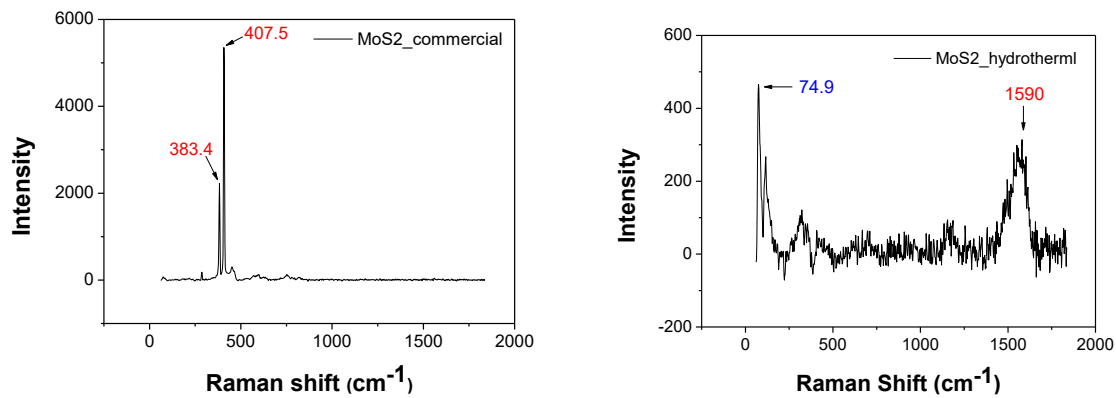


Figura 4: Confronto analisi RAMAN tra due campioni di MoS₂: commerciale (a sinistra), idrotermale (a destra)

Sempre durante questa prima fase di sintesi sono stati poi prodotte tre diverse tipologie di materiali compositi: IN SITU, EX SITU, idrotermale. Per la realizzazione di questi compositi sono stati utilizzati i materiali (PANI Italiana, PANI Portoghese, MoS₂ commerciale) e i processi di sintesi già ottenuti precedentemente. Prima di procedere con la sintesi vera e propria dei compositi è stato necessario però mettere a punto un processo di esfoliazione per MoS₂ commerciale e portarlo dalla sua forma bulk alla forma di singoli o pochi nanosheets. Per farlo si è deciso di procedere con un processo ad ultrasuoni durato 9 ore, svolto su una soluzione contenente acqua e polvere bulk di MoS₂. La forma esfoliata del MoS₂ è stata utilizzata sia per l'ottenimento dei compositi IN-SITU che per quelli EX-SITU.

- **Compositi IN-SITU:** nella soluzione contenente MoS₂ esfoliato è stata fatta avvenire la polimerizzazione della PANI secondo il protocollo portoghese. Attraverso le analisi FESEM (Figura 5) è stato possibile osservare una morfologia molto simile a quella riscontrata per la PANI Portoghese ma nessuna evidenza della presenza del MoS₂. Anche le analisi RAMAN (Figura 5) hanno permesso di identificare i picchi caratteristici della PANI nella forma emeraldina ma non ha messo in mostra i picchi caratteristici del MoS₂ commerciale. È stato ipotizzato dunque che l'MoS₂ abbia reagito con le altre sostanze utilizzate per la polimerizzazione della PANI. A causa dell'incompleta comprensione del processo di sintesi, questo composito è stato scartato per la realizzazione dei Double-Layers

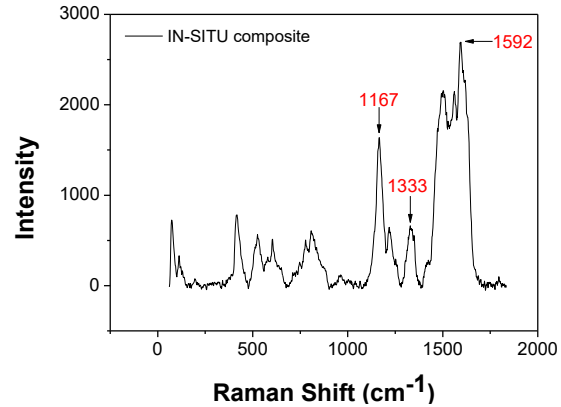
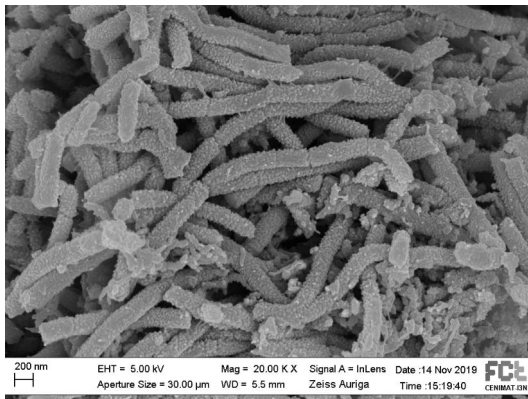


Figura 5: Analisi su composito IN-SITU: FESEM (a sinistra), Raman (a destra)

- Composti EX-SITU: per la realizzazione di questi compositi sono stati miscelati in un becher contenente acqua, l'MoS₂ commerciale e la PANI (Italiana o Portoghese), secondo opportuni rapporti (30:70 e 70:30). Le soluzioni così ottenute sono state poi sottoposte a un processo ad ultrasuoni per la durata di 9 ore, al fine di ottenere contemporaneamente l'essfoliazione del MoS₂ e la miscelazione dei due composti. Al contrario del caso precedente, dalle immagini FESEM (Figura 6), è stato possibile osservare la presenza di entrambi i materiali.

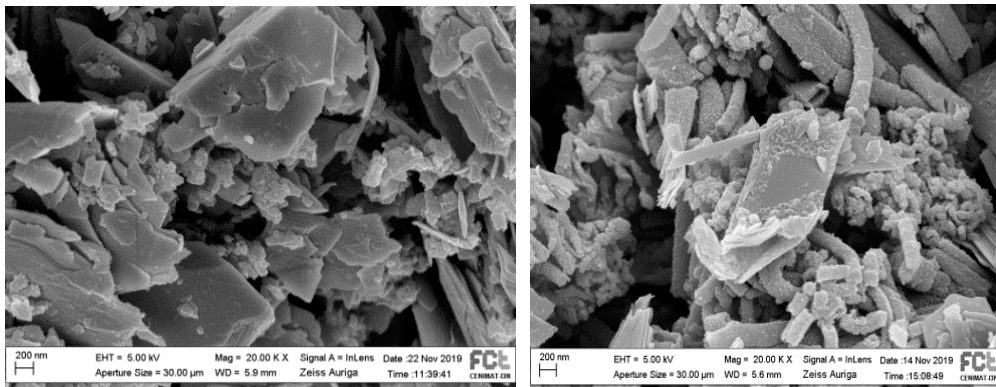


Figura 6: Analisi FESEM ottenute da compositi EX-SITU contenenti: 0.3 g PANI Italiana e 0.7 g MoS₂ commerciale (a sinistra), 0.3 g PANI Portoghese e 0.7 g MoS₂ commerciale (a destra)

I due materiali sono stati identificati anche attraverso le immagini RAMAN (Figura 7). Mentre però nel primo caso contenente un quantitativo maggiore di PANI è stato possibile riconoscere immediatamente tutti i picchi caratteristici dei due materiali, negli altri due casi (contenenti un quantitativo maggiore di MoS₂ rispetto alla PANI) è stato necessario, per vedere i picchi di quest'ultima, ingrandire la parte terminale del grafico.

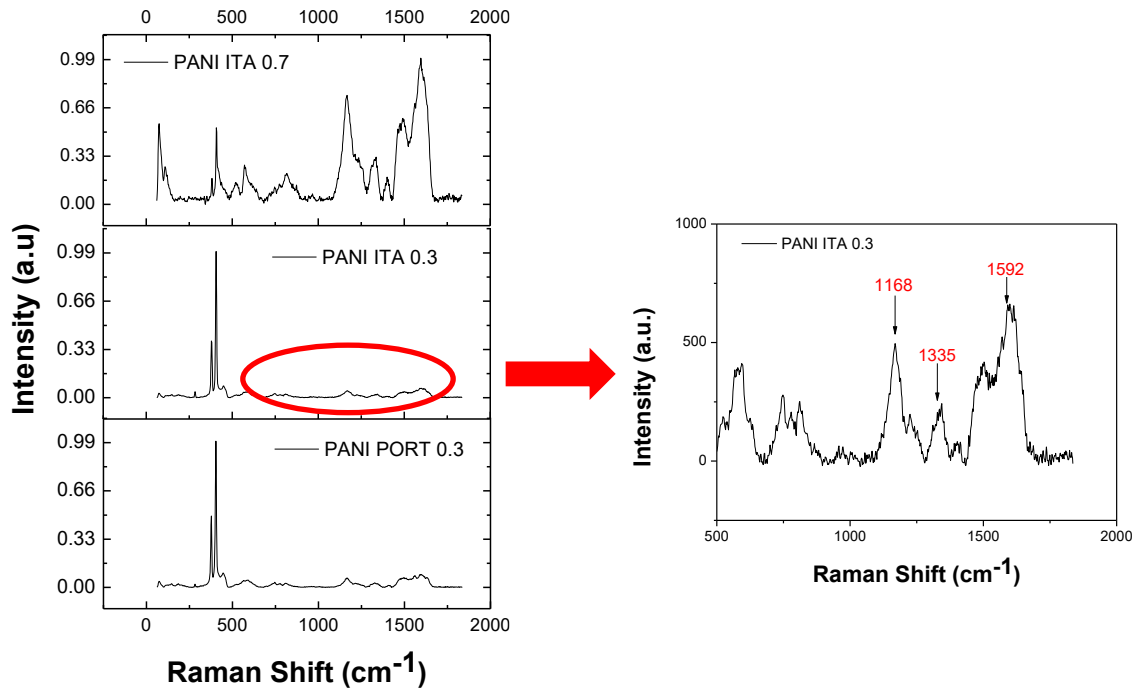


Figura 7: Confronto analisi RAMAN tra tre diversi campioni, contenente rispettivamente (partendo dall'altro): 0.7 g PANI Italiana e 0.3 g MoS₂ commerciale, 0.3 g PANI Italiana e 0.7 g MoS₂ commerciale, 0.3 g PANI Portoghese e 0.7 g MoS₂ commerciale

- **Composito IDROTERMALE:** per il suo ottenimento è stato seguito lo stesso procedimento già utilizzato per l'MoS₂ idrotermale, con la sola differenza che in questo caso è stata aggiunta nella soluzione di partenza un quantitativo in peso di PANI Portoghese, pari a quello di MoS₂ ottenuto attraverso il processo a microonde (0.0035g). Le immagini FESEM (Figura 8) rivelano una struttura a nanoflowers alternata a una struttura meno definita, riconducibile alla PANI. Anche in questo caso le immagini RAMAN (Figura 8) hanno evidenziato i picchi relativi alla PANI nella forma emeraldina e un picco a 74.9cm⁻¹ riscontrato anche nel caso del MoS₂ idrotermale.

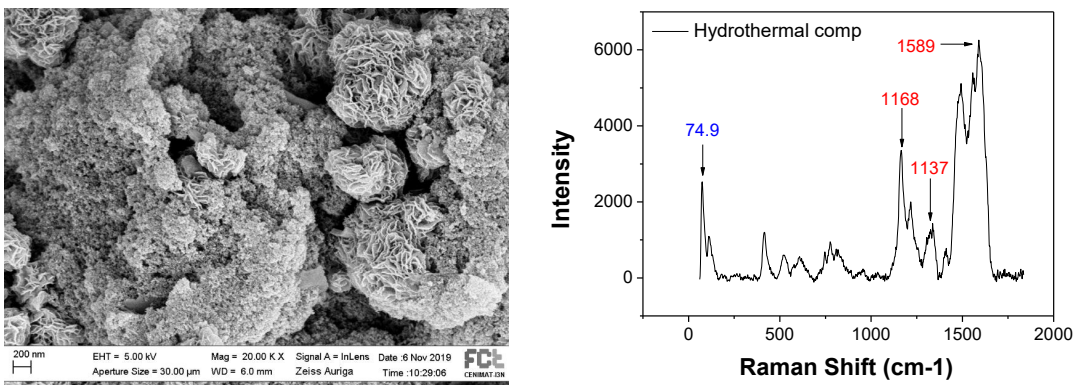


Figura 8: Analisi su composito idrotermale: FESEM (a sinistra), Raman (a destra)

Parte sperimentale: Assemblaggio celle e analisi elettrochimiche

Durante la seconda fase del lavoro sperimentale, alcuni campioni (Figura 9) sono stati scelti per essere analizzati da un punto di vista elettrochimico, al fine di evidenziarne le performance e le possibili applicazioni.

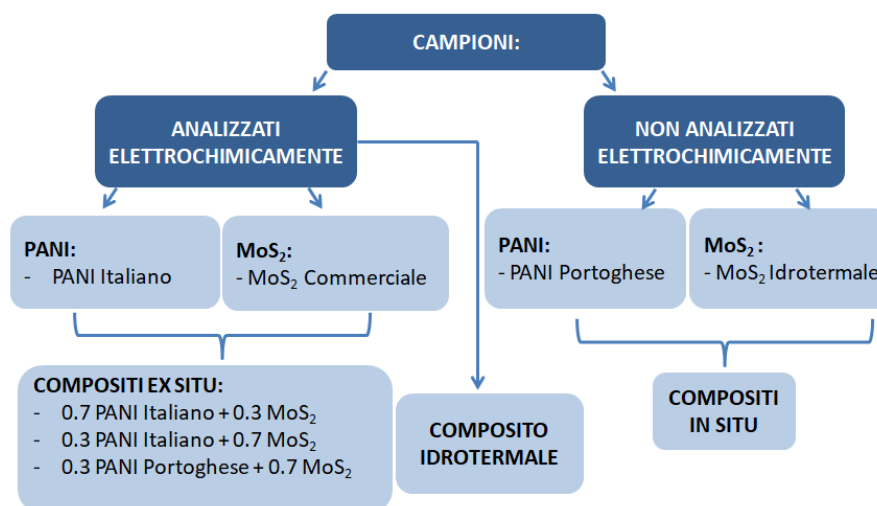


Figura 9: Quadro riassuntivo dei campioni ottenuti durante la parte di sintesi, qui classificati in: analizzati e non analizzati elettrochimicamente

Prima di procedere con le analisi vere e proprie è stato necessario realizzare il catodo su cui andare a depositare successivamente il Double-Layer. Per la creazione del catodo è stata scelta una composizione 70:20:10 in cui il valore maggiore del rapporto si riferisce al materiale attivo (lo Zolfo), mentre gli altri si riferiscono rispettivamente al carbone mesoporoso Ketjenblack (KJB), addizionato per migliorare la conducibilità del catodo, e al binder polimerico Polyvinylidene fluoride (PVDF). Il PVDF, invece, viene aggiunto all'interno della composizione catodica per favorire l'adesione tra il collettore di corrente su cui viene depositato il catodo, e la composizione catodica stessa.

I tre materiali sono stati così inseriti in un Eppendorf insieme a un solvente, N-Methyl-2-Pyrrolidone (NMP) e processati attraverso Ball Milling per 15 minuti a 30 Hz. La sospensione è stata poi depositata su un collettore di Alluminio attraverso un Doctor Blade, capace di regolare lo spessore della stesa a 200 μm . L'elettrodo ottenuto è stato infine posto in forno e lasciato ad asciugare per un'ora a 50°.

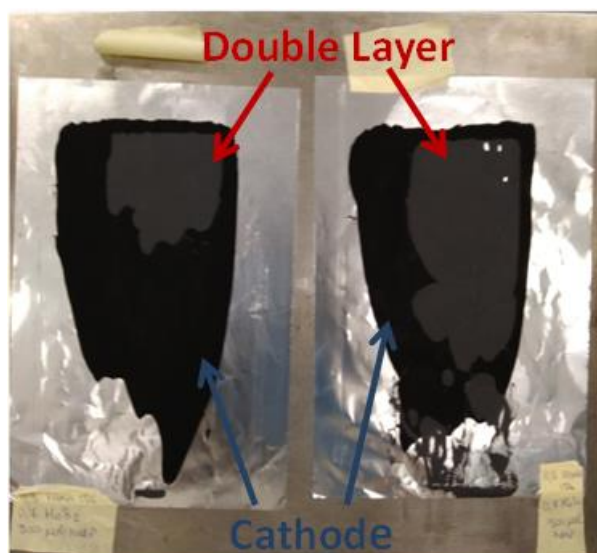


Figura 10: Foto di un catodo (70:20:10) su cui è stato depositato un Double-Layer

Per la realizzazione dei Double-Layers (Figura10) da applicare sui catodi è stato seguito un procedimento molto simile a quello appena illustrato. In questo caso però è stata scelta una composizione 80:10:10 dove il valore maggiore si riferisce alla quantità di materiale da analizzare da un punto di vista elettrochimico (i composti, MoS₂ commerciale e la PANI Italiana) mentre gli altri due valori si riferiscono sempre al KJB e al PVDF.

Anche in questo caso, ai tre elementi è stato addizionato l’NMP e la sospensione è stata processata per 15 minuti a 30 Hz tramite Ball Milling. Dopodiché il composto è stato depositato, con uno spessore di 150 µm, sul catodo precedentemente ottenuto.

Dopo il processo di essiccazione in forno, i catodi rivestiti sono stati fustellati in dischetti di 15 mm e posti in un forno a vuoto (Büchi) a 40° per 4 ore. Infine, sono state montate le celle. Durante questa fase, il catodo coperto dal doppio strato è stato posizionato nella coppa inferiore (acciaio inossidabile) della cella a bottone. Segue un separatore (Celgard 2500) che viene posto sopra il catodo e bagnato con 20µl di elettrolito LiMFSI (LiC₂F₆NO₄S₂) 1M electrolyte in DIOX: DME (1: 1v) + 0.25M LiNO₃. Successivamente, l’anodo di litio metallico, un distanziatore e una molla ondulata completano l’assemblaggio della batteria.

Poiché i risultati più incoraggianti sono stati quelli sui composti EX-SITU, si è proceduto alla loro ottimizzazione realizzando materiali contenenti rispettivamente 0.7g di PANI Italiana-0.3g di MoS₂ commerciale e 0.3g di PANI Italiana-0.7g MoS₂ commerciale. Sono state realizzate dunque quattro stese da applicare come Double-Layer sul catodo di cui due contenenti i materiali composti e due contenenti rispettivamente solo PANI Italiana e solo MoS₂ commerciale. Per avere un confronto anche con il catodo non trattato è stata assemblata infine una cella (STD) priva di coating.

Dalle analisi elettrochimiche effettuate su queste celle (in particolare Ciclazioni Galvanostatiche, Voltammetria ciclica e monitoraggio della capacità specifica su numero di cicli) è stato possibile osservare come il *Double-Layer* applicato non modifica il tipico comportamento delle batterie Li-S essendo chiaramente visibili le reazioni di ossidazione-riduzione tipiche dello Zolfo e dei relativi polisolfuri:

- il plateau a circa 2.3 V è relativo alla riduzione dello Zolfo ottaedrico in polisolfuri a catena lunga
- il plateau a 2-2.1V si riferisce alla riduzione a Li_2S_2 e Li_2S (Figura11)

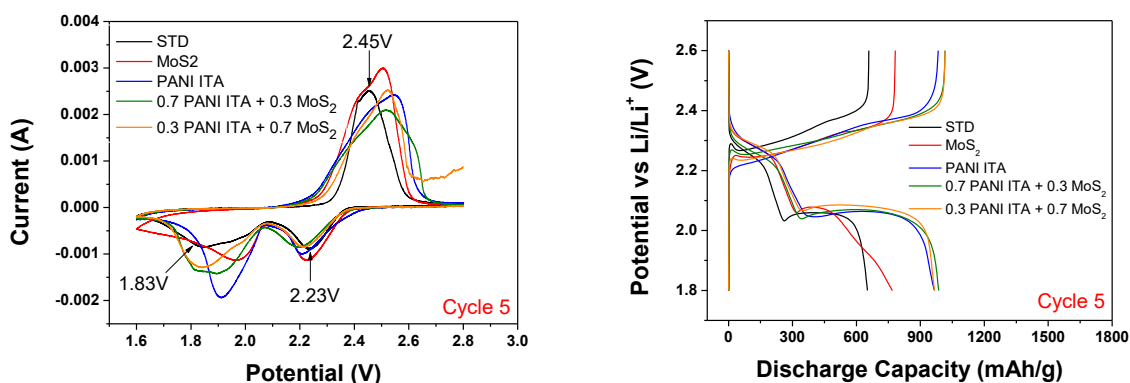


Figura 11: Analisi di voltammetria ciclica (a sinistra), ciclazioni galvanostatiche (a destra)

È evidente inoltre (Figura11) come le due celle contenenti i materiali composti presentino una minore polarizzazione e una maggiore capacità specifica. La polarizzazione (ΔE) di una cella è rappresentata dalla differenza di potenziale tra la curva di carica e la curva di scarica e permette di avere informazioni sulla cinetica del processo: in particolare, un minor valore di questa caratteristica è indice di un trasporto ionico e elettronico più efficiente e quindi di una cinetica ottimale. La capacità specifica invece è legata alla quantità di Zolfo ridotto durante il processo: un elevato valore di questa caratteristica è dunque desiderabile poiché segnale di un'elevata attività dell'elemento in questione.

Inoltre, attraverso i grafici riportanti la capacità specifica sul numero di cicli (Figura12) è stato possibile fare delle considerazioni sul valore iniziale di questa caratteristica, e sul suo andamento con l'aumentare del numero di cicli. I due composti, così come la PANI Italiana hanno mostrato valori di capacità iniziali più elevati rispetto a quelli delle altre due celle. A differenza della PANI però, le celle contenenti i composti hanno mostrato un andamento della capacità costante e una decrescita dei suoi valori piuttosto contenuti, raggiungendo dopo 500 cicli un valore di 600 mAh g^{-1} . Sempre da questi grafici è emerso che solo la curva relativa allo standard STD mostra il fenomeno dello Shuttle. Il fenomeno si presenta come una forte instabilità nei valori di capacità specifica e una repentina diminuzione di questa caratteristica.

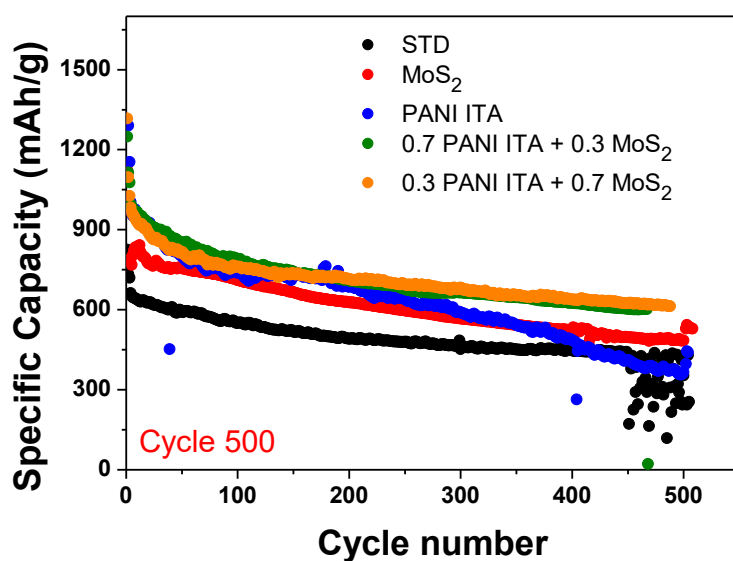


Figura 12: Capacità specifica su numero di cicli

Infine, attraverso delle analisi TAFEL (Figura13) sui due elementi di base principali (PANI Italiana e MoS₂ commerciale) e il Ketjen Black (carbone meso-poroso usato sia nella composizione catodica che per la realizzazione dei Double-Layer) è stato possibile evidenziare la forte attività catalitica del MoS₂ grazie agli elevati valori di corrente di scambio rilevati.

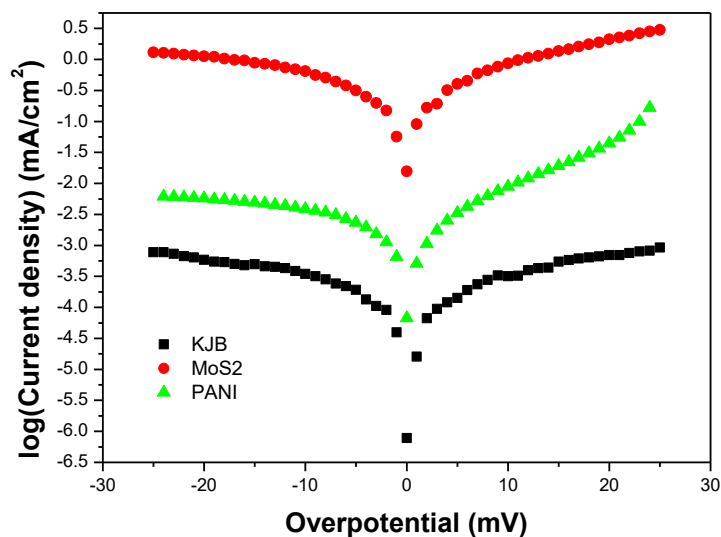


Figura 13: Analisi Tafel su KJB, MoS₂ e PANI

Conclusioni

Durante la fase di sintesi del lavoro sperimentale, sono stati ottenuti e analizzati con successo mediante analisi FESEM, XRD e RAMAN, i seguenti materiali:

- due tipi di PANI (Polianilina): attraverso reazioni chimiche ossidative
- due tipi di MoS₂: la forma commerciale (solo analizzata) e quella idrotermale ottenuta da un processo idrotermale con microonde
- tre tipi di compositi: IN-SITU, EX-SITU, IDROTERMALE

Tra questi campioni sono poi stati selezionati: la PANI Italiana, MoS₂ commerciale e due compositi EX-SITU (contenenti rispettivamente: 0.7g PANI ITA e 0.3 g MoS₂ commerciale; 0.3 g PANI ITA e 0.7 MoS₂ commerciale e analizzati da un punto di vista elettrochimico. Questi campioni sono stati infine confrontati con una cella standard (STD) priva di Double-Layer.

A fronte delle analisi effettuate è stato possibile dedurre che la presenza di un Double-Layer (sia questo costituito da sola PANI Italiana, solo MoS₂ commerciale o da entrambi i compositi) permetta di prevenire il fenomeno dello Shuttle. È stato inoltre possibile affermare che le celle contenenti i compositi presentino performance elettrochimiche migliori rispetto alle altre, sia in termini di capacità specifica che di polarizzazione, confermando l'azione catalitica e di ancoraggio dei materiali che li costituiscono nonché il raggiungimento dell'obiettivo di tesi.

Index

1. INTRODUCTION	1
1.1. Aim of the work.....	2
2. BIBLIOGRAPHIC PART	5
2.1. Rechargeable cells and batteries	5
2.1.1. Introduction on batteries	5
2.1.2. Types of batteries.....	6
2.1.3. Components of a secondary battery	7
2.2. Electrochemistry basics	10
2.2.1. Electrode-electrolyte interfaces.....	12
2.2.2. Practical cell measures	14
2.3. Why Lithium- Sulphur batteries?	19
2.3.1. Lithium-ion batteries.....	19
2.3.2. Lithium-ion vs Lithium-Sulfur batteries.....	23
2.3.3. Other storage solutions.....	28
2.4. Lithium-Sulphur battery	30
2.4.1. Cell.....	30
2.4.2. Cathode.....	30
2.4.3. Anode	35
2.4.4. Electrolyte	39
2.5. Sulphur and reactions	41
2.5.1. Polysulfides	42
2.6. Challenges	45
2.6.1. Critical aspect	45
2.6.2. Shuttle Mechanism	46
2.6.3. Possible strategies.....	49
2.7. PANI	53
2.7.1. Conductive polymers.....	53
2.7.2. Polyaniline	55
2.7.3. Synthesis	57
2.7.4. Other structures	59
2.7.5. Conductivity	60
2.7.6. Ionic conductivity	62
2.8. MoS₂	64
2.8.1. Other crystallographic structure of MoS ₂	65
2.8.2. Electronic bandstructure.....	66
2.8.3. Exfoliation process	67

2.8.4.	Top-down approach	68
2.8.5.	Bottom-up approach	70
3.	SINTHESYS PART	75
3.1.	Aim of the Work	75
3.1.1.	PANI.....	75
3.1.2.	MoS ₂	77
3.2.	Synthesis Work	79
3.2.1.	Materials	80
3.3.	PANI	81
3.3.1.	Italian PANI synthesis	81
3.3.2.	Portuguese PANI synthesis.....	82
3.3.3.	PANI ITA vs PANI PORT	83
3.4.	MoS₂.....	87
3.4.1.	MoS ₂ commercial	87
3.4.2.	MoS ₂ Hydrothermal synthesys	88
3.5.	Composites.....	92
3.5.1.	Exfoliation process	92
3.5.2.	IN-SITU Composite	93
3.5.3.	EX-SITU Composites	98
3.5.4.	Hydrothermal Composite.....	102
3.6.	Conclusion:	106
4.	ELECTROCHEMICAL PART	107
4.1.	Cell Preparation	107
4.1.1.	Cathode preparation:	107
4.1.2.	Double layer preparation:	108
4.1.3.	Cell assembling:.....	109
4.2.	Electrochemical Analysis.....	109
4.2.1.	Cyclic Voltammetry	110
4.2.2.	Galvanostatic cycling.....	115
4.2.3.	Catalytic Effect (TAFEL)	124
5.	CONCLUSION.....	127
	Abbreviations.....	130
	Simbols	133
	Figure Index	136
	Table Index	140
	Bibliography.....	141
	Appendix: Instruments and Operation Conditions	147
	Acknowledgments	148

1. Introduction

At the beginning of 1800s, energy acquired its primary role within societies thanks to the high abundance of fossil fuel and the ease way with which it could be obtained.

The availability and cost of energy have always been two factors capable of determining the birth or death of economic sectors and the development of entire countries. Not by chance, the industrial revolution, probably the most significant socioeconomic transformation in human history, found fertile ground in those countries that presented abundant and affordable energy such as coal-rich Northern England. The industrial revolution, however, was not the only phenomenon which caused a radical change in people's way of life; shortly afterwards urbanization, modernization and information technology took over, helping to build the foundations of the society as we know it today.

All these trends are united by nature, with an important need for energy, that can therefore rightly be considered as the basis of modern life. [1] [2] This energy need has also been exacerbated by the exponential population growth that has been registered in recent decades. [3] [4]

In the beginning, the energy was entirely obtained by the extraction and combustion of fossil fuels (petrol, oil, coal and natural gas). However, over the years, an increasing number of experts begun to show their concerns about these resources.

One of the first observations regarded the finite and non-renewable nature of fossil fuels. On one side the time required for their regeneration and on the other the speed which with they are consumed nowadays, make difficult to imagine their unlimited use over time while making easy to portend their depletion shortly.[1] [4] Alongside economic motivation, other social and environmental concerns soon arose. Recent studies show that the extraction and consumption of fossil fuels generate 85% of the CO₂ emissions released into the environment with devastating consequences on the climate and human health. It has been shown in fact that the abnormal increase in CO₂ in the atmosphere is one of the leading causes of global warming and climate changes. Moreover, the International Energy Agency (IEA) estimates that more than six million people around the world die every year for the consequences of combustion exhaust gas. [5] [6]

To limit the damage associated with the consumption of fossil fuels and to comply with the provisions of the Paris climate agreements (keep global warming below 2°C), it appears evident that it is necessary to reduce the CO₂ emissions drastically.[5]

In order to approach this goal, alternative technologies based on renewable sources started to be developed and adopted. Among these, solar and wind energy have become the most popular applied strategies all over the world. However, despite their development, the market penetration of solar and wind energies is still low: 30% and 10% respectively. The main disadvantage of these systems is that naturally variable wind resources and solar availability cause voltage and power fluctuation problems at the load side. Another significant question regards the storage of the energy generated for future use when no wind and sun are available. [7] [8]

The introduction of technologies based on renewable sources was, therefore, quickly followed by the development of electric energy storage systems (EES). EES, play a vital role in the entire chain of the

energy system, from energy generation to transmission, distribution and accumulation. Within this category, rechargeable batteries are one of the most viable options.

In recent years, batteries have also taken on a primary role in the automotive sector. [8] [3]

Transport in fact is one of the primary examples of unsustainable use of energy. This is due to both the high energy consumption of this resource (27% of the global energy) and almost its complete dependence (about 94%) from fossil fuels. These two aspects make transport the second source of CO₂ emissions globally. Another worrying aspect is that 60–70% of CO₂ road transport emissions, concern passenger vehicles (Figure 1.1). [9]

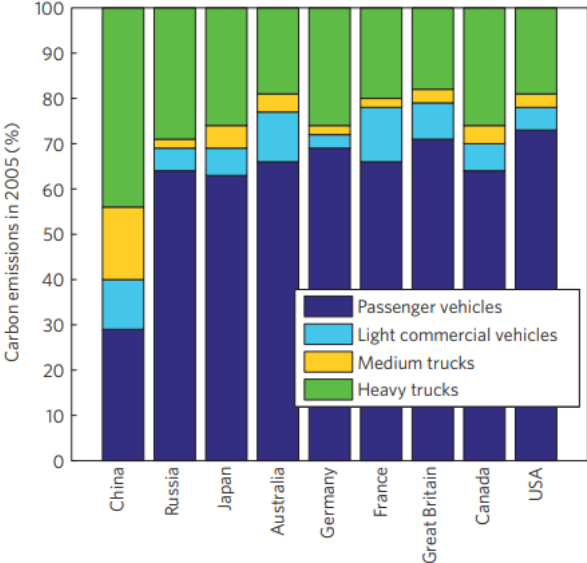


Figure 1.1: Impact of passenger vehicles on total CO₂ emissions in different countries (2005): [9]

In this scenario, the batteries introduction can be a winning strategy for the decarbonisation of transport: some studies even estimate a 70-85% reduction of CO₂ emissions by 2030. [9]

To encourage car manufacturers to undertake an electrification path, the European Parliament (European Commission – Climate Action) passed a law requiring all vehicles manufactured after 2020 will emit less than 95 g km⁻¹ of CO₂ into the atmosphere. The law enacted by the European Parliament is probably only one of the restrictive measures that will be approved shortly. New limitations on CO₂ emissions into the environment are expected for 2025. [10]

1.1. Aim of the work

The following master thesis aims to deepen the state of the art of one of the most recent and promising classes of batteries, the Lithium-Sulfur one. During the first part of the work, particular attention is paid to polysulfides (intermediate species, negatively charged, generated during the regular operation of the cell) and to the Shuttle phenomenon.

This phenomenon involves the migration of polysulfides inside the cell and a series of parasitic reactions with the electrodes. The suppression of the Shuttle mechanism is crucial because of the side effects that influenced the performance of the cells: shorter battery life, low coulombic efficiency, a significant drop in potential, moderate use of active materials and a high propensity to self-discharge.

To achieve this goal, Double-Layer composites were generated to be applied on the cathode in order to limit the severity of the Shuttle effect. The purpose of protective coatings, in fact, is to block polysulfides both from a chemical and physical point of view.

In the second part of the thesis, the methods of synthesis and the characterization of composite materials (the so-called IN-SITU, EX-SITU, Hydrothermal) are presented. These materials are made of conductive polymer, PANI (polyaniline) and metallic dichalcogenide, molybdenum disulfide (MoS_2) which present interesting properties that could act in coherence with the target.

A series of electrochemical analysis (galvanostatic cycling, cyclic voltammetry and Tafel plot) is therefore proposed to evaluate the performance of these materials and their applicability within batteries.

Finally, in the last part of the thesis, the principal results and conclusions are reported.

2. Bibliographic part

2.1. Rechargeable cells and batteries

2.1.1. Introduction on batteries

A battery is an electrochemical device that converts, through an electrochemical oxidation-reduction (redox) reaction, the chemical energy contained in its active materials directly into electric energy (Figure 2.1). A battery is a complex system in which there are both electro-chemically active and non-active components, but only the first ones are directly involved in the redox reactions. All other types of materials, even if are define like passive components, are not necessarily inert and can nevertheless be involved in other side reactions taking place during charge and discharge of the cell. [11] [12]

The conversion from chemical to electric energy allows for both energy storage, such as a direct method of producing Direct Current (DC) electricity. During these reactions, electrons are transferred via an external electric circuit from one electrode to another. At the same time, ions are transferred inside the cell, through the electrolyte, to maintain the charge balance. [11]

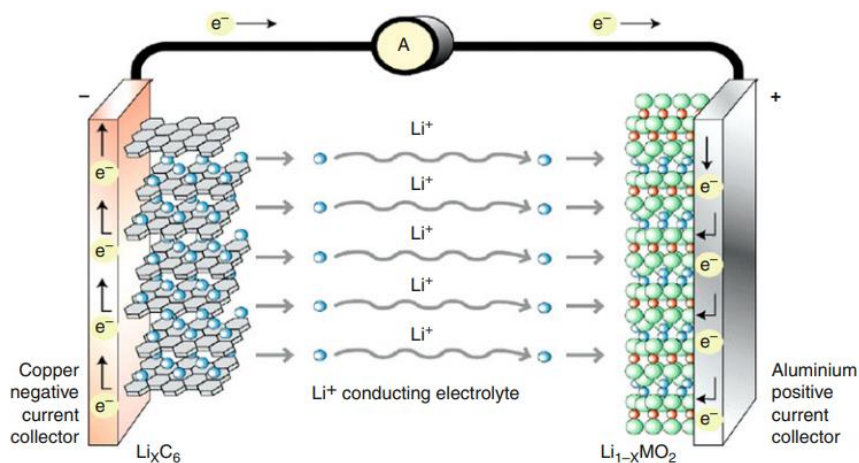


Figure 2.1: Operational scheme of an electrochemical battery. [13]

Based on the conversion process, batteries can be classified as electrolytic or galvanic. Correctly: in an electrolytic battery, the electrical energy is converted into chemical energy while in a galvanic battery, the process occurs oppositely. For an electrochemical battery, both definitions are correct; during the charging phase, it behaves like an electrolytic battery while during the discharge phase it behaves like a galvanic battery. [11]

The basic electrochemical unit of a battery is the "cell". A battery consists of one or more cells, connected in a different way (series or parallel, or both). How the cells are connected allows obtaining different outputs in terms of voltages and currents. Cells connected in series, for example, share the same current I and if the cells are identical to each other, the total voltage is the sum of the voltages of the individual cells. On the contrary, if the cells are connected in parallel, they share the same voltage V , and if the

cells are identical to each other, the current divides equally between the various cells, resulting in increased battery capacity. [11] [12] [14]

2.1.2. Types of batteries

Batteries can be classified into four groups:

- **Primary cell** (non-rechargeable): is entire of galvanic nature (it can only convert chemical energy to electric energy) and can be discharged only once. It represents an inexpensive and lightweight solution for portable electronic and electric devices. On the market, it is also possible to find high capacity primary batteries which are generally used for military applications (signalling, standby power). The general advantages of primary batteries are high energy density at low discharge rates, good shelf life and little maintenance.
- **Secondary cell** (rechargeable): can operate both as galvanic and electrolytic cells and can be easily recharged by a reversal of the process. The recharging operation consists of passing the current through them in the opposite direction respect the discharge current. These batteries are commonly the primary energy source for cell phones and tablet computers. Secondary batteries can be used as a back-up for another power source. For this reason, secondary cells are also known as "storage batteries" or "accumulators". They can also be used as the main energy source instead of primary cells in order to reduce waste, and in applications requiring power drains higher respect the capability of primary batteries. Secondary batteries are characterized by high power density, high discharge rate and good low-temperature performance, but their energy densities and charge retention are generally lower than those of primary batteries.
- **Reserve Batteries:** Unlike the "active" batteries (primary and secondary cells), these present one component, such as the electrolyte, physically separated to avoid chemical deterioration or self-discharge. This feature makes the battery more stable and able to be stored for a long time. The battery can then be activated only when necessary in the thermal battery this happening heating the system and causing the melting of the solid electrolyte, which in this way becomes conductive. These batteries are typically used in weapon systems to deliver high power for relatively short periods.
- **Fuel Cells:** Their function through a redox reaction like batteries (and unlike most capacitors) but are considered a battery only by some source. These batteries in facts differ in that the active materials are not an integral part of the device. The combustion cell is fed with fuel from outside the reaction chamber. It continues to function until the reagent is introduced. The electrode materials of the fuel cell are inert, but they have catalytic properties which enhance the electro-reduction or electro-oxidation of the reactants (active materials). Fuel cell technology can be classified into two categories: direct systems and indirect systems. In the second ones the fuel, such as natural gas or other fossil fuel, is first converted by reforming to a hydrogen-rich gas which is then fed into the fuel cell. Fuel cells have not matured to a point for use in mobile electronics and mechatronic devices. Only recently fuel cell technology has moved towards portable applications. [12] [14]

2.1.3. Components of a secondary battery

All batteries are composed of two electrodes (cathode and anode). During charge and discharge of a battery, the nomenclature of the electrodes is reversed. Conventionally, it was decided to adopt the terminology characteristic of the discharge process. For this reason, the negative electrode is called anode while the positive electrode is called cathode, regardless of the electrochemical state in which is the cell. [15] [14]

The electrodes are both electrically and ionically conducting materials that constitute the active components of batteries. Depending on the nature and the category of these materials, the electrochemical reactions can develop in different regions of the electrodes:

- Blocking electrodes: in which the electrochemical reactions take place only at the outermost surface layer due to the presence of reaction products capable of accumulating on the external surface preventing any further reactions. Metallic materials make up this category
- Insertion, or non-blocking electrodes: redox reactions take place at the surface as well as in the bulk of the electrode. For rechargeable batteries, this type of materials is the most used. [11]

The two electrodes are electronically isolated in the cell to prevent internal short-circuiting but are surrounded by an ionic conductor, the electrolyte. The element responsible for keeping the two electrodes electronically and mechanically divided is the separator which, like the electrolyte of which it is soaked, must allow the ions to move. The system is finally completed by two collectors which connect the electrodes to the external electronic circuit. Through this, electrons pass from one part to the other of the cell (Figure 2.2).[12]

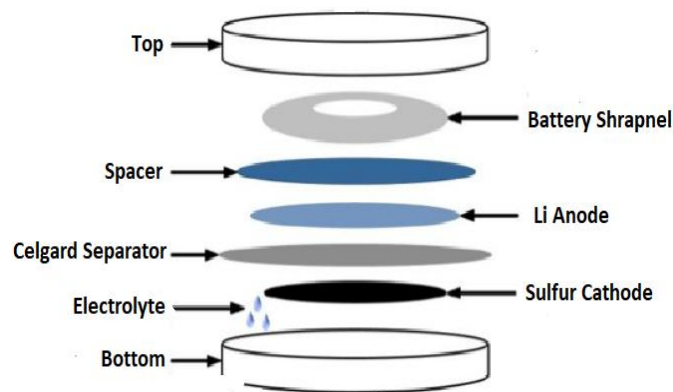


Figure 2.2: Typical structure of a coin cell. [16]

Going to the components in more detail:

- **The anode or negative electrode**—reducing electrode— gives up electrons to the external circuit (electron donor) and undergoes oxidation during the electrochemical reaction. The anode has to submit some peculiar properties: efficiency as a reducing agent, high coulombic output (Ah/g), good conductivity, stability, ease of fabrication, and low cost. The materials mainly

used as an anode are metals like Zinc and Lithium that present high value of electrochemical equivalence. [17][12]

- **The cathode or positive electrode**—oxidizing electrode— accepts electrons from the external circuit (electron acceptor) and undergoes reduction during the electrochemical reaction. The cathode must be an efficient oxidizing agent, stable when in contact with the electrolyte, and have a good working voltage. Most of the common cathode materials are metallic oxides.[12] [18]
- **The electrolyte**—ionic conductor— allows passage of charge, as ions, inside the cell between the anode and cathode. In order to not limit the redox reaction and increase resistance, the ion conductivity should be fast. For these reasons, a liquid phase electrolyte such as water or other solvents, with dissolved salts, acids, or alkalis able to increase ionic conductivity is typically used. Nevertheless, the use of aqueous solutions is not recommended with batteries that contain lithium anode due to the reaction that can eventually occur between the two elements. More generally the electrolyte must be compatible with the electrodes without losing its performance over time and be stable within the full voltage range of the cell. Liquid electrolytes, although excellent ionic conductors have shallow mechanical properties necessary to separate the electrodes and avoid short circuits. To overcome these limitations in recent years also solid-state electrolytes are gaining in importance, those made of polymeric materials that are more flexible and can be made in several shapes. The drawback of polymers and the solid-state electrolyte is the lower ion conductivity. A suitable electrolyte must provide a compromise between these two needs. [19] [12]
- **The separator:** as the electrolyte, the separator must be a good ionic conductor, but at the same time it has to: prevent the active materials from making direct contact, prevents electrons passing internally between the electrodes and maintain good electronic insulator properties. In order to meet these prerequisites, the separator must be permeable to the electrolyte, have excellent mechanical stability and strength without causing an excessive increase in resistance inside the cell, for this reason, it has to be as thin as possible. Another essential aspect to keep under control is its chemical inertia towards the other components. The separator is most often a porous membrane soaked in electrolyte. [11] [12]
- **The current collectors:** The primary function of the current collectors is to transfer electrons from one electrode to another in order to ensure the correct charging and discharging process. For this to happen, it must have excellent conductive properties and be suitably connected to the external electrical circuit that joins the two electrodes. The best candidates to perform this function are Aluminium and Copper used in the form of thin sheets or grids. In addition to electrical conductivity, also thermal conductivity plays a predominant role within the collectors. During the operation of the cell, in fact, heat is unavoidably generated, and the current collectors are responsible for its disposal without redox or parasite reactions taking place. Finally, the current collectors add mechanical strength, especially necessary in the case electrode materials based on nano-sized composites. [11]

The electrochemical cell can be eventually included in a casing. The casing is used to create the final mechanical stability for the cell and limit any outside influence. The casing can be made in different shapes (cylindrical, button, flat, and prismatic) and materials (plastic or metallic, hard or soft) and sealed

in a variety of ways to prevent leakage and dry-out. Some cells are provided with venting devices in order to allow accumulated gases to escape. [11] [12]

In the latest generation devices, it is also possible to witness an ever-increasing presence of sensors capable of verifying battery operation by effecting in situ characterizations. For particularly delicate applications such as in military devices, environmental monitoring systems and intelligent constructions these sensors are mounted inside the batteries in the form of wireless sensors networks. Most wireless devices are made up of small sensors that can independently collect information from the environment in which they are located and re-process it. The information collected allows evaluating the performance and overall life of the batteries. [20]

2.2. Electrochemistry basics

During the electrochemical reaction, two types of processes occur at the electrodes. They can be classified in faradaic and non-faradaic reactions. [21]

- Faradaic processes: also called electron /charge transfer reactions are those in which the electrons transfer through the electrode/electrolyte interface involves a change in the oxidation state of individual species. These processes obey to Faraday's law: this means that there is proportionality between the current (passing through the system), and the chemical reaction occurs. [18]
- Non-faradaic processes: involve changes in the structure of the electrode/electrolyte interface or double electrical layer. This kind of process occurs when the applied potential change without charge transfer (like during adsorption and desorption). [18]

The two processes are governed by some fundamental physical relationships that also control the main aspects of the chemical reactions within the battery. Thermodynamic and kinetic features linked with the faradaic process can be studied considering the general semi-reaction (2.1):



Where O is the oxidized (more positively charged) form of the species that accepts z electrons and R is the reduced (more negatively charged) form.[21] [22]

A first property based on thermodynamic relations is the theoretical cell voltage, E_{cell} . This characteristic represents the maximum voltage level possible during an ideal charge and discharge process. It can be expressed as the standard potential difference (2.2):

$$E_{cell} = E_{positive} - E_{negative} \quad (2.2)$$

Under rest conditions, the cell has an Open-Circuit Voltage (OCV), which usually is close to the theoretical voltage. The theoretical cell voltage is also referred to as the electrochemical force (emf) that is primarily expressed as Gibbs free energy of the charge of the cell, ΔG_{cell} . Under open-circuit conditions, no current flow (the trend for a species to move in one direction or another) and no reaction occurs (conversion of one species to another).

However, an electrostatic force appears, due to the potential difference between the electrodes (2.3). A chemical force must balance this force:

$$\Delta G_{cell} + nFE_{cell} = 0 \quad (2.3)$$

When the reaction occurs, there is a decrease in the free energy of the cell, according to (2.4):

$$\Delta G_{cell} = -nFE_{cell} \quad (2.4)$$

where n is the number of electrons exchanged, and F is the Faraday constant $96.485 \text{ C mol}^{-1}$. [12] [23] The product of nF and E_{cell} represents the electrical work needed to transfer electrons from the anode to the cathode.

The free energy associated with the reaction, ΔG_{cell} , is the difference between the sum of free energy of the products and reactants (2.5):

$$\Delta G_{cell} = \sum \Delta G_{prod} - \sum \Delta G_{react} \quad (2.5)$$

During the discharge phase, the reaction occurs spontaneously by converting chemical energy to electrical energy, i.e. $\Delta G_{cell} < 0$ and $E_{cell} > 0$. Thermodynamically a process will occur spontaneously if it lowers the free energy of a system. During the charging phase (i.e. when $\Delta G_{cell} > 0$ and $E_{cell} < 0$), instead, it is necessary to supply energy for the electrochemical reaction to take place.

Related to free energy is the chemical and electrochemical potential. In particular, the change in Gibbs free energy can also be presented as (2.6):

$$\Delta G_{cell} = \sum \mu_{prod} - \sum \mu_{react} \quad (2.6)$$

Where μ_i is the chemical potential of species i , the chemical potential defines the change in Gibbs free energy when an infinitesimal number of moles of species i is added to a point in the system from a point outside of it. This term can be used to derive expressions for the system behaviour.

The chemical potential is also dependent on the activity a of the species i according to (2.7):

$$\mu_i = \mu_i^0 + RT \ln a_i \quad (2.7)$$

Where μ_i^0 is the standard chemical potential for species i , R is the gas constant, and T is the temperature in Kelvin.

When a metal anode is placed in contact with an electrolyte containing ions of the same metal, at the interface between the two materials, a reaction occurs until a spontaneous equilibrium take place. Consequently, charge accumulation is formed on each side of the electrode-electrolyte interface which can be described in terms of electrostatic potential in the electrode, $\phi_{electrode}$, and in the electrolyte, $\phi_{electrolyte}$. The difference between these two terms generates a difference in electrical potential, $\Delta\phi$, known as Galvani potential (2.8):

$$\Delta\phi = \phi_{electrode} - \phi_{electrolyte} \quad (2.8)$$

The electrochemical potential, μ_i , must be consider. This additional term, therefore, can be defined as the combination of the chemical potential and the Galvani potential according to (2.9):

$$\mu_i = \mu_i^0 + RT \ln a_i + nF\phi_i \quad (2.9)$$

If an electrochemical cell has two electrodes having different potentials and different activities of species i , a_i , the electrochemical potential can be expressed as (2.10):

$$\Delta\mu_i = \mu_{i,+} - \mu_{i,-} = RT(\ln a_{i,+} - \ln a_{i,-}) + nF\phi_i = RT \left(\frac{a_{i,+}}{a_{i,-}} \right) + nF\phi_i \quad (2.10)$$

The electrochemical potential is more or less directly related to the cell potential: combining the chemical and electrochemical potentials with Gibbs free energy is possible to obtain the Nernst equation (2.11) that gives another expression for the theoretical voltage of a cell:

$$E_{cell} = E^0 - \frac{RT}{nF} \left(\frac{a_+}{a_-} \right) \quad (2.11)$$

The Nernst equation is a fundamental thermodynamic relationship that must always be obeyed in an electrochemical process. For this reason, any kinetic model for the reaction rate must be reduced to this expression at equilibrium. [24]

Values of the standard state reduction potentials for many reactions are measured and commonly tabulated but is considered impossible to measure E^0 of a specific electrode practically. Therefore, in order to establish a scale of half-cell standard potential, they are quoted relative to a second reference reaction potential agreed and set as zero. By convention, ‘zero’ is defined as the standard potential of the H_2/H^+ (aq) reaction. [22]

As can be seen from the Nernst equation, the cell potential is dependent on the temperature and the number of electrons involved in the redox reactions.

In an electrochemical cell, the chemical reaction rates affect overall cell performance. The electrode kinetics determines how quickly the chemical energy can be converted to electrical energy, i.e. the power capability of the cell. For this reason, phenomena such as mass transfer, diffusion and transfer of electrons, capable of modifying the kinetics of the whole system, are considered processes of great importance. These processes, in turn, are strongly dependent on the materials used to build batteries.

The rate at which the chemical energy is converted into electrical energy is expressed as current. At equilibrium, the anodic (positive) and the cathodic (negative) currents are equal in magnitude and correspond to the exchange current, i_0 .

During cell operation, non-equilibrium states are reached and accompanied by a deviation of the electrode potential known as overpotential, η : that represents the difference between the cell potential value when a current I is passing and the potential E calculated with the Nernst equation

The relationship between the current, i , and the overpotential, η , can be expressed with the Butler–Volmer equation:

$$i = i_0 \left(e^{\frac{\alpha n F}{RT} \eta} - e^{-\frac{(1-\alpha) n F}{RT} \eta} \right) \quad (2.12)$$

where n is the number of electrons involved in the electrochemical reaction and α is the fraction of the electrode potential involved in the reaction known as “transfer coefficient”. [22][25] [11]

2.2.1. Electrode-electrolyte interfaces

From an electrochemical point of view, in any electrochemical cell, the interfaces between various materials are particularly interesting. In fact, the characteristics of the cell performances (for example capacity and duration) and the formation of any collateral reactions and/or limiting processes depend on the interactions that are generated in these areas.

The most striking interaction is that is formed when an electrode is placed in contact with an electrolyte. At the interface between these two materials, coulombic and chemical interactions act as a driving force for a charge accumulation on the electrode surface. The electroactive species (ions) are transported to the electrode by migration and/or diffusion and adsorbed at the surface, resulting in a first layer that is electrically charged. In order to maintain system neutrality, excess charge is counterbalanced by an accumulation of ionic species, close to the first layer.

The resulting structure is known as the electrochemical Double Layer. In this region, the electrochemical reactions take place through a charge-transfer process (Figure 2.3 a).

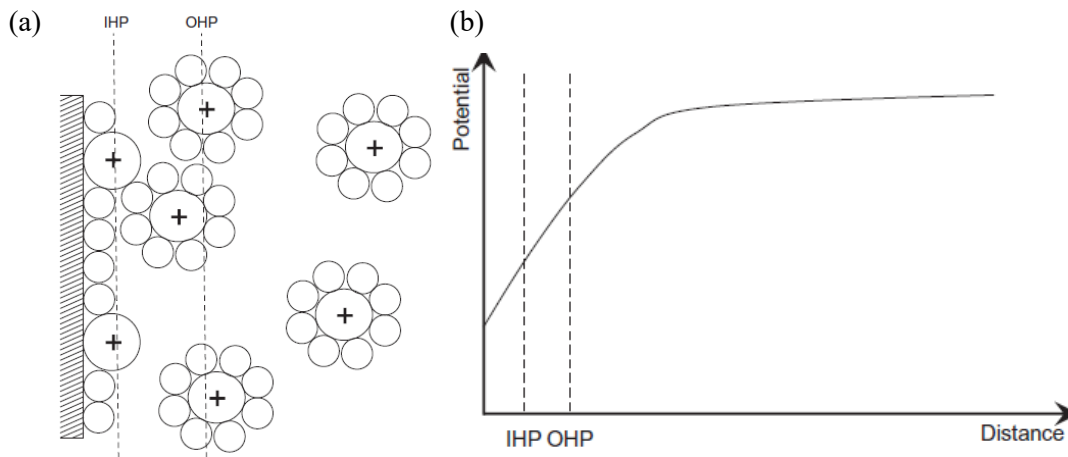


Figure 2.3: (a) Double-layer structure and (b) the potential distribution through it. [11]

Several models have been formulated to explain what happens at the electrode-electrolyte interface. The most used one is based on Helmholtz theories according to which:

- *Inner Helmholtz Plane (IHP)*: is the layer closest to the electrode surface. IHP is formed by ions (positive or negative) that are chemically adsorbed and actively interacting with the atoms of the electrode.
- *Outer Helmholtz Plane (OHP)*: the second layer that comprises ions attracted to the first layer charged surface. OPH is due to electrostatic forces which interact only weakly with the electrode surface. Unlike the ions that make up the Inner plane, these tend to keep their solvent shell from the bulk electrolyte intact. [21]

The presence of the double layer creates a potential variation that varies with the distance from the electrode surface considered. (Figure 2.3 b). Moreover, the electrochemical double-layer is by nature a capacitor, where the electrode surface and the Outer plane can be considered as the capacitor planes.

Due to the close distance between the planes, the double-layer capacitance can be quite large, causing an increase in polarization and losses. This phenomenon generates an impact on the dynamics of the electrochemical cell, such as a limitation in power rates. [11] [12]

2.2.2. Practical cell measures

Before entering more in detail with the description of the batteries and their function, it is necessary to introduce some characteristic properties of the cells.

These properties generally depend on several factors. Some are closely related to the system chemistry: active materials within the electrodes, type of electrolyte, current collector materials. Others, depend on the way the battery is design as: the configuration used, the thickness of the electrodes and the collectors, electrolyte amount. [11]

1. Open-Circuit-Voltage (OCV)

The open-circuit potential is the voltage, resulting from the difference in electric potential between the terminals of a cell, measured in the absence of an external load and electric current. It represents the maximum voltage available to the discharge phase, and it is used as a useful means to analyse the changes in electric energy that occur within the electrodes and estimate the battery State Of Charge (SOC).[11] [20]

This characteristic can be obtained from the variation of Gibbs free energy in standard conditions (2.13):

$$OCV_{cell} = E_{anode}^0 - E_{cathode}^0 = \Delta E^0 = - \frac{\Delta G^0}{nF} \quad (2.13)$$

2. Cell voltage under load

The OCV value is by nature only valid for cells in the rest condition. When a cell relates to an external load, electrons flow from the anode (where oxidation take place) to the cathode (where reduction occurs). During this process, known as the discharge phase, the cell transforms its chemical energy into electrical energy. This conversion leads to the generation of a potential difference between the two electrodes known as cell voltage (measured in volts). Electrochemical cells have different cell voltages according to their exactly chemistry. [23]

The cell voltage is limited by the theoretical cell voltage (that is determined by the Nernst equation), but they do not necessarily correspond, in fact, as a result of the passage of a current, potential losses are generated (Figure 2.4). The potential losses are caused by various types of polarisation or overpotential and have the effect of lowering the voltage value below the OCV. The overpotential, during the discharge phase, can, therefore, be defined as the difference between OCV and cell potential.

The polarisations can be classified as:

- *Activation polarisation*, η_{ct} : linked to the electrochemical reactions that occur at the surfaces of the electrodes and to the charge transfer between them.
- *Concentration polarization*, η_c : originated by the different concentrations of charged species between the electrodes surface and the bulk electrolyte. This polarisation is governed by the transport property (in terms of ions and mass) of the electrolyte
- *Ohmic polarization*, IR: is the most dominant sources of losses in an electrochemical cell. The voltage drop occurs during the discharge and is directly proportional to the current applied during this phase. If the applied current is small or negligible, the cell works for potentials close to OCV, and most of the theoretical energy is available. These Ohmic losses are associated with

the internal resistance which is the sum of various contributions: ionic resistance in the electrolyte, electronic resistance in the active electrode materials, and interface resistances between electrode/electrolyte or within the separator.[11]

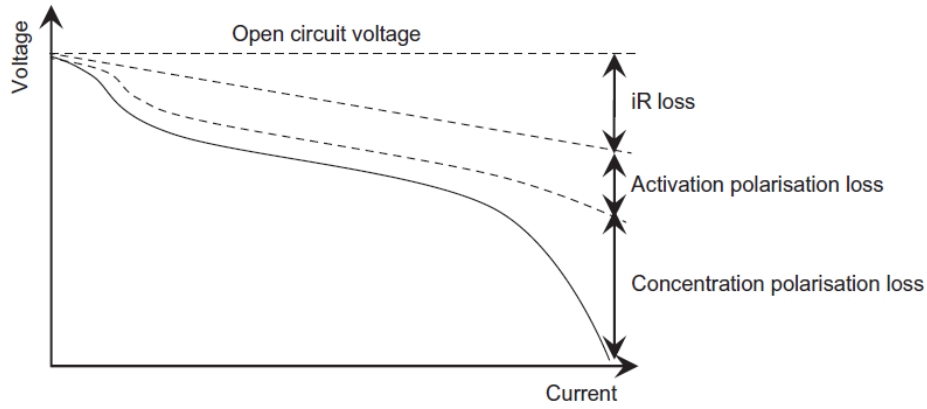


Figure 2.4: Effect of different types of polarisation on the voltage-current graph. [11]

The practical cell voltage can now be described as (2.14):

$$E_{cell} = E_{pos} - E_{neg} - [\eta_{ct} + \eta_c]_{pos} - [\eta_{ct} + \eta_c]_{neg} - iR_{cell} \quad (2.14)$$

where i is the current, and R_{cell} is the internal resistance of the cell. The polarisation losses do not assume constant values over time, but they are influenced by the degree of use of the cells and by the degradation processes. [12]

3. Charge and discharge rates

The rate at which the discharge (and charge) take place is defined as the C-rate, which express the current capability of an electrochemical cell. This parameter can also be associated with the constant current charge or discharge rate the cell can sustain for a specific time (the time required for the cell to charge/discharge completely)

A cell discharged at 1C rate, for instance, will deliver its rate capacity in one hour. In reality, what is possible to witness is a slightly shorter discharge time than the one foreseen as the cell often works in non-ideal conditions (temperature and the age of the cell may induce side reaction capable of modifying the discharge process and therefore the time in which this occurs).

At the same time, the charging and discharging currents are generally expressed as multiples of C. In particular, nC is defined as the current required to fully discharge or charge a battery in a time equal to 1/n hours based on the theoretical capacity of the electrode material.

Through the C-rate it is possible to evaluate the behaviour of a specific active material at different charging or discharging speeds, or more generally of an electrochemical system. A given material exhibits different values of specific capacity as the current changes. When increasing the current, or C-rate, the cut-off voltage is reached faster (much less charge has been delivered, due to massive polarisation), and hence a lower capacity will be achieved. [8][11]

4. Capacity

The total charge Q is the amount of charge that is carried by the current during a certain period. It can, therefore, be expressed as the integral of the current over time (2.15):

$$Q = \int_{t_1}^{t_2} I(t)dt \quad (2.15)$$

The cell *capacity*, on the other hand, is expressed with the ratio of the total charge and the mass, Q/weight (mainly cell weight is used). Capacity is related to the amount of active material within electrodes and cell dimensions. For this reason, two cells with the same chemistry, but different size present equal OCV but different capacity: the smaller cell, shows lower capacity.

The *theoretical capacity* of an electrode is related to the charge transferred in a specific reaction or the amount of charge that can be stored per unit mass of the material. It is often given according to the discharged state of the active material, and it could be express (2.16) in terms of specific capacity (Ah/kg or mAh/g) or volumetric capacity (Ah/L):

$$Q_{th} = \frac{nF}{M_w} \quad (2.16)$$

where Q_{th} is the theoretical specific capacity in Ah/kg or mAh/g, n is the number of transferred electrons, F is Faraday's constant (96485 As/mol), and M_w is the molecular weight of the electrochemically active material within the electrode (g/mol). From the expression of the specific capacity, it is easy to notice an intrinsic linkage with the type of material (molar mass) and the nature of the reaction (number of electrons involved).[12]

The fraction of the stored charge an electrochemical cell can deliver depends on several factors, including chemistry, discharge rate, voltage level, and temperature. For instance, when the discharge rate is too high, the cut-off voltage will be reached before the full capacity has been delivered.

Finally, knowing the capacity of the cathode and that of the anode, it is possible to calculate the resulting battery capacity as (2.17):[8]

$$\frac{1}{c(\text{battery})} = \frac{1}{c(\text{cathode})} + \frac{1}{c(\text{anode})} \quad (2.17)$$

5. Energy and power

The *energy* of an electrochemical cell is the amount of useful work that the cell can perform until the cut-off voltage has been reached, and it is defined as (2.18):

$$\text{Energy} = \int_0^{t^{\text{cut-off}}} V(t)Idt \quad (2.18)$$

corresponding to the area under the discharge profile.

The *specific energy* is the amount of energy that can be stored per unit mass of electrode materials [Wh/kg]. It can be related to the active electrode material only or both the active and the non-active materials in the cell.

The *energy density* is the amount of energy that can be stored per unit of volume, and it is expressed in Wh/l. The energy density depends on cell voltage and capacity; to increase the energy density is necessary to enhance these two values, e.g. by increasing the amount of the active materials.

The *power* of an electrochemical cell, generally indicated as [W/kg], is defined as the energy delivered during a specific time, namely the rate with which the useful work is performed. This characteristic is expressed as (2.19):

$$Power = \frac{\int_0^{t_{cut-off}} V(t)Idt}{\int_0^{t_{cut-off}} dt} \quad (2.19)$$

The energy depends on the kinetics of the electrodes and the electrolyte but in particular on the rate at which reactions occur at the interfaces between these components.

Contrary to what happens for energy, increasing the power means reducing the potential drop between the two electrodes with an increased current which can be achieved using thinner electrodes in order to reduce diffusion limitations. Therefore, inside the cells, there is a lower presence of active material.

It is, therefore, evident that it is not possible to achieve both maximum energy and maximum power density at the same time. It is necessary to decide if optimize the battery from an energetic point of view or in terms of power. The choice can be made according to the applications and performance required to the battery; for example, cells used in hybrid electric vehicles (optimized concerning power) cannot be used for fully electric vehicles and vice versa.

The power of a battery is also given by the product between the current and the working potential; therefore applications that require low powers will work at rates between C / 10 and 1C while for applications that require high powers the charge and discharge rates can be 5C or 10 C or more. [11][8]

6. Efficiency

The performance and efficiency of a cell depend both on charge and mass transport. When the ionic current through the electrolyte (inside the cell) is equivalent to the electric current through the electric circuit (outside the cell), the cell is defined ideal.

These two parameters, in turn, are influenced by the materials that compose the cell and the characteristic of the battery itself like diffusion rate, the stability of the materials during operation conditions and ionic conductivity.

The efficiency of a cell can be expressed in two different ways:

- The *Coulombic efficiency* is defined as (2.20) the charge transferred during the discharging process, Q_{dis} , over the charge transferred during the subsequent charging process, Q_{cha} :

$$\eta_{Coulombic} = \frac{Q_{dis}}{Q_{cha}} = \frac{\int_{dis} Idt}{\int_{cha} Idt} \quad (2.20)$$

This parameter is an indicator of the reversibility of the process: for a coulombic efficiency equal to 1, the process appears as completely reversible.[8]

- *Energy efficiency* is defined similarly, but expressed in energy terms (2.21):

$$\eta_{Energy} = \frac{\int_{dis} V(t)Idt}{\int_{cha} V(t)Idt} \quad (2.21)$$

The batteries used in the automotive sector require high-efficiency values (of both types) close to the unit. [11]

7. Cycle life

The cycle life of a battery corresponds to the number of charges, and discharge cycles that an accumulator can make before its performance (measured in terms of capacity or energy storage efficiency) are excessively reduced and reach some arbitrary limit.

This parameter is mainly used in the automotive field to control the performance of batteries in electric cars. In this field, the limit beyond which a battery is considered "depleted" corresponds to 80% of capacity compared to the value initially submitted.[8]

8. Current density

The current density (j) is defined as (2.22) the ratio between the total current (I), that flows through the electrode, and its normal surface (A). This quantity is therefore expressed in A/m^2 . [8]

$$j(t) = \frac{I(t)}{A} \tag{2.22}$$

2.3. Why Lithium- Sulphur batteries?

2.3.1. Lithium-ion batteries

In the 1980s, the development of portable electronic products (such as video cameras, cell phones and laptops) gave rise to a growing need for high capacity rechargeable batteries. Soon, in addition to the demand, also the complexity of electronic devices that require the use of batteries increased. In this scenario, battery systems which had been used for over a century in a variety of applications such as lead-acid, nickel-cadmium, nickel-metal hydride batteries appeared inadequate in terms of energy density, size and weight. [23] [26]

In order to accommodate the needs of the market, intense activity research began and in 1991 a new type of high-performance batteries was introduced: the Lithium-ion battery. [23]

Since then, the lithium-ion market has continued to expand rapidly for over 15 years, making these batteries the dominant power storage solutions in portable electronic devices (Figure 2.5). Their success was due to their high energy density, low self-discharge property, high open-circuit voltage, long lifespan and negligible memory effect (an undesirable phenomenon that generates a loss in the storage capacity when repeated charging cycles are performed without having completely discharged the batteries). [26][27]

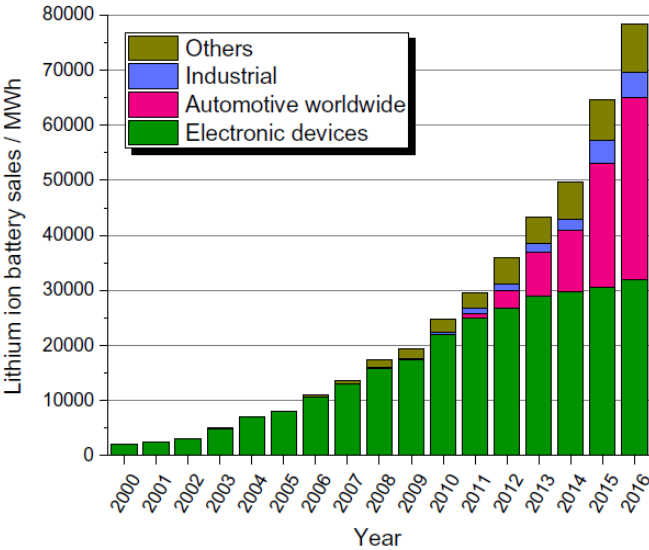


Figure 2.5: The graph shows the number of lithium-ion batteries sold in the world (from 2000 to 2006) and the application field in which they were used. [6]

The rapid growth of the Lithium-ion market was also due to the safe and efficient principle on which these batteries are based: a reversible intercalation process of Li ions that involves the cathode (typically Lithium metal oxide) and the anode (a carbonaceous material with a specific crystalline structure able to provide higher capacity respect with the amorphous ones). [23]

The chemical process consists of several steps: at the beginning, the lithium atoms are contained only inside the cathode of which they are part. During the charging phase, lithium ions leave the cathode (lithium source) and migrate to the anode (lithium sink) where they remain temporarily blocked, allowing energy to accumulate. During the discharge process, the opposite situation is found, and the ions return to the anode releasing the previously accumulated energy.

Inside the batteries that use the principle of intercalation or insertion, host materials are used to create the electrodes (Figure 2.6). These materials have free sites where the guest species (ions) can move and react without causing significant changes in the atomic structure. In contrast, the electronic structure of the host undergoes to modifications.

The host structure involves transition metals which change their oxidation state during the insertion/extraction reactions. Initially, the electronic bonding and anti-bonding levels of the host are arranged in well-defined bands. As the insertion process proceeds, the electrons of the guest species are added to the conductive bands of the structure. The Fermi level of the structure passes to a higher energy level, and the insertion process proceeds until the conductive band has been filled and the oxidation state of the host structure has reached its limit.

The limitations on the number of ions that can participate in the process reduce the capacity that the ion batteries can reach during their operation. [11]

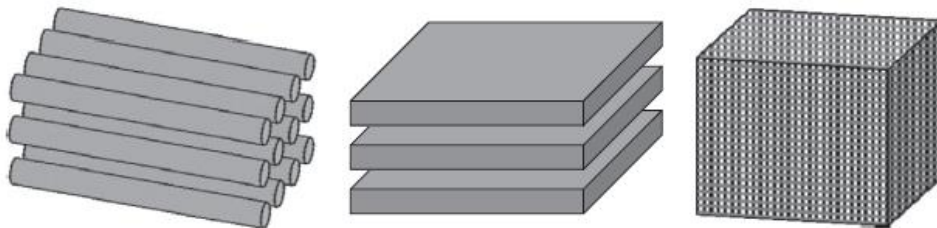


Figure 2.6: Three different examples of host structures that can be used as electrode materials: 1D (a), 2D (b), 3D (c). [11]

The main parameter capable of modifying the capacity of the insertion materials is the number of interstitial sites within the host material. This number depends on the type of structure used for the creation of the electrodes and the diffusion pathways between two host sites. The pathways developing in several directions can create 1D, 2D, and 3D interconnections (Figure 2.6), which correspond to different performances and properties of the electrodes. For this reason, during the electrode preparation, it is necessary to carefully control the type and degree of porosity contained in the material. [11]

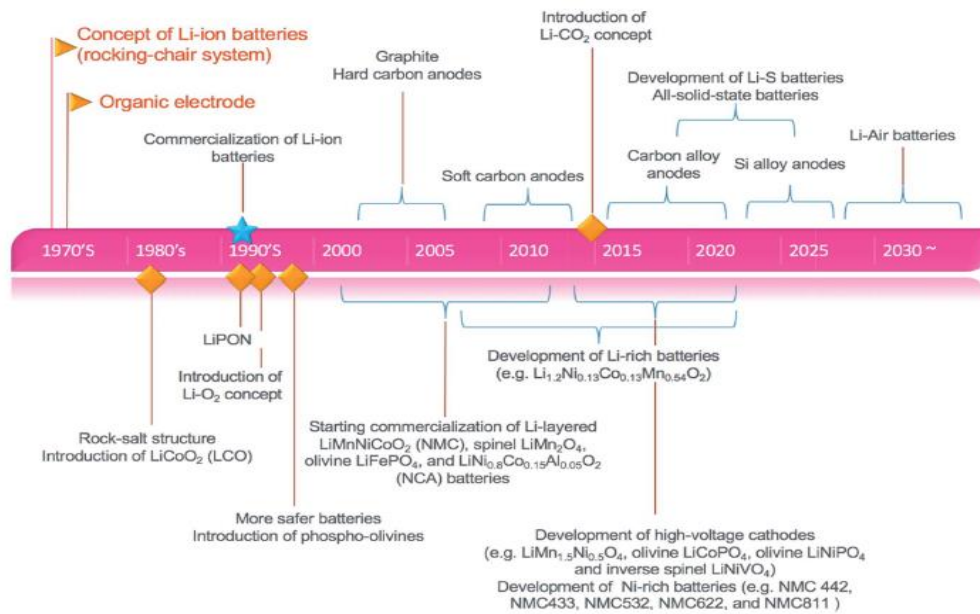


Figure 2.7: Summary diagram of the temporal evolution of lithium-ion batteries. [26]

The history of lithium-ion batteries began with the introduction of the rocking-chair batteries having graphite as intercalation materials (Figure 2.7). It has been demonstrated that graphite is very suitable as a host material due to its lamellar structure. During the same period, some studies on $LiCoO_2$ were conducted by Goodenough and collaborators to establish its applicability as a stable intercalation cathode able to accommodate Li-ions reversibly.[23] Since their earliest commercialization in the 1990s, batteries consisting of a $LiCoO_2$ (LCO) cathode and a graphite anode have proven to be very competitive in terms of energy density and power compared to traditional batteries (Figure 2.8). [24] Even today, cathodes composed of $LiCoO_2$, remain one of the most suitable solutions for ion batteries thanks to the excellent cycling performance and low self-discharge. [6] [15] [26] [27]

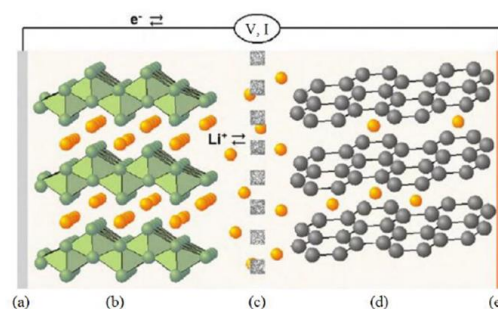


Figure 2.8: Schematic diagram of a LCO battery structure. [24]

During the charging and discharging phase of these batteries, Li ions migrate through the electrolyte according to the reaction (2.23):



The specific capacities of the two materials used as electrodes are 140 mAh/g for $LiCoO_2$ and 372 mAh/g for graphite that give rise to a specific theoretical energy of 387 Wh/Kg and a theoretical energy density of 1015 Wh/L. These values are well suited to uses related to consumer electronics.

These findings opened the door to the modern lithium-ion battery; however, the high cost due to the low cobalt availability, low thermal stability, and fast capacity fading at high currents led the researchers to investigate new cathode materials.

The materials that were studied in this regard can be classified according to their crystalline structure and their ion diffusion pathways in (Figure 2.9):

- One-dimensional $Li[M]PO_4$ with $M=Fe, Mn, Ni, Co, (Fe_yMn_{1-y})$
- Two-dimensional $Li[M]O_2$ with $M=Co, Ni, (Ni_xCo_{1-x}), (Ni_xMn_yCo_z)$
- Three-dimensional $Li[X]_2O_4$ with $X= Mn, (Mn_{1-y/2}Li_{y/2}), (Mn_{3/4}Ni_{1/4})$ [24]

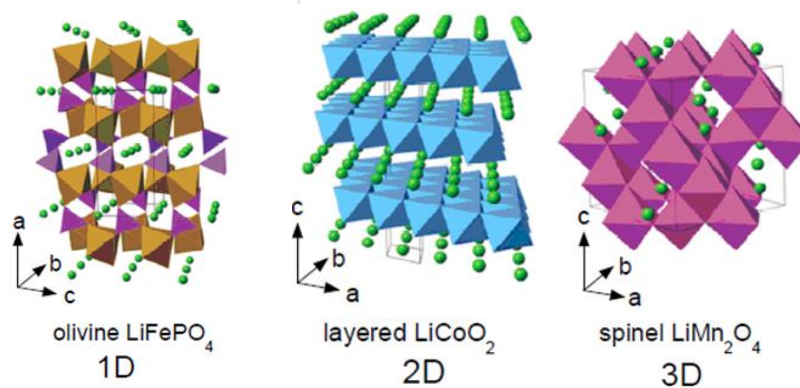


Figure 2.9: Possible cathodic material for Lithium-Ion batteries. [24]

The spinel $LiMn_2O_4$ (LMO) was proposed as a cathode material thanks to its environmental friendliness, excellent safety characteristics and high-power capability, but this never managed to gain an essential slice of the market. The major disadvantage of LMO is the considerable capacity fading linked to the structural transition from spinel to tetragonal structure due to reactions that can occur in contact with the electrolyte. This behaviour prompted to replace part of the Mn contained in the cathode with other metal ions. Also, $LiNi_{0.8}Co_{0.15}Al_{0.05}O_2$ (NCA) never reached a significant diffusion. However, these two classes of materials are still preferred for some specific applications that require certain properties. [24]

The LCO's market started to be gradually eroded only in 2010 with the introduction of $LiNi_{0.33}Mn_{0.33}Co_{0.33}O_2$ (NMC), a ternary system with nickel, manganese and cobalt thanks to their appealing properties such as high-capacity, excellent rate capability and greater availability of raw materials that involve a lower cost of the final product. In more recent years also phosphates with an olivine structure have been classified as a promising new class of cathode with $LiFePO_4$ (LFP) being the most common since they are low cost, environmentally friendly and show high thermal and chemical stability. Nevertheless, they present intrinsically low ionic and electronic conductivity. [26] [27]

Although their technology has evolved considerably since the first commercial unit was produced, (thanks also to the studies aimed at optimizing the chemical composition and electrolyte), conventional

lithium-ion batteries, cannot offer the high charge capacities ($> 300 \text{ mA hg}^{-1}$) required for particular applications and are therefore inadequate to meet all market needs (Table 2.1). [24]

Table 1.1: Possible structure and related properties of the cathodic materials used in Li-ion batteries. [24]

Framework	Compound	Specific capacity* (mAh/g)	Average potential (V vs. Li^0/Li^+)
Layered	LiCoO_2	272 (140)	4.2
	$\text{LiNi}_{1/3}\text{Mn}_{1/3}\text{Co}_{1/3}\text{O}_2$	272 (200)	4.0
Spinel	LiMn_2O_4	148 (120)	4.1
	$\text{LiMn}_{1.5}\text{Ni}_{0.5}\text{O}_4$	148 (120)	4.7
Olivine	LiFePO_4	170 (160)	3.45
	$\text{LiFe}_{0.5}\text{Mn}_{0.5}\text{PO}_4$	170 (160)	3.4/4.1

*Value in parenthesis indicates the practical specific capacity of electrode.

The need for alternatives solutions justifies the intense search for new types of electrochemical accumulators capable of offering high performances.

Among the solutions proposed, great attention has been given to advanced lithium insertion cathode such as high capacity Li and Mn-rich, layered oxides or $4.8\text{V LiMn}_{1.5}\text{Ni}_{0.5}\text{O}_4$ spinel. [24] However, the increase that can be observed in energy density hardly exceeds a few tens of per cent compared to existing cutting-edge systems. [26] [27]

The most promising technology, currently, are the Lithium-Sulfur batteries (both for energy density and safety).

2.3.2. Lithium-ion vs Lithium-Sulfur batteries

According to some studies, lithium-ion batteries are reaching their practical, specific energy limit (200-250Wh / Kg) confirming the inadequacy of these batteries to meet market needs. The achievement of the practical energy density limit, inside Li-ion batteries, can be conferred considering that the relationship between the theoretical and maximum practical energy density hardly exceeds 1/3. For this reason, an optimization of the cathode materials inside lithium-ion batteries is not sufficient to guarantee the performance required in some applications.

On the contrary, Li-S batteries with a current state of 200-500 Wh / kg, have a wide margin of improvement in terms of practical capacity. According to some authors, shortly, this type of batteries will reach a value of 900 Wh / Kg namely a value four times greater than what could be achieved by a lithium-ion battery.

Li-S batteries are presented as a promising technology thanks to the advantages linked with the replacement of the metals usually used as the cathode in lithium-ion batteries with Sulfur. Li-S technology is not just another modification on the Li-ion chemistries: the replacement of the metal cathodes with those based on Sulfur, in fact, allows the batteries to perform differently, making some concepts learned from lithium-ion batteries unused. [10]

The first Li-S battery composed of a sulfur cathode and a lithium metal anode dates back to the '60s however, intensive research and development on rechargeable Li-S batteries started only in the 2000s, as can be seen by the exponentially increasing number of publications (Figure 2.10 and 2.11). [15] [28] [6]

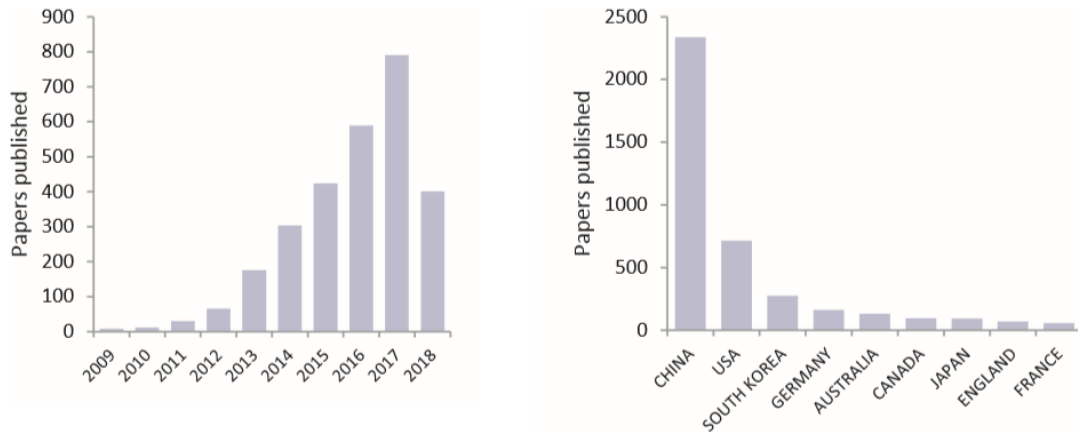


Figure 2.10: Spatial and temporal evolution of publications concerning lithium-sulfur batteries. [10]

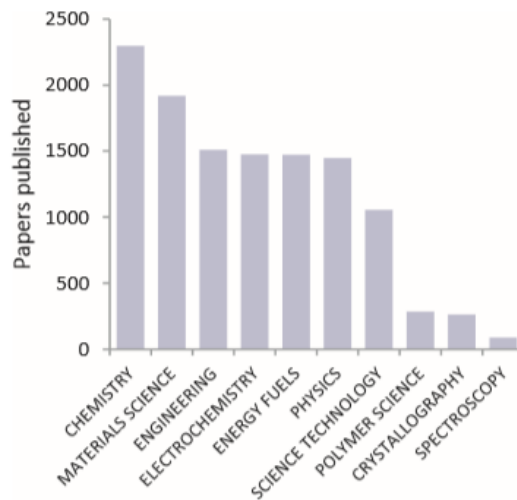


Figure 2.11: Diagram showing the number of publications on lithium-sulfur batteries and the topics they have involved. [10]

One of the main differences between these two technologies lies in the fact that in Li-S batteries, the intercalation process does not occur. On the contrary, Sulfur in its reduced state (S_8) reacts with lithium ions, through a series of intermediate products, until lithium sulfide (Li_2S) is obtained. [29]

Unlike typical lithium-ion batteries, in which the range of cathode materials is extensive (varying from Lithium Cobalt Oxide (LCO), Lithium Manganese Oxide (LMO) or Lithium Nickel Manganese Cobalt Oxide (NMC)) in Li-S batteries sulfur has remained the primary used cathode material over the years thanks to its structure and electrochemical properties (Figure 2.12).

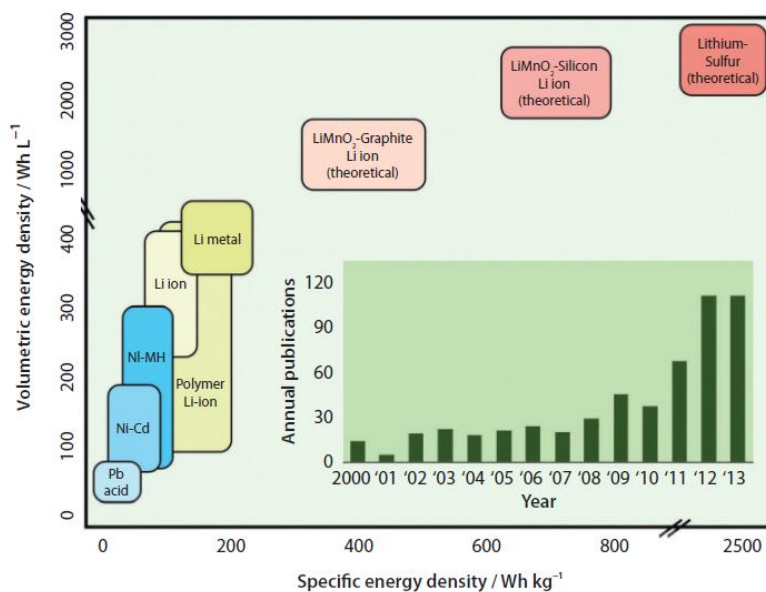


Figure 2.12: Comparison between different types of batteries in term of gravimetric and volumetric energy densities [30]

One of the most attractive electrochemical properties of Sulphur is its very high theoretical capacity of 1675 mAh/g (an order of magnitude higher than those of the transition-metal oxide cathodes and 4–5 times that of today’s Lithium-ion batteries). However, due to the high electrical resistance of elemental Sulfur and its reduction products, this element cannot be used alone but must be diluted with conductive materials.[31]

Consequently, Li-S batteries have a theoretical gravimetric energy density of around 2500 Wh/kg, an entire magnitude of order higher than typical Li-ion batteries and a practical energy density of 200 and 600 Wh/kg. [10][28] [32]

The high capacity is based on the conversion reaction of Sulfur to form lithium sulfide (Li_2S) by reversibly incorporating two electrons per sulfur atom compared to one or less than one electron per transition-metal ion in the insertion-oxide cathodes, due to the instability of higher redox states. [28][31]

Furthermore, Li-S cells can function correctly for all SOC ranges (state of charge), making full use of all the capacity. On the contrary, in lithium-ion batteries, it is necessary to leave a safety margin, usually corresponding to 20% of SOC.

In addition to an analysis of the performance of lithium-sulfur batteries compared to lithium-ion batteries, it may be interesting to examine other aspects of these technologies, such as the corresponding environmental impact.

In order to characterize the environmental performance of batteries, the Life Cycle Assessment methodology (LCA) has been used by some researchers. LCA-based studies can provide information on all phases of a battery's life starting from the production of the cell constituents, up to the end of life of the materials (from the cradle to the grave). In order for this to happen, it is necessary to insert coherent boundary conditions in the analysis model and consider all the steps involved in the life of the battery (including the acquisition of raw materials, transportation, the amount of energy used for the production of pieces). [10]

One of the aspects that emerged from these studies is, for example, that half of all the environmental impact of electric vehicle production is recognized for lithium-ion batteries in electric cars. However, it is necessary to highlight that, within the different classes of lithium-ion batteries, appreciable differences appear in terms of the energy consumption linked to the production of cathode materials.

Among these classes, the NMC lithium-ion battery technology can be considered as the most polluting, but also the most widespread one in electric cars. Therefore, NMC batteries present themselves as excellent representatives of lithium-ion batteries in comparison with Li-S batteries.

In addition to analysing the environmental impact related to Green House Gas (GHG) emissions, which considers the kg of CO₂ equivalent emitted, it is interesting to consider additional categories of impact. Among these additional categories, the main differences between lithium-sulfur batteries and lithium-ion batteries are found in (Figure 2.13):

- Human Toxicity Potential (HTP) category: where Li-S batteries show an 85% lower value
- Materials Depletion Potential (MDP) category: with a 74% reduction compared to NMC batteries
- Global Warming Potential (GWP, which is the category that better explains the impact of humankind in a globalized world) and Fossil resources Depletion Potential (FDP): where Li-S batteries confirm a lower value (of around 20%) [10]

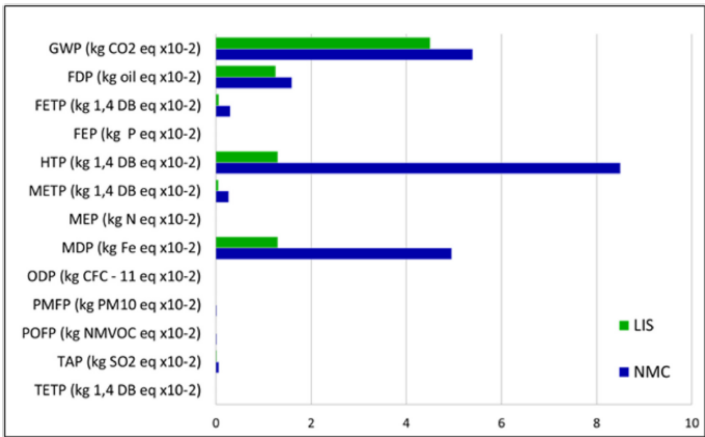


Figure 2.13: Comparison between life cycle impact of Li-S and NCM batteries. [10]

In conclusion, it can be affirmed that Li-S batteries have a lower environmental impact than lithium-ion batteries, well represented by the NMC class. Moreover, it is reasonable to hypothesize a further reduction of this impact following the optimization of the production process on a commercial and industrial scale.

Finally, among the aspects that contribute to making lithium-sulfur batteries competitive respect to lithium-ion batteries, there is a consideration about costs. Considering the three Li-ion battery variants with higher practical specific energy (Wh/kg):

- LCO (Lithium Cobalt Oxide),
- NMC (Lithium Nickel Cobalt Manganese Oxide)
- NCA (Lithium Nickel Cobalt Aluminium Oxide).

The main chemical elements present are Cobalt, Nickel, Manganese and Aluminum. All of these have much higher prices than Sulfur. In particular: the price of Sulphur is 32 times cheaper than Aluminium, 243 times cheaper than Nickel, 550 times cheaper than Cobalt and 20 times cheaper than Manganese.

Costs related to electrodes production and cells assembly, also contribute to the final price. Unfortunately, large-scale manufacturing strategies have yet to be developed for lithium-sulfur batteries, so it is not so easily making a direct comparison between these two technologies.

However, some studies in this direction have already been done. In particular, Erik J. Berg et al. made a comparison between the prices of the cathodes used in lithium-sulfur batteries and those used in lithium-ion batteries, showing that between a cathode for NMC (33 \$ / kg) and a cathode for Li-S (0.05 € / kg) there is a difference of about 660 times.[10] [31]

Nevertheless, the introduction on the market of lithium-sulfur batteries is very recent compared to that of lithium-ion. Also, for this reason, before being able to overcome the predominance of the latter, Li-S technology needs to overcome a series of technical challenges and limitations (Figure 2.14). [10]

	Li-ion				Li-S
	NMC	NCA	LCO	LFP	
Cell voltage (V)	3,70	3,60	3,65	3,20	2,15
Theoretical specific energy (Wh/kg)	400-600	400-600	400-600	300-400	2600
Practical specific energy (Wh/kg)	220	260	240	120	200-550
Practical/Theoretical correlation	≈ 1/2,5	≈ 1/2,5	≈ 1/2,5	≈ 1/2	≈ 1/10
Power density (W/L)	320	270	450	200	100-200
Cycle life (cycles)	1000-2000	500	≈ 700	1000-2000	≈ 50
Self-Discharge Rate (month)	1%	1%	1%	1%	8-15%
Thermal runaway (°C)	210	150	150	270	120
Work window (SOC)	15-95%	15-95%	15-95%	15-95%	0-100%
Memory effect	No				Yes
Properties	High voltage, good specific capacity, high safety risk, good lifetime	High energy, high density, expensive	High safety risk, good lifetime	Long lifetime, high stability, basic low cost	High energy density, cheap, low environmental impact, low safety risk
Applications – Automotive	EV, HEV, PHEV	EV, HEV, PHEV	EV, HEV	EV, HEV, PHEV	EV

Figure 2.14: Comparisation between Li-S and Li-ion performances and characteristics. [10]

Among these, insufficient capacity stability (and therefore a short duration of the cell) is one of the biggest problems to be solved. Nowadays, Li-S batteries have an extremely rapid decrease in capacity, lasting for less than 50 cycles, which is between 10 and 40 times less than what Li-ion commercial batteries are offering.

Other critical challenges concern low coulombic efficiency and high self-discharge rate, both attributable to the shuttling phenomenon of the polysulphides and progressive collector corrosion. Li-S

batteries, in particular, have a self-discharge rate of 8-15% per month, namely 10-15 times higher than that of lithium-ion batteries. Some studies, including those conducted by Yousi et al., shown that the phenomenon of self-discharge increases with increasing SOC. Therefore, it would be advisable to store Li-S batteries at low SOC, which unfortunately is not always possible, as most applications require that the battery be fully charged at the beginning of the operating process.

Finally, consideration can be made on the power density of Li-S batteries. Although Li-S have a higher energy density, they have lower power density about ten times less than Li-ion (capable of reaching 2-50 Ah / cell), which is the primary concern for car manufacturers. Therefore, Li-S cells low power and high capacity make this chemistry more suitable for EV's (Electric Vehicles) than for PHEV's (Plug-in Hybrid Electric Vehicle). The limitations in terms of power reached are mainly regulated by:

- the diffusion of the ions in the electrodes (which is mainly connected to the battery design and electrode materials)
- the high sensitivity to cycling parameters such as current profile or temperatures due to slow diffusion of species through the electrolyte, ions and polysulphides kinetics, and reduced availability of active species and active surfaces.[10]

In conclusion, Li-S batteries are ahead of lithium-ion batteries in terms of energy density, safety, price and environmental impact. In contrast, Li-S batteries are slightly less attractive in other essential aspects such as life cycle, self-discharge, power density and modelling (Figure 2.15). [10] [31]

	Li-ion				Li-S
	NMC	NCA	LCO	LFP	
Energy density	+	+	+	+ -	+ + +
Power density	+ +	+ +	+ +	+	+ -
Lifecycle	+ +	+ -	+	+ +	--
Self-discharge	+ +	+ +	+ +	+ +	--
Safety	+	-	-	+ -	+
Price	-	+ -	+ -	+	+ + +
Model	+ +	+ +	+	+ -	-
Environmental	-	-	--	+ -	+ +

Figure 2.15: Summary scheme of the advantage and disadvantage aspects of Li-ion and Li-S batteries. [10]

The advantages of lithium-sulfur batteries justify the great attention paid to this class of cells, while the limits currently still in force explain the numerous researches carried out in this field.

2.3.3. Other storage solutions

Lithium-ion batteries and lithium-sulfur batteries are undoubtedly among the best known and most studied accumulators on the market, but they are not the only ones. Li-S (metal /sulfur) cells belong to a broader category of "new generation" batteries known as post-lithium ion batteries (PLIBs). Within this category, other very promising examples appear, such as metal /air and metal/oxygen batteries.[6]

Metal /air batteries, proposed in the 1970s, are considered as possible sources of energy for electric vehicles thanks to their: high specific capacity, high specific energy values and energy density. The cell is composed of a metal anode (typically zinc, aluminium, iron, magnesium and lithium) and a cathode in which the active material is the oxygen present in the air. The oxygen reaction takes place on the surface of a conductive medium. [6][31]

Among the various types, the most promising technology is undoubtedly the one with a lithium anode. Its interest grew enormously when in 1996 Abraham and coworkers introduced the first non-aqueous Li-air battery by using a porous carbon cathode and a carbonate-based polyvinylidene gel polymer as an electrolyte membrane. Inside the mesoporous carbon cathode, catalyst metals (manganese, cobalt, platinum, silver) were also added to improve the kinetics of the reduction process.

In 2006, Ogasawara et al. introduced MnO_2 as a catalyst, which, in combination with an organic electrolyte, proved to be capable of promoting the reversibility of the Li_2O_2 discharge product. This discovery contributed to increasing scientific interest in this technology.

From a theoretical point of view, these batteries have fascinating characteristics compared to Lithium-ion batteries, first, a high theoretical specific energy. However, before proceeding with a broad commercial diffusion, it is necessary to fine-tune the sophisticated technology of these accumulators and solve some of the significant drawbacks such as inadequate rate capacity, decomposition of electrolytes during charging phase, the high reactivity of the lithium metal anode and related safety problems, as well as high overvoltages. All this leads to reduced cycling and poor Coulombic efficiency.

Another next-generation battery approach is aiming at the so-called “post-lithium technologies” (systems without Li), which are based on an alternative single (Na^+ , K^+) or multivalent ions (Mg^{2+} , Ca^{2+}). It is a very young technology and therefore, the object of an intensive study. [6]

Nowadays the ever-increasing need for new and efficient storage systems pushes the academic and industrial interests in an in-depth evaluation and comparison of these different battery systems in terms of theoretical and practical specific energy ($Wh Kg^{-1}$) and energy density ($Wh L^{-1}$) as well as costs.

Although there are more suitable and mature technologies than others to meet market needs, it is clear that the winning strategy will not be to move towards a technological monopoly governed by a single technology, but rather, move towards a technological diversity, capable of offering different storage systems (to be used alone or combined) to meet the multiple applications. [6]

2.4. Lithium-Sulphur battery

2.4.1. Cell

Before going into details of the components that make up a lithium-sulfur battery, it is interesting to make some general observations on the cell design.

Looking at the diagram below (Figure 2.16) appears evident that the weight of the cells is only partly made up of active materials (lithium and Sulfur) while inactive components still dominate it. This feature creates a severe impact on the battery performances. [18]

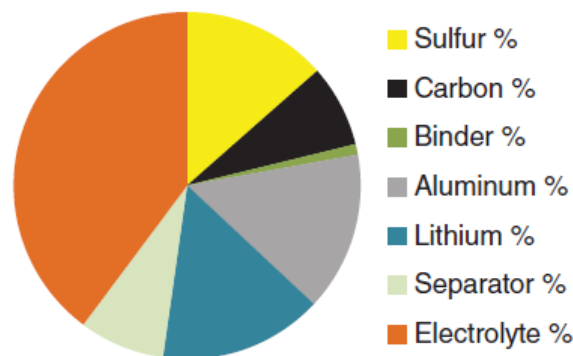


Figure 2.16: Pie chart showing the weight distribution of the various components that make up a Li-S cell. [18]

The most critical elements are the electrolyte and current collectors.

The electrolyte has the most significant impact on the total weight of the battery. This can be explained considering that cathodic conversion reactions involve dissolution and precipitation of active material species in the electrolyte and that, in order to ensure a high conversion efficiency, a rather high amount of electrolyte is required.

The other element which significantly contributes to the total weight of the device is the metal collector (in aluminium for the cathode and in copper for the anode). In order to limit its effect, in the case of the cathode, one possibility could be to replace aluminium foil with a lighter material such as thin carbon sheets.[3] However, the specific resistance of carbon is 100 times higher than that of aluminium, and currently, this solution is used only for devices that have low power requirements.

Although to a lesser extent, also the carbon and polymeric binder amount, used for the realization of the cathode, negatively influence the cell performances. It is therefore evident that, in order to optimize the specific energy of the cell or more generally the performance of the device, is necessary to operate at the whole-cell level considering all the components, in particular the inactive ones. [18]

2.4.2. Cathode

The positive electrode of a Li-S battery, the cathode, is formed by a layer of active material deposited on a metal support. The three main constituents of the active layer are elemental Sulfur, carbon materials and a polymeric binder.

Obtained the slurries by mixing the three components, the solution is coated onto a current collector in a reel-to-reel coating process. The collector is generally composed, as for lithium-ion batteries, of thin

aluminium sheets with a thickness of 10-20 μ m. After the coating, the solvent is removed by drying process generating a 20- 200 μ m layer.

Conductive carbon materials are added inside the composition to limit the adverse effects related to the low electrical conductivity of the sulfur and its discharge products (lithium(poly)sulfide(s)) and therefore to increase the specific energy of the cell. Polymeric binders are added to improve the materials cohesion inside the cathode and the adhesion of the cathodic slurry to the current collector.[16] [32]

Within the cathode, the relative amount of the three constituents are:

- Carbon materials: 20–50 wt%
- Polymer binder: 3–20 wt%
- Sulfur: 45–75 wt%

For the correct design of the cathode, the quantity of most considerable interest is the sulfur-carbon ratio. While maximizing the active material is one of the main objectives to be achieved, on the other side, an excessive increase in the latter inevitably leads to negative consequences such as high area currents at a given C-rate, problems related to coating and drying processes (for cathodes with a thickness greater than 100 μ m) and excessive increase in ionic and electronic resistance. All these aspects lead to a reduction in rate capability. Recent studies have shown that a reasonable compromise can be reached with an amount of Sulfur of 70-80%. [18]

Porous and Nanostructured Carbons as Conductive Cathode Scaffolds

In addition to Sulfur (discussed later), the essential components within the cathode are carbon materials, responsible for holding multiple roles.

They, in fact, actively participate in the electrochemical conversion of sulfur species through a charge transfer on their surface. The rate with which this transfer takes place and therefore the conversion itself depends on the carbon surfaces nature.

Moreover, carbon materials supported by the binder form a porous and conductive scaffold which provides mechanical resistance during all battery operating phases and guarantees a certain free volume amount to the electrode. The free volume between the carbon materials (added to any pores within the particles) determines the accessibility and mass transport of Sulfur and electrolyte, as well as their possibility of being retained inside the electrode.

Depending on their morphologies (pore shape and size) and the chemical properties of the surface (functionality), carbon materials can also interact with polysulphides and under certain conditions hinder their movement and limit the shuttling phenomenon. [18]

Carbon materials that are mainly added inside lithium-sulfur cathode can be divided in (Figure 2.17):

- *Graphite-Like Carbons*: carbon hexagons form a 2D structure or layered structure wherein each layer. Each hexagon is in turn composed by sp^2 hybridized carbon atoms tightly bonded through strong covalent bonds. Individual layers are called graphene and are held together by weak van der Waals forces that act perpendicularly to the carbon hexagons. Graphite-like carbons are often used as additives within electrodes as they combine several favourable properties such as high electrical conductivity, acceptable chemical durability, low material costs and in the right circumstances electro catalyzing properties for electrochemical reactions.
- *Carbon Black*: generated by incomplete combustion of hydrocarbons. Their structure includes spherical primary particles (with diameters between 10 and 500 nm) joined by covalent bonds. The main Carbon Black characteristic is the very high specific surface which gives interesting conductive properties to the material: in fact, a tiny mass fraction of these particles is enough to reach the critical percolation threshold and allow the electrons to flow. What limits the conductive properties of this material are impurities (especially oxygen), that are created during the production process.

- *Activated Carbons*: usually used like adsorbent they can also represent the most inexpensive choice for sulfur cathode architectures. In most cases they show a granular form and high quantity of open pores with different dimension (micro-, meso-, and macropores): pores with a narrow opening, in some cases, are not accessible for electrochemical processes (e.g. for the electrolyte molecules and ions). Granular form and dimensions of the pores influence their specific surface as well as the pore size distribution. Activated carbons are available with a vast spectrum of properties, and a variety of processes can be used to realize the activation of the carbon material.
- *Carbide-Derived Carbon*: Carbide-derived carbons (CDCs) present narrow pore size distributions: typically, microporous carbons that have a relatively high specific surface (up to $2800 \text{ m}^2\text{g}^{-1}$). However, by adapting the synthesis process temperature and / or the post-treatment step (e.g. activation), the CDC nanotexture can be modified to introduce different pore shapes and sizes (also mesoporous coals) and functional surface groups. This characteristic makes them attractive materials for ion transport applications, such as double-layer electric capacitors. This type of carbon materials is generally synthesized at high temperatures by selective extraction of a metal or semi-metallic ions from a hard metal precursor (ZrC, SiC, Mo₂C, TiC, B₄C) through supercritical water, halogen gases or decomposition under vacuum. [18]

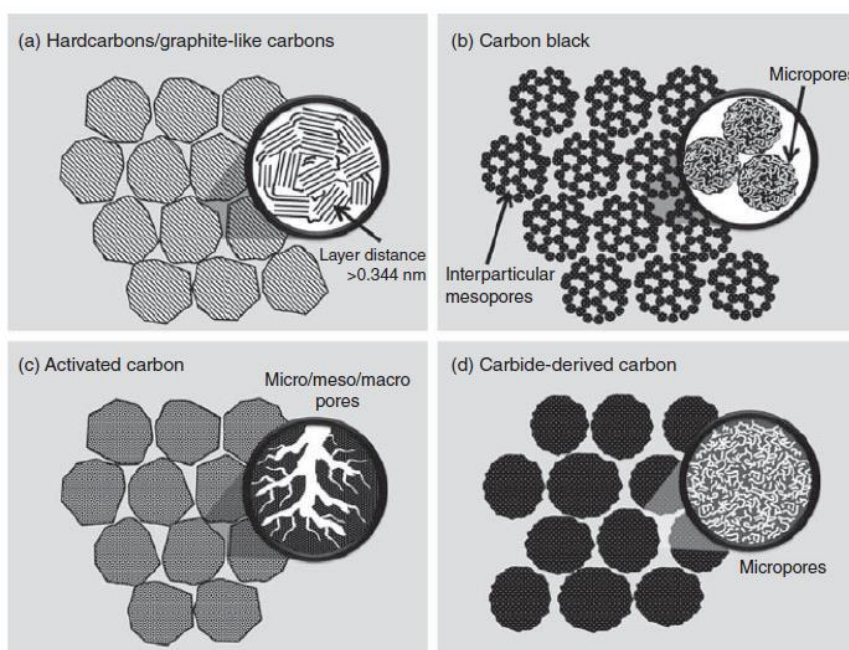


Figure 2.17 : Morphology comparison of carbon materials used for the preparation of the cathodes. [18]

Carbon-Sulfur Composite Cathodes

Carbon materials can be added directly to the cathode slurry or provided as a sulfur host material. For the composite preparation, it is necessary to use carbon materials able to accommodate enough Sulfur (Figure 2.18). In the literature, it is possible to find examples of synthesis processes in which: microporous ($d < 2\text{nm}$), ultra-microporous ($d < 0.7 \text{ nm}$), mesoporous ($2 < d < 50 \text{ nm}$) and macroporous carbons ($d > 50\text{nm}$), hierarchical carbons, hollow carbon spheres ($d \sim 200\text{nm}$ and a mesoporous shell $\sim 3\text{nm}$), carbon nanotubes and graphene thermally expanded ($d < 47.5 \text{ nm}$) are used. [33] [29]

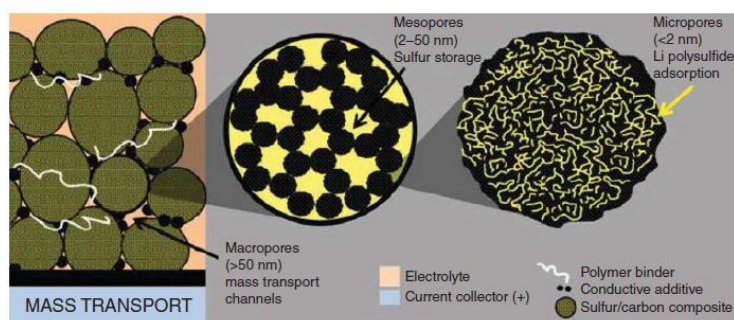


Figure 2.18: Comparison between three different types of porosity (macro, meso and micro) and their functions within the cathodes. [18]

Microporous carbons present high specific surface area (usually higher than $2000 \text{ m}^2\text{g}^{-1}$.) but also a relatively low pore volume fraction with values below $1 \text{ cm}^3\text{g}^{-1}$. These pore sizes severely limit the amount of Sulfur embedded in the composites ($\text{S} < 55\%$ by weight) and the possibility for the electrolyte to reach the cavities. Therefore, the rate capability cannot reach high values. The diameters of the pores, however, are close to the size of Sulfur and polysulphide molecules. This characteristic leads to the generation of high absorption forces between the polysulphide molecules and the micro-pore walls, with consequent polysulphides storage and shuttling phenomenon reduction. [34] [35]

In order to increase the amount of Sulfur contained in the carbon-based composites, it is necessary to enhance the pore size. Moving to a meso-type porosity (with pore volumes higher than $\gg 1 \text{ cm}^3\text{g}^{-1}$), it is possible to gain percentages of incorporated Sulfur up to $\sim 60\text{--}85\%$. Also, mass transport results significantly improved. By contrast, the retention of active materials is lower due to the smaller specific surface, as well as the potential adsorption for the physisorption of polysulfide molecules.

By further increasing the size of the pores (macroporosity), carbon particles result ineffective as regards LiPS retention, but they do not pose limitations on the transport and absorption of the electrolyte. Furthermore, if the electrolyte used is viscous, the cell can be very stable: the viscosity limits the mobility of the LiPS while the size of the pores allows the accessibility of the internal areas even during the precipitation of Li_2S .

Recent studies show that a combination of different pore sizes guarantees the best compromise to meet the requirements of dissolution/deposition cathode chemistry. The structure, with a multimodal pore size distribution (micro, meso and macro), is called hierarchical. Its presence in Li-S cathodes allows the combination of several attractive properties such as compensation of volume variation during electrochemical reactions, high Sulfur storage capacity, easy access for electrolyte, a high number of accessible redox sites and better LiPS retention.[29]

Other recent but promising solutions concern the introduction of hollow carbon spheres and graphene-like sulphur host.[3] [18]

In order to obtain carbon-sulfur composites, it is possible to proceed in several ways (Figure 2.19):

1. *Sulfur melting diffusion method* (in an inert atmosphere or under vacuum and with possible infiltrations of additional solution): The operation is carried out in the range temperature in which Sulfur viscosity reaches its lowest values (generally at $155 \text{ }^\circ\text{C}$). In the first phase, Sulfur and carbon materials are ground together to obtain a homogeneous mixture. Thermal treatment follows and, sometimes, even a post-treatment at a higher temperature ($300 \text{ }^\circ\text{C}$) in order to remove the non-adsorbed Sulfur by evaporation. This type of cathode preparation is a widely used method as it is a simple and inexpensive method.[29]

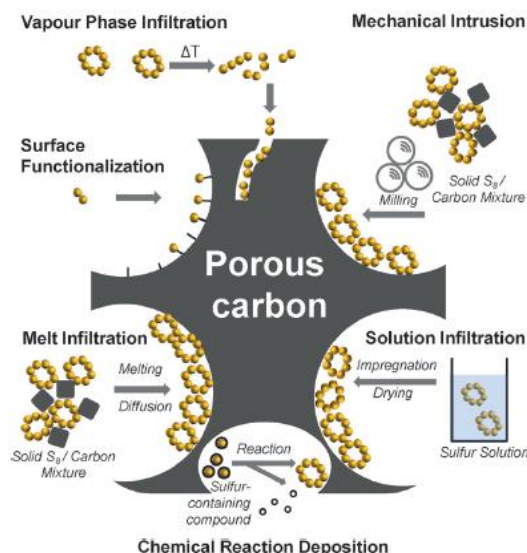


Figure 2.19: Different approach to obtain carbon-sulfur composites. [29]

2. *Sulfur vaporizing method:* different Sulfur allotropes can be obtained depending on the temperature used. At melting temperature (445 ° C) almost the Sulfur molecules are S_6 - S_8 rings while starting from 550 ° C, the smaller S_2 - S_4 allotropes prevail. Smaller molecules result very suitably for microporous infiltration; for this reason, the process is carried out at these temperatures.
3. *Solution infiltration:* This method involves the use of solvents able to make Sulfur soluble at room temperatures, such as carbon disulfide and some aromatic hydrocarbons (benzene or toluene). At the end of the infiltration process, the solvent must be removed (generally by evaporation).
4. *Mechanical intrusion:* Mechanical forces are used to get Sulfur into the carbon pores, or more often, to make it adhere to particles with large external surface areas. These forces can be produced by ball milling, pestling or agitation processes. Mechanical intrusion is economical, scalable and eco-friendly (no waste products) method; by contrast, the interactions that link Sulfur to carbon are weak.
5. *Chemical reaction deposition:* most of the sulfur-containing compounds show a better solubility compared with elemental Sulfur; for this reason, are usually preferred for process infiltration. PS solutions such as Na_2S_x (synthesized by the reaction of Na_2S and Sulfur) can be used to infiltrate carbon host. Subsequently, through a redox reaction, PS anions are oxidized to S_0 by oxidizing agents such as formic acid: as a result, Sulfur precipitates within the carbon material. Another way to induce sulfur precipitation can reduce pH by adding, for instance, sulfuric acid or hydrochloric acid. PS solutions have an exact stoichiometry which allows obtaining well-defined model cathodes.
6. *Sulfur surface functionalization:* A more recent approach requires to binding through covalent interaction Sulfur and conductive polymers (e.g. polyaniline PANI). This process can be done by combining polymer mixture and Sulfur molecules in the presence of inert atmosphere at 300 ° C.
By this way it is possible to obtain a very homogeneous distribution of Sulfur through the material and a reduction of the polysulphides shuttling phenomenon. [29]

2.4.3. Anode

Lithium

Lithium is the third element on the periodic table (and the first in the alkali metal group) with an atomic mass of 6.94 g / mol and a very low density (0.59 g cm⁻³). It was discovered in 1817 by the Swedish chemist Johan August Arfwedson inside the mineral petalite. Arfwedson, however, never managed to isolate pure metallic lithium. In 1821, the English chemist William Thomas Brande managed to achieve the goal through the electrolysis of lithium oxide. After him, in 1855, the German chemist Robert Wilhelm Eberhard Bunsen and the English chemist Augustus Matthiessen isolated lithium from lithium chloride by electrolysis. Their production method was later marketed on a large scale. [36]

Its lightness and the high reactivity make it an ideal candidate for battery technology designed for high gravimetric energy density. [37] Lithium has, in fact, an extremely high theoretical specific capacity of 3860 mAhg⁻¹ and the lowest electrochemical potential - 3.040 vs the standard hydrogen electrode. These properties make it the most polarizing element among all alkaline metals and a material able to store chemical energy in a very effective way. [38] [4]

Lithium exists in nature as two stable isotopes Li₆ (with an abundance of 7%) and Li₇ (with an abundance of 93%). Due to its significant reactivity with oxygen, it cannot be found as a pure metal but always in the form of various salts and minerals. [37]

Lithium Industrial Resources

Lithium is not a particularly rare metal as it is widely distributed globally. However, there are only a few sources (resources: a term that refers to the amount of the minerals located in well-defined deposits in terms of grade and quantity) that contain high concentrations of this mineral and that justify the extraction processes. Some studies show that 57% of the world's lithium resources are contained only in three locations: the Salar de Atacama, in Chile; Salar de Uyuni, Bolivia, and the Kings Mountain belt in the United States (Figure 2.20 a).

New sites, such as those in Ireland and Afghanistan, are still excluded from the market. However, they are being researched as potentially crucial shortly.

Making a correct estimation of the places and quantities of lithium present in the world is not a simple undertaking. Even in literature, the data that can be found are often conflicting or inaccurate.

Regardless of geographic location, there are two main types of resources in the world: minerals and mineral rich-brines [24]:

- *Lithium minerals*: can be classified into complex aluminium silicates, phosphates and micas but only a few lithium minerals such as spodumene, petalite and lepidolite are economically useful for the extraction of lithium. Typically, lithium is extracted from minerals such as lithium carbonate and, regardless of the considered mineral, the process initially follows the same sequence of operations. The first stage involves a crushing and grinding (comminution) process, to free the lithium minerals from the rock matrix. Given the abrasive and hard nature of aluminosilicates, this operation is very energy-intensive and represents up to 50% of the processing costs. A separation process (which can be carried out physically, electrically or magnetically) and a chemical processing follow. Finally, a separation step by flotation and/or by different density media is used in order to concentrate the lithium. The three largest lithium mines in the world are in Australia, Canada and Zimbabwe. Among these, that of Greenbushes pegmatite in south-west Australia is currently the biggest one. [39] [36]
- *Mineral-rich brines*: brines (a high concentration salt solution) are an essential source of lithium. There are different types of brine deposits, but the main one consists of interior saline

desert basins created by evaporation of the water previously contained. The most abundant sources of lithium-rich brine are found in South America, particularly in Argentina, Bolivia and Chile, collectively known as the lithium triangle as it contains 50% of the world's lithium reserves.[39] In all these countries, the sources are located at high altitudes, where the atmospheric pressure is low, and the ability of the water to evaporate is high. Some studies show that essential quantities of lithium are also found in geothermal waters (due to the higher leaching capacity of hot waters compared to cold ones) and in oil fields brines. [24] Currently, lithium is not yet extracted from these sources, but they could constitute a valid alternative for the future. Lithium, instead, is mostly extracted as lithium carbonate or lithium chloride from saline desert basins thanks solar evaporation. Evaporation helps to concentrate lithium in a gradually smaller brine volume. After reaching a sufficient concentration of the brine, lithium is extracted by chemical means, as lithium chloride or, more commonly, lithium carbonate, through precipitation, adsorption, and / or ion exchange. The whole process can take 18 to 24 months. [39] [36]

Nowadays, it is estimated that around 25% of the world's lithium resources are found in minerals, 59% in brines and the remainder in clays, geothermal waters and oil fields brines.

Initially, all lithium was extracted from hard rock mineral sources, but since the 80s, the discovery of mineral-rich brines such as those found in the Andes (Latin America), led to a change in trend, resulting in the closure of several lithium mines. However, there was never a definitive transition between these technologies as often the high lithium concentration in mineral sources can offset the high costs associated with the extraction processes.

For this reason, lithium present on the market today can be divided as follows (Figure 2.20 b):

- 50% from salt brines (dry saline lake beds)
- 40% deriving from the extraction of minerals from mines
- 10% from clay deposits and other sources [36]

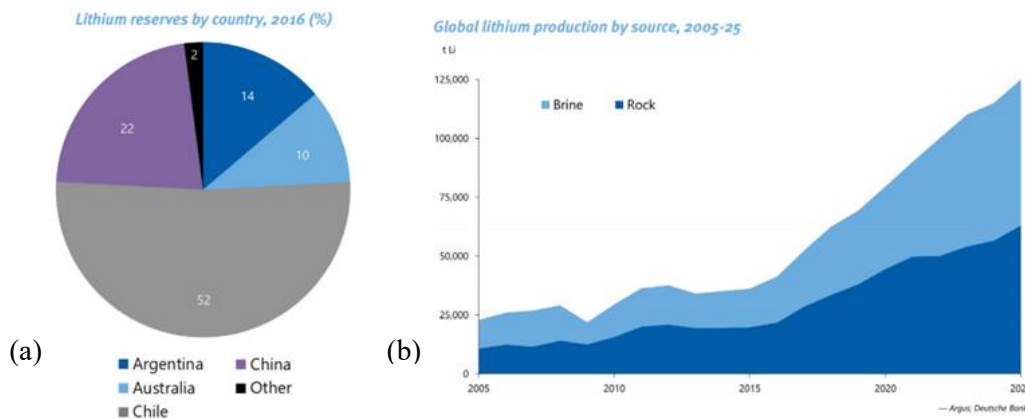


Figure 2.20 : (a)Lithium distribution by country in 2016 and, (b) by source. [39]

Even though China needs to import a massive quantity of lithium, economically, it dominates the manufacturing industry of lithium products thanks to its ability to sell low-cost products. On the other hand, even if the European Union is one of the biggest consumers of lithium in the world, it manages to produce only a negligible amount of metal (1-2%).[39] [36]

The substantial discrepancy between these two world powers worries researchers. According to some studies, thanks to the discovery of new deposits, and advancement of extraction technology and

recycling techniques, Europe will be able to meet its future demand. According to others, the lithium demand could exceed the extraction and production ability in the future not only at European level but worldwide.

Currently, lithium is not considered like a CRM (Critical Raw Material) as it is quite abundant on a global level and because on the market, there are other materials able to replace lithium in certain technologies (e.g. manganese and nickel in batteries). However, it is estimated that due to the uncertainties surrounding the supplying of this metal, lithium could become part of the CRM category shortly. [36]

Nowadays LIB (Lithium Ion Battery) production consumes the most significant percentage of lithium on the market (Figure 2.21 and 2.22), however not all LIBs require the same amount of lithium carbonate. This quantity depends on the applications and capacity required for the device. A smartphone battery, for example, needs about 3g of mineral, a PC battery a quantity varying between 10 and 30 g, a power tool battery of 40-60 g and a battery for electric vehicles of 8-100kg. [39] [36]

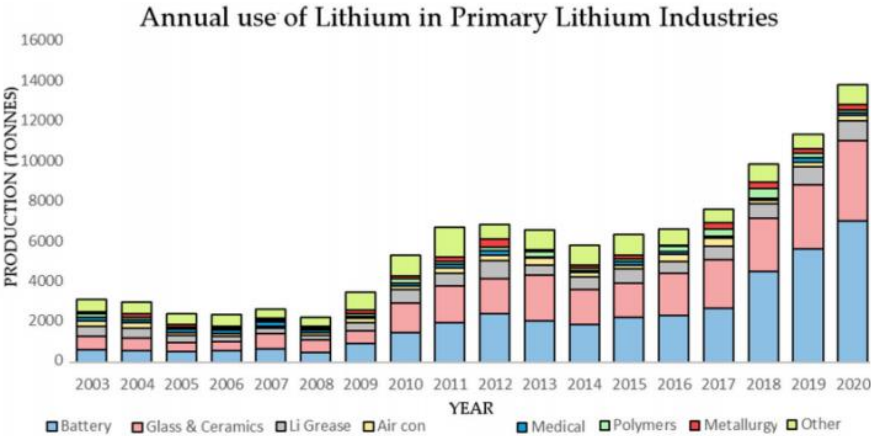


Figure 2.21: Diagram showing the annual consumption of Lithium and the industrial sector in which it is used [36]

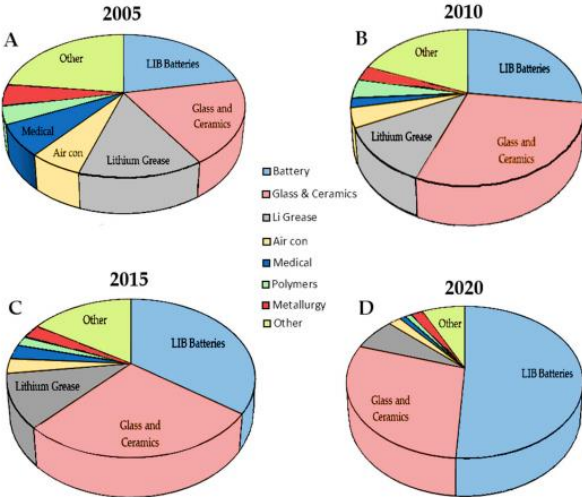


Figure 2.22: Several pie charts (one in each year considered) which shows how Lithium consumption varies in the various industrial sectors over time [36]

According to a recent study a 60 kWh LIB in each car (currently 1 billion) would consume 50% of the world's lithium reserves. This scenario does not take into account goods vehicles that usually require batteries at least ten times larger than a generic electric vehicle. [36]

SEI formation

As previously seen, the intrinsic lithium properties make it an extremely reactive material, with both positive and negative consequences on the performance of the cells.

On the one hand, this characteristic allows it to significantly contribute to the high voltage of the cells, making lithium an optimal electrode material. On the other hand, its uncontrollable reactivity leads it to react also with most of the elements which come into contact, giving rise to unwanted reactions. These side reactions are at the basis of an irreversible consumption of lithium and a consequent capacity fade, early degradation of the cell or both. [40]

One of the most famous side reactions inside the cell is that involves the solvent, present in the electrolyte, and lithium anode: during the reaction the solvent is consumed causing an increase in the electrolyte viscosity and changes in the kinetics system. However, this reaction produces also an unexpectedly positive effect: in the contact area between lithium and electrolyte, an interface known as SEI (Solid-Electrolyte Interface) is formed. This passivation layer can protect lithium from further unwanted reactions, reducing degradation phenomena and therefore improving the cyclical life of the cell. [17]

The growth of the SEI proceeds if the transfer of electrons (electron tunnelling) is allowed. This phenomenon generally occurs up to a thickness of a few tens of angstrom. The rate at which the SEI layer grows must guarantee the layer homogeneity and its ability to regenerate at each cycle. A too-fast growth rate proves to be ineffective in order to create a uniform layer as well as a too slow reaction rate, does not allow the layer to regenerate in time for the next cycle, leaving areas of the anode uncovered.

The resulting layer can ideally be split into two sub-layers: a porous outermost film (in contact with the electrolyte) and a film in close contact with the lithium anode, with a compact structure. The outermost layer porosity is linked to the reduction of the species in solution, which does not occur homogeneously over the entire surface. Due to the nature of the process, reactions occur more easily near defective areas such as surface holes where electrons can tunnel to the surface. If the surface has many defective zones, the formation of dendrites can be induced.[41] Moving towards the lithium anode lower oxidation states are found which make the SEI more compact. The morphological variation occurs gradually within the layer.

The SEI layer is also the region where the first electrochemical reactions occur, for this reason, the nature of the layer can heavily influence the reaction kinetics: a disordered structure, for example, can favour ionic conductivity. However, if the structure is too rough during the charging and discharging phases, irregular plating and depleting phenomena can occur. This phenomenon generates an increase in lithium ions and a new SEI formation, with consequent consumption of lithium and electrolyte and early cell degradation. Also, the thickness of the SEI may have an impact on the performance of the cell. An increase in thickness layer causes an increment in internal resistance and a slowdown in the kinetics of the electrochemical process. An ideal SEI should, therefore, allow lithium ions to pass but it should also be chemically stable, compact, uniform and have rigidity and elasticity such as to adapt to the volume changes that involve the material.[17] [29]

In order to obtain the best compromise between these properties, it is necessary to control the electrolyte and additives composition. In this scenario, lithium nitrate, an additive that is usually added to limit the shuttling effect, has also proven to be an excellent ally for the formation of a protective SEI layer. Furthermore, unlike most oxides, sulphides and halides, which undergo reduction by the lithium metal, the nitride anion shows unique stability due to its intrinsic properties and through passivation characteristics. By contrast, lithium nitrate is depleted during regular cell operation due to the constant repair of the SEI, in which it is involved. For this reason, its effectiveness is reduced with time.

Moreover, although it is the most followed approach nowadays, the addition of additives negatively affects the energy density of the cell, internal resistance and cyclic stability. For this reason, researchers are also looking for other solutions that do not provide their use. [29] [31]

In conclusion, SEI is a fundamental element for the correct functioning of the cell, as its presence allows to reduce excessive consumption of the solvent and the problems that this entails. At the same time, if not correctly designed, the SEI can negatively influence the performance of the cell. For this reason, many research works are focus on the attempt to develop new solvents and reactive additives capable of forming resistant SEI or even to develop artificial SEI. [17]

2.4.4. Electrolyte

The electrolyte is a fundamental component of batteries that performs much more than just transport of ions: solvent molecules play an active role in the lithium polysulfides (LiPS) solvation and the determination of their solubility. Furthermore, cathodic conversion reactions occur inside the electrolyte, which leads to the dissolution and precipitation of active species. This phenomenon explains why it is essential to have a high amount of electrolyte in order to have a high conversion efficiency. An increase in the electrolyte amount also has a positive effect on the viscosity, ionic mobility and cell life. However, an excessive increase in its quantity can adversely affect specific energy and energy density. A good compromise can be obtained for an amount of electrolyte equal to four ml per gram of Sulfur.[19] [40]

Liquid Electrolyte Solutions

Currently, liquid electrolytes (often with solvent mixtures) with dissolved lithium salts are widely applied as they present: a high ionic conductivity over the whole temperature range of operation, a relatively cheap and straightforward production method and an optimal wetting of the electrodes (necessary to give good contact between the battery components).

Liquid electrolytes of lithium-sulfur batteries are based on two main types of solvents:

- *organic carbonates*: such as ethylene carbonate (EC), propylene carbonate (PC), dimethyl carbonate (DMC), and diethyl carbonate (DEC);
- *ethers*: such as 1,3-dioxolane (DOL), 1,2-dimethoxyethane (DME), and tetra(ethylene glycol) dimethyl ether (TEGDME).

Often to meet several requirements that electrolytes must have and to increase cell performance, just one type of solvent is not enough. Moreover, given the significant instability of carbonate solvents and their tendency to react with reduced sulfur species, efforts are made to avoid this category of electrolytes in favour of ethereal ones. [19] [40]

Ester-based solvents (especially those with large donor number) are advantageous as they allow to achieve a high solvation capacity of long-chain polysulfides. Among these, the composition of the electrolyte solution most used by Li-S research groups is up to 1 M of either lithium triflate or lithium bis(trifluoromethanesulfonyl)imide (LiTFSI, $\text{Li}(\text{CF}_3\text{SO}_2)_2\text{N}$) in a 1: 1 mixture of TEGDME and DOL.

Although still widespread, liquid electrolytes suffer from too high a solubility for PS, with consequent loss of active material and generation of parasitic reactions with the anode, high flammability and high volatility. Due to the high solubility of PS in the liquid phase, the shuttle phenomenon is almost inevitable and the standard lithium-sulfur cell, which usually works with an electrolytic liquid, generally offers a high initial capacity, but discharge capacity and the efficiency generally low. It may also show short cycle times and safety problems. Various strategies have been developed over the years in order to reduce this phenomenon.[29]

In liquid electrolytes, there is also a further loss in the capacity due to the nature of the electrolyte and the phenomena that commonly involve liquid media, such as diffusion, migration, solubility and precipitation. [19]

Some researchers started then to investigate the possibility to use a solid-state electrolyte. This type of electrolyte generally has excellent properties in terms of stability at high temperature, mechanical strength, low flammability and safety (avoiding the problem of liquid leaks during operation). It can also protect the lithium metal anode and minimize dendrite formation. [29]

These reasons make solid-state electrolytes an exciting alternative for the future.[19]

Alternative Electrolyte

Alternative electrolytes include solid electrolytes and liquid electrolytes with very low polysulphide solubility. Both technologies force the active material into the solid-state, thereby changing the full conversion mechanism.[3]

- **Absorbed Liquid/Gelled Electrolyte:** Gel polymer electrolytes are generally made up of solid polymer matrices able to ensure specific mechanical stability and a liquid electrolyte responsible for the ions transport. This idea was born for lithium-ion batteries, where the presence of a polymeric medium capable of absorbing an organic electrolyte solution is more and more frequent. A widely used polymer in this field is poly (vinylidene difluoride) (PVDF) which can be transformed quite easily into thin and microporous membranes able to host liquid electrolyte. It has been shown that the presence of this polymer slows down the ionic conductivity, without changing the chemistry of the solution. Another polymer widely used for lithium-ion batteries is polyethylene oxide (PEO). During the last years, considerable attention has also been paid to the optimization of the polymeric composition in order to make it exert an active role on the migration of the polysulphides: PEG borate esters incorporated in mixtures of PEG-methacrylate copolymers is an example. Up to now the most surprising solution, however, have been reached with the addition of nanometric silica particles to a polymeric media in order to create a mesoporous structure able to block polysulphides and to facilitate Li-ions transport.
- **Solid Polymer Electrolytes:** In order to reduce the polysulphides solubility and mobility, many studies have been done on solid polymers electrolytes (with or without ceramic charges). Although the intrinsic flexibility of these materials and their low cost are exciting features, none of the solid polymer systems studied has been able to show performance comparable to liquid systems, even for temperatures above 60 ° C (typical minimum T for the conductivity of the solid polymer). The data obtained so far show that the conductivity at room temperature is inevitably very low with substantial repercussions on the electrochemical performance of the cell. Nevertheless, within this electrolytes category there are some promising examples, such as: (i) PEO/LiTFSI; (ii) poly(ethylene-methylene oxide) (PEMO) with LiTFSI; and (iii) a composite made by mixing fumed silica with PEGDME and LiTFSI.
- **Non-polymer Solid Electrolytes:** an alternative to organic-based solid electrolytes (polymeric electrolytes) can be found in inorganic systems composed by a ceramic matrix. Particularly interesting are the sulfur compounds which allow obtaining solid amorphous electrolytes with quite high conductivity for metal ions (Li). Currently, the inorganic systems based on $\text{Li}_2\text{S}-\text{P}_2\text{S}_5$ glasses seem to be very promising even if the best results obtained so far are similar to those of standard liquid electrolyte systems, with an excellent initial capacity (about 1000 mAhg^{-1}) that the can lasts for 100-200 cycles. [19][29]

2.5. Sulphur and reactions

The chemistry of Li-S batteries depends on the reversible conversion, due to redox reactions, between Sulfur and lithium sulfides (Figure 2.23).

Elemental Sulfur is commonly extracted from underground deposits through a method known as the Frasch process. Nowadays, however, the trend is to recover Sulfur as a by-product of oil and coal refinery, through a desulphurization process of crude oil. The sulfur recovery allows having this material available at low cost and on a large scale.

The octasulfur (cyclo- S_8), which crystallizes at 25°C as orthorhombic $\alpha\text{-}S_8$, is the most stable allotrope at room temperature as well as the allotrope used inside the cathode of Li-S batteries. This kind of Sulfur is made up of crownlike eight-membered rings since elemental Sulfur atoms show a strong tendency to form long homoatomic chains or homocyclic rings of various sizes with a phenomenon known as catenation. The catenation phenomenon occurs because Sulfur tends to form single bonds with itself (σ and π) rather than double bonds. As a result, Sulfur aggregates into extended structures and larger molecules. [3]

Orthorhombic α -sulfur has a density of 2.069 g cm^{-3} and close to room temperature is an excellent thermal and a good electrical insulator $5 \times 10^{-30}\text{ cm S}^{-1}$. In the low sulfur electrical conductivity lies one of the significant issues related to its use. [18] [42]

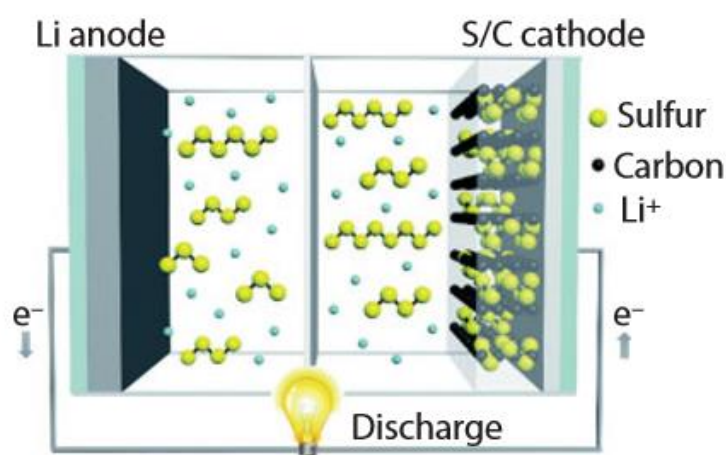


Figure 2.23: Schematic diagram of the operation of a Lithium-Sulfur cell and the reactions products. [15]

Since the Sulfur is in the loaded state, the cell operation begins with the discharge phase. [29] During this phase, reactions can be divided based on where they occur. For instance:

the anodic reaction (on the negative electrode) involves the oxidation of the lithium and can be expressed as (2.24):



while the cathodic reaction (at the positive electrode) involves the reduction of Sulfur according to the reaction (2.25):



For the overall cell reaction to be satisfied, on discharge, the lithium reaction must run to the left (electrochemical oxidation), with ions and electrons being formed from the lithium metal. In contrast, the C/S reaction must run to the right (electrochemical reduction), with electrons being consumed and ions being formed by the reaction of solid-phase Sulfur. Writing in this way the reactions it is easier to

understand how the electronic charge is generated inside the electrodes. Once the electrodes are connected, the charge will then flow in the form of current through the external circuit.

The overall discharge process can be expressed as (2.26) the lithium and Sulfur react to form lithium sulfide, Li_2S :



However, as previously mentioned, the Sulfur used in the cathode exists as octasulfur (S_8) rings; for this reason, the previous reaction must, therefore, be changed to (2.27): [22]



These electrochemical reactions allow regenerating the charge on the electrodes when an external current flow. If this did not happen, the voltage would drop rapidly to zero, and the cell could not continue its operation.

Although both reagents involved in the electrochemical reaction are present inside the cell, the reaction does not take place directly. The presence of the separator avoids the contact of lithium and Sulfur and makes the reaction mechanism more complex.

In order for the species to react with each other, they must enter the electrolyte in solution. [4] This process occurs through non-electrochemical reactions that consume / release electrons on the surfaces of the electrodes. As for the cathode, the reaction that allows solid Sulfur to enter in the solution is a dissolution reaction, while the anode is involved in a chemical precipitation reaction between lithium ions and Sulfur to form Li_2S : [18] [22]

- Sulfur dissolution: $S_{8(s)} \rightleftharpoons S_{8(a)}$
- Li_2S precipitation: $2Li^+ + S_2^- \rightleftharpoons Li_2S$

2.5.1. Polysulfides

As mentioned above, the electrochemical reactions are not the only ones that take place inside the cells. Other chemical interactions (such as disproportionation and chain growth reactions) complete the whole process making it very complicated and partly still unknown, despite the intense research carried out in recent years. [32] [31]

What makes particularly hard this study is the high number of factors that can contribute and influence the development of the reactions involved, such as the operating conditions, the electrolyte composition and its quantity, the structure of the cathode and the design of the cell. The pathways of the individual reactions and the discharge profile of the sulfur electrode can, therefore, show significant differences between the various systems examined.

The result of this complex set of reactions and interactions generates intermediate species formed by sulfur anions, known as polysulphides. Multiple polysulphide species appear and exist in equilibrium since the free energy of Gibbs formation (ΔG_f) of the polysulphide species formed by the Sulfur reduction in the presence of Li ions are very close. [31]

Polysulphides are commonly divided into two groups: "high order" species with chain lengths from four to eight atoms Li_2S_x ($6 < x \leq 8$), and "low order" species with chain lengths from one to two atoms Li_2S_x ($2 < x \leq 6$). The sulfur reduction is therefore defined by the gradual formation of four intermediate polysulphides, Li_2S_8 , Li_2S_6 , Li_2S_4 and Li_2S_2 and by the final reduction that Li_2S produces. [3]

The detailed reactions in the discharge process are listed (2.28 – 2.32): [15]





Once the battery is assembled and the electrodes connected to the external circuit, the cell is ready to start supplying energy.

The first redox reaction that takes place inside the cell involves the oxidation of the metallic lithium at the negative electrode with the consequent release of lithium ions and electrons. The former, migrate (due to a concentration gradient) from the anode to the cathode through the electrolyte. In the same moment, the electrons migrate to the cathode through the external circuit.

At the same time, the solid Sulfur which constitutes the cathode dissolves into the electrolyte as S_8 . The S_8 cycle is then reduced, and the ring-opened, determining the formation of high order lithium polysulfide. During cell discharge, lithium ions continue to reach the cathode promoting the further reduction of Sulfur. As the process advances, the polysulphide chains are reduced until the final product, lithium sulphide (Li_2S), is formed at the end of discharge. [16] [27]

At the end of the discharge process, S_8 is entirely reduced to S^{2-} (Li_2S), and the anode no longer contains Li metal.

Depending on the structure of the polysulphides and the length of their chains, the intermediate products can have different physical properties: the most important one lies in the different solubility within the electrolytes. Long-chain polysulphides are soluble in most commonly used organic solvents, while short-chain sulphides are insoluble: solubility increases with increasing chain. [4]

Referring to the following scheme (Figure 2.24) it is possible to see a high voltage plateau at ≈ 2.3 V that refers to the open ring reduction of the cyclic S_8 to S_8^{2-} , S_6^{2-} and S_4^{2-} . The following plateau, in the region of ≈ 2.1 V, is associated with the further reduction of these polysulfides to Li_2S_2 and Li_2S . [3] [16] [43]

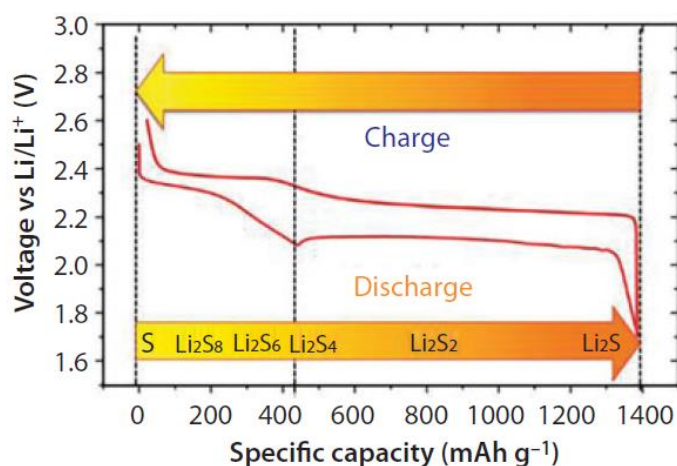


Figure 2.24: Typical voltage profile of a Li-S cell. [15]

As better illustrated later, the presence of polysulfides and their migration inside the cell (shuttling phenomenon) constitutes one of the significant drawbacks of lithium-sulfur batteries. If not adequately prevented, this phenomenon can lead to a substantial loss of capacity, low columbic efficiencies and high self-discharge speed. [32] [29]

Once the discharge phase is completed, the charging process takes over. Although these reactions are equally important and complex compared to the discharge reactions, much less attention has been paid to their development; even in the literature, it is not easy to find much about these.

The charge process takes place in the opposite direction respect the discharge one, with Li^+ ions depositing at the anode as Li metal and low-order polysulphides oxidizing form insoluble products up to soluble polysulfide species, which are further eventually oxidized to elemental sulfur S_8 (s).

Affirm that the charging process is the inverse process of the discharging one, even if correct, it turns out to be improper. Using different in situ characterization techniques is possible to observe a significant hysteresis between the charge and discharge pathways.

This hysteresis can be explained considering that the Li_2S oxidation, due to its insoluble and insulating nature, is a process that occurs with difficulty. On the contrary, the reduction of elemental Sulfur, although it turns out to be even more insulating, occurs very easily as it is capable of being solubilized in aprotic solvents. This reaction generates a characteristic overpotential at the beginning of the charging phase, known as activation kick. [44]

2.6. Challenges

Although Li-S batteries are believed to be one of the most promising technologies among new generation rechargeable batteries, there are still many challenges to be faced before they can be used on a large scale: cycle life and efficiency values, in particular, are not adequate yet to meet all market needs.[32]

Polysulfide shuttling phenomenon plays a predominant role in these characteristics. However, other numerous factors contribute to determining the performance of the entire battery. The main ones are listed below.

2.6.1. Critical aspect

Referring to the cathode side, the first thing that can be put in evidence is the insulating nature of Sulfur (which has resistance values of $\sim 10^{-30} \text{ S cm}^{-1}$) and lithium sulfide ($\sim 10^{-14} \text{ S cm}^{-1}$). A certain degree of electrical conductivity is necessary for lithium ions and electrons migration to occurs. When this does not correctly happen, the cathode is submitted to a significant polarization, and the active material shows low values of specific capacity and high charge and discharge current. A possible solution to mitigate this limitation involves the incorporation of conductive additives (e.g. carbon) into the electrodes or Sulfur scaling process into nanometer-sized particles. On the other hand, an excessive increase in carbon amount can reduce too much the volumetric energy density of the cells (if the carbon content reaches about 30% of the total weight of the cathode, the energy density of the cell can decrease by about 25 %).[3] [16]

Another problematic aspect concerns the high-volume variation (about 80%) that occurs during the electrochemical conversion of Sulfur into lithium sulfide. This phenomenon is related to the different density of the two materials (2.03 g cm^3 for S and 1.66 g cm^3 for polysulphide).[29] The change in volume can produce fragmentation of the active material and a contact loss with the collector. Therefore, a significant loss of capacity occurs. Some studies show that use a full lithium-sulfur cathode (Li_2S) allows eliminating the expansion and breakage of the active material thanks to the safest combinations of anodes without lithium-metal.[3] [16]

In addition to the structural and morphological variation of the cathode, repetitive dissolution and deposition of reactive species may occur during the conversion of Sulfur to lithium sulfide. The electrodes tend to passivate, leading to a significant increase in impedance. An example is given by Li_2S nucleation, which occurs in some areas due to the high discharge rate. [3][16]

All these issues result in low utilization of the active material, poor cycle life, and low system efficiency. [32]

Even when moving the anode part, is possible to find new problems related to the passivation of the electrode (in this case known as SEI layer) and problems related to changes in morphology (dendrites). Both these problems are related to high lithium reactivity, which leads it to react with a huge number of substances. These side reactions can be irreversible, consuming lithium and other components of the cell, leading to a loss of capacity with cycling, cell degradation or both.[29]

As previously mentioned, the reaction between lithium and the solvent, responsible for the formation of the SEI, has both positive aspects (protection of the anode, reduction of solvent consumption) and negative aspects (an increase of the viscosity of the electrolyte, decrease of the active species present in solution decrease in ionic/electronic transport and a slowdown in process kinetics, decrease in cell voltage). This phenomenon makes the SEI layer a critical element but at the same time, a fundamental component for the correct functioning of the cell. In this scenario, its optimization is a mandatory issue.

In addition to the SEI formation, on the anode surface, stripping and plating of the electrode take place (Figure 2.25). These phenomena occur as a result of microscopic variations in the surface structure of the electrode, which make some areas more subject to these phenomena. Near the nucleation points, porosity and the reactive anode surface, increase over time according to a 3D mossy growth. This new

electrochemically active surface induces continuous breakage and reformation of the SEI layer according to a non-linear and random dynamic process. During dissolution, large parts can become detached electrically, as well as lithium which remains attached to its original position on the substrate due to passivation.[29]

A final problem relating to the metal lithium anode concerns the formation of lithium dendrites. The term dendrite covers several structures, including needle-like, snowflake-like, treelike, bushlike, whisker-like, and mosslike. In most cases, however, mossy growth is the most frequent one within Li-S cells. Dendrites are associated with safety problems due to the potential internal short circuit caused by their contact with the cathode: also, for this reason, a separator has to be inserted between the two electrodes inside the Li-S batteries. In order to avoid the formation of dendrites and related safety problems, research has focused on preventing their growth through more excellent stability and uniformity of the SEI. This goal can be achieved with optimization of electrolytic additives. [40] [41]

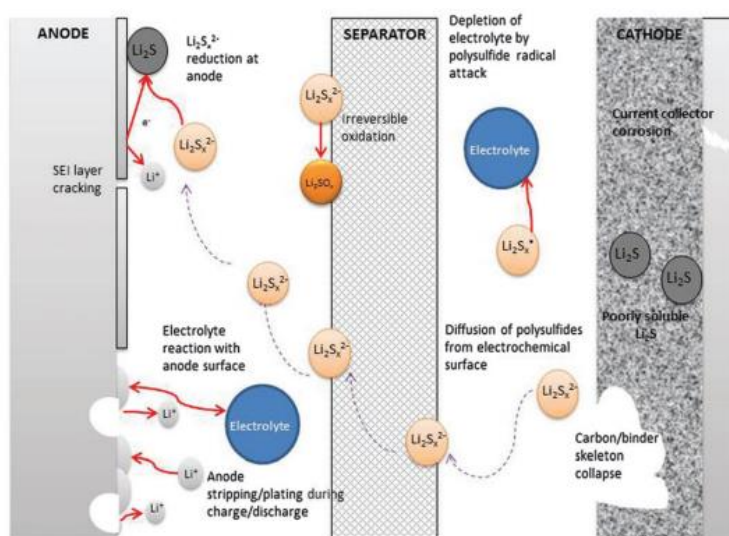


Figure 2.25: Degradation mechanism in Lithium-sulphur batteries [32]

2.6.2. Shuttle Mechanism

As mentioned above, the most feared and studied aspect within Li-S cells is that relating to the polysulphide shuttling phenomenon.

The main culprits of this process are the long-chain polysulphides Li_2S_x ($6 < x \leq 8$) produced during the charge reactions (Figure 2.26). Toward the end of the charge, the cell produces increasingly large quantities of high-order polysulfide species. [3]

Because these species have to accumulate in solution before the solid-phase Sulfur precipitates out again, they diffuse away from the cathode to the anode thanks to their solubility inside the organic solvents (glycol and dioxolane solvents) and the establishment of concentration gradients. Once they reach the anode, they are reduced with metallic lithium because of the small μe^- on the anode, and low order polysulphides are formed. In turn, low order sulphides migrate back towards the cathode, where through an oxidation reaction they are reconverted to the original polysulphides (Figure 2.27). [3]. When these two parasitic reactions occur cyclically, they give rise to the Shuttle effect.

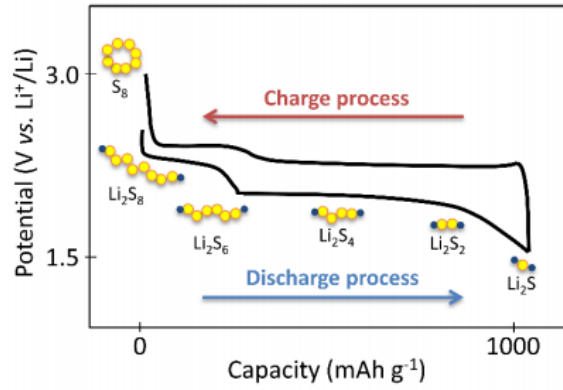


Figure 2.26: Voltage profile of a Li-S cell which also takes into account the transformations of the polysulphides. [4]

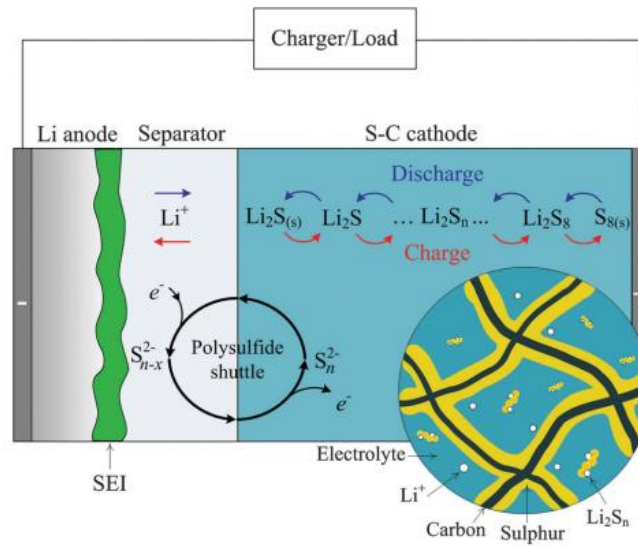


Figure 2.27: Effects of shuttle phenomenon [32]

The charge current and the diffusivity of the polysulphides are two parameters used by Mikhaylik and Akridge to evaluate the degree of shuttle phenomenon, through the definition of a charge shuttle factor (2.33):

$$f_c = \frac{k_s q_{pu} [S_{tot}]}{I_c} \quad (2.33)$$

where I_c , k_s , q_{pu} , S_{tot} and represent, respectively, the charge current, shuttle constant (can be obtained when small charge currents are applied by measuring the charge capacity output from the upper plateau. The lower is the shuttle constant, slighter are shuttle effect, specific capacity of Sulfur (fixed and equal to 419 mAh g^{-1} , about a quarter of the full theoretical capacity of Li-S batteries), and total Sulfur concentration.

Looking at the simulated charging profiles (Figure 2.28), it is possible to note that when f_c approaches zero the curve has a markedly vertical course which allows to reach very high voltages and does not suggest the presence of the shuttle effect. This profile may correspond to three different scenarios: a

system with a considerable current density, an infinitely small shuttle constant or a negligible Sulfur concentration. [3]

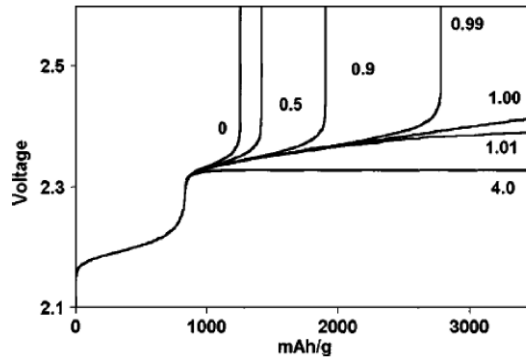


Figure 2.28: Influence of the charge shuttle factors f_c on the charge plateaus. [3]

When $f_c > 1$, the curves tend to flatten. This potential reduction allows protection against overcharge, but on the other hand, prolonged Shuttle reactions might cause corrosion phenomena of the Lithium anode and a reduction in the cycle life. Besides, the extension of the upper plateau is consumed in the polysulfides migration with repercussions on the charging efficiency.

In addition to the concentration of the active material present in the cathode, it is possible to express the concentration of high order polysulphide in the upper plateau as (2.34):

$$\frac{d[S_H]}{dt} = \frac{I_C}{q_{up}} - k_S[S_H] \quad (2.34)$$

where $[S_H]$ represents the concentration of high order polysulfides. From the concentration of higher-order polysulphide also depends on the upper plateau capacity and then the shuttle constant K_S . [3] [32]

The shuttle phenomenon opens the door to numerous problems. The main ones are listed below:[15] [29]

- The polysulphide species carrying the electrons from the anode to the cathode inside the cell, generate an internal parasitic current. The shuttle current counteracts the charging current at the top of the charge, and overcharging is prevented. Furthermore, if the Shuttle rate corresponds to the charging rate, the charging current is neutralized by avoiding the full charge of the cell (reduced charge efficiency or low Coulombic efficiency).
- The establishment of a parasitic current inside the cell also causes another undesirable effect: an excessive increase in temperature. If not controlled and monitored the temperature can cause severe problems to the functioning of the cell and a drastic drop in performance [45]
- A further effect related to the current Shuttle concerns the formation of a mixed potential at the anode responsible for a drop in cell voltage and the C-rates (up to 10 times) that Li-S can reach (compared to Li-ion: which can reach 20-50 Ah / cell)
- A phenomenon underlying the shuttle effect lies in the reaction between the polysulfides and the active materials present in the electrodes. The same could be said for their dissolution within the electrolyte. These reactions reduce the active material useful for the electrochemical reactions and generate a loss of capacity, low coulombic efficiencies and reduce the life of the cells. [46]
- The shuttle phenomenon can also contribute to the self-discharge of the cells when they are left to rest in a charged state. Also, in this condition, the active material continues to dissolve

gradually and migrate towards the anode where it reacts with the metallic lithium, with consequent reduction of the open-circuit voltage OCV and discharge capacity. Another observable phenomenon by the discharge pathways is the disappearance, after the dissolution of Sulfur in the electrolyte, of the upper discharge plateau for longer rest times (more than a week). The self-discharge rate is 10-15 times faster (Figure 2.29) than lithium-ion batteries (8-15% self-discharge per month), and some studies show that this value increases further with increasing SOC (state of charge). [3] [45]

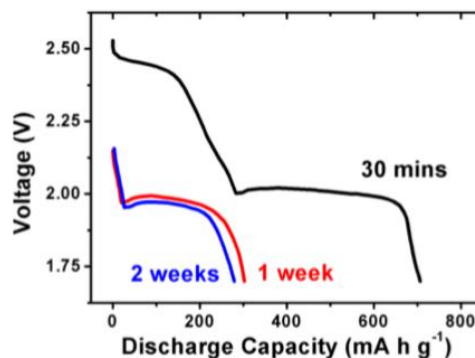


Figure 2.29: Self-discharge phenomenon of pristine sulfur cathodes at different resting times. [3]

It is therefore evident that limiting the polysulphide shuttle phenomenon is a mandatory issue in order to increase the performance of these batteries and their access to the market.

2.6.3. Possible strategies

Numerous approaches have been studied in the last few decades to try to limit the polysulphide shuttle phenomenon. [47] The most significant examples are reported:

1) Preventing PS shuttling by using alternative electrolytes.

Although there are precautions to limit the Shuttle phenomenon, this seems to be inevitable when liquid electrolytes are used.

An alternative to liquid electrolytes is provided by IL ionic liquids (relatively hydrophobic and electrochemically stable salts of TFSI anion). Ionic liquids (IL) are salts that can be liquid below 100 °C or even at room temperature (molten organic salts), widely used in electrochemical energy storage applications.

Their use has been studied because inside Li-S batteries they can reduce polysulphides shuttle phenomenon thanks to their high viscosity (Figure 2.30). Furthermore, the solubility of the PS strongly depends on the anionic structure of the IL: it is, therefore, possible to improve battery performance by choosing ionic liquids with an appropriate donor number (stronger donor ability leads to the higher solubility of PS). Other IL exciting properties are strong electrochemical, thermal and chemical stability, low volatility and flammability, good eco-compatibility and rather high ionic conductivity. Despite these positive aspects, ILs have not reached a significant diffusion within Li-S batteries, probably due to their high cost, low wetting power towards the electrode, high hygroscopicity, and high viscosity. However, it is undeniable that ILs can play an essential role in Li-S batteries if adequately mixed with organic solvents to counter the polysulphide phenomenon.[31]

In this scenario, attractive candidates are also solid electrolytes able to retain Ps at the cathode, preventing their migration to the anode and gel polymer electrolytes that aim in the same direction.

Various gel polymer electrolytes as well as other solids, such as $\text{Li}_2\text{S-P}_2\text{S}_5$ powders, and thio-LISCONs (lithium super-ionic conductors), have been investigated during the years.

On the other hand, neither gel polymeric electrolytes nor other solid electrolytes can guarantee sufficient ionic conductivity at room temperature, and the high resistance between the electrodes and the electrolyte remains a severe problem.[29]

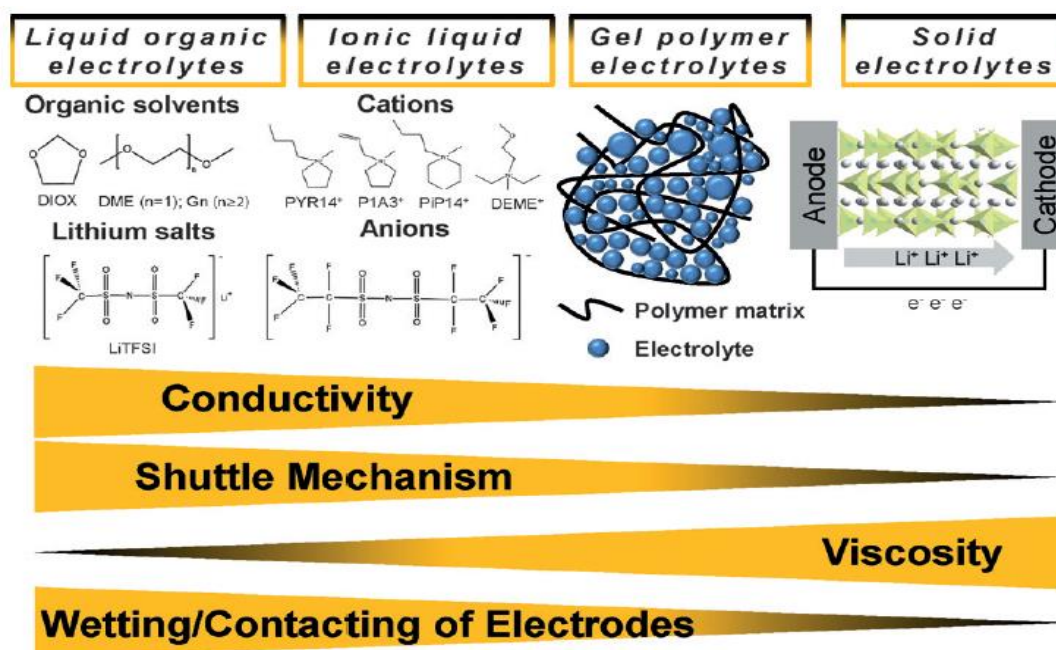


Figure 2.30: Comparison in terms of conductivity, ability to act positively on the shuttle effect, viscosity and wettability of the electrode, between different electrolyte systems used in Li-S batteries. [29]

2) Trapping PSs with porous additives.

Under certain conditions, such as when a liquid electrolyte is used, it is impossible to avoid the complete formation of polysulphides inside the cell. In this case, the most followed approach, to limit the shuttle phenomenon consists in the removal of polysulphides from the electrolyte through surface adsorption processes. [15]

This strategy is made possible by the anionic polar nature of most polysulphides which allows it to show a high affinity towards polar adsorbents having positive surface charges. Oxide additives, such as $\text{Mg}_{0.6}\text{Ni}_{0.4}\text{O}$ of nanometric size, are considered excellent candidates as they can promote the catalytic activity of Sulfur redox reactions and absorb PS species. The polysulfides are thus confined within the cathode with improvements in terms of capacity and rate capability.

Another widely used class of materials is that of high surface oxides such as mesoporous silicas which, thanks to their well-defined nanometric pores, can capture polysulphides effectively.

For this strategy to be efficient in pursuing the goal, some possible drawbacks must be considered. First, the constant absorption of the polysulphides could cause a progressive depletion of the active mass. For this reason, it is necessary to guarantee certain reversibility in the adsorption process. Furthermore, most of the absorbent additives are insulating from an electrical point of view and electrochemically inactive; therefore, an excessive increase in their content can have severe repercussions on the energy density of the device. [29]

3) Trapping PSs due to surface functionalization and polymer coatings.

Another approach to remove the polysulphides from the electrolyte, and to limit their migration inside the cell, consists in increasing the active sites for PS absorption on the carbon cathodes through suitable

surface modifications. Usually, these modifications are linked to functionalization processes which involve the introduction of heteroatoms or polymeric coatings.

- Heteroatoms: can modify the conductivity of the materials by changing the electronic properties of carbon materials. They also help to regulate its binding properties: functionalization can improve the absorption of Sulfur and PS inside the carbon host with a consequent reduction in irreversible losses of active material. For example, N-doped CNTs are widely used since pyridine nitrogen, and the graphene structures surrounding quaternary N are excellent sites for the adsorption and deposition of polar PS and Li_2S . Also, boron, by introducing a positive polarization on the carbon surface, can favour the chemisorption of PS (anionic) and Sulfur. Other studies instead suggest a functionalization linked to the introduction of Sulfur and phosphorus as adsorbent agents.
- Polymer coatings: (e.g. PEDOT: PSS, PPy, PANI) can improve the cycle stability and the kinetics of the lithium / delitiation process and therefore, the performance of the Li-S battery. This improvement is made possible by the polymers elastic nature, which allows suppressing mechanical stress that occurs during the process and to compensate for changes in volume following the reactions. The use of conductive polymers (electrically and ionically) also allows increasing the electrical conductivity of the entire system thanks to the establishment of an additional three-dimensional conductive network. However, what makes these materials truly attractive is their ability to adsorb polysulphides and reduce the depletion of active material acting as a physical barrier. Finally, they can be processed in thin nanometric sheets. Too high thicknesses could act negatively on the cell's performance.[29]

4) Using ion-selective membranes and separators.

Selective separators can hinder the migration of some specific species, such as polysulfide ions directed towards the anode. These separators manage to perform their function through careful design of porosity and composition.

Typical choices involve polyolefins (polypropylene) and glass fibre-based materials. Nafion (a cation-selective material), lithiated Nafion ionomer and Nafion-coated polypropylene also showed improved cycle performance due to a reduction in the crossing of anionic polysulphides. Nonetheless, the role of the separator is often overlooked.[29] [3]

5) Trapping PSs within the pore structure of the carbon.

The use of carbon materials, as mentioned above, can be a viable way to avoid the formation of long-chain polysulphides. The pores retain Sulfur through absorption processes (avoiding excessive release inside the electrolyte) and ensure its complete electrical contact. Furthermore, based on the size of the pores, carbon limits the size of the sulfur species growing during the charge. An ultramicropore ($d_p < 0.7$ nm), for example, does not allow access to the large S_8 species, allowing small non-cyclic allotropes of S_2^{-4} instead to enter. This kind of pore avoids the non-flavoured transition from S_8 to S_4^2 and the consequent formation of high order PS.

However, the volume of microporous materials is somewhat limited and does not allow high sulfur load. In order to increase the amount of active material inside the cathode, carbon materials with hierarchical porosity or hollow spheres (single shell or multi-shell) with appropriate hole dimensions and shell thickness can be used. Careful control of the characteristics of the hollow spheres can be pursued through various templating methods.

Finally, another approach may concern the introduction of permeable porous carbon papers between the cathode and the separator. These are layered structures made with various types of carbon materials (graphene, CNT, activated carbon, carbon derived from biomass or carbon black).[29]

6) Anode protection

Anode protection has proven to be an effective solution for reducing the shuttle phenomenon. Using a solid electrolyte, the electrolyte itself can protect the electrode surface. However, it is not always

convenient to work with such electrolyte due to the internal resistance that it induces and its limited ionic conductivity. When it is necessary to adopt a liquid electrolyte, various approaches can be used to reduce the shuttle problem, such as surface coating (fluorinated polymers and organosulfur compounds) or passivating additives within the electrolyte.[15]

As regards the passivation of the anode, various reactive chemicals have been proposed, such as SO_2 , SO_2Cl_2 , H_3PO_3 , or H_3PO_4 . All these substances have proven effective in improving cycle stability; however, the most used additive is LiNO_3 . Its oxidative effect allows the anode to form a very favourable surface layer made up of Li_xNO_y and Li_xSO_y . The composition of the passivating layer manages to effectively prevent the reduction of PS on the anode surface with excellent consequences on coulombic efficiency

However, while the presence of nitrates is beneficial for the extended cycle of the lithium anode, some studies show that adverse effects on the cathode may occur. First, the contribution to the oxidation of Sulfur to oxy-sulfur species that are deposited in the cathode constitutes lost active materials. Secondly, LiNO_3 is irreversibly reduced to the cathode below 1.6 V, and also makes the final discharge product (Li_2S) even more difficult to recharge, with a negative impact on the capacity and reversibility of the battery. This adverse effect can be avoided by not discharging the cell above 1.6 V. Although many research teams are using LiNO_3 additives (or co-salts) in the electrolyte, its problems of continuous consumption and safety due to its strongly oxidative character problems remain. [31]

Even the same PS have been used as additives able to reduce PS dissolution by the cathode. When high-order PSs, such as Li_2S_9 , are used as electrodes, it is called a catholyte. In this case, the cathode is made up of a porous carbon laid on the collector. These cells are generally better in terms of specific capacity and capacity conservation. [29]

7) Use other anode materials

Finally, one of the most promising strategies is to replace the metal lithium anodes with non-lithium lithium materials, such as silicon, tin and graphite. Among these, silicon and tin have high electric capacities, air stability and more excellent safety. [3] Silicon is a very attractive cathode material thanks to its high theoretical specific capacity of 3579 mAh g^{-1} . On the other hand, during operation of the battery, silicon undergoes enormous volume changes ($> 300\%$) with consequent breakage of the electrode and detachment from the collector. Graphite also has promising properties (it is widely used in lithium-ion batteries); however, it undergoes delamination in contact with most of the ether-based electrolytes, and this limits its practical applications. When no lithium anodes are inserted into the battery, a cathode material consisting of Li_2S can be used. The insertion of Li_2S inside the batteries makes the process safer (it is as if the battery was assembled in the discharged state) and guarantees high theoretical capacities. [48] [29][31]

Recent studies show that the best approach to increase the performance of Li-S cells is to combine different strategies able to avoid the polysulphide phenomenon. [47]

2.7. PANI

2.7.1. Conductive polymers

Conductive polymers (CP) acquired, since their discovery, growing interest. What makes them attractive is the fact that to the standard characteristics of the polymer materials (high flexibility and lightness, low cost, ease of production and processing), are added those related to semiconductor materials, as they can conduct. [49]

Conductive polymer materials can be divided into two sub-groups:

- *Extrinsically conductive polymers (ECP)*: are obtained adding conductive fillers (carbon black, carbon nanotubes, metal powders, etc.) inside an insulating polymer matrix. Compared to the starting material, these polymers show good electrical (10^{-5} and 10^3 Scm^{-1}) and thermal conductivity, good mechanical properties and corrosion resistance. However, the electrical conductivity values are still insufficient for many applications.
- *Intrinsically conductive polymers (ICP)*: also known as conjugated polymers, under certain conditions can show exceptional electrical (10^{-10} to 10^5 Scm^{-1}) and optical properties, compared with other polymers or extrinsic polymers. They also have excellent environmental stability and an easy synthesis process. On the other hand, they do not show good mechanical properties. Polyaniline (PANI) belong to this second category.

These organic materials, which are generally made up of C, H and simple heteroatoms N and S, owe their intrinsic conductivity to the π conjugation, originated by the overlap of π -electrons. Conjugation presents itself as an alternation of single and double bonds. Double bonds, or conjugated, consist of a localised "sigma" bond which forms strong chemical bonds and a weaker and less strongly localised "pi" bond (Figure 2.31). [49] [50]

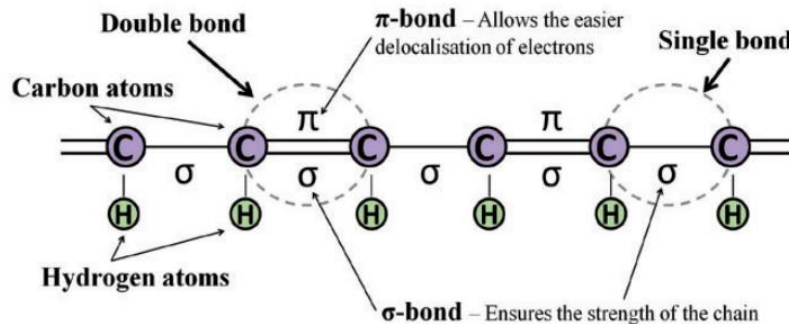


Figure 2.31 : Representation of single and double bonds that make up the backbone of extrinsic conductive polymers [50]

The bond conjugation, although it is a fundamental prerequisite, is not enough to make the polymer material conductive. For this to happen the polymer structure must be disturbed (Figure 2.32): among several ways to introduce charge carriers or to dope the conjugated polymers the most widely used are electrochemical and chemical oxidation (p-doping), reduction (n-doping).

The charges, possibly distributed in a highly delocalised way, are responsible for achieving an energetically favourable conformation while the orbital system allows charge carriers to move along the polymer backbones. [50]

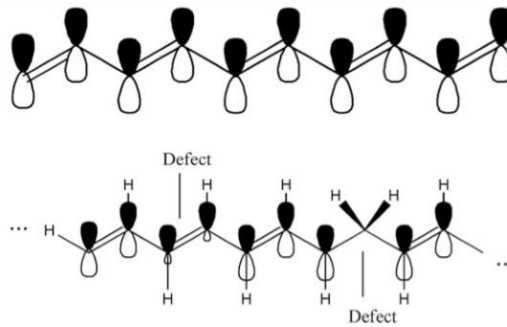


Figure 2.32: In the top: representation of the π -conjugation typical of conducting polymers. In the bottom: the same structure in the presence of defects. [49]

This kind of reactions is performed by several pure species: oxidants or reductants, called dopants (Figure 2.33). They can be small anions or cations (ClO_4^- or Na^+), but also large polymeric species such as poly (polyelectrolytes) poly (styrene sulfonic acid) and poly (vinyl sulfonic acid) are used.

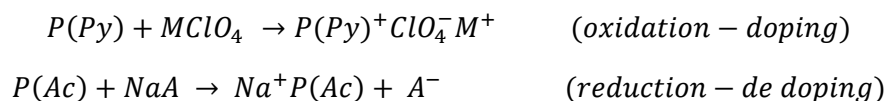
Usually, dopants are incorporated into the material at the time of synthesis; however, it is possible to incorporate them later by chemical (by exposure the material to a solution of vapour of the dopant), electrochemical (by applied a specific potential) or a host of other means. Other oxidation centres (e.g., $\text{C}=\text{O}$ bonds) can be generated due to the interaction of the CPs with the environment, air and humidity making the charge centres distribution of the of not very homogeneous inside the chains.

The number of doping elements incorporated per monomer units gives an idea of the extent of oxidation/reduction through what is called the doping level (the ratio of counterion and monomers in the polymer). Increasing the doping level means increasing the number of charges on the polymer chain and their mobility and therefore increasing the conductivity. [49] However, the doping level can also modify the surface and the structural properties (colour, porosity and volume) and cause relaxation of the polymer geometry. [51] [52]

Dopant	Structure/formula
<i>Anionic</i>	
Chloride	Cl^-
Perchlorate	ClO_4^-
Tetrafluoroborate	BF_4^-
Tos, <i>p</i> -toluene sulfonate	$\text{CH}_3\text{-C}_6\text{H}_5\text{-SO}_3^-$
Trifl, trifluoromethane sulfonate	CF_3SO_3^-
Hexafluorophosphate	PF_6^-
PSS, polystyrene sulfonate	$[\text{-CH}_2\text{CH}(\text{C}_6\text{H}_4\text{SO}_3^-)]_n^{n-}$
<i>Cationic</i>	
Proton	H_3^+O
Sodium	Na^+
Potassium	K^+

Figure 2.33 : Typical dopant elements used for CPs.

In any case, if the formation of charges occurs through an oxidation reaction, some electrons are removed from the valence band generating a positively charged polymer and an associated anion. If instead the charges are created through a reduction reaction, a charge is given to the CP structure generating a negatively charged polymer and an associated cation.



Where M and A are any cation and anion.[49]

In "doped" CPs the overlap π bands become the valence band while the π^* bands become the conduction band generating a bandgap generally greater than 1 eV, like in the most semiconductor materials. If the gap is further reduced, leading to an overlap of the valence and conduction bands, with the latter now partially filled, metallic conduction occurs. Conjugation originated by the overlap of π -electrons, therefore allows them to progressively leave the typical behaviour of semiconductor materials and acquire tunable electronic, magnetic and optical properties similar to those of metallic materials.[51]

Since the discovery of the first conductive polymer, polyacetylene (PAC), many others have been developed and produced (Figure 2.34). Among these: polyaniline (PANI), polypyrrole (PPy), poly (3,4-ethylene dioxythiophene) (PEDOT), poliparaphenylene (PPP) and others. [49] [50]

Recently, nanostructured conductive polymeric materials have also attracted significant attention, as they can guarantee properties that are not obtainable with bulk conductive polymers. Future challenges include controlling electrical conductivity extended to conductive polymers of various sizes and morphologies and developing new synthesis methods capable of producing CP nanomaterials in large quantities. [51][52]

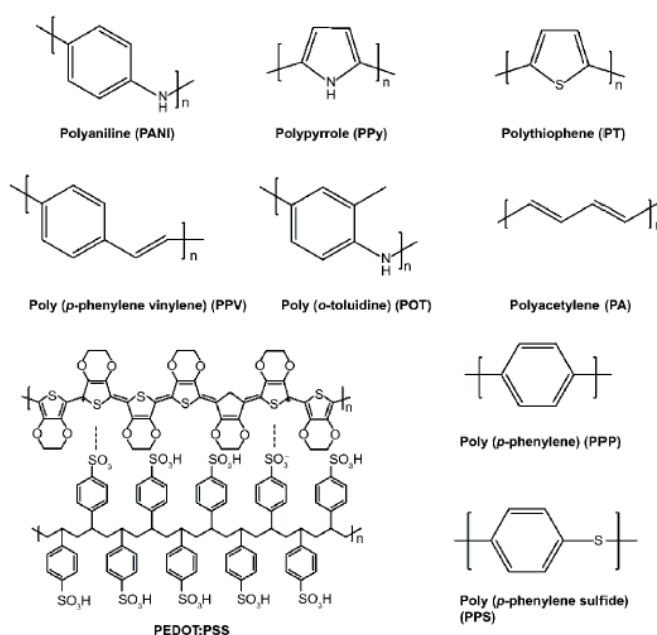


Figure 2.34 : Some examples of conductive polymers and their respective properties (conductivity and type of doping).

2.7.2. Polyaniline

Among the conductive polymers listed above, PANI is acquiring great interest thanks to its exceptional electronic properties (high conductivity, reversible convertibility between redox states), high chemical and environmental stability, economical and straightforward synthesis process. Recent applications see PANI in Li-ion batteries (LIB), Li-S batteries (LSB) and supercapacitors (SCP) both as an electroactive component in the electrode materials or as a coating in LSB due to its strong physical affinity and

chemistry for S and polysulphides. [52] Besides, the flexibility and easy workability typical of polymers make it applicable also inside sensors and actuators. [51]

PANI is a homopolymer, which can contain benzenoid and quinonoid rings. The deprotonated (undoped) form of PANI (Figure 2.35) consists of reduced base units (R: which contain the first type structure), and oxidised base units (O: made up of the other structure class). [53] [52]

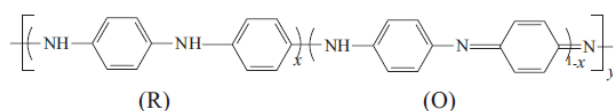


Figure 2.35 : Deprotonated form of PANI with reduced and oxidized units [52]

where $x: 0 \leq x \leq 1$. [54]

Based on the ratio of the two types of structures (benzenoid: quinonoid, i.e., m:n) that appear within the polymer chain, PANI can be classified in different oxidation states (Figure 2.36).

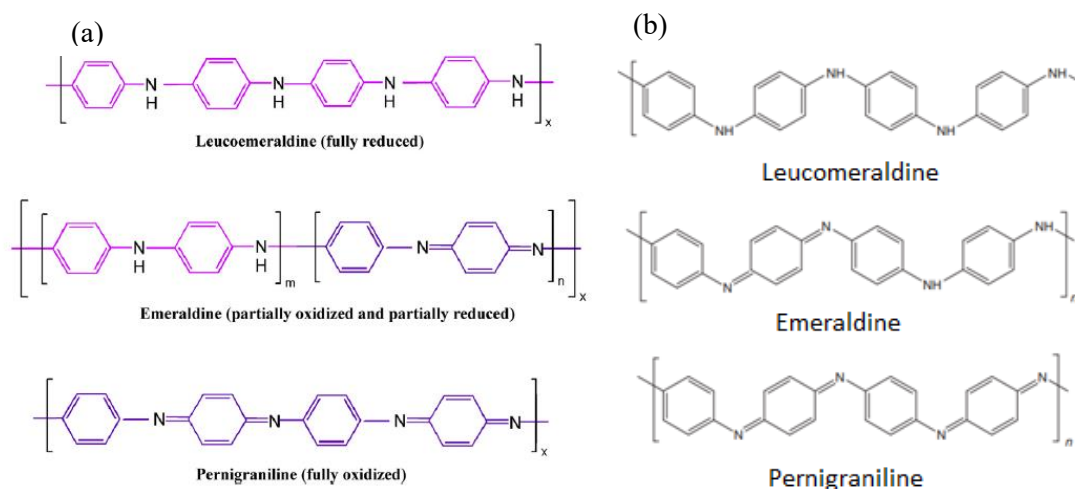


Figure 2.36 : (a), (b): Representation of the three typical PANI oxidation states. [53] [55]

There are mainly three typical PANI oxidation states, including fully reduced leucoemeraldine base (LEB), semi-oxidised emeraldine base (EB) and fully oxidised pernigraniline base (PE) that can be interconverted by oxidation or reduction:

1. *Completely reduced leucoemeraldine state*: consists of benzenoid state in which the hydrogen atoms are attached to the nitrogen atoms. For the wholly reduced leucoemeraldine the proportion between benzenoid and quinonoid, m: n, is ideally 1: 0.
2. *Partially oxidised emeraldine state*: with a ratio of 1: 1, can be adjusted by varying the synthesis procedure and the doping amount.

3. *Completely oxidised pernigraniline state*: quinonoid state in which no hydrogen atom is attached to the nitrogen atoms. For the wholly oxidised form, the ratio is 0: 1.[51] [53]

2.7.3. Synthesis

Polyaniline exists mainly as an emeraldine green salt (hydrogen sulfate) obtained from the oxidative polymerisation of aniline in the presence of dopants (Figure 2.37). This synthesis process is by far the most accessible and most explored approach to directly prepare emerald salt as well as most conductive polymers. Polyaniline is obtained starting from an aqueous solution with a sufficiently high acidity $1 < \text{pH} \leq 3$ in which aniline is added drop by drop. Another approach is to solubilise aniline in toluene followed by addition of acid and oxidant. The oxidant can be iron (III), cerium (IV), silver (I) or dichromate.

In most cases, however, it is preferred to use ammonium peroxydisulfate because of the faster and simpler solubility capable of guaranteeing higher yields (90%) and conductivity ($\sim 1.2 \text{ S / cm}$) than the final conducting salt. The oxidation started under alkaline conditions; on the other hand, mainly leads to the obtainment of aniline oligomers. The aniline oxidation process takes place with the release of two hydrogen atoms in the form of protons when an aniline molecule is added to the growing polymer chain. This reaction is exothermic, and in fact, one can witness an increase in temperature during the reaction; for oxidation that starts at acid pH and leads to polyaniline, an initial or intermediate induction period is typical, in which the temperature variations are low. PH, on the other hand, decreases due to the release of sulfuric acid as a by-product of the reaction. The changes in pH can be used to monitor the progress of the reaction. [53] [49]

In the emeraldine, salt half of the nitrogen atoms in the polymer chain are present as secondary amines, the other as protonated imines. [56]

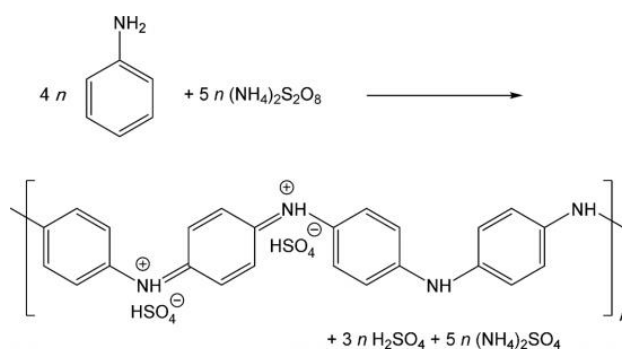


Figure 2.37 : Oxidation process of aniline under acidic conditions. [56]

Another way in which emeraldine salt can be obtained is the electrochemical process. The electrochemical synthesis of polyaniline involves oxidation of aniline on a conducting electrode (made of inert material) thanks to the application of electric potential and not by oxidant agent. Electrochemical methods include potentiostatic, galvanostatic oxidations with constant potential or current, or potentiodynamic cyclic voltammetry polymerisation using a two or three-electrode system. The reaction takes place inside an electrolytic medium composed of an aqueous solution to which background electrolytes and acid are added.[56] The most commonly used acids are those of an inorganic nature such as sulfuric, phosphoric, perchloric, nitric acid or in solutions of organic acids or polymeric acids.

The physical properties of polyaniline salts, including conductivity, density and hydrophilicity, depend both on the backbone of polyaniline and on the acid that constitutes a salt with polyaniline. Based on the concentration of aniline, the density of current applied, the properties of the solvent used, polyaniline can be synthesised with different properties and morphologies. From this type of synthesis, it is possible to obtain a purer product (free of additives, unreacted monomer and initiator) with a well-defined polymer structure or morphology. However, it is limited by the fact of having to use conductive surfaces; it is therefore used only for specific applications.[49] [53][56]

Focusing on two different synthesis methods (chemical process and electrochemical process) the first step involves the formation of a radical cation. What distinguishes the two polymerisation mechanisms lies in the following steps, in fact:

- In the **chemical case**: a great abundance of monomeric molecules is present in the starting solution. The radical cation can, therefore, quickly attack one of these molecules generating a weaker radical cation. The new cation, in turn, can attack another monomeric molecule allowing the chain to grow until the end of the process.
- In the **electrochemical case**: the concentrations of the radical cations is much higher than that of the neutral monomers. For this reason, near the electrode, where the reactions take place, radical-radical coupling reactions occur more quickly. The quick nature of the reaction leads to the formation of a radical dication capable of generating a neutral dimer following the loss of two protons. The dimer is then oxidised to the radical cation so that the propagation reaction can proceed to the termination. In this second case, it may be necessary to wait for a certain period of "gestation", necessary to ensure that enough radicals accumulates. After this has occurred, the polymerisation proceeds rapidly. [49]

Regardless of the synthesis process, emeraldine salts can be converted to the corresponding bases (Figure 2.38).

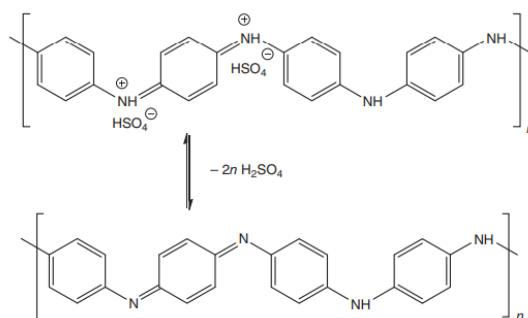


Figure 2.38: Conversion reaction from emeraldine salt to emeraldine base. [56]

It is possible to pass from the salt structure of polyaniline to the base structure, treating the salt with alkaline solutions such as ammonium hydroxide 0.1–1 M (dedoping process). The transition from one form to another causes significant changes in the electrical and optical properties: while emeraldine salt (green colour) is conductive, the base (blue colour) is not able to conduct. The different characteristics presented by the two materials mean that the applications in which they are used may not be the same.[56]

This salt-base transition is reversible. The polyaniline can be re-protonated in the salt form when immersed in an aqueous solution with a sufficiently high acidity $\text{pH} < 3$ (Figure 2.39). [56]

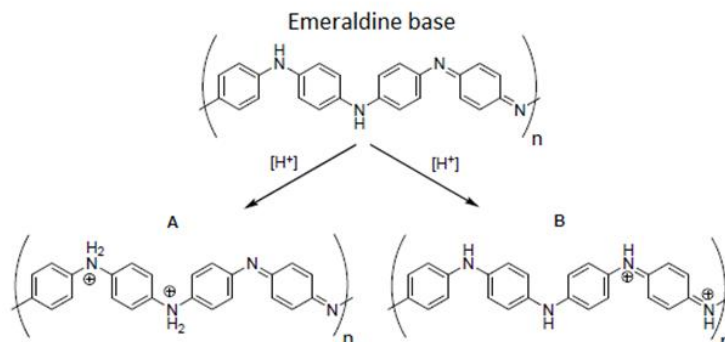


Figure 2.39 : Different structures of protonated Emeraldine. [57]

2.7.4. Other structures

As mentioned above, in addition to the emerald form, PANI can present itself with two other structures: leucoemeraldine and pernigraniline (Figure 2.40). The transition from one state to another causes variations in colours, stabilities and properties, in particular in electrical conductivity: leucoemeraldine (colourless) and pernigraniline (blue) are not conductive materials, while emeraldine (in the doped state, emeraldine salt) is conductive. [56]

- *Pernigraniline*: is composed of aminobenzene fragments alternating with quinonediimine. Since the latter group is not very stable in the presence of nucleophiles, pernigraniline and its salts tend to decompose in the air, compromising the stability of the whole compound. The completely oxidised form (pernigraniline salt) is generated during the oxidation process, due to an excess of oxidant. Furthermore, even for pernigraniline, it is possible to pass to its basic form through a dedoping process. In this case, the material takes on a blue-purple colour.
- *Leucoemeraldine*: is a colourless substance composed of benzene and amino groups. As pernigraniline, it cannot conduct electrically, also following the oxidation phenomena that involve its groups when left in air contact. Leucoemeraldine is obtained mainly in the basic form, although some studies show that it can also exist in salt forms. To obtain this structure, however, it is necessary to work in highly acidic conditions.[51] [53]

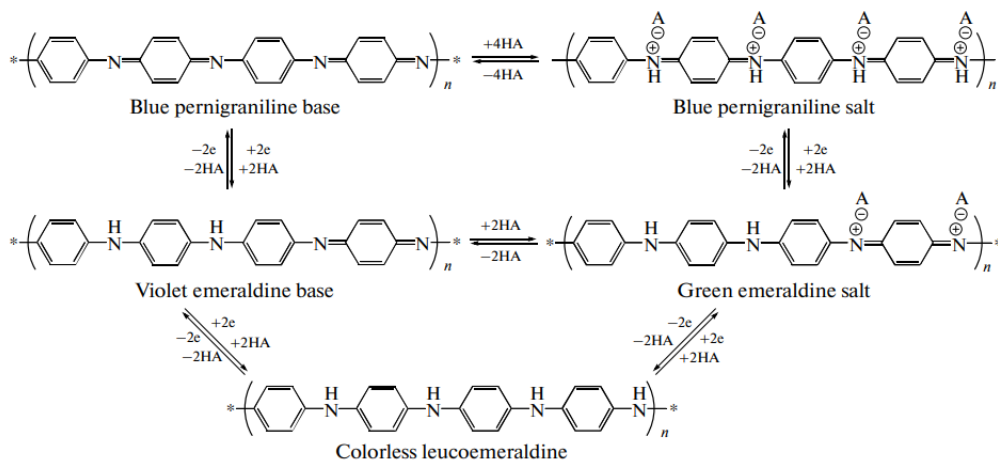


Figure 2.40: Different structures and reaction that could involve PANI.

2.7.5. Conductivity

As mentioned above, the electronic structure of pristine conjugated polymers (such as the emeraldine base or the pernigraniline or leucoemeraldine forms) does not allow current conduction. The situation is different when sufficient charge carriers are made available along the conjugated molecular chain of polyaniline: that is when the conversion into emeraldine salt occurs.

In order to make this transition happen, it is possible to adopt different approaches such as a reduction phase from pernigraniline, an oxidation step from leucoemeraldine or a doping process starting from the emeraldine base. Unlike the first two conversion mechanisms, the doping process does not take place through a change in the number of electrons but a non-redox process involving proton acids. This process is called "protonation" and involves organic and inorganic acids.

During the doping process, the proton acid interacts mainly with the nitrogen atoms of the imine group of the quinone ring, which are part of the PANI chain. The proton then binds to the N of the quinone ring by reducing it to a benzene ring (Figure 2.41).[53] [49]

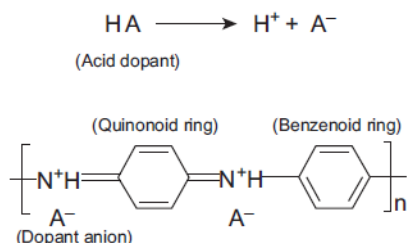


Figure 2.41: Schematic representation of the doping process by a proton acid. [53]

As a result, bipolarons (positive paired charge) are generated in the chain. The polymeric chain is therefore positively charged, and an anion then approaches the polymer chain to maintain charge neutrality. Bipolarons increase the total energy of the system, originating an electronic redistribution.

The electronic charge, in turn, causes, without variations in the number of electrons contained in the system, the formation of isolated cationic radicals (polarons). The polarons formation is not found instead in the PE and LEB chains, although doped, as their chains have a lower regularity. The polarons are delocalised (by an intramolecular mechanism) beyond a certain conjugation length and are responsible for the electron conductivity of the polymer (Figure 2.42). Another way in which the delocalisation of cation radicals can take place is through the intermolecular mechanism: in this case, the polymer chains must be oriented in a particular direction in order to guarantee the transfer of electrons π from one chain to another. This process is made possible by the Van der Waals interactions that develop between the benzene and quinoid rings of the PANI. Electronic conductivity, in this case, can reach higher values. [56]

In the half-oxidised EB with alternating quinoid and benzenoid rings experiences 50% doping the entire quinoid ring, which is ideal for the formation of polarons is protonated. For this reason, the highest conductivity is achieved compared to doping levels below or above 50 %. [51]

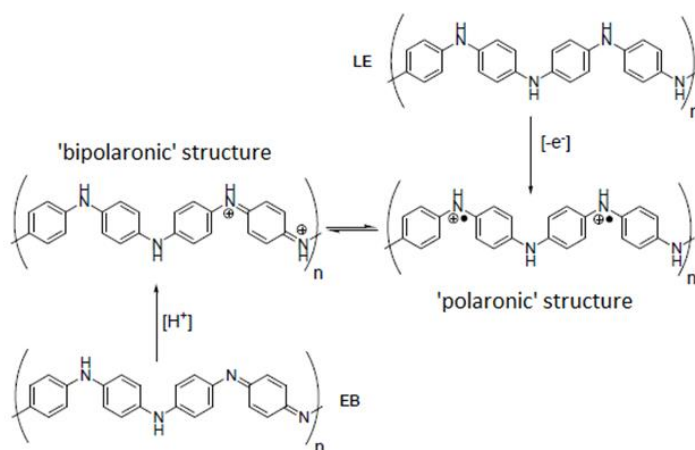


Figure 2.42 : Schematic diagram of doping process for PANI. [57]

Polaron and bipolarons are in thermodynamic equilibrium (Figure 2.43).

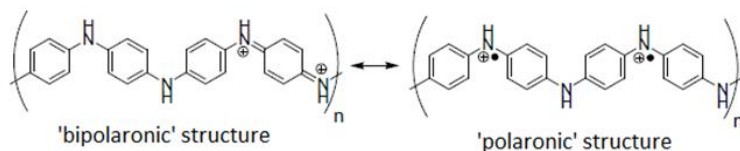


Figure 2.43 : Bipolaronic and polaronic structures. [57]

As stated above, the electronic structure of non-doped conjugated polymers (such as the polyaniline base) does not allow active charge transport and the behaviour of the material is comparable to that of insulating materials. Things change when sufficient charge carriers are present on the chain (emeraldine

salt): in this case, the conductivity shows a semiconductor but, in some cases, also metallic behaviour. The transition from semiconductor to metal can be induced by an external magnetic field or pressure following a doping process. [49]

The electrical conductivity of the polyaniline salt varies from 10^{-10} to 10^2 Scm^{-1} depending on its degree of oxidation or protonation, morphology (orientation of the chains and crystallinity) and method of synthesis (acids, oxidising agents and synthesis conditions).[53] [56]

Polyaniline conductivity in the emeraldine form increases by ten orders of magnitude when the degree of protonation is increased from 0 to 20%. Based on the degree of protonation, the conductivity extends from 10^{-10} Scm^{-1} for the emeraldine base up to units of Scm^{-1} for the fully protonated emeraldine salt. Another particularly important factor is the acidity level reach during the synthesis and the type of counterions. [52] As can be seen from the figure below (Figure 2.44), conductivity (as well as density and hydrophilicity) of polyaniline prepared in the solutions of various acids differs substantially.[49][56] The use of different acids, instead, does not change the kinetics and performances of the process. [57]

Acid	Conductivity, S cm^{-1}	Density, g cm^{-3}
Hydrochloric	11.9	1.386
Sulfuric	10.1	1.397
Methanesulfonic	9.7	1.385
Phosphoric	4.8	1.466
Hydrobromic	4.7	1.526
Camphorsulfonic	3.1	1.345
Picric	2.3	1.461
Citric	1.0	1.375
Succinic	0.28	1.348
Formic	0.21	1.344
Acetic	4.2×10^{-2}	1.375
No acid ^a	4.4	1.333

Figure 2.44: Comparison of the properties (conductivity and density) obtainable, according to the type of acid used during the synthesis process. [56]

However, the highest conductivity was obtained in the form of thin films cast from solution and protonated with camphor sulfonic acid (400 Scm^{-1}) or by stretching the protonated films with 2-acrylamide-2-methyl-1-propansulfonic acid (670 Scm^{-1}).

Finally, when samples with a specific conductivity are required, it is possible to proceed in two different ways:

- the copolymerisation of aniline with p-phenylenediamine ($10^{-10} \text{ Scm}^{-1}$)
- partial reprotonation: synthesis of the polyaniline base and subsequent immersion of the base in solutions with different level of acidity (and therefore pH). [56]

2.7.6. Ionic conductivity

The ionic conductivity is linked to the presence of acids in the protonated form of the emeraldine structure in which: for each acid molecule, there are two constitutional units of aniline. It is, therefore, possible to affirm that polyaniline in the protonated emeraldine state is a mixed conductor of both electrons and protons.

In the emeraldine salt, while the acid anion interacts with a polaron guaranteeing the stabilisation of the positive charge, the proton acid (which has become relatively free) allows the proton conductivity of the material through a hopping mechanism. This mechanism that guarantees the movement of the proton from one polaron to the other offers better mobility and therefore higher proton conductivity than the classic diffusion ion conduction mechanisms.

As for electrical conductivity, it is possible to improve the conductivity values with increasing acid saturation and the degree of wettability of the polymer. Another factor that raises these values is the environmental humidity or the presence of aqueous solutions: in aqueous media, it is possible to register greater proton mobility. [56]

2.8. MoS₂

MoS₂ belongs to the class of Transition Metal Dichalcogenides (TMD), known for their classic structure MX₂ in which M represents a transition metal from group 4 to 6 and X a chalcogen (typically S, Se and Te). Currently, more than 40 types of layered structure TMD have been explored. Among these, MoS₂ remains the most studied thanks to its attractive properties, such as: [58] [59] [60]

- Sizable bandgap and layer-dependent electronic properties
- Considerable interlayer distance (0.615 nm) [61]
- High lithium storage theoretical capacity of 670 mAh g⁻¹ [61]
- Outstanding optoelectronic performance
- Good chemical adsorption and catalytic performance
- Abundant adsorption and catalytic sites
- Excellent current on/off ratio of 10⁵ -10⁷
- High carrier mobility up to 200-700 cm² (Vs)⁻¹ at room temperature
- Ambient stability
- Natural availability

These characteristics make it competitive in many sectors like energy storage, electronics to photovoltaic systems (solar cells), photonic to the piezoelectric device, sensor. [60] [62]

In determining its peculiar properties, the structure plays a predominant role (Figure 2.45).

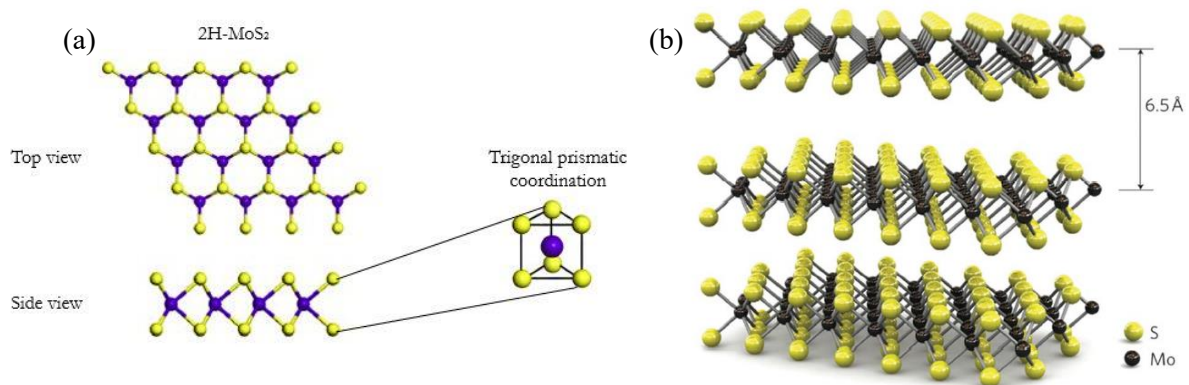


Figure 2.45 : (a) 2H-MoS₂ structure with trigonal prismatic coordination both from top view and side view [63].
(b) 3D representation of 2H-MoS₂ structure. [60]

In a single layer of the MoS₂ film, the constituent atoms are part of a sandwich structure in which: two layers of S atoms are held together with a hexagonal layer of Mo atoms through covalent bonds (S-Mo-S unit). [58]

Crystalline MoS₂ mainly exists in its polymorphic 2H form. This structure is made up of vertically stacked layers (each 6.5 Å thick) that interact with each other through Van der Waals forces. The weak nature of the bonds generated by Van der Waals forces makes these materials easily exfoliate in few layers or even in a single layer such as graphene and other 2D materials.[4] [60]

Many properties depend on the number of layers and therefore, on the exfoliation process. The bandgap and other photoluminescence-photophysical properties tend to increase as the number of layers joined

decreases. Single nanosheets, however, present also other improved properties, such as excellent in-plane stiffness ($180 \pm 60 \text{ Nm}^{-1}$), extremely high Young's modulus ($270 \pm 100 \text{ GPa}$ up to 0.3 TPa) and high elasticity. [58]

It can be said that, for this type of material, moving from the bulk form to single or a few nanolayers structure is often advantageous since, in addition to the properties of the bulk material, the improved characteristics of the exfoliated phase are added. [59]

2.8.1. Other crystallographic structure of MoS₂

The 2H (hexagonal) structure, also known as the trigonal prismatic phase, due to its structural symmetry, is found in nature as a molybdenite mineral and represents the more thermodynamically stable structure of MoS₂. [61]

However, bulk MoS₂ can exist in other two crystal phases, namely 1T, and 3R, where the letters imply the crystal system (T-trigonal, and R-rhombohedral) and the digit represents the numbers of monolayers in the unit cell. Such as in 2H structure, in the 3R phase, the coordination Mo-S is trigonal prismatic, while in the 1T phase, the coordination is octahedral (Figure 2.46). [64] However, both phases are metastable: in fact, they are not found in naturally occurring minerals, but only in the synthetic MoS₂. [58] [60]

Another way to obtain the 1T polymorph is to carry out an exfoliation process starting from 2H-MoS₂. [60] In fact, during the exfoliation step, part of the bulk MoS₂ undergoes a structural transformation from the 2H-MoS₂ type to the 1T-MoS₂ type (monolayer). As better explained later, 2H-MoS₂ is an intrinsic semiconductor, while the 1T-MoS₂ type is metallic. [59]

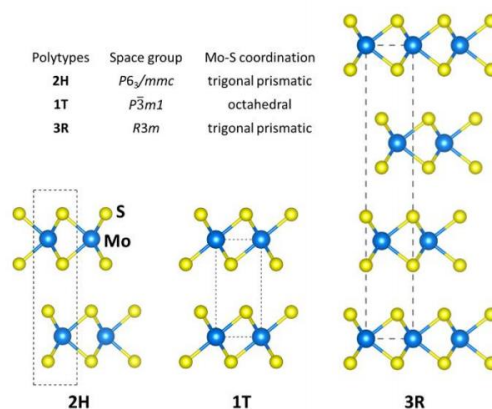


Figure 2.46 : Structure comparison between the main three different MoS₂ polymorphs. [59]

Overall, five polymorphs have been proposed for the atomic structure of a monolayer, including 1H, 1T, 1T', 1T'' and 1T''' (Figure 2.47). Among these, the 1H monolayer has trigonal prismatic coordination, like the bulk form, while the 1T monolayer adopts octahedral coordination (as mentioned above). The 1T phase can generate in turn other metastable polymorphs superstructures (1T'', 1T''' and 1T''') which differ from each other for the unit cells. These metastable polymorphs often coexist within a monolayer. [59]

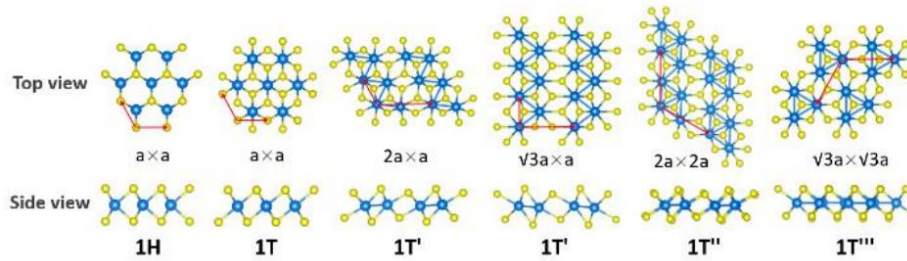


Figure 2.47 : Structure comparison between the different MoS_2 polymorphs that have been proposed for a monolayer. [59]

2.8.2. Electronic bandstructure

The electronic band structures of different MoS_2 phases are strongly related to the crystalline structures of the materials. For all TMD, the main contribution to the regulation of the electronic properties of the phases is the filling of the "d" orbitals, which are non-bonding from groups 4-10.

According to the crystal field theory, when the orbitals are filled, they display semiconducting properties. This occurs for 2H- MoS_2 where the trigonal prismatic coordination of the material leads to the filled d_{z^2} and empty d_{xy} and $d_{x^2-y^2}$ orbitals. Such an electronic configuration of $\text{Mo}^{4+} 4d^2$ (d_{z^2} , $d_{x^2-y^2}$) makes 2H MoS_2 a semiconductor.

On the contrary, when the orbitals are partially filled, the materials exhibit metallic properties: this is the case of phase 1T / T' in which $\text{Mo}^{4+} 4d^2$ orbitals in an octahedral crystal field are split into the configuration of e.g. orbitals ($d_{x^2-y^2}$, d_{z^2}) over t_{2g} orbitals (d_{xy} , d_{xz} , d_{yz}), whose two electrons are filled in t_{2g} states and may become itinerant electrons to induce metallic conductivity (Figure 2.48). [63] [59]

The band structures of bulk MoS_2 in 1T and 2H phase can be described by Density Functional Theory (DFT) calculations based on the known crystal structures while for metastable phases of MoS_2 monolayer, the only theoretical calculation is conducted. From the DFT calculations is possible to say that:

- Bulk 2H MoS_2 , whose Conduction Band (CB) and Valance Band (VB) mainly consist of Mo 3d orbital, and S 2p orbital presents a semiconductor behaviour with an indirect bandgap of 1.29 eV [59] [60]
- Bulk 1T MoS_2 , whose density of states consist of Mo 3d orbital and S 2p orbital distribute at the Fermi level, shows a metallic behaviour. 1T- MoS_2 is approximately 10^7 times more conductive than semiconducting 2H phase resulting in higher electrical conductivity and better electrochemical performances. [61] [64]

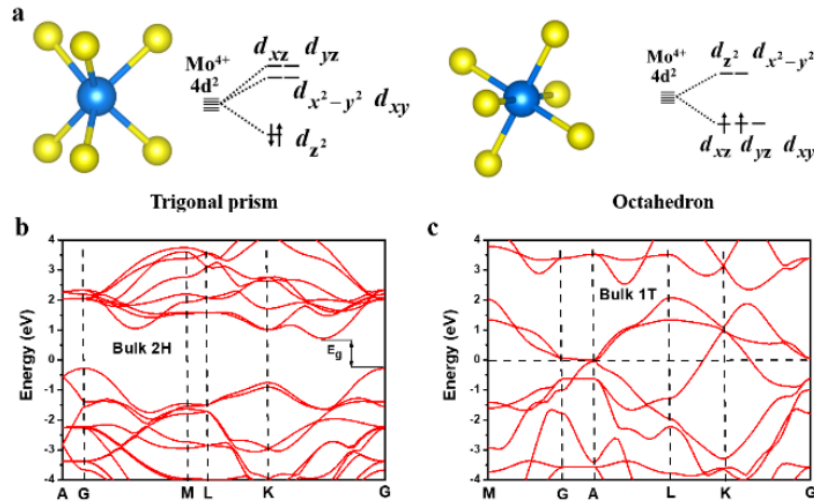


Figure 2.48: Electronic structure of 2H and 1T bulk MoS₂. [59]

In a confined system, even the size of a solid and its thickness, have a significant impact on energy levels especially in those solids (such as TDM) that can be easily exfoliated due to the weak Van der Waals forces that characterize their bulk structure. In these materials, the number of layers of which a specific phase is composed can seriously affect the electrical conduction.

The 2H MoS₂ in the bulk form, for example, shows an indirect bandgap of 1.2 eV (typical of indirect semiconductors). However, by decreasing the number of the layers (with an exfoliation process), the bandgap tends to increase from 1.2 to 1.7 eV. [61] [64] It is also possible to observe a transition from the indirect to the direct band. When the material shows the indirect bandgap, the Valence Band Maximum (VBM) is at Γ point of Brillouin zone and Conduction Band Minimum (CBM) at the middle between Γ and K points of Brillouin zone. With the change into direct bandgap, VBM and CBM coincide both at K point of Brillouin zone. [63] [60] [63]

The transition that is complemented by strong photoluminescence reflects the interlayer interaction, quantum confinement, surface effects and long-range Coulomb effects of 2D TMDs.

The correlation between the layers number and the band structure is not entirely known for the 1T phase and its polymorphisms. [59]

2.8.3. Exfoliation process

MoS₂ in the form of nanosheets allows to add properties not otherwise achievable to the properties of the bulk material. For this reason, over the years, numerous synthetic strategies have been proposed to obtain the material in this form. Currently, most synthetic methods can be divided into two macro-categories:

- 1) *Top-down methods*: that provide the exfoliation of 3D bulk materials (raw materials) in 2D scaled-down products, through the application of external stress or chemical intercalation.
- 2) *Bottom-up methods*: that provide the formation of MoS₂ nanosheets through the assembly of single atoms into target nanomaterials or through intermediate products at high temperatures, during chemical reactions. [61]

According to the different used synthetic methods, different MoS₂ structures can be obtained and therefore, it is legitimate to foresee different properties and applications.

2.8.4. Top-down approach

Physical exfoliation

Physical exfoliation strategies exploit the weak nature of the van der Waals bonds that regulate the vertical stacking of MoS₂ individual layers. The following belong to this category:

- *Micromechanical exfoliation*: inspired by the typical "Scotch tape method" (Figure 2.49) initially used for graphene and subsequently introduced in 2005 as a new method to produce MoS₂ nanosheets. The process involves the use of adhesive tape, able to extract single atomic planes from the MoS₂ bulk crystal and of a substrate on which the nanosheets of the material will then be transferred. This method allows to obtain single crystals of considerable size, high purity and with excellent stability under ambient conditions. However, it is a method that requires a great deal of time and has a low yield in terms of the amount of material obtained; for this reason, it is not used on an industrial scale. Moreover, with this exfoliation process, it appears difficult to control the thickness, size and shape of the final product.[61]

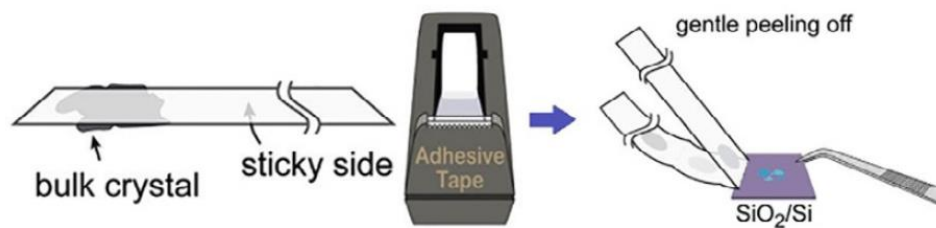


Figure 2.49: Schematic representation of the "Scotch tape method". [61]

- *Plasma assisted exfoliation*: allows to obtain nanosheets down to monolayer with the help of an Ar⁺ plasma. This process is very reliable, easily scaled up, and lead to improving the yield of the MoS₂ monolayer.
- *Shear exfoliation and liquid- phase exfoliation*: involves an aqueous surfactant solution in which the final nanosheets obtained can vary widely in amount and average dimensions (»40–220 nm for the length and» 2–12 layers for the thickness) depending on the concentration and type of surfactant used.

Generally speaking, physical exfoliation methods are easy to implement; however, they have numerous limitations in terms of yield and control of the final dimensions (lateral dimensions and thickness) of the obtained nanosheets. [60]

Chemical exfoliation

Chemical exfoliation is often presented as an alternative to physical exfoliation that can guarantee higher yields. The process can be considered composed by two different stages: an initial one in which small host species (e.g. pure atomic species, alkali metals, polymers and organometallic species) are intercalated between one layer and another and a second phase in which the crystal expanded through the help of external forces able to break the van der Waals bonds and form 2D nanomaterial.[61]

- *Intercalation exfoliation:* MoS_2 can be exfoliated in single- or few-layers employing an intercalation process with lithium ions, followed by reaction with water. Lithium is widely applied, thanks to its high reduction potential and its high mobility in the interlayer spacing of MoS_2 . In most cases, lithium is inserted into the process in the form of large organolithium compounds, such as $n\text{BuLi}$ and $t\text{BuLi}$, (more efficient lithium precursors than small compounds such as MeLi). During the reaction between organolithium compounds and bulk MoS_2 , Li^+ cations (or ions of other alkali metals such as Li^+ , Na^+ and K^+) are inserted into the interlayers spacing. After the intercalation process, the Mo^{4+} cations are almost totally reduced to Mo^{3+} . Subsequently, upon the contact of the obtained Li_xMoS_2 with water, most of the Mo^{3+} cations are re-oxidized, and the water undergoes a reduction reaction to hydrogen between the layers. The gaseous hydrogen produced tends to expand, helping to disassemble the bulk MoS_2 easily (Figure 2.50). Microwave-assisted intercalation and ultrasonication-assisted intercalation make the exfoliation process even easier by increasing the efficiency and rate of the lithiation step.

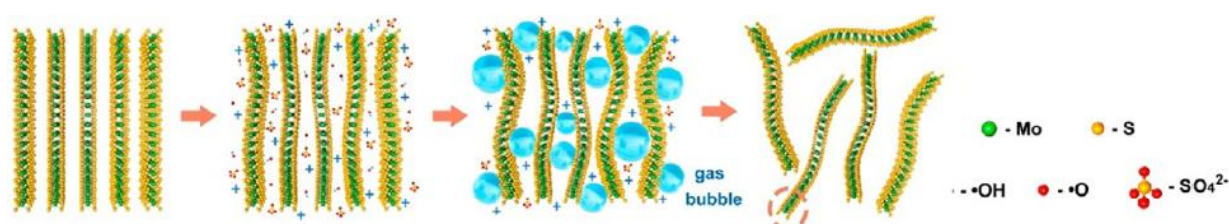


Figure 2.50: Schematic representation of MoS_2 bulk exfoliation through a lithiation process. [60]

- *Electrochemical lithiation process:* in this case, the process is carried out inside an electrochemical cell in which bulk MoS_2 is used as a cathode. During the discharge process of the battery, lithium is intercalated between the layers of MoS_2 bulk. After the lithiation process, compounds are treated by ultrasonication in water or ethanol to obtain single layers. This process (Figure 2.51) presents some improvements compared to the traditional $n\text{-Bu-Li}$ intercalation method, such as lower execution temperatures, shorter time and guarantees a high -yield of 92%.

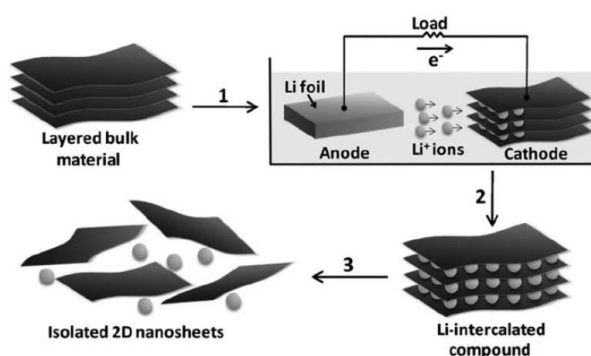


Figure 2.51 : Schematic representation of electrochemical intercalation and exfoliation process. [61]

Chemical exfoliation, the most popular method of which is lithium-ion intercalation, is a promising candidate for obtaining high yields of MoS₂ nanosheets. However, the organo-lithium compounds used in the process (toxic and expensive) make this process environmentally harmful and challenging to apply on a large scale. In order to overcome these limitations, non-lithium intercalants have been developed in recent years (SO₄²⁻, Na⁺, K⁺, N₂H₄). Besides, to have excellent environmental compatibility, these also allow obtaining comparable or even better performance than organo-lithium compounds. [60] [61]

Solvent-assisted exfoliation

- *Solvent-assisted exfoliation*: has been developed in order to prepare thin-layer MoS₂ in a simple but powerful way. This method requires to start from a solution containing solvents (with variable surface tension) and surfactants (for better synergistic effects) able to guarantee an effective exfoliation mechanism (Figure 2.52). In order to be efficient, solvents must have a surface tension as close as possible to the surface energy of MoS₂. Nowadays, the most promising are DMF, N-cyclohexyl-2-pyrrolidone (CHP) and N-methyl-2-pyrrolidone (NMP). The surface tension of NMP (40 mJ/m²) is very similar to the estimated surface energy for few-layered MoS₂ (46.5 mJ/m²). However, all these solvents are environmentally dangerous (toxic) and challenging to remove due to their high boiling points. Surfactants agents can also play a vital role in the process, stabilizing the nanosheets in the selected solvent and helping to increase the yield of the exfoliation process. Once the solution is obtained, bulk MoS₂ it is dispersed in this. Subsequently, the solution is subjected to a sonication phase and finally to an optional centrifugation step. During sonication, the presence of oxygen and dissolved moisture in the organic solvent also plays a critical role the redox-active species formed in situ through a self-oxidation pathway can help exfoliation by oxidation at of reactive edges sites of MoS₂. [61]

Solvent assisted exfoliation is considered a highly efficient, reproducible and scalable approach; however, most of the products obtained are multi-layer with a small lateral dimension (few hundred nanometers). [60]



Figure 2.52: Schematic illustration of solvent assisted exfoliation procedure. [61]

2.8.5. Bottom-up approach

Chemical synthesis

The bottom-up approach is generally characterized by a series of chemical reactions involving Mo and S precursors and a subsequent thermal annealing treatment. The most significant examples in this category are hydrothermal synthesis and chemical vapour deposition. Unlike the technologies

previously seen, with these strategies, it is simple to obtain different morphologies from nanosheets (such as nanoflowers and nanotubes, nanoflakes) and therefore, different properties.

- *Hydrothermal/solvothermal methods* are a widely used approach for the growth of layered MoS₂ materials. What makes them so widespread is the pure, ecological and controllable nature of the process, also because it takes place within a closed and protected system. The reactions between the precursor's Mo and S occur inside a Teflon-lined stainless-steel autoclave after it has been opportunely closed and heated (Figure 2.53).



Figure 2.53: Schematic representation of hydrothermal/solvothermal methods. [61]

Temperature, such as the concentration of the precursor, the pH value and the reaction time, allow obtaining MoS₂ with different morphologies, particle sizes, phases and crystallinity. By inserting templates and additives inside the autoclave, it is also possible to obtain the formation of hollow microspheres, double-shell microspheres and core-shells or yolk-shell structures. To vary the crystalline phase of MoS₂, instead, it is possible to apply magnetic fields: from the XPS (X ray Photon Spectroscopy) analysis, it has been shown that with the increase of magnetic fields the percentage of phase 1T unstable in the final product increases while stable 1T-MoS₂ can be obtained if the magnetic field strength reaches a critical point. Regardless of the process parameters and operating conditions set, after the reactions, products must be finally rinsed and dried in order to guarantee the purity of the product. [60] [61]

- *Chemical Vapour Deposition (CVD)*: which does not require an ultrahigh vacuum environment, it is one of the most suitable and scalable methods to produce MoS₂ nanosheets (Figure 2.54). The new proposed process involved Mo sulfurization after its deposition on a suitable substrate. However, this strategy has proven inadequate in ensuring adequate thickness control. For this reason, instead of pure Mo, a precursor was introduced and deposited on a SiO₂ / Si growth substrate. In this case, it is possible to control the number of layers by adjusting the sulfurization annealing time. Various precursors such as MoO₃, MoO₂, have been applied for the production of MoS₂ monolayers. Wang et al. for example, developed a CVD approach for the production of MoS₂ flakes by the layer-by-layer sulfurization of MoO₂ microcrystals, while Lee et al. synthesized large area MoS₂ directly on SiO₂ / Si substrates using the CVD method based on the sulphurization of MoO₃. Through the reaction between S vapour and MoO₃ carried out under moderate temperature conditions, it is possible to obtain a large area MoS₂ film with high crystal quality. For this to occur, however, the substrate lattice must be oriented appropriately; otherwise, it may harm electrical properties and mobility of large-area films. Atomically smooth sapphire preheated in the air for 1 hour at 1273 K immediately before the growth process allows optimal growth of MoS₂ by controlling the lattice orientation. [61]

Unlike conventional CVD, Metal-Organic Chemical Vapour Deposition (MOCVD) is a method based on the use of a gas phase precursor: typically $[\text{Mo}(\text{CO})_6]$ (as a precursor) and H_2S (as a gas flow). The obtained product grown with this method presents high crystallinity and optoelectronic quality; however, the poisonous by-products and the risk of substrate degradation still limit their diffusion. To limit the risk related to precursors, the use of metal-organic precursors has proven to be significantly advantageous in terms of purity, safety and convenience (thanks to a low-temperature, fast, and simple process). [63] [60]

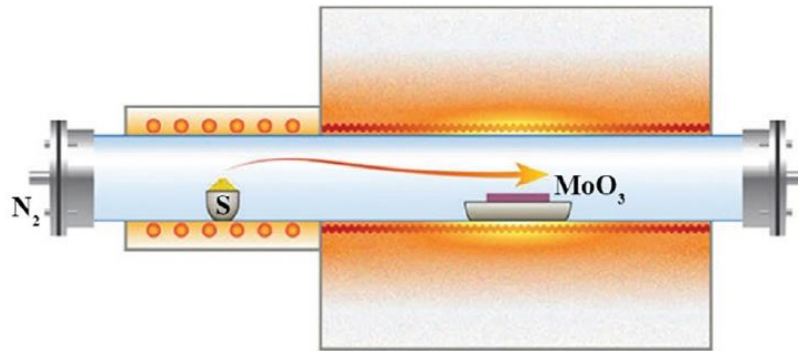


Figure 2.54: Schematic illustration of chemical vapor deposition process. [61]

Therefore, the hydrothermal method is easy to operate, but difficult to control in terms of size and morphology of the products obtained (in order to overcome this drawback, high-temperature annealing processes have been proposed).

The CVD method, on the other hand, allows having a more accurate control of the number of layers and the quality. Through this technology, it is also possible to obtain large-scale production of MoS_2 nanosheets, but it often requires controlled work environments with very high vacuum and high temperatures. [60]

A summary scheme with the methods that can be used in order to obtain MoS_2 in its exfoliated form is reported (Figure 2.55).

Methods	Dimensions		Advantage	Disadvantage
	Lateral	Thickness		
Mechanical exfoliation	Up to several micrometers	1–6 layers	Mild condition	Low yield
Shear exfoliation	~40–220 nm	~2–12 layers	High yield, easily processing	Large distribution of size and thickness
Li-ion intercalation	From 300 nm to several micrometers	1 to 8 layers	Higher energy of mono-layers	Toxic and expensive reagents required
Hydrothermal CVD	— Up to several micrometers	— 1–10 layers	Easily processing	Uncertain morphology
Solvent assisted exfoliation	A few hundreds of nanometers	Multi-layers	large-scale, high-quality, precisely controllable layer numbers large quantities yield, easily processing	Ultra-high vacuum environment and high temperature required Difficult control in size and thickness

Figure 2.55 : Comparison in terms of achievable size, advantages and disadvantages of the various approaches that can be used to obtain MoS₂ in the form of nanosheets. [60]

3. Synthesis part

3.1. Aim of the Work

The purpose of this work is to obtain a composite material to be applied as a double layer on the cathode component. As already seen, this represents one of the approaches used in lithium-sulfur cells to block polysulphides (Figure 3.1).

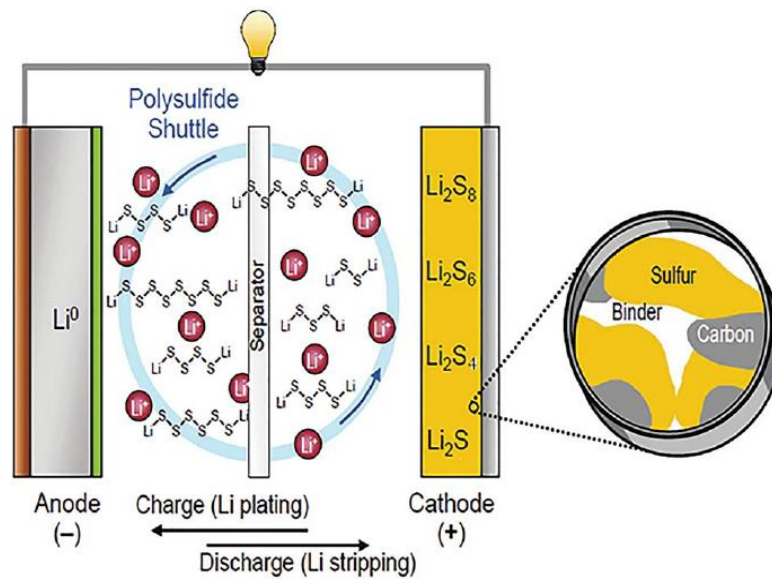


Figure 3.1 : Constitutive diagram of a Li-S battery. [4]

The use of mesoporous carbons (characterized by a large specific surface) or hollow carbon spheres, as materials constituting the cathode, can help to limit the phenomenon of shuttling. However, carbon materials can only guarantee the physical confinement of the polysulfides. [42] [54] At the same time, the chemical interactions between the non-polarity of the carbon host materials and the polar Li_2S_n are often insufficient. [4] [65]

For this reason, other polar materials are often introduced into cells, to provide strong chemisorption anchoring sites for polysulfides. [66]

PANI and MoS_2 were selected as starting materials to obtain a composite material to be applied as the coating. They are reported in the literature as materials capable of acting positively on the anchoring of polysulfides both from a chemical and physical point of view.

3.1.1. PANI

Conductive polyaniline was introduced in lithium-sulfur batteries thanks to its ability to enhance conductivity and prevent the shuttling phenomenon. It was demonstrated that:

- The repetitive phenylenediamine and quinone diimine units give to polyaniline specific electrical conductivity and unique redox behaviour. In fact, inside PANI, the N- containing groups can act as highly efficient redox mediators.[54] The quinonoid imine group ($-\text{NH}^+ = / -\text{N} =$), in particular, promotes the redox kinetics of sulfur species showing an electrocatalytic effect on these reactions. [51] [67]
- PANI can reduce the shuttling phenomenon through physical and chemical entrapment (Figure 3.2). Polysulfides dissolution into the electrolyte, in particular, can be reduced through chemical interaction between heteroatoms and $\text{Li}_2\text{S} / \text{LiS}$: Lewis base N site interacts with Lewis acid Li^+ ion of polysulfides. [54] Polyaniline presents multi-anchoring sites for polysulphides. Specifically, the protonic acid-doped polyaniline has three types of nitrogen atoms: quinonoid imine, benzenoid amine and the positively charged nitrogen. Among these, the quinonoid imine represents a unique anchoring site for polysulphides. Reversible chemical bonds between the quinonoid and polysulphides could improve the performance of the Li-S battery cells. [67]

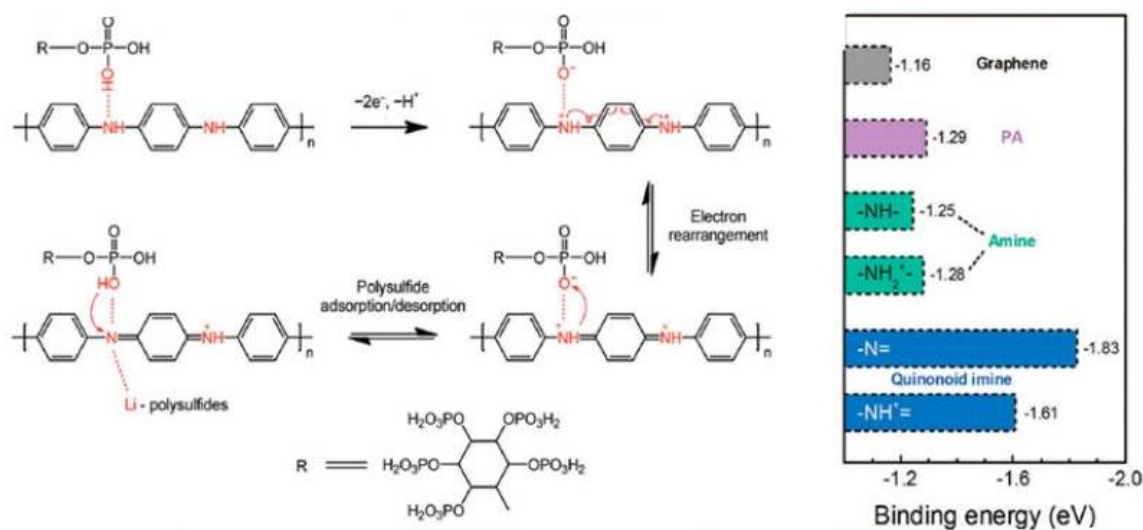


Figure 3.2: Schematic representation of quinonoid imines formation (left) and polysulfides binding energies on different materials. [67]

However, polyaniline inside Li-S batteries is not configured as an electrochemically active material: its electrical conductivity results unchanged during the charging-discharging process of Li-S battery. Therefore, when too much polyaniline is used as a coating material, the inactive weight in the cathode tends to increase while the total energy density decreases. [54]

Another drawback lies in H^+ present in the polyaniline chains. This group can easily introduce side reaction with polysulphides with consequent loss of active materials. Moreover, H^+ can also lead to current collector corrosion. [42]

Recent studies are considering the creation of protective layers even with dedoped PANI. [42]

3.1.2. MoS₂

Two-dimensional molybdenum disulphide (MoS₂) nanosheets have attracted intense research interest in electronic devices thanks to their physical and chemical properties, tunable surface features, unique electronic structures, earth abundance and low cost.

In lithium-sulfur batteries, however, MoS₂ is mainly introduced for its roles as:

- *Polysulfide immobilizer*: polar metal–sulfur bonds can bind polysulfides through strong chemical bonds (Figure 3.3), or by a dipolar interaction with the polarized surface. [65] [66] These interactions can effectively inhibit polysulfides dissolution inside the electrolyte. [4] [61]

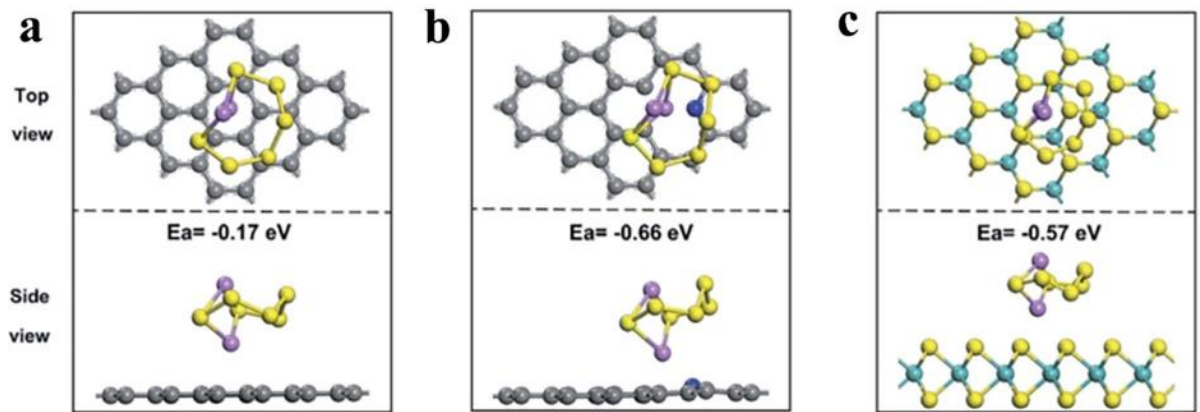


Figure 3.3: Examples of structures and binding energy for three different materials: carbon matrix (a), NC (b) and MoS₂ (c) [4]

- *Catalyst*: due to its strong interactions with LiPS and its high electronic conductivity, MoS₂ is considered catalytically active for polysulphides conversion (Figure 3.4). It, therefore, manages to promote the redox reaction kinetics of LiPS (from long-chain to short-chain polysulfide) during the discharge/charge process and act as a lithium conductor. For this reason, MoS₂ is often used as a cathode material. The fast conversion of the soluble polysulfides, in fact, decreases their accumulation in the sulfur cathode and inhibits their subsequent loss from the electrode. [4] [66] [64]

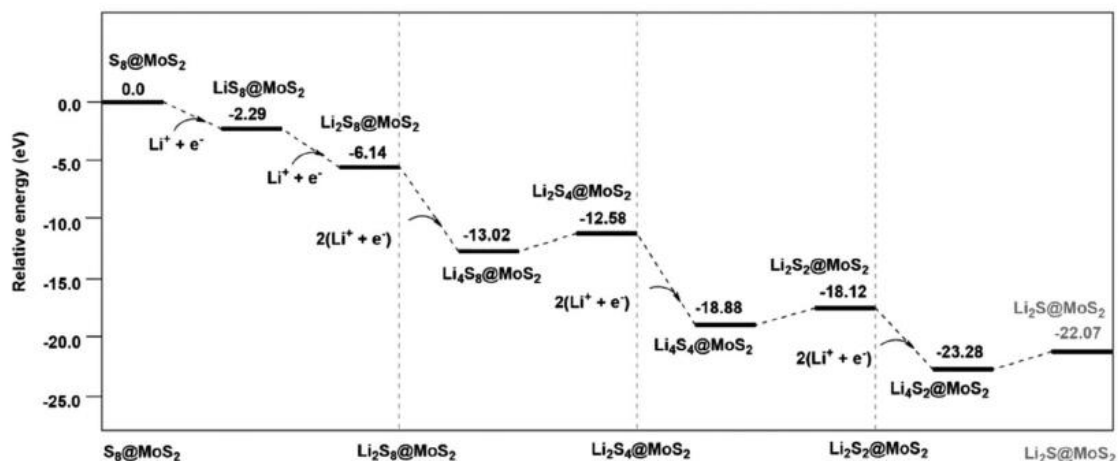


Figure 3.4 : Energy profile of polysulfide reaction on MoS_2 surface. [4]

Both the absorption of the polysulphides and the catalytic activity depend strongly on the chemical composition, the surface functionality and the intrinsic electronic structure of the catalyst.[65] [61] [64]

In particular, the redox reactions occur through strong polysulfides adsorption, rapid interfacial charge transfer and product deposition. Manipulating the surface adsorption behaviour can tune the activation energies of chemical reactions and promote the redox reaction kinetics.[66]

MoS_2 with sulfur-free locations, for example, has a higher electrochemical activity. [68]The same applies for the edge sites of MoS_2 which show stronger interactions with Li_2S than those of sites on the basal surface.[66] Finally, the different phase structures of MoS_2 (hexagonal (2H) and tetragonal symmetry (1T)) have different electronic and therefore, catalytic properties. [4] [61] [64]

3.2. Synthesis Work

The experimental part of this thesis was conducted partly in Italy and partly in Portugal thanks to a collaboration between Politecnico of Turin and FCT (Faculdade de Ciências e Tecnologia) Nova of Lisbon Universities.

During the period spent in Portugal, the synthesis processes of the base materials constituting the composites (PANI and MoS₂) and those relating to the composites themselves were initially developed. In this phase already consolidated protocols such as oxidative polymerization for PANI and hydrothermal process for MoS₂ have been adopted.

Subsequently, chemical-physical analyses (FESEM, Raman, XRD) were conducted to carry out an in-depth investigation of the morphologies and properties achieved.

The samples (Figure 3.5) were finally transported to Italy to undergo further characterization and electrochemical analysis processes.



Figure 3.5 : Samples obtained during the experimental part done at FCT University of Lisbon.

In Italy, a new PANI synthesis process was conducted according to a different protocol. Even in this case, the material has been obtained from an oxidative chemical reaction. However, unlike the PANI previously collected, the reagents and their amounts were varied.

The samples obtained were then compared both from a chemical-physical and an electrochemical point of view.

To carry out the electrochemical analysis, cells, in which the samples (in the form of single elements or composites) were previously coated on the cathode, have been finally assembled and tested.

3.2.1. Materials

Below, to distinguish the PANI synthesis protocol followed in Portugal from that observed in Italy, the materials obtained are generally defined as Portuguese PANI and Italian PANI.

Composite materials are classified into three categories: IN-SITU, EX-SITU and hydrothermal composites. The first two designations refer to the polymerization process of PANI occurred respectively during (IN) and before (EX) the production of the composite material. In particular:

- IN SITU composites: was obtained starting from a solution containing water and MoS_2 in which the polymerization reaction of the polyaniline has been carried out
- EX SITU composites: was obtained starting from the mixing of the base materials (PANI and MoS_2) inside a beaker containing water, after these were synthesized separately. The base materials have been introduced with different ratios (30:70 and 70:30) to understand better the influence each has on the final properties of the material

The last composites category refers to a synthesis process in which the already synthesized PANI is placed in a microwave with the MoS_2 reagents. This procedure, except for the addition of the PANI, is the same as the one followed to obtain a type of MoS_2 defined hydrothermal.

However, only commercial MoS_2 , suitably exfoliated, was used to produce composite materials.

Due to the availability of the analysis machinery and the time needed to carry out the analysis, it was not possible to test all the samples from an electrochemical point of view. For this reason, the samples can finally be divided into two macro-categories: those that have been tested inside a lithium-sulfur cell (as a double layer deposited on the cathode) and those that have not yet been analyzed (Figure 3.6). The thesis work focuses primarily on the former.

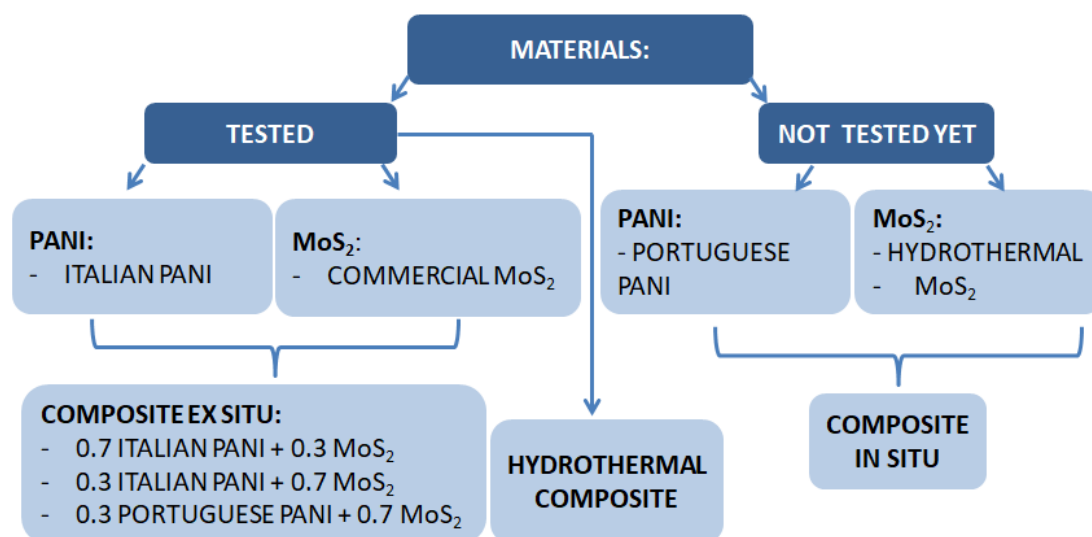


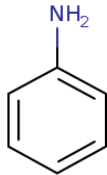
Figure 3.6 : Schematic representation of the samples obtained and their subdivision into samples electrochemically analysed and not yet analysed.

3.3. PANI

3.3.1. Italian PANI synthesis

The reagents used for the synthesis were (Table 3.1):

Table 2.1: Reagents used for the synthesis of Italian PANI.

Materials	Chemical structure/formula
Aniline	
Sulfuric Acid	H ₂ SO ₄
Ammonium peroxydisulfate (PSA)	(NH ₄) ₂ S ₂ O ₈

The synthesis procedure was the following (Figure 3.7):

- A monomer solution was prepared (100 mL): [Aniline] = 0,2 M; [H₂SO₄] = 0,5 M.
- The solution was chemically treated with (NH₄)₂S₂O₈ (PSA) 1M, which was added drop by drop until the colour of the samples turned to dark green. Then the reaction was left on magnetic stirring for a whole night.
- The precipitates obtained were washed with distilled water and ethanol several times. During this process, the solution was divided into several falcons and located inside a centrifuge set at high speeds. At the end of each centrifugation process (10 minutes), the excess liquid was removed using a pipette, and new water/ethanol was inserted into the falcons. The process was repeated until a neutral pH is reached.
- Finally, the powder was collected in a petri dish and dried in the oven at 50 ° C.

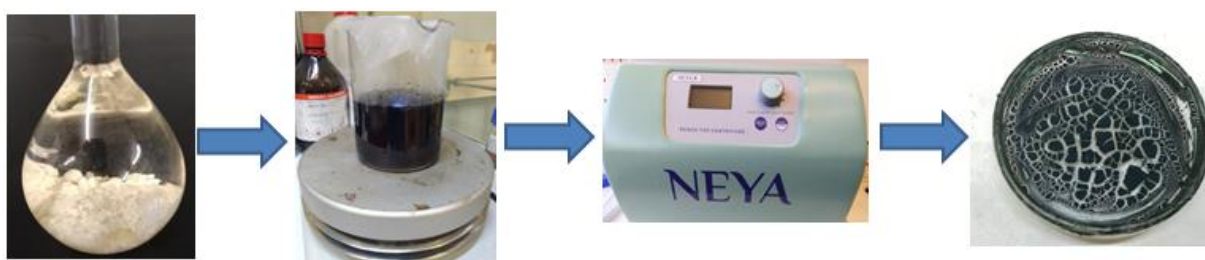
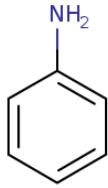
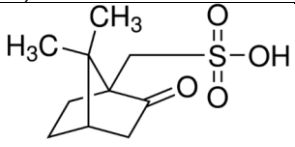


Figure 3.7 : Schematic representation of the significant steps necessary to obtain Italian PANI.

3.3.2. Portuguese PANI synthesis

The reagents used for the synthesis were (Table 3.2):

Table 3.2: Reagents used for the synthesis of Portuguese PANI.

Materials	Chemical structure/formula
Aniline	
Hydrochloric acid	HCl
Ammonium peroxydisulfate (PSA)	$(\text{NH}_4)_2\text{S}_2\text{O}_8$
Camphor-10-sulfonic acid, beta (CSA)	

The synthesis procedure was the following (Figure 3.8):

- Two different solutions were prepared:

- 1) [Aniline] = 0.164 M; [Camphor-10-sulfonic acid] = 0.043 M
- 2) $(\text{NH}_4)_2\text{S}_2\text{O}_8$ = 0.395 M; [HCl] = 0.163 M

After obtaining the two solutions separately, they were placed in an ice bath and left to rest for 30 minutes

- The solution containing Aniline (1) was then poured into the solution containing APS (2), and the final solution was left in the ice bath for another hour and a half. During this time, the solution generally changes colour from brown to green until purple-blue shades.
- The solid material obtained was separated from the liquid of the solution by the use of two filter papers and subsequently washed 6-7 times with deionized water and the last time with methanol
- Finally, the filter containing the powders was placed in the oven (without vacuum) and left to dry at 60 ° C for 24 hours.

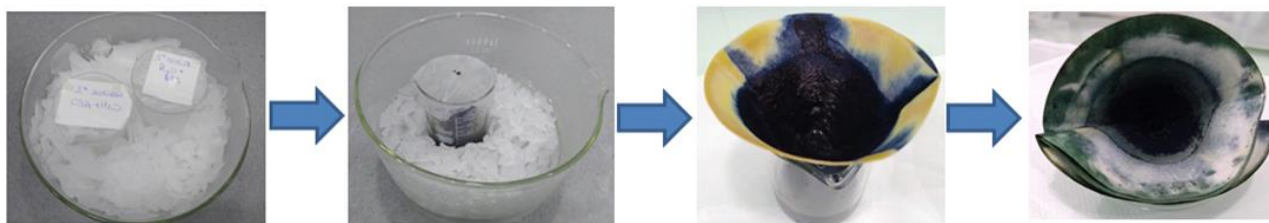


Figure 3.8 : Schematic representation of the significant steps necessary to obtain Portuguese PANI.

3.3.3. PANI ITA vs PANI PORT

The two synthesis processes present evident differences in the composition and typology of the reagents, as well as in the process itself. Referring to the Portuguese PANI its synthesis, compared to that of the Italian PANI, presents:

1. **ICE BATH (1,5 h):** helps to control the crystallinity and conductivity of the polymer. A high crystallinity is desirable since a greater packing of the chains favors the charge transport inside the material. [69] The presence of the ice bath also allows reducing the reaction time
2. **CSA:** surfactant and co-dopant, can increase the conductivity,[53] [51] modify the morphology and help the formation of the tubular structure
3. **HCl:** doping agent, responsible for an increase in conductivity [52] (in the synthesis of the Italian PANI, sulfuric acid was used with the same objective)

FESEM Analysis:

The first analysis that has been carried out on the PANI is a FESEM (Field Emission Scanning Electron Microscopy) analysis from which it is possible to observe the morphology of the compound (Figure 3.9). [70] For the Italian PANI, the structure appears irregular and not well defined in the form (with a morphology that could be described as "fragmented") but repeated uniformly in space. For the Portuguese PANI, the morphology appears instead very delineated according to a "tubular" geometry with a dimension (length) much higher despite the others.

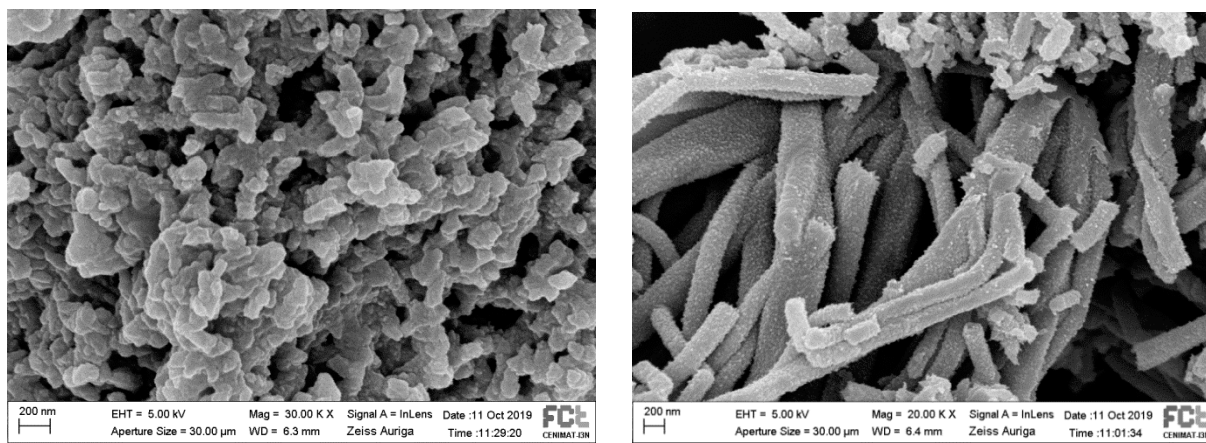


Figure 3.9 : Comparison between the FESEM analysis of Italian PANI (left) and Portuguese PANI (right), at 200 nm magnification.

Looking at the compounds with smaller magnifications (Figure 3.10), Italian PANI appears very compact and the polymer fragments firmly adhered to each other. In the case of the Portuguese PANI, on the other hand, the compound has a more open morphology in which the individual tubular elements result evident and well defined.

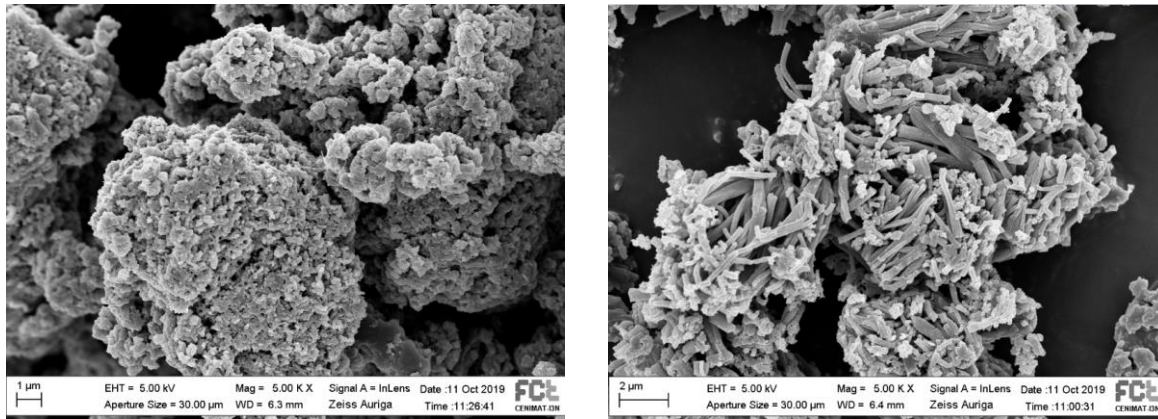
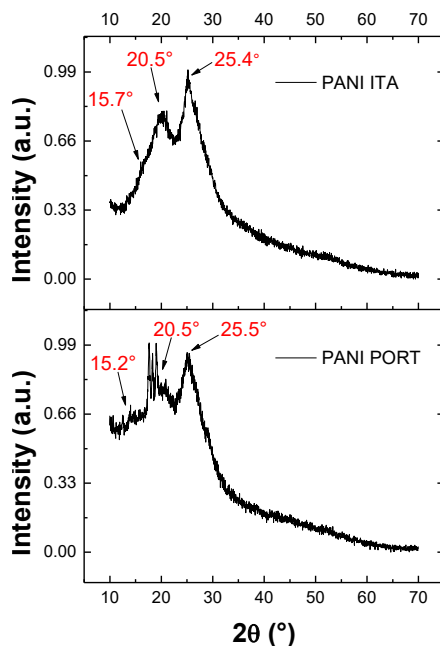


Figure 3.10 : Comparison between the FESEM analysis of Italian PANI (left) and Portuguese PANI (right), at 1-2 μm magnification.

XRD Analysis:

X-ray diffraction (XRD) is a bulk analytical technique that is used to reveal details in the atomic structure of crystals. The parameters that can be determined by this technology are lattice parameters and interlayer spacing, space group, degree of crystallinity, residual stress. The interference generated between the atomic crystal structure and the incident X-rays leads to obtain this crystal information.

From a typical diffractogram, it is also possible to derive the average size of the crystals and the deviations from a perfect crystal starting from the shapes and widths of the peak (measuring the width of the peak at half-height). [71]



Peaks:	Planes:
15.1°	(001)
20.5°	(020)
25.5°	(200)

Figure 3.11: Left: Comparison between the XRD analysis of Italian PANI (top) and Portuguese PANI (bottom). Right: table with the characteristic peaks of PANI in the emeraldine form.

Generally, for the emeraldine salt, there are three crystalline peaks at $2\theta = 15.1^\circ$, 20.5° and 25.5° which correspond to (011), (020) and (200) planes of pure PANI (also reported in the table). [72] The peaks at higher angles (near $2\theta = 20^\circ$ and 25°) are attributed to the periodicity parallel and perpendicular to the polymer chain, respectively (Figure 3.11). [62] [53]

By subjecting the two types of PANI to the XRD analysis, these peaks result evident for the Italian PANI. On the other hand, in the case of the Portuguese PANI, the graph appears noisier and the peaks slightly shifted. However, from both graphs polyaniline results a semicrystalline polymer. Its characteristic reflections with low intensity and wide width, in fact, indicate that this material is not entirely amorphous.

In general, PANI exhibits low to medium range of crystallinity. However, by modifying the synthesis process and the initial composition of the reagents, it is also possible to obtain highly crystalline PANI.

Raman Analysis:

When monochromatic light is irradiated on to a surface sample produces scattered light. Some of this scattered photon maintain the same frequency as the source of incident light (Rayleigh scatter) other instead change their frequency because of an energy exchange with the samples phonons (Raman scattering). Raman scattering is therefore, a phenomenon of inelastic dispersion of light. [73]

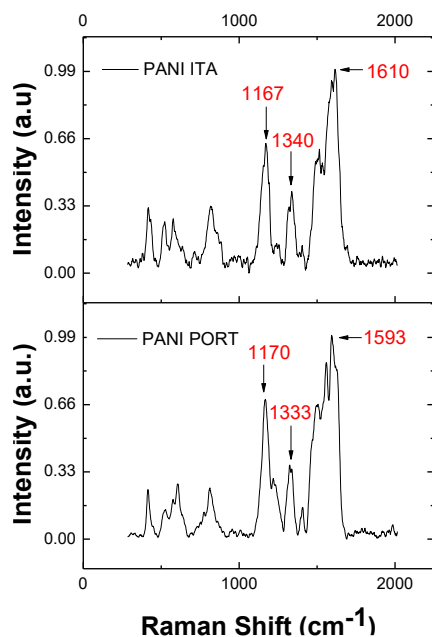
By studying the different wavelength obtained, it is possible to trace the molecular vibrations of the molecules responsible for the light dispersion. From these vibrations, moreover, derive information on the structure, symmetry, the electronic environment and the bond of the molecules considered, thus obtaining a quantitative and qualitative analysis of the individual compounds. [70]

Raman spectra depend on the excitation wavelength. Based on the energy of the laser excitation line, polyaniline behaves differently, and the electronic transition of the benzenoid or quinonoid constitutional units can be more or less enhanced.[56]

Using the blue laser excitation, the characteristics of the reduced leucoemeraldine form of this polymer are improved. In contrast, red laser excitation implements the attributes of oxidized forms. In the latter case, the vibration bands originating from the oxidized quinonoid units are enhanced. To obtain spectra of more uniform intensity (both from reduced and oxidized forms), it is necessary to use a green laser line at 532 nm (Figure 3.12). [74]

Raman spectra of polyaniline can be divided into three central regions. Each region can provide information on the oxidation level and the degree of protonation of the polymer. These are:

1. 1100-1210 cm^{-1} region: in which the C - H bending vibrations fall
2. 1210-1520 cm^{-1} region: in which the stretching vibrations of C - N, C = N and C~N⁺ bonds, can be observed
3. 1520-1650 cm^{-1} region: where C - C and C=C bonds, respectively of the benzene and quinone rings, predominate [74] [75]



Peaks:	Bending:
1167 cm^{-1}	C – N ⁺ stretching
1336 cm^{-1}	C – H bending
1592 cm^{-1}	C = C bending

Figure 3.12 : Left: Comparison between the Raman analysis of Italian PANI (top) and Portuguese PANI (bottom). Right: table with the characteristic peaks of PANI in the emeraldine form.

Data reported in the table were found in the literature. These values refer to a sample of PANI doped with HCl 1M and analyzed with green laser line conditions. Although the positions of the peaks obtained with the Italian PANI and the Portuguese PANI have slightly shifted concerning these values, general considerations can be drawn.

First, the peak at 1167 cm^{-1} corresponds to the in-plane C-H bending of benzene or quinoid units. This peak is evident after a doping process takes place.

Another characteristic peak of the doped forms of PANI is that at 1336 cm^{-1} . This peak is not observable in the spectrum of PANI in its non-conductive forms and is expected only when the quinoid rings are converted into benzenoid rings. This band is assigned to the radical cation (C-N⁺ stretching) and is often the result of protonation of the PANI with HCl or the oxidation of PANI after complexation. It provides information on the delocalized polaronic structures vibrations.

Another critical peak to highlight is the one observed at 1592 cm^{-1} . This peak relates to C = C stretching vibrations in a quinoid ring (partially mixed with C-H bending). When the PANI is doped, its position within the spectrum shifts to higher wavenumbers. [75]

The Raman spectrum is dotted with numerous other peaks. Among these, the most important are: [76]

- 1491 cm^{-1} in PANI, which is assigned to the C = N stretching of the quinoid units. Its shift towards higher wavenumbers is indicative of a decrease in the number of quinoid units in the PANI chain.
- 1418 cm^{-1} of the quinoid CC stretching
- 1219 cm^{-1} related to C-N benzenoid stretching [62] [75]

3.4. MoS₂

3.4.1. MoS₂ commercial

Commercial MoS₂ is undoubtedly the most economical and readily available solution for this material. MoS₂ can be found on the market in the form of bulk black powder with a multilayer structure. In the bulk composition, before any exfoliation treatment, the layers are strongly adhesive and stacked together through van der Waals forces. This configuration is evident in the FESEM image (Figure 3.13) shown at lower left, where sections of the stacked MoS₂ sandwiches are visible. It is possible to observe, in fact, a vast stacking of compressed and curled MoS₂ layers with a few micrometres in length and hundreds of nanometers in thickness.

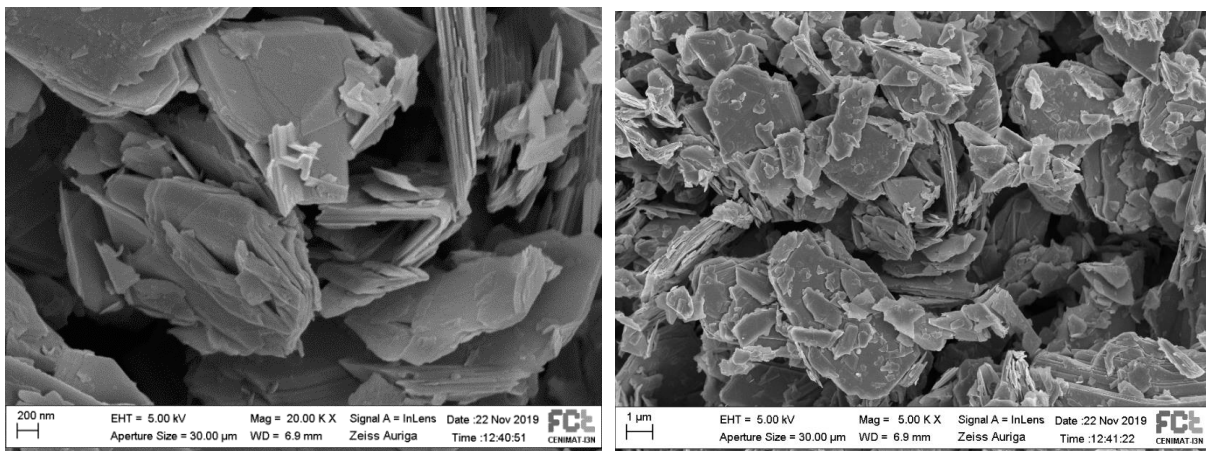


Figure 3.13 : Comparison between the FESEM analysis of MoS₂ commercial at 200 nm magnification (left) and MoS₂ commercial at 1 μm magnification (right).

The two main MoS₂ peaks studied in literature through Raman analysis are E_{21g} and A_{1g}. [77] [78]

- E_{21g}: in-plane vibration modes of the S atoms
- A_{1g}: out-off-plane vibration modes of the S atoms

Their position within the graph is not fixed but may vary according to the number of layers that make up the material: the peak frequency is layer dependent (Figure 3.14).

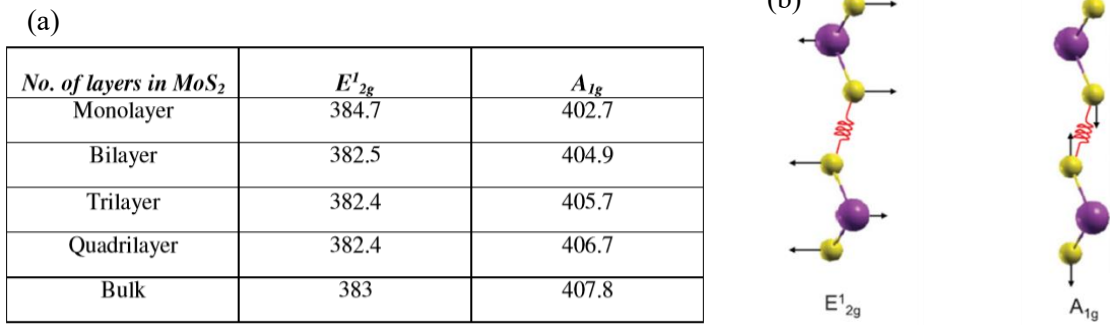


Figure 3.14 : (a) Correlation between the number of layers and the phonon vibration modes [58]. (b) In-plane and out-of-plane phonon modes. [78]

Some studies have been demonstrated that as the number of layers increases, E_{12g} moves towards lower frequencies while A_{1g} shows a shift towards higher frequencies. These variations in the position of the peaks occur due to partial Coulombic interactions and the charge that is induced while stacking the intra layers.[64] In particular, the downshift of the E_{12g} mode with an increasing number of layers can be explained by an increase of the dielectric screening which reduces the long-range Coulomb interaction between the effective charges. [58] [78]

The Raman spectrum obtained (Figure 3.15) from commercial powders confirms that the material is in its bulk form: the E_{12g} peak is a 383,4 while the A_{1g} peak is located at 407,5.

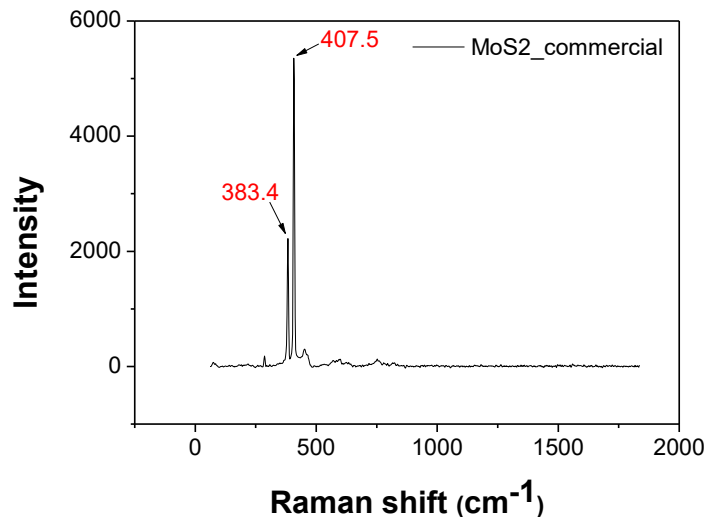


Figure 3.15 : Raman analysis of commercial MoS₂ with characteristic peaks of the bulk form.

3.4.2. MoS₂ Hydrothermal synthesys

As seen in the bibliographical part, MoS₂ can be synthesised in various ways and with different morphologies. To have a comparison with the bulk form just presented, it was carrying out a synthesis

process starting from a solution containing Thiourea and Sodium molybdate (Table 3.3). The selected process is called Hydrothermal and involves the use of a microwave

Table 3.3: Reagents used for Hydrothermal MoS₂ synthesis.

Materials	Chemical structure/formula
Sodium molybdate	Na ₂ MoO ₄
Thiourea	CH ₄ N ₂ S

The synthesis procedure was the following (Figure 3.16):

- A reagent solution was prepared: [CH₄N₂S] = 0,7 M; [Na₂MoO₄] = 0,175 M and dissolved on a heating plate for 15 minutes at 80°C and 700 rpm
- Once the solution became utterly transparent, it was poured into a flask and placed inside a microwave. The process parameters (shown below) have been set in the microwave
- After the microwave process took place, the resulting powder was washed five times with a centrifugation process (4500 rpm, 15 minutes) in which water and ethanol were alternately used
- Finally, the material was placed in a vacuum dryer for 12 hours at 80 ° C



Figure 3.16: Schematic representation of the significant steps necessary to obtain Hydrothermal MoS₂.

The process parameter used were (Table 3.4):

Table 3.4: Process parameters for the microwave synthesis of hydrothermal MoS₂.

Temperature:	200°C
Time:	60 min
Pressure:	280
Power:	100 W
Stirring:	off
Pre-Stirring:	off

One of the most significant differences compared to bulk MoS₂ probably lies in morphology. As can be seen from the FESEM images (Figure 3.17), the material produced using the microwave has nanoflower shape. Each nanoflower is still composed of many nanosheets, but these are no longer stacked on each other. Layers, in this case, are arranged to form a spherical shape like a rose. The nanoflowers appear well defined and arranged according to a very open and porous structure.

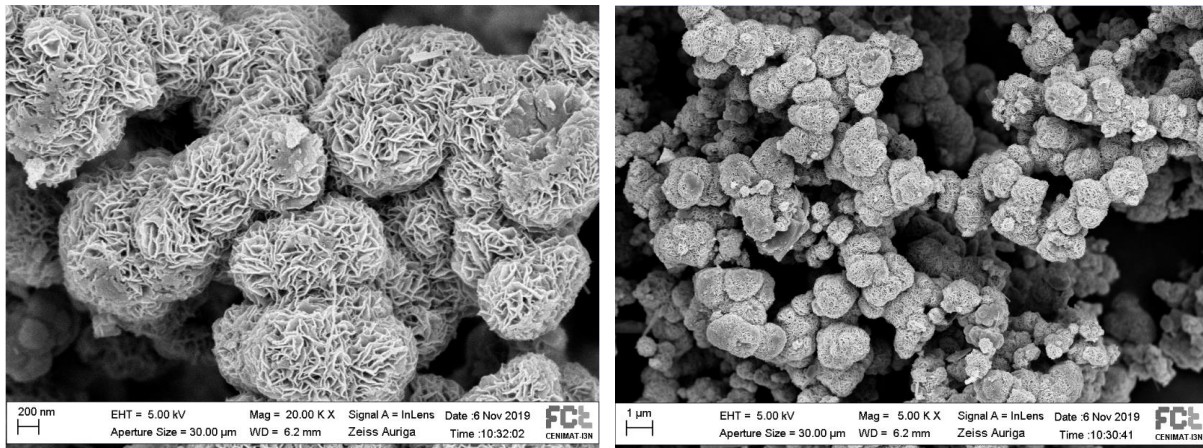


Figure 3.17 : Comparison between the FESEM analysis of MoS₂ hydrothermal at 200 nm magnification (left) and MoS₂ hydrothermal at 1 μm magnification (right).

Another difference lies in the Raman graph performed on the synthesized powders. In this case, the graph is noisy and disturbed. This can be due to various causes:

- the presence of a more amorphous material
- a sub-optimal powder washing process
- a too small amount of analysed material

In particular, the diffraction peak enlarged to about 1590 cm⁻¹ can come from residues of reagents contained in the thiourea, which is in reasonable compliance with the synthesis process (Figure 3.18). [79]

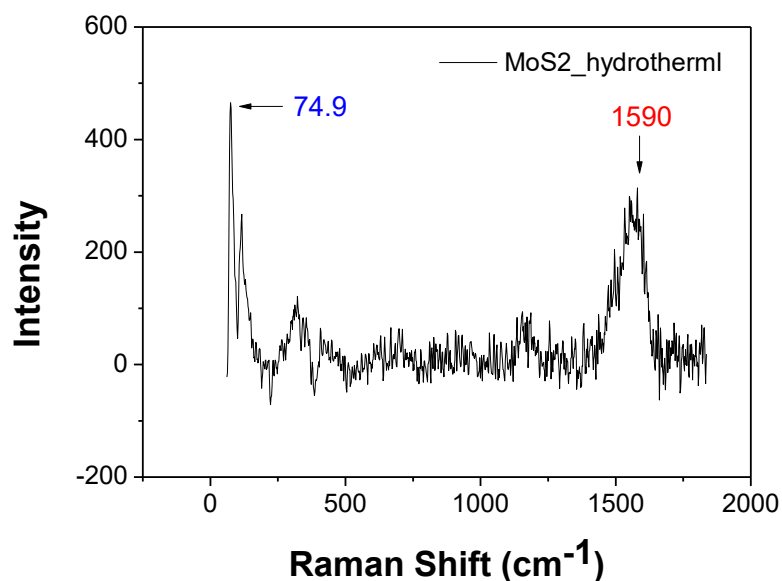


Figure 3.18 : Raman analysis of hydrothermal MoS₂ with its main peaks.

In the small amount of material obtained from the synthesis, about 0.0035 g, (and therefore analyzed), lies the most significant problem of this approach. Although the morphology of the nano-flowers has attractive configuration with high surface area capable of improving the sulfur loading rate and the battery capacity, this approach is too demanding for MoS₂ production. Therefore, microwave synthesis process has not been used for MoS₂ powder but only to obtain an hydrothermal composite with the addition of PANI, (presented later).[4]

The materials which have been analysed from an electrochemical point of view, alone (as a reference) or in the form of composites double layer, are Italian PANI, Portuguese PANI and commercial MoS₂.

3.5. Composites

During the experimental part, three different types of composite materials were synthesized: IN-SITU, EX-SITU and hydrothermal. In the preparation of these materials, the synthesis processes just presented have played different roles. They have been used for:

- obtain the composite material directly: *IN SITU composites*. In this case, to get the composite, an oxidative polymerization of Portuguese PANI was carried out with the addition of commercial MoS₂.
- obtain the elemental materials: *EX SITU composites*. In this case, the two forms of PANI (Italian and Portuguese) were obtained separately and only later they were combined through a sonication process with commercial MoS₂.
- both: *hydrothermal composites*. In this case, the PANI previously synthesized through the Portuguese protocol was added to the microwave synthesis process used to obtain MoS₂.

3.5.1. Exfoliation process

As seen in the literature, since few MoS₂ layers have significantly better properties than the bulk form, an exfoliation process was carried out on commercial MoS₂ before using it in the preparation of composites (Figure 3.19).

This operation has been mainly concerned with the synthesis processes of IN-SITU and EX-SITU composites.



Figure 3.19: Schematic representation of the significant steps, and process conditions, necessary to obtain the exfoliation of commercial MoS₂.

Among the various methods to obtain exfoliated MoS₂, it was adopting a "solvent-assisted exfoliation" process.

Generally, solvents with surface tension as close as possible to the surface energy of MoS₂ are used to perform this operation. However, since in this case, the solution in which the exfoliation process takes place is also the one in which the oxidative reaction of the Portuguese PANI occurs (IN-SITU

composites), it was decided to use only water. This choice was made up to avoid possible influences by the solvent on the polymerization process and therefore on the formation of the composite.

The commercial MoS₂ powder was then placed in a beaker containing 30 ml of water and subjected to an ultra-sonication process for 9 hours at 300 W.

Some differences can be seen from the FESEM analysis (Figure 3.20) obtained on the pristine sample (left) and that earned on the material after 9 hours of ultra-sonication process (right).

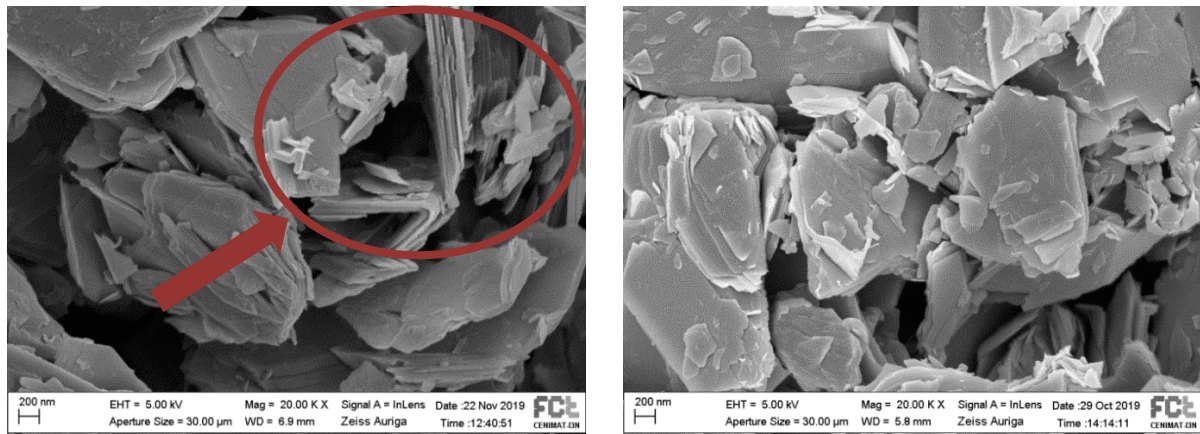


Figure 3.20: Comparison between the FESEM analysis of commercial MoS₂ in its bulk form (left) and exfoliated MoS₂ (right), at 200 nm magnification.

While in the image on the left, it is easy to observe MoS₂ blocks made up of several stacked layers, in the image on the right they are not evident. Furthermore, passing from one picture to another, the size of the sheets and their shape seems to be unchanged.

This process was therefore adopted in the synthesis of composite materials.

3.5.2. IN-SITU Composite

This first type of composite material was obtained through an IN-SITU polymerization reaction of PANI, inside a solution containing commercial MoS₂ (Table 3.5). For the IN-SITU composite synthesis, an oxidative polymerization was carried out according to the Portuguese protocol (in the presence of HCl and an ice bath, with the addition of CSA).

Table 3.5: Reagents and polymerization protocol used for IN-SITU composite synthesis.

Reagents:	Amount:
MoS ₂ commercial:	0.3 g
PANI Portuguese:	IN-SITU Polymerization

A beaker containing 30 ml of water and 0.3 g of commercial MoS₂ in its bulk form, underwent an ultrasonication process for nine hours. Then, the solution was divided into two different beakers: one containing 10 ml and the other 20 ml of solution.

The reaction [(NH₄)₂S₂O₈] = 0.395 M; [HCl] = 0.163 M was carried out in the first container; while in the other, the reaction: [Aniline] = 0.164 M; [Camphor-10-sulfonic acid] = 0.043 M was carried out.

Then, according to the Portuguese protocol, the beakers were placed separately in an ice bath for half an hour. At the end of this time, the solutions were combined in a beaker and left in the ice-bath for another hour and a half. Finally, the mixture was washed with water and dried in the oven.

FESEM Analysis:

The FESEM images (Figure 3.21) show the morphology of the composite obtained. From the image at higher magnifications (200 nm), it is possible to observe the tubular morphology already encountered by the synthesis of the PANI according to the Portuguese protocol. It is not possible to see instead MoS₂ layers: this could suggest that this material has been completely incorporated and covered by the PANI (image at lower magnifications, 1 μm)

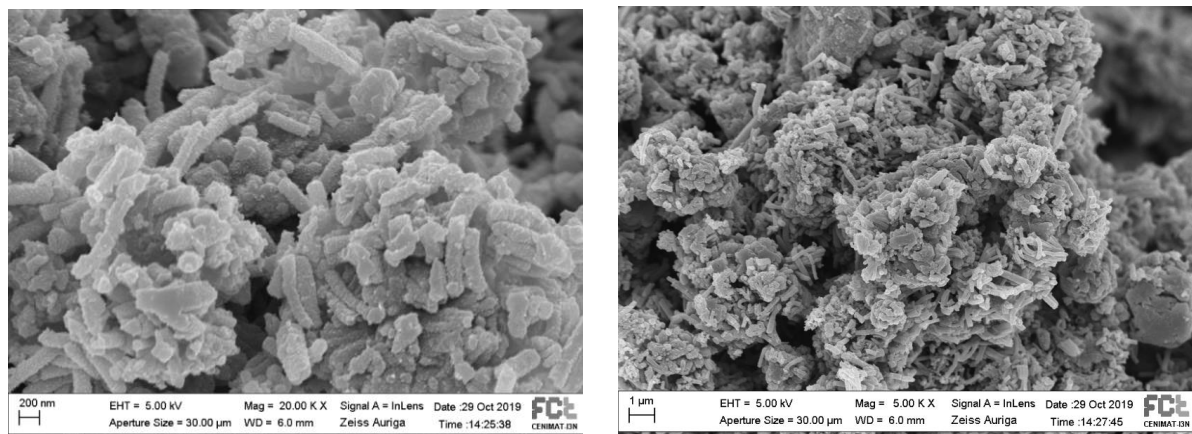


Figure 3.21 : Comparison between the FESEM analysis of IN-SITU composite (with 0.3g commercial MoS₂) at 200 nm magnification (left) and at 1 μm magnification (right).

However, by repeating the same synthesis process with a smaller initial MoS₂ amount (0.03 g), what is obtained is (Figure 3.22 and 3.23):

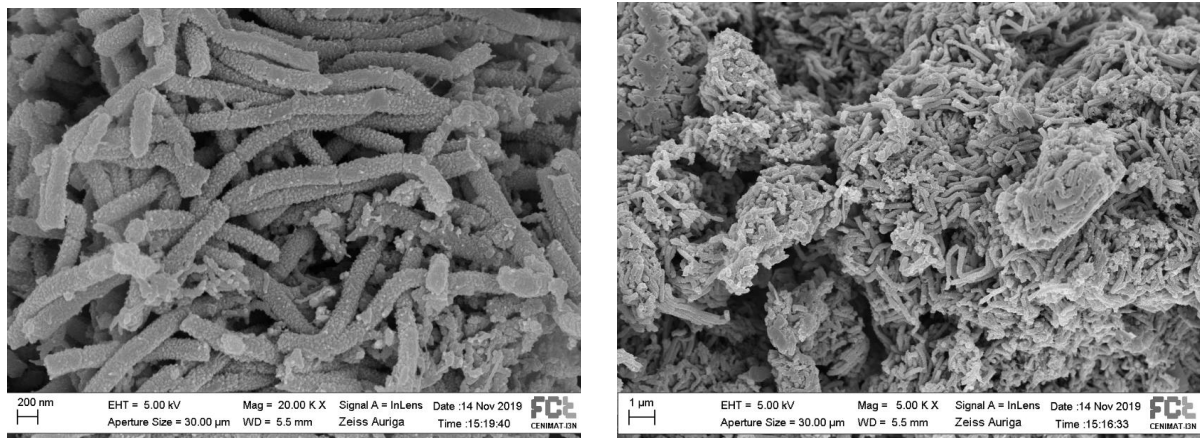


Figure 3.22 : Comparison between the FESEM analysis of IN-SITU composite (with 0.03g commercial MoS₂) at 200 nm magnification (left) and at 1 μm magnification (right).

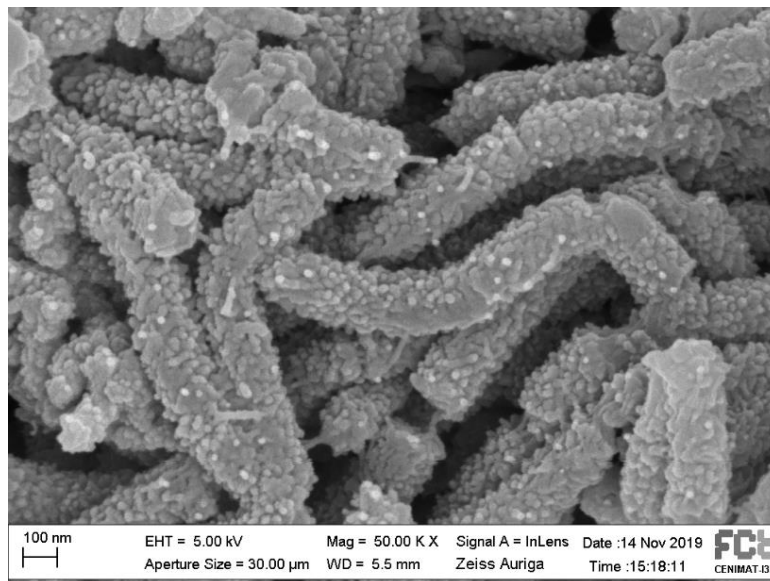


Figure 3.23: FESEM analysis of IN-SITU composite (with 0.03g commercial MoS₂) at 100 nm magnification.

In this case, the tubular structure of the PANI is much more pronounced and well defined. At the same time, it is more difficult to imagine the presence of MoS₂ in the form of layers, as observed immediately after the exfoliation operation.

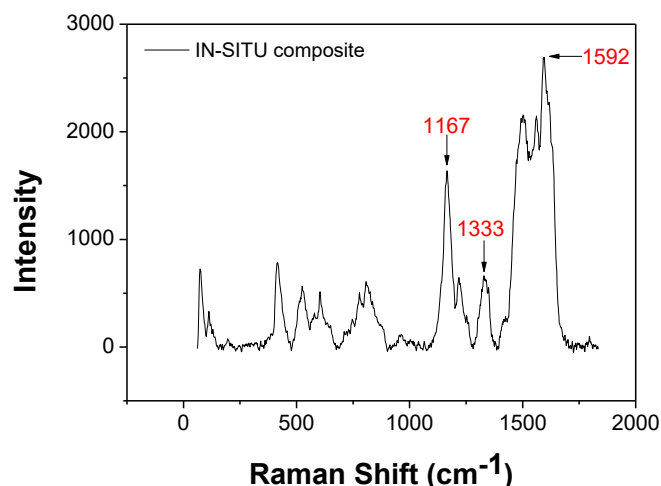
During the composite synthesis, therefore, a reaction between MoS₂ and the PANI polymerization reagents may have occurred.

To draw more precise conclusions, it is necessary to conduct a more in-depth analysis in which try to separate the influence that each reagent (of the CSA and HCl) has on MoS₂. For this reason, it was

decided to wait for further investigations on the synthesis process of this material before proceeding with electrochemical analyses.

Raman Analysis:

The RAMAN analysis carried out on the IN-SITU composite containing 0.3 g of MoS₂ is shown below (Figure 3.24).



Peaks:	Bending:
1167 cm ⁻¹	C – N ⁺ stretching
1333 cm ⁻¹	C – H bending
1592 cm ⁻¹	C = C bending

Figure 3.24: Left: Raman analysis of IN-SITU composite. Right: table with the characteristic peaks of PANI in the emeraldine form.

From the graph, it is possible to observe the peaks already identified in the case of the Portuguese PANI. The values that correspond to the emeraldine form of PANI (1167, 1333 and 1592 cm⁻¹) are particularly highlighted.

There is also a less pronounced peak at about 400 cm⁻¹.

However, the shape and height of this peak do not recall those already seen in the case of commercial MoS₂: this supports the hypothesis of a possible reaction between the MoS₂ contained in the starting solution and the PANI reagents

EDS Analysis

Energy Dispersion X-ray Spectroscopy (EDS) is generally used to quantify and qualify the elemental compositions of a sample surface. During this analysis, the atoms on the surface are excited by an electron beam. From the interaction of the surface with the incident electrons, X-rays with specific wavelengths are generated. By analysing the wavelengths of the emitted rays, through an energy dispersion detector, it is possible to trace the elements that make up the surface and therefore, the composition of the sample. [70]

For completeness, the EDS image obtained on the sample containing 0.3 g of MoS₂ is also reported (Figure 3.25 and Table 3.6).

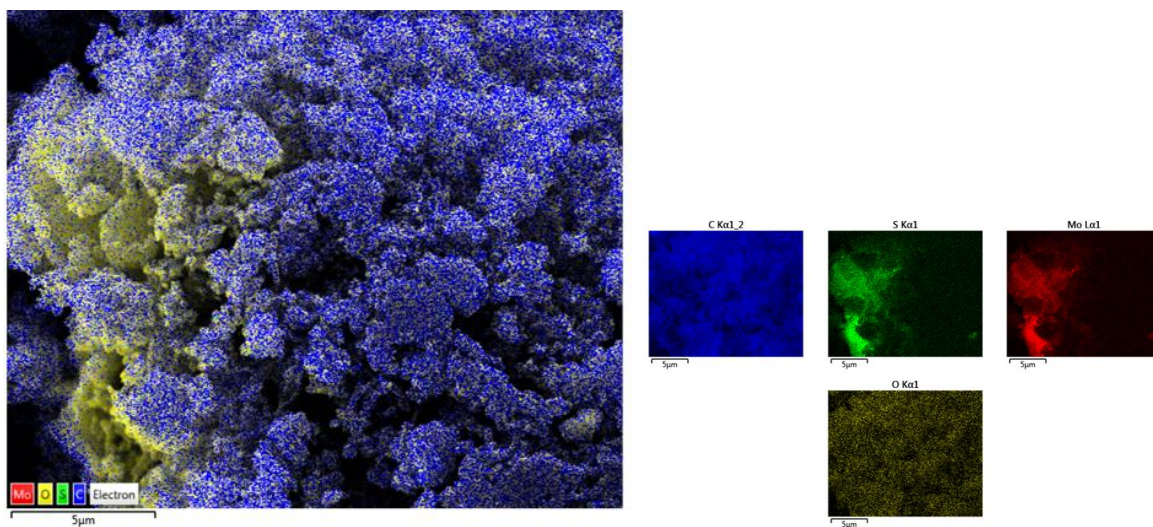


Figure 3.25: EDS images of IN-SITU composite.

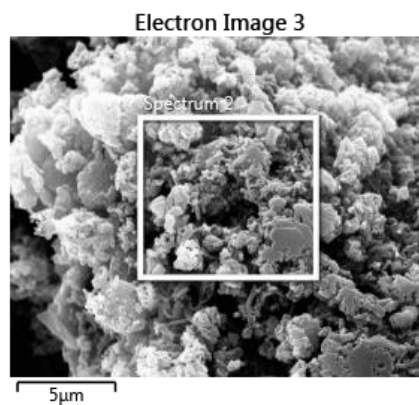


Table 3.6: Element table of EDS analysis.

Element	Line Type	Apparent Concentration	k Ratio	Wt%	Wt% Sigma	Atomic %	Standard Label	Factory Standard	Standard Calibration Date
C	K series	4.49	0.04495	72.71	0.53	86.46	C Vit	Yes	
O	K series	0.93	0.00313	11.10	0.32	9.91	SiO2	Yes	
S	K series	0.70	0.00600	4.11	0.20	1.83	FeS2	Yes	
Mo	L series	1.57	0.01574	12.07	0.50	1.80	Mo	Yes	
Total:				100.00		100.00			

3.5.3. EX-SITU Composites

The first step, to obtain this class of composite materials involves the synthesis of the constituent elements: Italian and Portuguese PANI.

Once the two different polyaniline powders were obtained, these were added in three different backers each containing, in 30 ml of water, a certain amount of commercial MoS₂ (in its bulk form).

The ratio adopted between Italian PANI and MoS₂ were 70:30 and 30:70 (Table 3.7). This choice was made to separate the contribution of the individual elements on the final performance of the component. In the case of the Portuguese PANI, the ratio adopted was 30:70. The inverse proportion was not chosen for a practical reason: much less material can be obtained from any synthesis carried out according with the Portuguese protocol.

Table 3.7: Constituent elements of the three EX-SITU composite materials and their relative quantities.

Samples:	MoS ₂ :	PANI:
1	Commercial: 0.3 g	Italian: 0.7 g
2	Commercial: 0.7 g	Italian: 0.3 g
3	Commercial: 0.7 g	Portuguese: 0.3 g

Sample 1:

From the FESEM analyses (Figure 3.26) of the first sample, with 0.3 g of MoS₂ and 0.7 g of ITALIAN PANI, a highly compact structure can be observed. The morphology is very similar to that already found in the case of Italian PANI (both for dimension and shape). Moreover, for smaller magnifications (1 μ m), some well exfoliated MoS₂ nanosheets, can be identified.

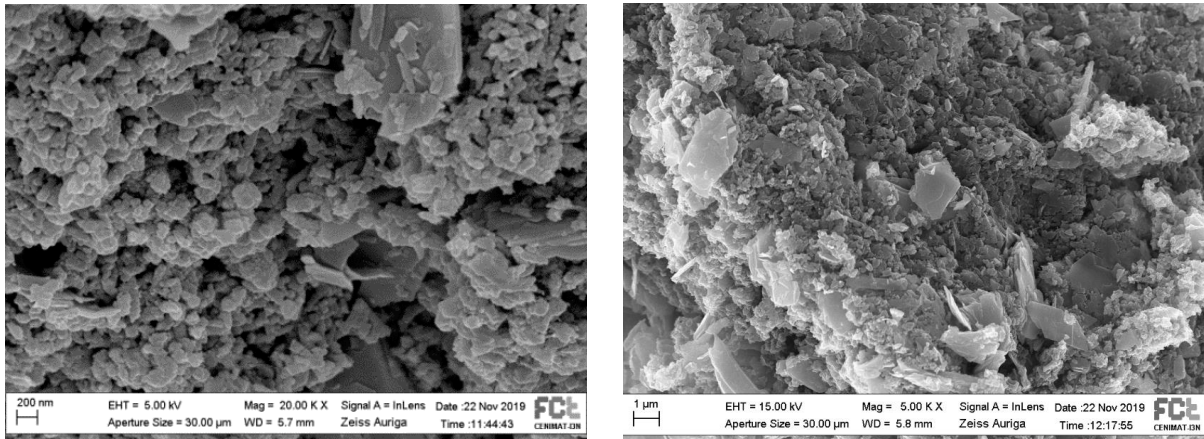


Figure 3.26: Comparison between the FESEM analysis of EX-SITU composite (with 0.3g commercial MoS₂ and 0.7g Italian PANI) at 200 nm magnification (left) and at 1 μ m magnification (right).

Sample 2:

The images below show the FESEM analyses (Figure 3.27) performed on the second sample: containing 0.7 g commercial MoS₂ and 0.3 g Italian PANI. In this case, the morphology is much more open, and the presence of the individual MoS₂ sheets appears predominant.

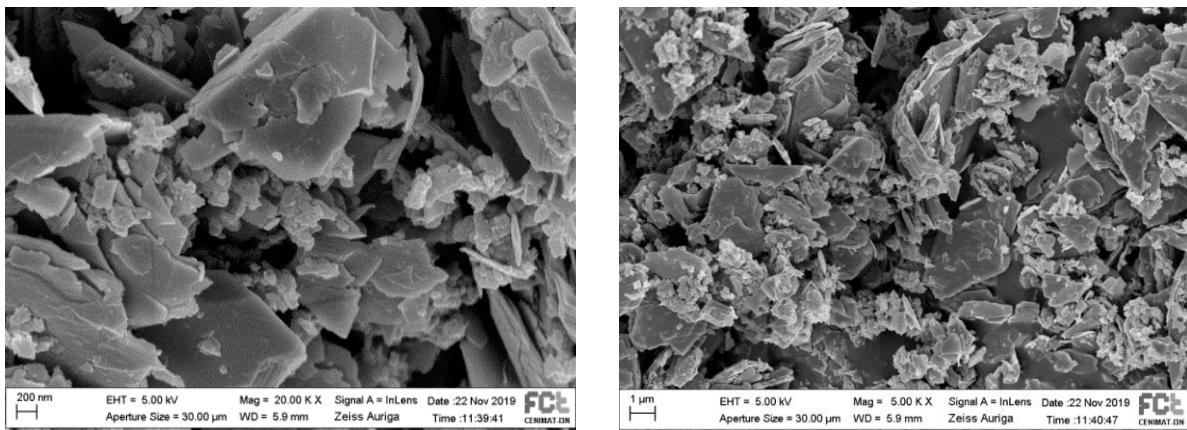


Figure 3.27: Comparison between the FESEM analysis of EX-SITU composite (with 0.7g commercial MoS₂ and 0.3g Italian PANI) at 200 nm magnification (left) and at 1 μ m magnification (right).

Sample 3:

Unlike the other two EX-SITU samples, in this case, the FESEM analysis (containing 0.7 g of MoS₂ and 0.3 g of Portuguese PANI) shows the tubular nature of the PANI that composes it (Figure 3.28). From these images, it can be deduced that the ultra-sonication process, manages to preserve the PANI morphology, in addition to exfoliating the MoS₂.

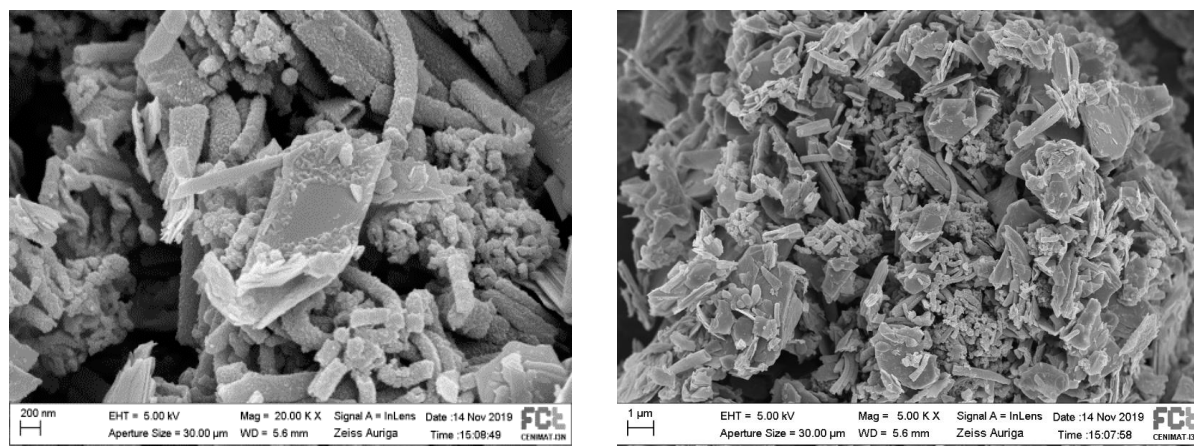


Figure 3.28: Comparison between the FESEM analysis of EX-SITU composite (with 0.7g commercial MoS₂ and 0.3g Portuguese PANI) at 200 nm magnification (left) and at 1 μm magnification (right).

Raman Analysis:

A comparison of the Raman analysis obtained from the three EX-SITU composites is reported (Figure 3.29).

In the first sample (PANI ITA 0.7), containing a quantity of PANI higher than that of MoS₂, it is possible to notice, in addition to the typical peaks linked to the presence of PANI in the emeraldine form, a signal at about 400 cm⁻¹ which could be associated to MoS₂.

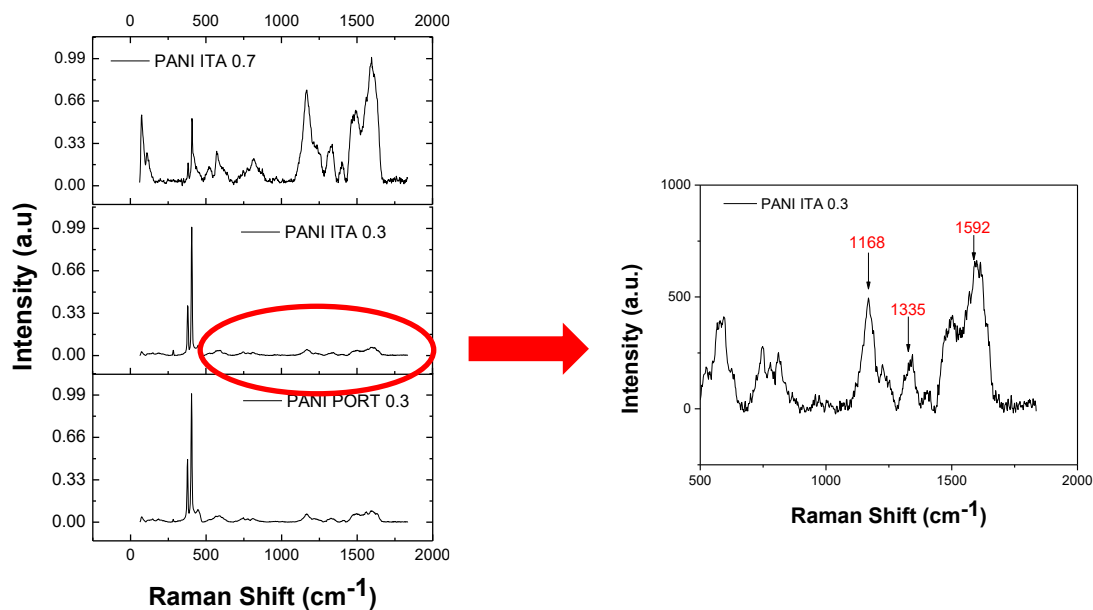


Figure 3.29: Left: Comparison between the Raman analysis of the three EX-SITU composites. Right: Zoom in the Raman chart to highlight the characteristic peaks of PANI in the emeraldine form.

In the following two graphs, corresponding to the EX-SITU composites containing a higher quantity of MoS₂ (0.7 g), only two peaks (at about 400 cm⁻¹) can be seen and associated with MoS₂ itself. However, it is not possible to observe other peaks at longer wavelengths, where those of the PANI are usually found.

For these materials, it is possible to obtain the typical signals of emeraldine form, expanding the terminal portion of the graphics. In this case, the peaks previously presented for polyaniline are visible. [62]

EDS Analysis:

EDS image obtained on the sample containing 0.3 g of Italian PANI and 0.7 of MoS₂ is also reported (Figure 3.30 and Table 3.8).

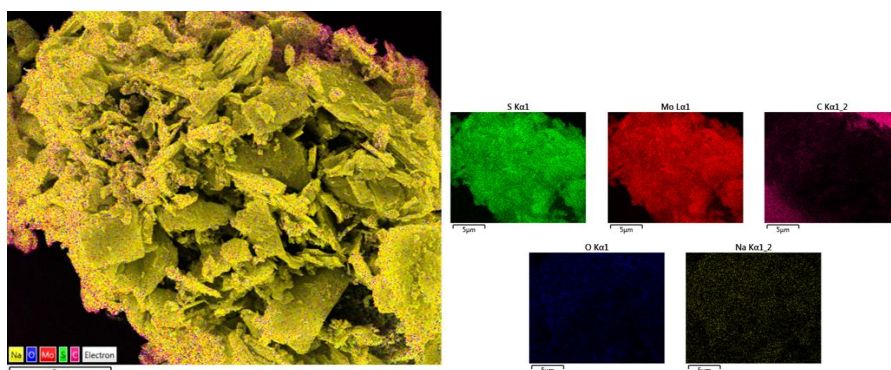


Figure 3.30 : EDS images of EX-SITU composite with 0.3 g of Italian PANI and 0.7 of MoS₂.

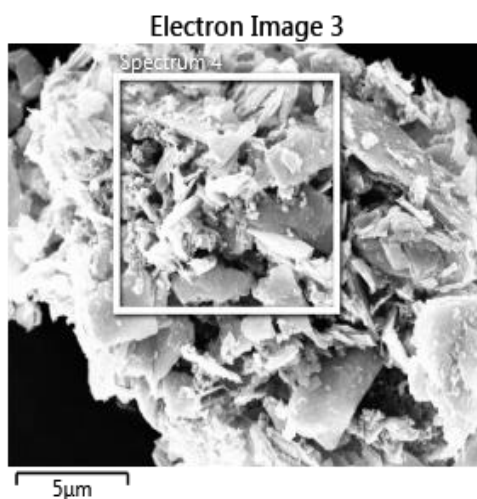


Table 3.8: Element table of EDS analysis.

Element	Line Type	Apparent Concentration	k Ratio	Wt%	Wt% Sigma	Atomic %	Standard Label	Factory Standard	Standard Calibration Date
C	K series	0.69	0.00692	27.74	0.49	63.64	C Vit	Yes	
O	K series	0.38	0.00126	3.89	0.16	6.70	SiO2	Yes	
S	K series	3.88	0.03346	17.53	0.26	15.06	FeS2	Yes	
Mo	L series	8.67	0.08668	50.84	0.47	14.60	Mo	Yes	
Total:				100.00		100.00			

3.5.4. Hydrothermal Composite

To obtain this material, the protocol already adopted for the hydrothermal MoS₂ was followed. The only difference has been the addition of a certain amount of Portuguese PANI during the microwave process (Table 3.9).

Table 3.9: Reagents and synthesis protocol used for the Hydrothermal composite.

Reagents:	Amount:
PANI Portuguese:	0,0035 g
MoS ₂ :	Hydrothermal Synthesis

- A reagent solution was prepared: $[\text{CH}_4\text{N}_2\text{S}] = 0,7 \text{ M}$; $[\text{Na}_2\text{MoO}_4] = 0,175 \text{ M}$ and dissolved on a heating plate for 15 minutes at 80°C and 700 rpm.
- Once the solution became completely transparent, it was poured into a flask together with 0.0035 g of Portuguese PANI. Then the flask was placed inside a microwave oven, with the previously selected process parameters.
- After the microwave process took place, the resulting powder was washed five times with a centrifugation process (4500 rpm, 15 minutes) in which water and ethanol were alternately used
- Finally, the material was placed in a vacuum dryer for 12 hours at 80°C

The amount of PANI that has been added within the process is equal to the quantity of MoS_2 , which can usually be obtained from a single hydrothermal synthesis. In this case, therefore, the ratio between the PANI and MoS_2 should be around 50:50.

FESEM Analysis:

From the FESEM images obtained (Figure 3.31 and 3.32) on the hydrothermal composite, it is possible to notice the characteristic nanoflowers, already seen after the synthesis of the hydrothermal MoS_2 , combined with a more formless mass. This second phase corresponds to the PANI added during the process.

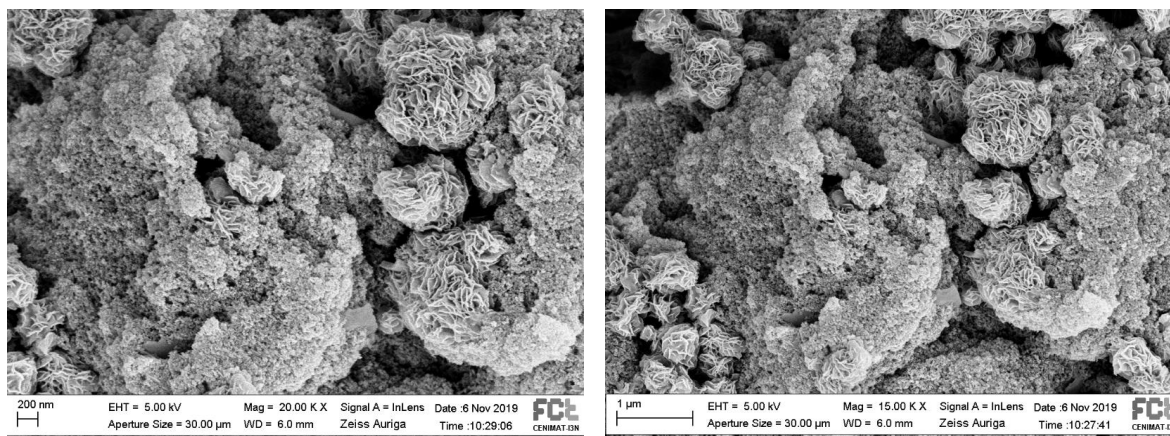


Figure 3.31: Comparison between the FESEM analysis of Hydrothermal composite at 200 nm magnification (left) and at $1\mu\text{m}$ magnification (right).

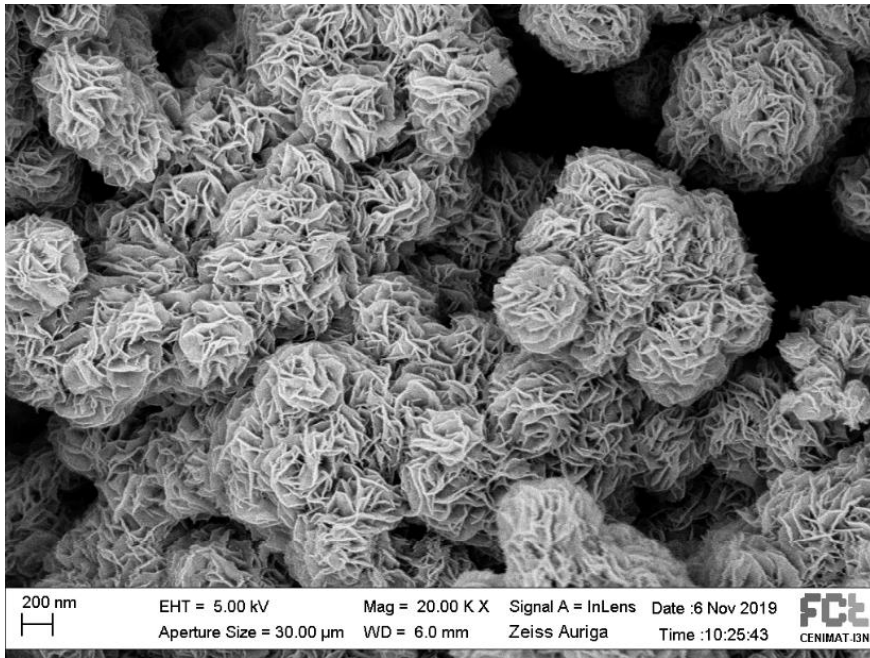


Figure 3.32 : FESEM analysis of Hydrothermal composite at 200 nm magnification.

RAMAN Analysis:

As with all other types of composite materials, also in the case of the hydrothermal one, Raman analysis (Figure 3.33) highlights the characteristic peaks of PANI in the emeraldine form. There is also a peak at 74.9 cm^{-1} found in the MoS_2 graph obtained through the same process.

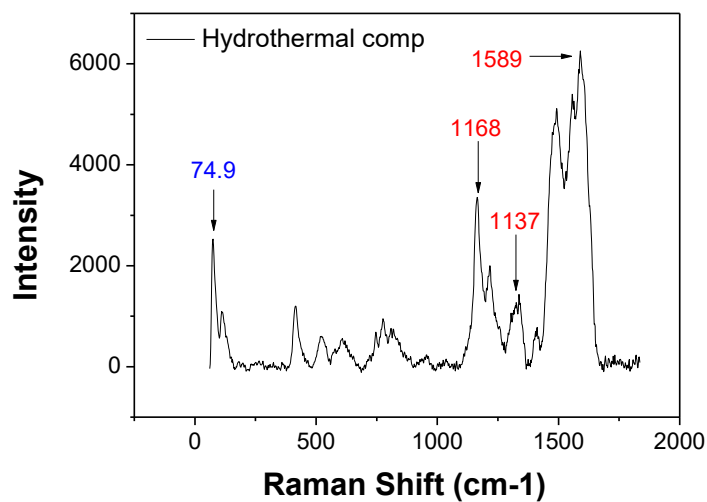


Figure 3.33 : Raman analysis of Hydrothermal composite with the characteristic peaks of PANI in the emeraldine form and that of Hydrothermal MoS_2 .

EDS Analysis:

EDS image obtained on the Hydrothermal composite is reported (Figure 3.34 and Table 3.10).

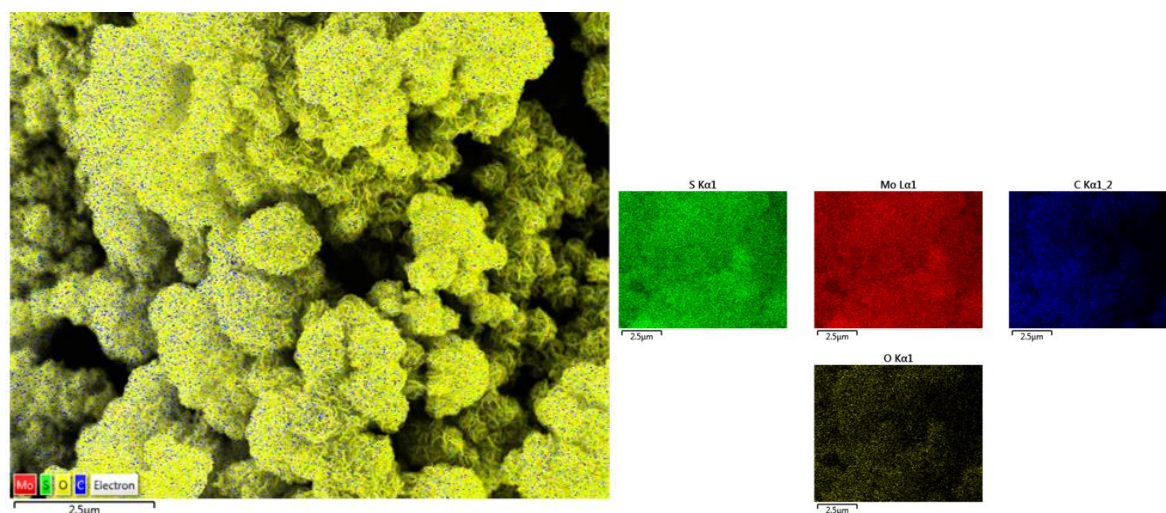


Figure 3.34: EDS images of Hydrothermal composite.

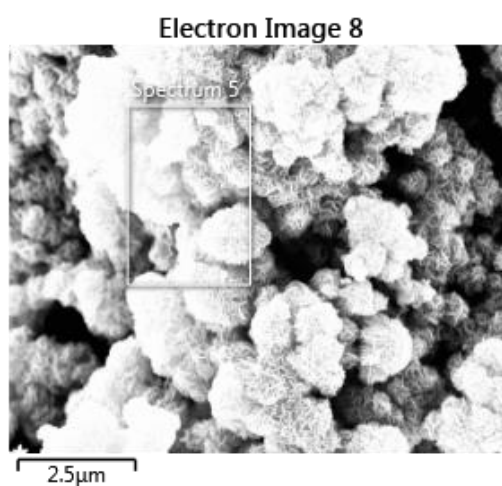


Table 3.10: Element table of EDS analysis.

Element	Line Type	Apparent Concentration	k Ratio	Wt%	Wt% Sigma	Atomic %	Standard Label	Factory Standard	Standard Calibration Date
C	K series	0.66	0.00658	31.25	0.52	65.80	C Vit	Yes	
O	K series	0.51	0.00171	6.88	0.21	10.87	SiO2	Yes	
S	K series	2.20	0.01893	13.36	0.25	10.54	FeS2	Yes	

Mo	L series	6.14	0.06136	48.51	0.50	12.79	Mo	Yes	
Total:				100.00		100.00			

3.6. Conclusion:

During the synthesis phase of the experimental work, the following materials were successfully obtained and analysed through FESEM, XRD, and RAMAN analysis:

- two types of PANI (Polyaniline): through oxidative chemical reactions
- two kinds of MoS₂: the commercial form (analysed only) and the hydrothermal one obtained from a hydrothermal process with microwave
- three types of composites: IN-SITU, EX-SITU, HYDROTHERMAL

In the following part of the experimental phase Italian PANI, MoS₂ commercial MoS₂, EX-SITU and HYDROTHERMAL composites were also characterized and tested from an electrochemical point of view.

4. Electrochemical part

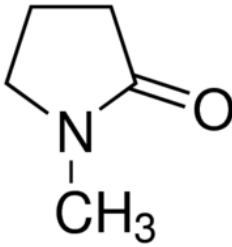
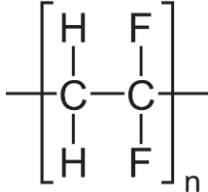
4.1. Cell Preparation

To proceed with the electrochemical analysis of the samples, it was necessary to produce the cathode on which to apply the double layer and, subsequently the double layer itself.

4.1.1. Cathode preparation:

For the cathode, it was decided to use a 70:20:10 composition in which the higher value refers to the active material (Sulfur), and the other two values indicate respectively the mesoporous carbon, Ketjenblack (KJB) and solvent (PVDF).

Table 4.1: Solvent and binder used for the cathodic composition.

Materials	Chemical structure and/or formula
N-Methyl-2-Pyrrolidone (NMP)	
Polyvinylidene fluoride (PVDF)	

The procedure followed was:

- 0.25 g of PVDF (Table 4.1) were poured into a 1.5 ml Eppendorf. PVDF is the most used binder, as it provides favourable thermal and chemical stability between the current collector and the deposited electrode materials. It is also soluble in NMP, which is usually introduced as a solvent into the composition to control the slurry viscosity.
- Then Sulfur (0.14 g) and KJB (0.04 g) powders were weighed on a laboratory balance, mixed and crushed on a mortar.
- The two elements were added to the Eppendorf with 1.2 ml of NMP. The alternate pouring operation of the solid fraction (NMP and Sulphur) and the liquid part (NMP) allows a more homogeneous consistency and facilitates the subsequent mixing process.
- Two zirconia spheres were inserted inside the Eppendorf. The container was then closed and brought to the ball milling where a 30 Hz mixing operation was performed for 15 minutes.
- The suspension was spread on an aluminium sheet through a film applicator (Doctor Blade technique) with a given thickness of 200 μm .
- The electrode thus obtained was finally dried in an oven at 50 ° C for one hour in order to allow the solvent to evaporate

The most critical parameter in the preparation of the cathode is the viscosity of the slurry: this must be high enough not to create voids in the cathode during the evaporation of the solvent but not too high, to prevent a homogeneous spread on the aluminium sheet. While optimizing the slurry composition, the viscosity can be controlled by the NMP amount. [80]

4.1.2. Double layer preparation:

To obtain the slurry which will constitute the double layer, a procedure similar to that used for the cathode was followed; however, the ratio adopted between the active material, KJB and PVDF was 80:10:10. In this case, with "active material", is indicated the sample which has to be characterized from an electrochemical point of view, therefore: composites (EX-SITU and hydrothermal), commercial MoS₂ and Italian PANI. MoS₂ and PANI are analyzed both as a constituent part of the composites and as single elements. In the latter case, the two materials act as a reference.

With 80:10:10 ratio, the amount of materials used for the preparation of the slurry was (Table 4.2):

Table 4.2: Double-Layer composition

Materials:	Amount:
Active material:	0.12 g
KJB:	0.015 g
PVDF (8% in NMP):	0.187 g
NMP:	400-500 ul (based on active material)

After pouring all the materials into a 1.5 ml Eppendorf (as explained in the case of the cathode preparation), the suspension was subjected to a mixing process by ball milling: 15 minutes at 30 Hz. Subsequently, the formed slurry was blade casted on the sulfur-carbon cathode (Figure 4.1). The thickness imposed on the applicator film, in this case, was 150 µm. The coated cathode was taken into an oven, to dry the solvent, for 1h at 50°C.

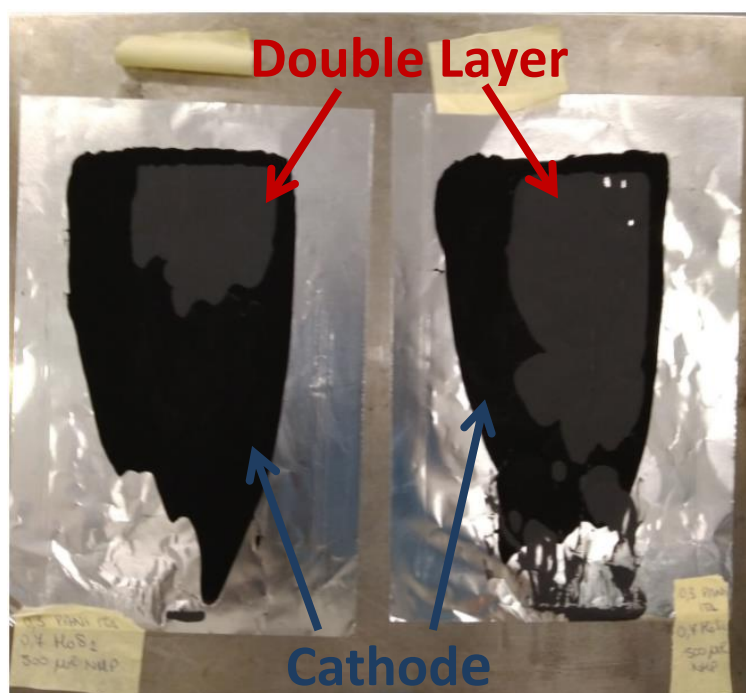


Figure 4.1: Double-Layer coated on a sulfur-carbon cathode

The obtained coated cathode was then cut into discs of 15 mm of diameter and inserted in a Büchi Glass oven B-585 at 40°C for 4h in vacuum.

4.1.3. Cell assembling:

To test the samples from the electrochemical point of view, the components were inserted inside a Li-S cell with a coin configuration. The cells were assembled inside a glovebox: a controlled atmosphere chamber in which water and oxygen values are kept below 1ppm. The box is filled with argon and has a slightly higher pressure than atmospheric one (overpressure) to limit the possibility that, during the opening/closing phase, the contaminants can reach the materials contained inside.

The assembly of the cell consists in overlapping the various layers (made up of active and non-active materials) one on top of the other, trying to keep them as parallel as possible (Figure 4.2). During this phase, the cathode covered by the double-layer was positioned in the bottom cup (stainless steel) of the coin cell. Then the separator (Celgard 2500) was placed over the cathode and wet with 20 μ l of LiTFSI ($\text{LiC}_2\text{F}_6\text{NO}_4\text{S}_2$) 1M electrolyte in DIOX: DME (1: 1v) + 0.25M LiNO_3 . Subsequently, the lithium metal anode, a spacer and a wave spring (both made of stainless steel) were placed over the separator. The spring is inserted as it helps compress the layers, improving the contact between the various materials placed inside the cell. Finally, the battery was sealed by crimping in a manual mechanical press.

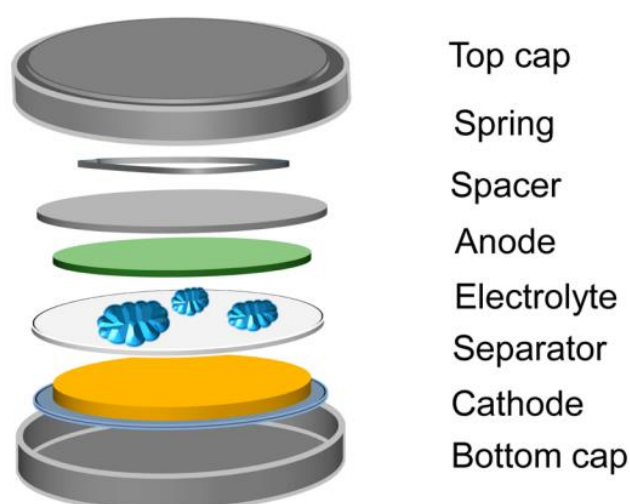


Figure 4.2: Schematic representation of an assembled cell. [81]

After having closed the cell, a short circuit test was carried out, conducted between 2 and 3 Volts through the use of a multimeter, to verify the success of the assembly operation.

4.2. Electrochemical Analysis

The assembled cells were then subjected to a series of electrochemical analysis:

1. Cyclic voltammetry
2. Galvanostatic cycling
3. Catalytic Effect (TAFEL)

All electrochemical analysis measurements were performed in Politecnico di Torino, Italy. Cyclic voltammograms were performed using CH Instruments 660D model while galvanostatic cycling and coulombic efficiency were achieved by Arbin 32-channel battery tester.

4.2.1. Cyclic Voltammetry

Cyclic Voltammetry (CV) is a standard tool used to investigate the thermodynamic and kinetic behaviour of an electrochemical reaction, but it can also be used to understand the structure-property relationship of the battery components. In lithium-sulfur batteries, it is often used in conjunction with the discharge/charge curves to describe the electrochemical redox process.[32] [82]

The typical configuration for this analysis involves the use of three electrodes: a Working Electrode (WE), a Counter Electrode (CE) and a Reference Electrode (RE). [83] However, in most application-oriented studies, two-electrode coin cells are mainly applied. In this case, an electrode functions both as CE to form a current circuit and as a load polarization. [82]

The analysis requires that a linearly swept potential per unit of time is applied to the electrode at a scan rate of mV. When a set potential ($E\lambda$) is reached, the potential is swept in the opposite direction. [84]

During the measurement, the potential (imposed on the system) is plotted on the x-axis, while, the current (the response) is plotted on the y-axis, resulting in a trace called voltammograms or cyclic voltammograms (Figure 4.3). [83]

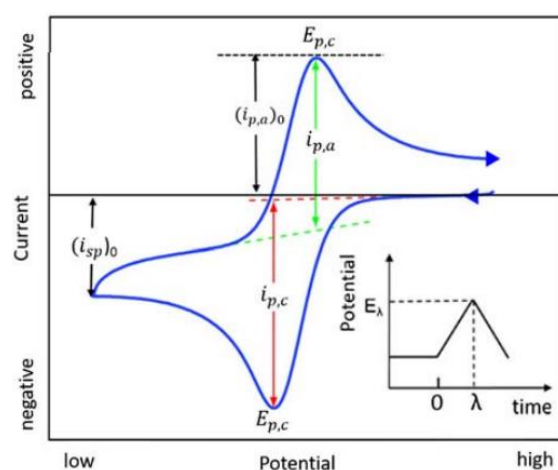


Figure 4.3: Schematic example of a CV curve depicting a simple reversible reaction. [82]

Cyclic voltammetry is an electrochemical characterization tool capable of providing information on:

- chemical and electrochemical reversibility of a reaction: if the reduction process is reversible the difference between the anodic and cathode peak potentials, (peak-to-peak separation, ΔE_p), is 57 mV at 25 °C and the maximum half-width on the forward scan of the peak is 59 mV. In the case, the reaction is not reversible the peak of the reverse scan would be absent or significantly reduced.[84] [83]
- electrochemical reversibility: refers to the electron transfer kinetics between the electrode and the electrolyte. When there is a low barrier to electron transfer, electrochemical reversibility occurs. Conversely, when there is a high barrier to electron transfer at the electrode/electrolyte interface (electrochemical irreversibility), electron transfer reactions are slow and more negative (positive) potentials are needed to observe the reduction (oxidation) process. In this case, the voltage variation imposed by the potentiostat undergoes a delay before being transferred to the electrode, giving rise to greater ΔE_p . [84] [83]

- the presence of multistep electrochemical reactions (one peak for each electrochemical step) and the presence of chemical reactions that occur before and after the electrochemical reactions (EC, CE and ECE mechanisms).[84]
- understanding of the amount of sulfur used for energy storage (in the case of lithium-sulfur). [85] [82]

The image below (Figure 4.4) shows a typical CV curve for a lithium-sulfur battery.

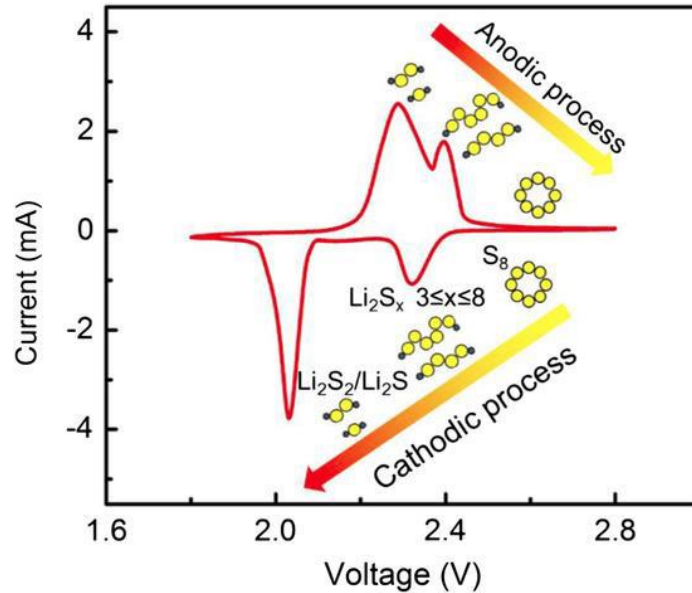
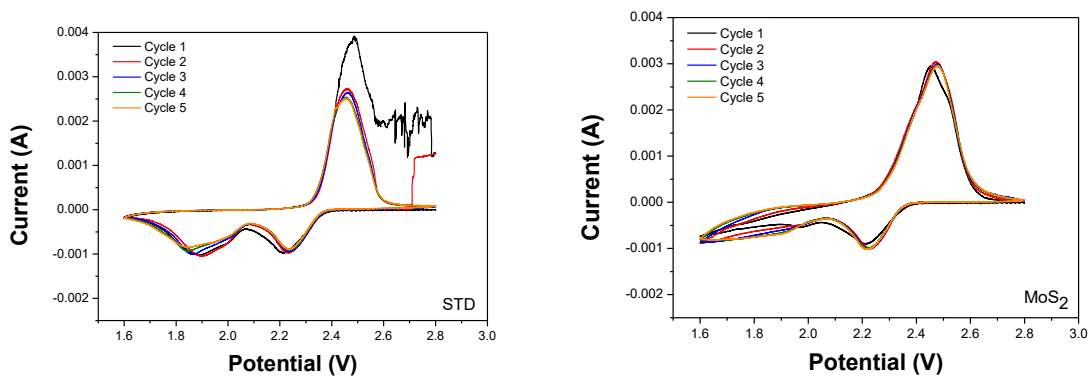


Figure 4.4: Typical CV curve obtained from a Lithium Sulfur battery with a scan rate of 0.1 mV s^{-1} . [82]

From this curve it is possible to see:[65]

- *Two cathodic peaks*: the first reduction peak positioned at 2.4–2.2 V involves the conversion of solid S_8 to soluble Li_2S_n ($3 \leq n \leq 8$) while the second peak at 2.1–1.9 V corresponds to the reduction of Li_2S_n to $\text{Li}_2\text{S}_2/\text{Li}_2\text{S}$.
- *Two anodic peaks*: positioned at 2.2–2.6 V and corresponding to the oxidation of lithium sulfide in LiPS/sulfur. During the anodic scan, the peaks may be overlapped or otherwise be very close to each other. [82]

The CV curves for each sample (5 cycles) are reported (Figure 4.5):



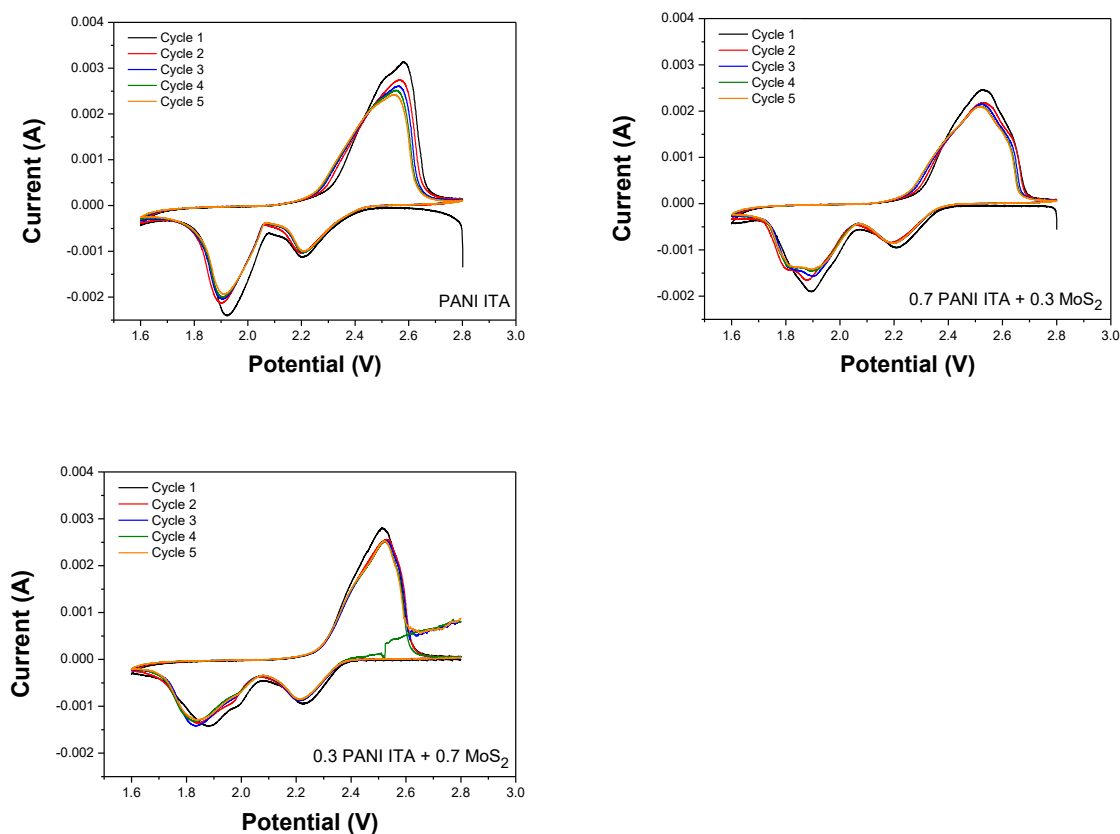


Figure 4.5: Diagrams reporting for each sample the cyclic voltammetry plot of the first five cycles.

In the following graphs (Figure 4.6), it is possible to see instead the CV curves of the first and fifth cycles of cells having the cathode coated with the following materials: MoS₂, PANI ITA and EX-SITU composites, containing respectively 0.7 and 0.3 g of PANI ITA. To these samples is added the Standard that contains only the cathode without double layer.

For both first and fifth cycles of the Standard component, are reported the values at which the oxidation and reduction reactions occur.

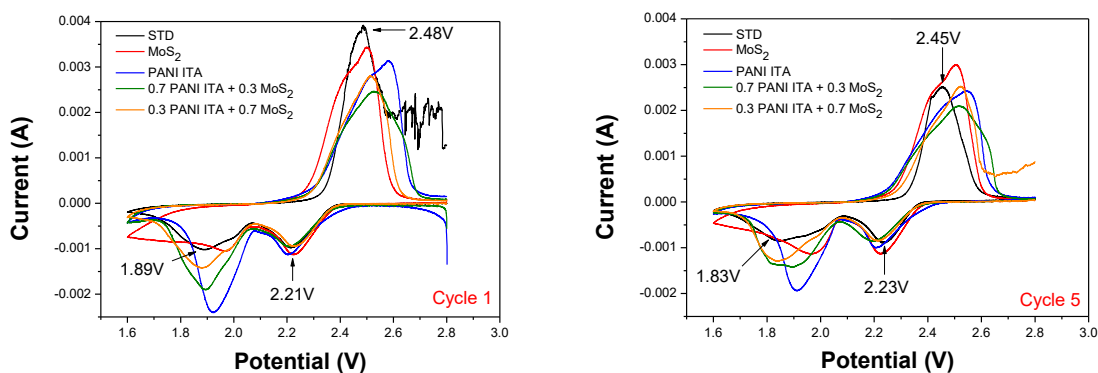


Figure 4.6: Comparison of the cyclic voltammetry diagram at cycle 1 (left) and cycle 5 (right) for all the samples electrochemical analyzed

From a first comparison with the data found in literature, it can be concluded that the positions of the peaks of the Standard sample are in line with those of a typical Lithium-Sulfur cell. The only value that is lower is that relating to the second reduction peak of the Standard sample at the fifth cycle (1.83V vs 2.1-1.9V). In addition, this peak is also more extended than the others.

Table 4.3: Comparison between the peak values found in the literature for a Li-S battery and those experimentally obtained for the standard (STD) at cycle 1 and cycle 5

Samples:	1st reduction peak:	2nd reduction peak:	Oxidation peak/s:
Literature	2.4–2.2 V	2.1–1.9 V	2.2–2.6 V
Standard (Cycle 1)	2.21 V	1.89 V	2.48 V
Standard (Cycle 5)	2.23 V	1.83 V	2.45 V

Looking more carefully at the graph relating to the first cycle (Figure 4.7):

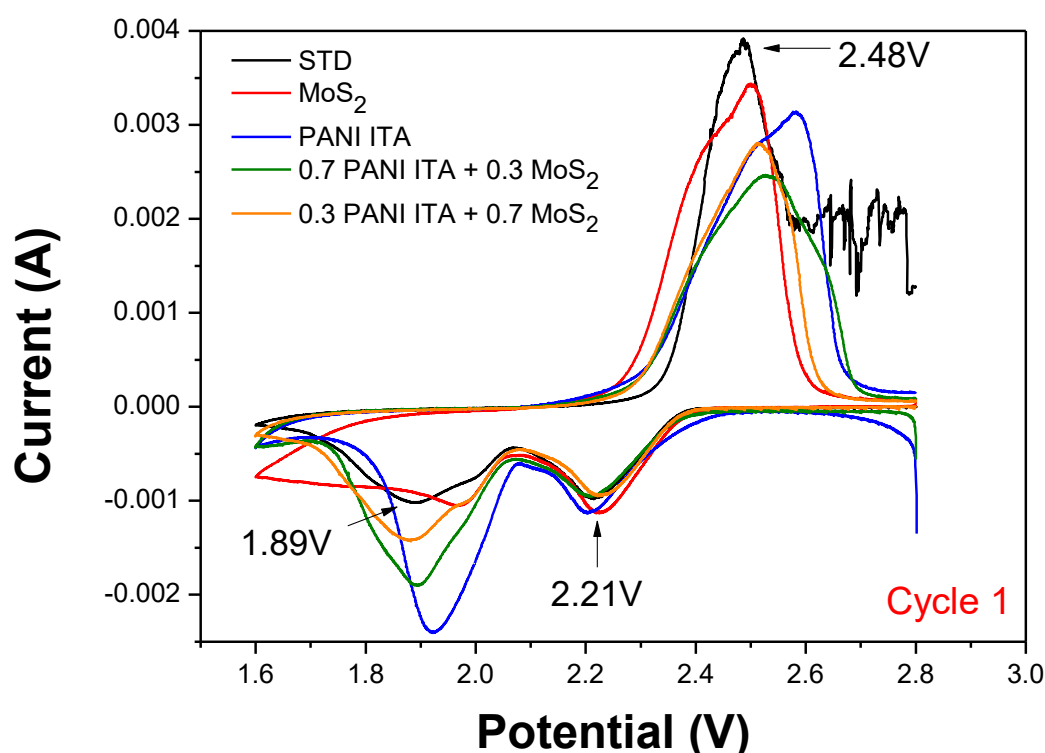


Figure 4.7: Cyclic voltammetry (cycle 1) in which are highlighted the peaks related to the standard STD

The first reduction peaks of all the samples are very similar in shape and height and almost superimposable. What changed markedly for the different materials are the second reduction peaks. In fact, while the peaks of the ex situ composites are well aligned with that of the Standard sample, those of MoS₂ (1.92 V) and PANI (1.97 V) are shifted towards higher potentials. It can also be observed that the PANI peak is the most defined and symmetrical one. This trend tends to decrease as the content of this material decreases within the cathodic composition. The sample containing only MoS₂ is just hinted at and asymmetrical. Similar considerations can be made for the STD cathode. Another interesting aspect is that the curves relating to the two composites seem to derive from the superposition of the curves containing respectively only PANI and only MoS₂. This behaviour can be deduced both from the intermediate height of these peaks with respect to that of the two single materials but also from the presence of small shoulders on both branches of the peak.

All the oxidation peaks tend to move towards increasing voltages. An enlargement in the peak itself often accompanies this shift. The extension over a wide range of voltages can indicate the presence of numerous species that undergo the anodic reaction at a different potential. These species can be polysulphides with different chain length.

The shift of the peaks mainly concerns PANI, which reaches a value of 2.58V and to a lesser extent, the two ex situ composites. Moreover, PANI and MoS₂ are the only samples with an evident shoulder, and this is located at lower voltages respect the two oxidation peaks. Composites, the one containing 0.7g PANI ITA, instead present a pattern with two small shoulders, one on the right and the other on the left of the peak.

Finally, the shift of the anode peaks compared to the cathode peaks also translates into a higher voltage range between them. This phenomenon could indicate an increase in cell polarization.

Looking at the graph (Figure 4.8) relating to the fifth cycle:

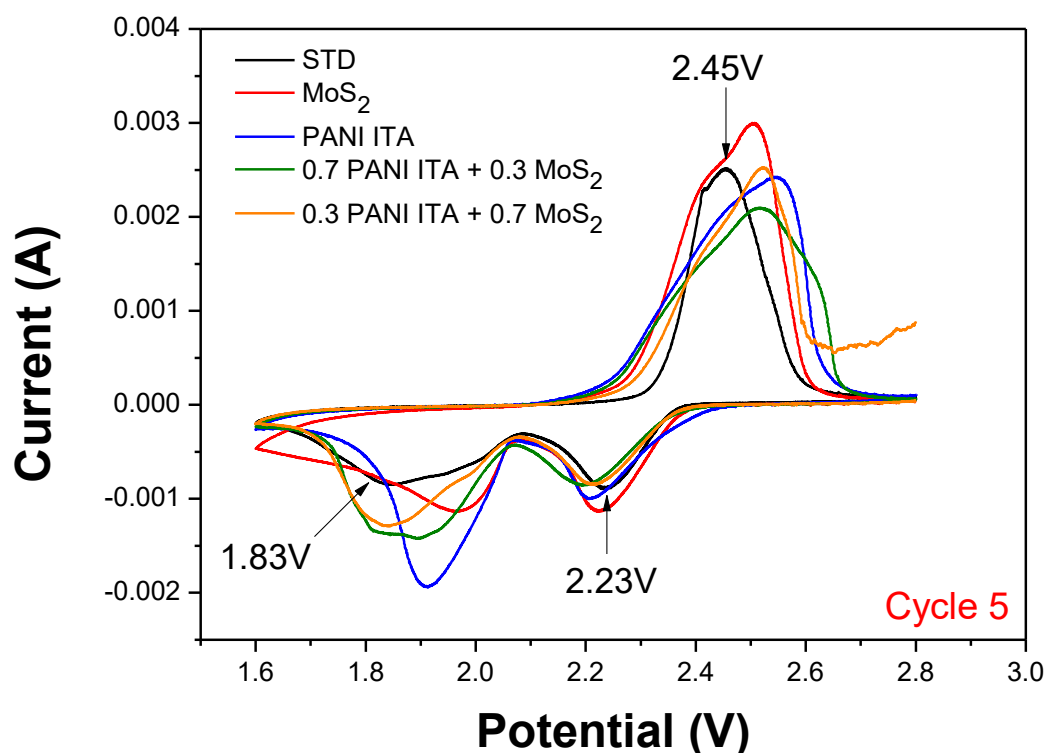


Figure 4.8: Cyclic voltammetry (cycle 5) in which are highlighted the peaks related to the standard STD

Also in this case, the considerations relating to the shift of the peaks towards higher voltages and those relating to the presence of shoulders remain valid.

The main differences, instead, lie in:

- the height of the oxidation peak (now the largest one is that of MoS₂)
- the first reduction peak, in this case, less superimposable to each other
- the area delimited by the CV curve which is overall less than the graph obtained for the first cycle. As the number of cycles increases, the amplitude of the reduction peaks decreases and with it the capacity. This loss may be since long-chain polysulphides are trapped in the double layer and that they can no longer be reduced or oxidized in the discharge and charge phases.

To separate the contribution of the two materials used for the realization of the double layers (MoS₂ and PANI) from the reactions involving the reduction-oxidation of sulfur and its products, two other cells without this element were mounted.

In this case (Figure 4.9), the layer previously applied as a coating for the electrode was used instead of the cathode.

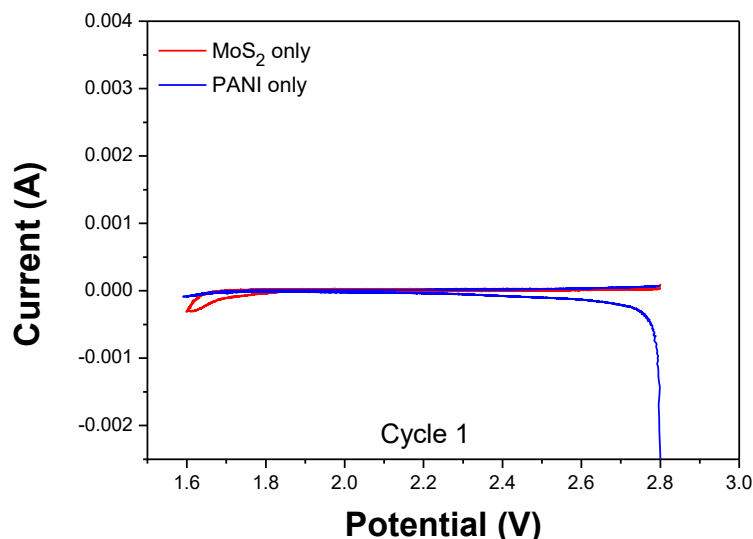


Figure 4.9: Cyclic voltammetry carried out only on the active materials (MoS₂ and PANI) in order to separate their contribution from that of sulfur.

Since no peaks appear in this curve, it can be deduced that PANI and MoS₂ are non-electroactive species in the voltage range investigated. However, a small background current still flows between the electrodes, also called capacitive current, double-layer current or non-Faradaic current. The intensity of the current varies linearly with the scan rate used and allows to verify that all the components of the cells are in good condition. [84]

4.2.2. Galvanostatic cycling

To study the electrochemical performance of a given material, two essential tools are usually used: galvanostatic and potentiostatic cycling methods. While the potentiostatic cycling focuses on the mass-transfer and diffusion process that occur during electrochemical reactions, the galvanostatic methods is used to establish the kinetics and reaction mechanisms of the electrode. [11]

Using the latter approach, the cells are practically subjected to charging and discharging cycles in which the current flowing through the cell is constant, at a specific C-rate. This current is imposed through an external source (Arbin cycle) and calibrated based on the quantity of sulfur (active material) contained in the cathodic composition.

During the analysis process, the potential variation (V) of the cell, as a function of time, is recorded. The output of this test, consists of a graph with the potential (V) on the y-axes and the time (or cell capacity, expressed in mAh g⁻¹) on the x-axes.

The potential profile of a lithium-sulfur cell generally shows the typical discharge plateaus, previously encountered:

- one at about 2.3V, relating to the reduction of octahedral sulfur in long-chain polysulfides (which contributes little to the loss of total capacity)
- the other at around 2 ~ 2.1V, relative to the reduction of Li_2S_2 and Li_2S (which contributes significantly to the loss of cell capacity). [25] [82]

It can, therefore, be noted that exists a complementary relationship between the cyclic voltammetry and the galvanostatic cycling process. However, in the first, the reactions are represented by peaks, while in the discharge-charge process through plateau.

The voltage profiles obtained can be used to evaluate the changes in electrochemical performance during cycling and for:

- qualitatively compare different cells with each other (determining if and for what voltage values the typical electrochemical reactions of a battery develop)
- determine the capacity of the cell as the number of cycles increases (quantity of electric charge that the cell can deliver), both during charging and discharging phase. The theoretical sulfur capacity, measurable from an ideal cell, should be 1675 mAh g^{-1} .
- follow the degradation processes that occur as a result of the use of the cells
- estimate the coulombic efficiency (ratio between the discharge and charge capacity of the battery)
- understand the reversibility of a cycling process and in particular, if a given cell can maintain a high capacity for the duration of the measurement. [86]

The analysis can be performed for different periods. For example, cycling can be stopped after a certain number of cycles or after a specific time interval. This approach is generally followed to evaluate specific cell characteristics (such as capacity and impedance) at predefined intervals. Another method, typically the most used, involves measuring for long periods of time until the EOL conditions (End Of Life, which is often made to correspond to 80% of the initial capacity) are reached.

Another critical parameter, as mentioned above, is the C-rate. By adjusting this, it is possible to modify the cycling mode. It is spoken, for example, of symmetrical cycles when the same C-rate (e.g. 1C) is used both during the charging and discharging phase or asymmetrical cycling when the rate is varied in the two stages. In this way, the type of C-rate allows for evaluating several characteristics. In general, to analyze the cell degradation process, it is better to use higher C rates and therefore, shorter recharge times. [86]

In this case, the analyzes were made at: $I = C / 10$ for the first three cycles and at $I = C / 5$ the remaining ones. This means that the process lasted for 10 hours in the first case, with a capacity discharge of 0.1675A per hour (if it is considered $C = 1675 \text{ mAh / g}$ like in the ideal case) and 5 hours in the second case with a capacity of 0.335A per hour.

For each sample, the graphs containing the charge-discharge curves at cycles 1-2-3-5-10-50-100 are shown below. The samples considered (STD, MoS_2 , PANI, the three ex-situ composites and the hydrothermal one) were compared with regards to capacity and polarization.

1. Capacity values are related to the sulfur quantity, which is reduced during the reactions. A high value of this parameter is consequently desirable since it indicates a higher sulfur activity and a plausible less motion of the polysulfides. [25] [87]
2. The polarization (ΔE) is the difference in voltage between the charge and discharge curve that gives instead information on the reaction kinetics. The voltage gap is related to the ionic and electronic transport paths and therefore, to the adsorption surfaces of the samples that can or not favour them. In this case, a reduction of this parameter is desirable. [25] [65] [66] [88]

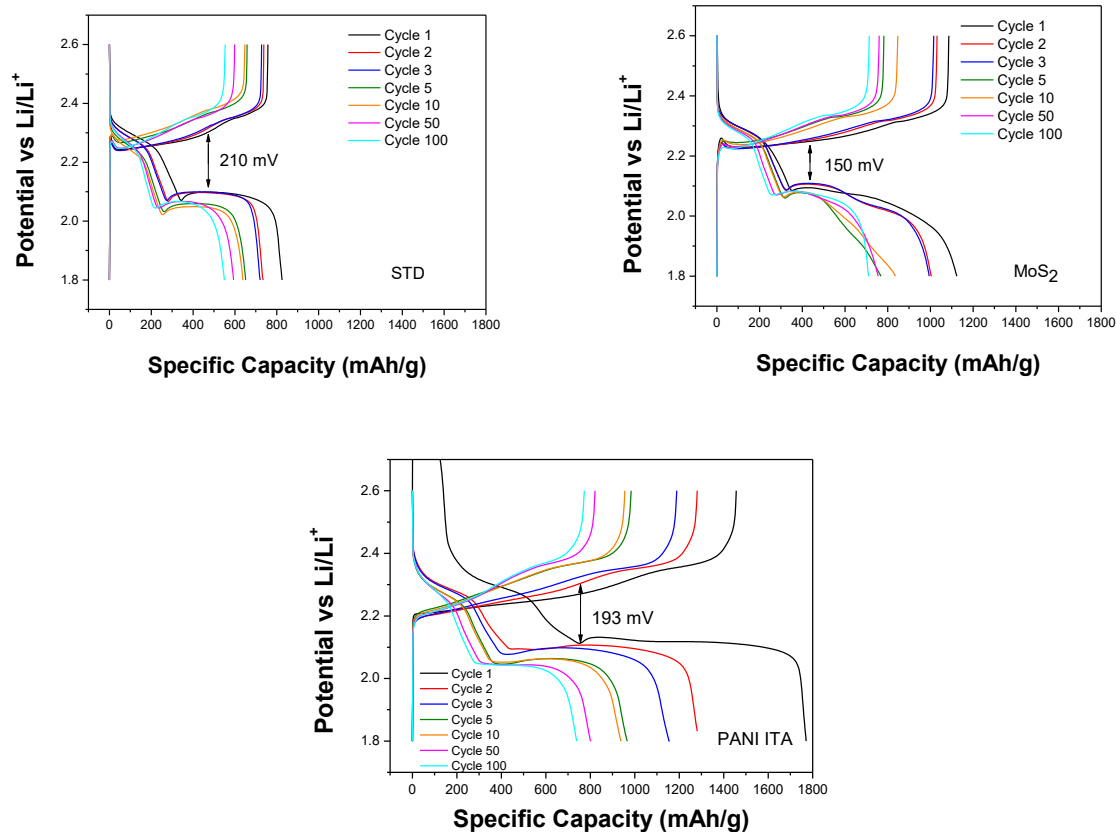


Figure 4.10: Galvanostatic cycling for STD- MoS₂ and PANI ITA with current $C/10$ for cycles 1-2-3 and current $C/5$ for cycles 5-10-50-100.

The three graphs (Figure 4.10) respectively show an uncoated cathode (STD), a cathode layered with only MoS₂ and one coated with Italian PANI. From these graphs, it can be easily seen how the cell containing a standard cathode present a low capacity (about 800 mAh g⁻¹ for the first cycle, which decreases with increasing of the cycles number). At the same, this cell has a rather high ΔE (210 mV) an indication of rather high polarization.

The cell containing the cathode coated with MoS₂ still presents low capacity, but at the same time shows a polarization lower than the other two cases. This aspect could be connected to a possible catalyst action by MoS₂. Another interesting feature of this component lies in the potential instability observable in the discharge curve. While the other cells show a second broader plateau indicating that the reactions from soluble S₄²⁻ to insoluble Li₂S₂/ Li₂S have a slow kinetic, the cell containing MoS₂ instead shows a very short second plateau followed by a third step.[65] [88] It seems, in fact, that a further plateau appears on this branch, and this is especially visible for the 2nd and 3rd cycles.

The cell containing PANI in the Double layer, instead, shows very high capacities (especially for the first cycles) and an intermediate ΔE compared to the two previous cases. Polyaniline in fact present a specific energy between 100 and 200 Wh/Kg which is one-tenth that of sulfur. [42]

These characteristics make the cell containing a conventional uncoated cathode the worse battery both in terms of available capacity (cell performance) and process kinetics (ΔE). It could, be said that regardless of the coating materials (MoS₂ and PANI), this element could help to increase the cell performances.

In the following graphs (Figure 4.11), the two EX-SITU composites containing respectively 0.7g Italian PANI-0.3g MoS₂ and 0.3g Italian PANI-0.7g MoS₂ are reported.

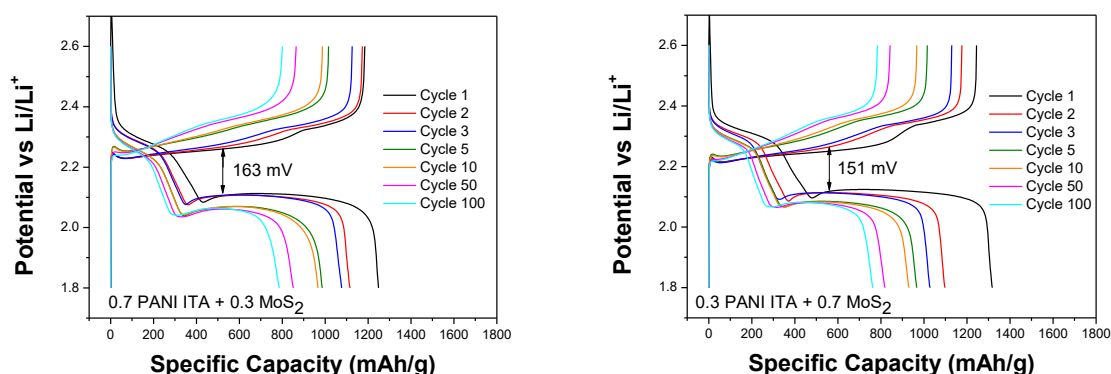


Figure 4.11: Galvanostatic cycling for the EX-SITU composites containing 0.7g PANI ITA -0.3 g MoS₂ and 0.3g PANI ITA-0.7g MoS₂ with current $C / 10$ for cycles 1-2-3 and current $C/5$ for cycles 5-10-50-100.

From a comparison between the two images, it appears evident that the ΔE values are in good accordance with what has been seen previously. In fact, in the sample containing a higher quantity of PANI, the polarization is more significant, while in that containing more MoS₂, the polarization rate is lower. The values of these gaps (163 mV in the first case and 151 mV in the second case) present intermediate values between that obtained for only PANI (193 mV) and that obtained for only MoS₂ (150 mV).

For what about the capacities values (excluding the first cycle) instead, they result very similar to each other.

Finally, the graphs relating to the EX-SITU composite containing 0.3g Portuguese PANI-0.7g MoS₂ and the hydrothermal composite (Figure 4.12) are shown.

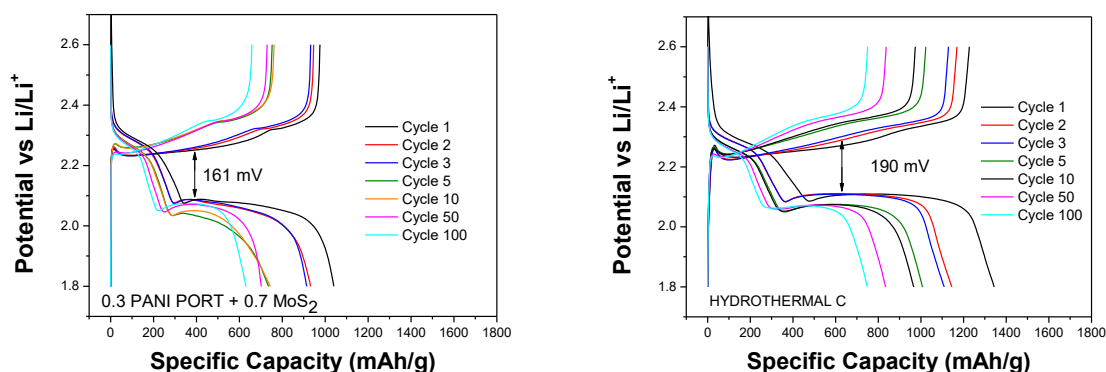


Figure 4.12: Galvanostatic cycling for the EX-SITU composites containing 0.3g PANI PORT -0.7 g MoS₂ and hydrothermal composite with current $C / 10$ for cycles 1-2-3 and current $C/5$ for cycles 5-10-50-100.

It is interesting to note that the graph concerning to the first sample is very similar to that already obtained for only MoS₂. This similarity involves both the achievable capacity values and the strong potential instability on the discharge curve. Also, in this case, it could be observed the presence of a curvature which could hint the presence of a third plateau.

As regards the hydrothermal composite, this presents instead a very regular potential profile (both in the charging and discharging phase). The capacity values are like those found in the case of EX-SITU composites with Italian PANI while the ΔE is slightly lower than that of the STD and the only PANI.

In conclusion, it can be said that all cells that have a double layer consisting of a composite material (EX-SITU or hydrothermal) on the cathode, present better characteristics than the one without coatings. Besides, composite materials generally have (especially as regards EX-SITU composites) intermediate properties between those relating to PANI only and those about MoS₂ only.

To better highlight, this latter aspect (especially concerning the obtainable capacity values) the STD cell and the samples containing as coating materials MoS₂, PANI ITA and the two EX-SITU composites (with Italian PANI), are shown in the same graph at specific cycle numbers.

For completeness, also the graph relating to the first cycle is shown. The reactions that occur during the first operation phase of the battery are multiple and complex, so deciphering this graph is not an easy issue. However, it is possible to observe what has been said above, namely that composites tend to present intermediate properties to those of only PANI and only MoS₂ and superior to those of STD. As the following graphs show (Figure 4.13), this trend remains unchanged until the fifth cycle.

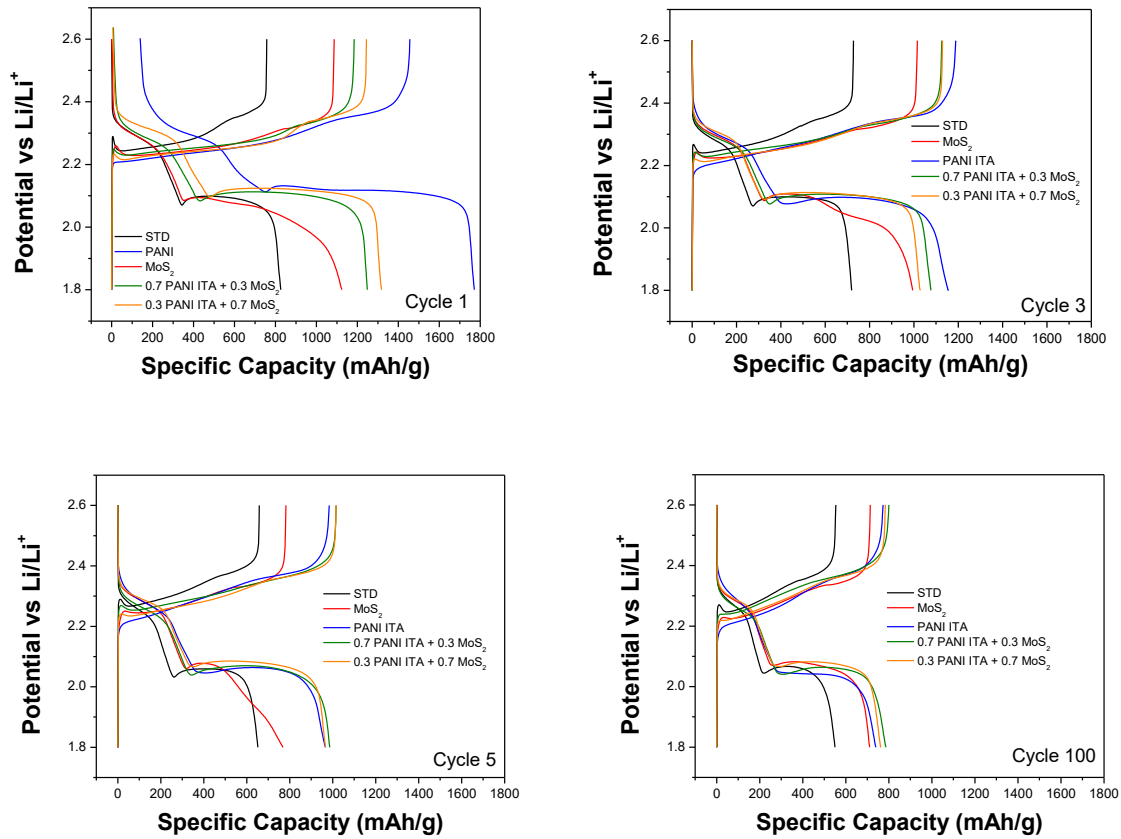


Figure 4.13: Comparative galvanostatic cycling analysis (at the same number of cycles) of all the samples analyzed. Current $C/10$ for cycles 1-3 and current $C/5$ for cycles 5-100.

Starting from the fifth cycle, the cell containing PANI shows a more significant loss in capacity compared to the two EX-SITU composites. The capacity of the STD remains the lowest obtainable; this justifies the insertion of a double layer on the cathode.

Further information that can be extrapolated from the data provided by the charge and discharge curves are the specific capacity values of the cell as a function of the number of cycles. These characteristics are obtained through graphs that report the capacity values on the y-axis and the cycles number on the x-axis.

By comparing the same materials (STD, PANI, MoS_2 , and the two EX-SITU composites with Italian PANI) on this kind of graphs, respectively at 100 and 500 cycles (Figure 4.14), what can be observed is:

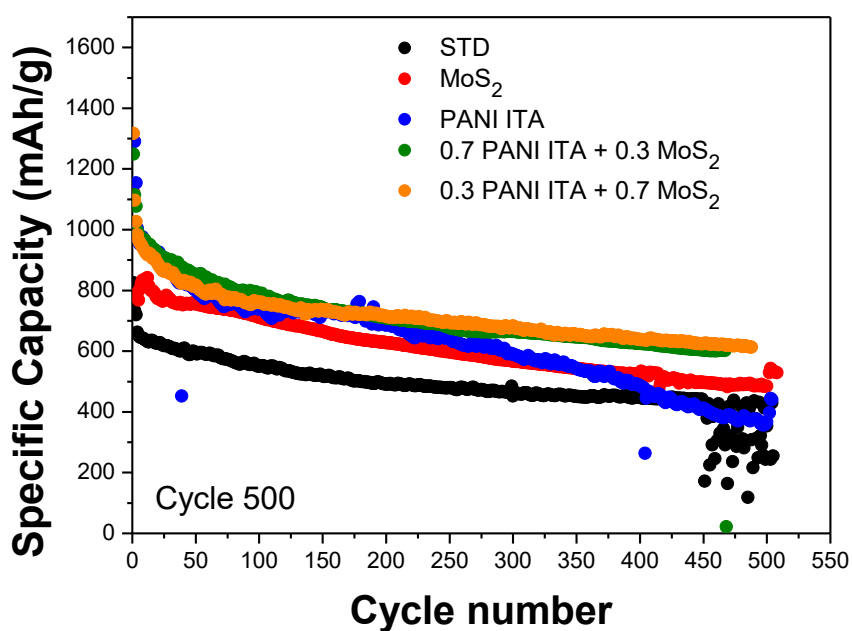
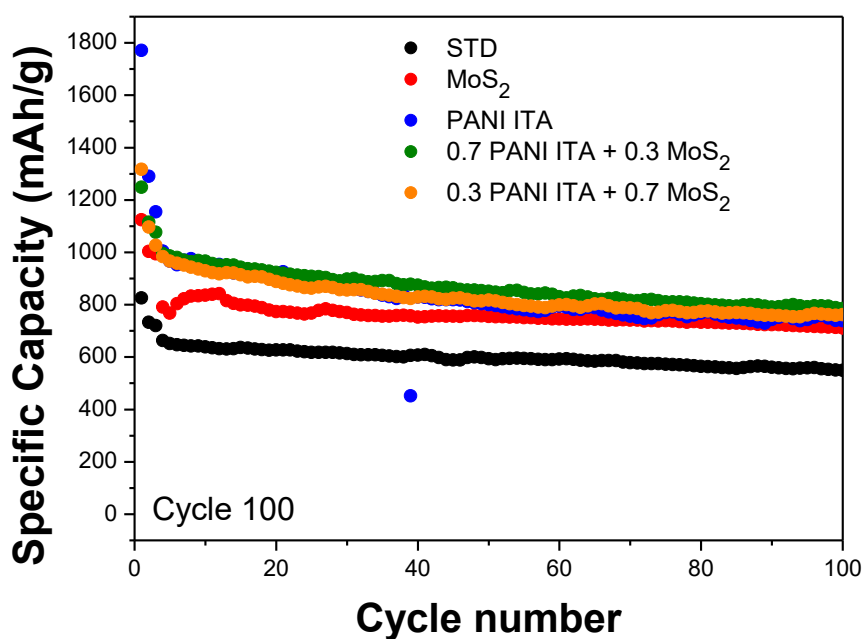


Figure 4.14: Comparison in terms of Specific Capacity on Cycle number between STD, PANI, MoS₂ and the two EX-SITU composites containing Italian PANI respectively at 100 (top) and 500 cycles (bottom).

From the two graphs above (Figure 4.14), among all the samples, the standard one has the lowest capacity values. The curve of the STD starting from 450 mAh g⁻¹ reaches in a linear and constant way the 550 mAh g⁻¹ value at 500 cycles. However, in close proximity to this cycle number, it is possible to witness the polysulfide Shuttle phenomenon highlighted by a strong instability in the capacity values

and a rapid decrease in this characteristic up to about 100-150 mAh g⁻¹. No other sample presents such behavior; therefore, the Shuttle mechanism can be excluded for them.

Then MoS₂ follows which, starting from 750-800 mAh g⁻¹, reaches mAh g⁻¹ after the same number of cycles. Also, in this case, the trend is almost linear, but the loss in capacity is more significant.

A different situation occurs for the Italian PANI. Initially, the curve appears to be mainly overlapping with that of the two EX-SITU samples. Still, starting from 150 cycles, the curve begins to rise again for drops suddenly after with an irregular profile. PANI thus passing from 1000 to 350 mAh g⁻¹, shows the most severe loss before 500 cycles, compared to all the other samples. The capacity increase (at about 200 cycles) could be related to the growth of a PS resistive layer on the PANI surface.[65] [88]

Finally, the curves of the two EX-SITU composites can be observed. These materials have a very straight and regular loss of capacity which, starting from 1000 mAh g⁻¹, reaches mAh g⁻¹ after 500 cycles. Initially, the composite containing 0.7g of Italian PANI and 0.3g of MoS₂ presents a slightly higher capacity. Then the two curves meet definitively at about 200 cycles and proceed in a superimposed manner until the end of the period.

The graphs just analyzed are shown below separately, with the addition of the charge curve and the coulombic efficiency (Figure 4.15). This characteristic is reported on the opposite axis to that of the specific capacity.

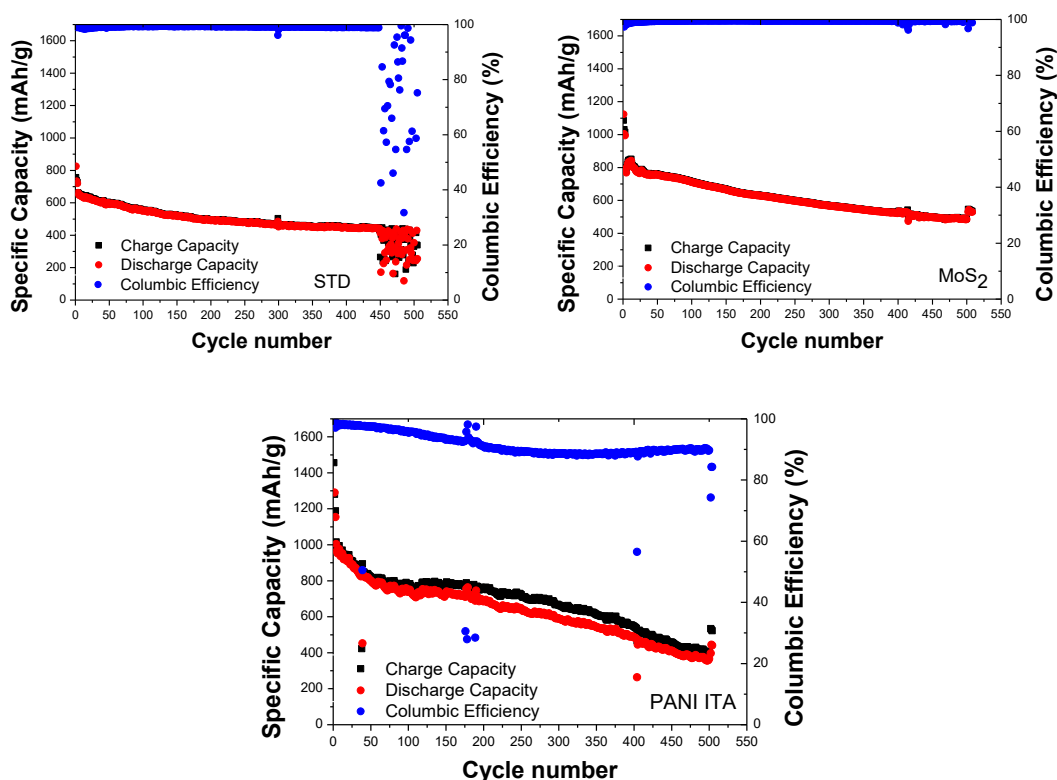


Figure 4.15: Columbic efficiency curves for: STD, MoS₂ and PANI ITA

From these images, the charge and discharge curves are in all cases, except for the Italian PANI, perfectly superimposable. The Italian PANI shows in the central area of the graph, a clear separation between the two curves, which then return to meet each other at high numbers cycles number (about 400). MoS₂ and STD exhibit, instead, excellent Columbic efficiencies. In the first case, these properties

remain equal to about 99-100% till the end, while in the second case it maintains at the same values until the Shuttle phenomenon occurs. At that point, Columbic efficiency decreases rapidly.

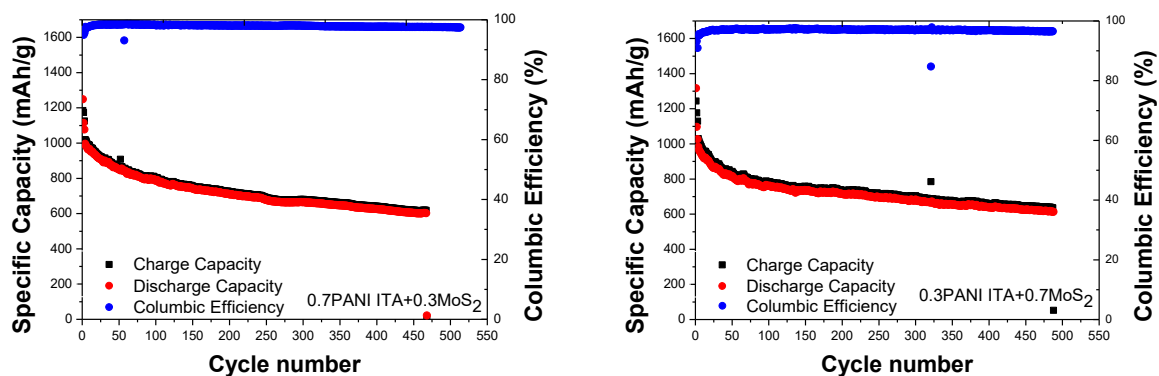


Figure 4.16: Columbic efficiency curves for the two EX-SITU composites with: 0.7g PANI Ita -0.3g MoS₂ (left) and 0.3g PANI ITA -0.7g MoS₂ (right)

As for the two composites (Figure 4.16), this parameter remains very high and constant (certainly more than the PANI) but at lower levels respect MoS₂. Moreover, the composite containing 0.7g PANI ITA has initially a very high efficiency, which then settles at values close to 97% in the final part of the graph. As for the composite with 0.3g PANI ITA efficiency does not decrease when the number of cycles increases but remains at a lower value corresponding to 96%.

4.2.3. Catalytic Effect (TAFEL)

The Tafel equation, and the corresponding graph, are used in electrochemistry to evaluate the kinetics and thermodynamics of chemical reactions and to understand their physical origin. This equation allows to obtain a quantitative relationship between the chemical reaction, the measurable electric current (i) and the external potential (U); therefore, a connection between the current electrochemical potential and the applied one.

The measurement of the electric current i , is that which allows establishing the rate of the reactions and therefore to deduce information on the process kinetics.

The relationship linking the various quantities within the Tafel equation is a linear correlation between $\log i$ and overpotential (η). [89]

$$\eta = a + b \log i \quad (4.1)$$

$$(\eta = U - U_0) \quad (4.2)$$

$$b = \frac{2.3RT}{\alpha F} \quad (4.3)$$

Parameter b represents the slope of the Tafel graph ($\log i$ vs η) and is a fundamental quantity as it allows to establish the catalytic performances of a given material.

This parameter can be obtained from an inverse proportionality relation to the Charge Transfer Coefficient (CTC), α in combination with the Arrhenius equation and the transition state theory. Also, α is an essential quantity in electrochemistry as it allows establishing the nature of the electron transfer in the elementary reaction. [89]

In this case, Tafel analysis was conducted to evaluate a possible catalyst function of MoS_2 and PANI with respect to the electrochemical reactions that occur in the cell; in particular, for those reactions that involve polysulfides conversion.

It has been shown that the "confinement" action of polysulfides has a relatively limited effect on improving battery performance. This phenomenon is because passively blocked LiPS have high activation energy at conversion and are challenging to reuse during reactions. [64] As a result, part of the active material is irreparably lost ("dead sulfur") and the internal resistance increases. [90] [66]

In this scenario, the use of materials which, in addition to blocking LiPs, allow their conversion to lithium sulfides (from long-chain soluble LiPS to insoluble short-chain $\text{Li}_2\text{S}_2/\text{Li}_2\text{S}$, from which the theoretical cell capacity derives, and vice versa) is consequently attractive. [64] Therefore, increasing the transformation speed of LiPS through materials capable of lowering the energy barrier of a redox reaction (by electrocatalysis) can be an excellent strategy to limit their transport (Shuttle effect) and develop a practically usable Li-S battery. [65] [66] [90]

To perform the measurement, a cell with a different configuration, respect the other seen so far has been mounted. In this case, the coating containing the material to be analyzed was made on a porous component called Gas Diffusion Layer (GDL). This material has a peculiar double-layer structure in which: one layer shows a macro-type porosity and a fibrous structure while the other a micro-type porosity. This hierarchical structure is chosen because it allows having a component that shows at the same time, excellent mechanical properties and a high surface.

As already done for other analysis, also in this case, a coating was created to be used as a reference (containing only Ketjen Black). Two additional samples were then made, providing MoS_2 and PANI. The ratios used between the various materials were 90%wt di Ketjen Black e 10%wt di PVDF and 80%wt di MoS_2 or PANI, 10%wt Ketjen Black e 10%wt di PVDF for the others.

In particular, the compositions that have been used for the coating layers are shown below (Table 4.4):

Table 4.4: Compositions used for the Tafel analysis

Samples:	KJB:	PVDF:	NMP:	MoS ₂ :	PANI:
1	0.09 g	0.125 g	1400 μ l	-	-
2	0.015 g	0.187 g	400 μ l	-	0.125 g
3	0.015 g	0.1875 g	400 μ l	0.125 g	-

After obtaining the cathodes, these were inserted into three different cells. A Celgard2325 separator was then placed on the electrodes. In this case, the Celgard was not wetted by a standard electrolyte but through a catholyte (20 microliters for each cell). Catholyte is a solution containing LiTFSF (1M) and Li₂S₆ polysulfides in which the long chain polysulfides act as the active material within the cells. A lithium anode was then placed on the separator, and the cells were closed and analyzed.

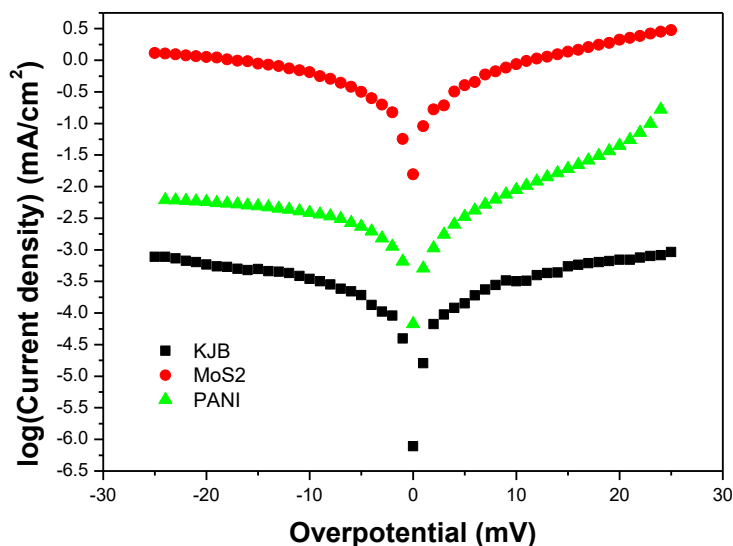


Figure 4.17: Tafel plot for KJB, MoS₂ and PANI ITA

From the test results (Figure 4.17), it can be seen that, in the case of the Ketjen Black cathode, the Tafel curve turns out to be quite symmetrical concerning the zero overvoltage value; this means that the presence of Ketjen Black does not significantly influence oxidation and reduction reactions. The same can be said for the MoS₂, which shows a similar trend. The sample containing the PANI instead presents the cathode branch with a markedly different curvature compared to that of the other two materials.

Another significant difference lies in the current values obtained. The three curves are translated along the y-axis. MoS₂ is the one with higher currents, followed by the PANI and finally by the KJB.

The higher exchange current density of MoS₂ compared to that of PANI and KJB shows its catalytic effect on the charge transfer kinetics (and therefore also on the kinetics of the electrochemical reactions). [90][64] These results (Figure 4.5) also suggest an increase in the conversion rate of LiPS. [4] [66]

Table 4.5: Exchange current density for the samples analyzed

	Oxidation	Reduction	Exchange current OX	Exchange current OX
KJB	-3.85262	-3.6228	0.00014*	0.00024*
MoS ₂	-0.42011	-0.42916	0.38009	0.37225
PANI	-2.73905	-2.56521	0.00182	0.00271

In literature, it is possible to obtain confirmations of these assumptions.[65] Arava and co-workers have discovered that the edge sites of atomically thin MoS₂ (which are also the ones that can show a much stronger interaction with Li₂S compared to the terrace counterpart) can lower the polarization and improve the kinetics of the electrochemical reaction. [4][61] [64]

5. Conclusion

During the first part of the experimental work, mainly aimed at the FCT University of Lisbon, various synthesis processes, both as regards the elemental components of the composite materials, and the composites themselves, were conducted. In particular:

- Two different forms of PANI (Italian and Portuguese) were successfully synthesised following the protocols provided in the two respective countries. FESEM, XRD and RAMAN analyses were then performed on obtained materials. Through the Field Emission Scanning Electron Microscopy, it was possible to highlight, between the two types of PANI, substantial morphological differences (poorly defined and compact structure for Italian PANI and a markedly tubular and open morphology for Portuguese PANI). Through the XRD analyses, it was also possible to put in evidence the semi-crystalline nature of both materials; while, with the RAMAN analyses, the characteristic peaks of the doped form of PANI, the only conductive structure of this polymer, have been identifying.
- Two different types of MoS₂ have been then analysed: the commercial form and the MoS₂ obtained through a hydrothermal process. For the synthesis of this second material, a solution with Sodium Molybdate and Thiourea was prepared, and let it react at high temperatures (200 °C) and pressures (280 Pa) in a microwave reactor. Characterisation analyses were then carried out. From FESEM analyses, it emerged that commercial MoS₂ has a bulk form consisting of numerous layers firmly adhered to each other while hydrothermal MoS₂ presents a nanoflower structure. RAMAN analyses allowed to recognise, in the first case, the phonon modes characteristic of the bulk of this material, while in the second case, the amorphous nature of the hydrothermal MoS₂. Although this material has an impressive structure, it has not been adopted in the creation of composite materials due to the minimal amount obtainable from each synthesis process.
- Finally, three different types of composite materials were produced. IN SITU composites (in which the polymerisation of Portuguese PANI was carried out within a solution containing commercial MoS₂); EX SITU (in which the two constituent materials, previously obtained independently, were mixed with different ratios through a nine-hour ultrasonication process), HYDROTHERMAL (in which, following the hydrothermal process already developed for the synthesis of MoS₂, the composite was obtained adding Portuguese PANI powder to the solution before it was subjected to the microwave process). FESEM analyses carried out on the three samples showed evident morphological differences within three types of samples. Furthermore, while for the EX-SITU and IDROTHERMAL composites, it was possible to identify both phases, this did not happen in the case of IN-SITU composites. RAMAN analyses also showed the lack of the MoS₂ peak. During this phase, a simple method to exfoliate commercial MoS₂ was also proposed.

During the second phase of the experimental work, totally done at the Politecnico of Turin University (Italy), the samples were analysed from an electrochemical point of view. Since the most encouraging results were those on EX-SITU composites, they were optimised by making materials containing 0.7g of Italian PANI-0.3g of commercial MoS₂ and 0.3g of Italian PANI-0.7g of commercial MoS₂ respectively. Therefore, four coating mixtures were made to be applied as Double-Layer (80:10:10) on the cathode, two of which containing composite materials and two containing respectively only Italian PANI and only commercial MoS₂. Finally, to have a comparison with the untreated cathode, a cell (STD) without coating was assembled.

- From the electrochemical analyses carried out (Galvanostatic Cycling, Cyclic Voltammetry), it was possible to observe how the Double-Layer applied does not change the typical behaviour of the Li-S batteries. From the graphs, it is possible to highlight also the typical oxidation-reduction reactions of Sulfur and the polysulfide species. In particular, the plateau at 2.3 V

relates to the octahedral Sulfur reduction in long-chain polysulphides while that at 2-2.1V relates to the reduction to Li_2S_2 and Li_2S . It was also highlighted that the two cells containing composite materials have less polarisation and higher specific capacity.

- Moreover, the two composites, as well as the Italian PANI, showed higher initial capacity values than those of the other two cells. Unlike the PANI, however, the cells containing the composites showed a steady trend in capacity and a rather slight decrease in its held values, reaching a value of 600 mAh g^{-1} after 500 cycles. It emerged also that only the curve relating to the STD standard shows the phenomenon of the Shuttle.
- In the end, TAFEL analyses on the two main essential elements (Italian PANI and commercial MoS_2) and Ketjen Black (mesoporous carbon used both in the cathodic composition and for the realisation of the Double-Layers) were carried out. From the Tafel plot, it is possible to highlight the intense catalytic activity of MoS_2 , thanks to the high exchange current values detected.

According to the results of the analyses carried out, it can, therefore, be deduced that the presence of a Double-Layer (whether it consists of only Italian PANI, only commercial MoS_2 or both composites) allows preventing the Shuttle phenomenon. It can also be said that the cells containing the composites have better electrochemical performances than the others, confirming the catalytic and anchoring action of the materials that make them up, as well as the achievement of the thesis aim.

Abbreviations

IEA – International Energy Agency

EES – Electrical Energy Storage

Li-S – Lithium-Sulfur

PANI – Polyaniline

PS – Polysulfides

DC – Direct Current

OCV – Open-Circuit Voltage

IHP – Inner Helmholtz Plane

OHP – Outer Helmholtz Plane

SOC – State Of Charge

LCO – $LiCoO_2$ – Lithium Cobalt Oxide

LMO – $LiMn_2O_4$ – Lithium Manganese Oxide

NCA – $LiNi_{0.8}Co_{0.15}Al_{0.05}O_2$ – Lithium Nickel Cobalt Aluminium Oxide

NMC – $LiNi_{0.33}Mn_{0.33}Co_{0.33}O_2$ – Lithium Nickel Manganese Cobalt Oxide

LFP – $LiFePO_4$ – Lithium Iron Phosphate

LCA – Life Cycle Assessment

GHG – Green House Gas

HTP – Human Toxicity Potential

MDP – Materials Depletion Potential

GWP – Global Warming Potential

FDP – Fossil Depletion Potential

PHEV – Plug-in Hybrid Electric Vehicle

EV – Electric Vehicles

PLIB – Post-Lithium Ion Batteries

CDC – Carbide Derived Carbon

LiPS – Lithium Polysulfide

PS – Polysulfide

CRM – Critical Raw Material

LIB – Lithium Ion Battery
SEI – Solid-Electrolyte Interface
EC – Ethylene Carbonate
PC – Propylene Carbonate
DMC – Dimethyl Carbonate
DEC – Diethyl Carbonate
DOL – 1,3-Dioxolane
DME – 1,2-Dimethoxyethane
TEGDME – Tetra (Ethylene glycol) Dimethyl Ether
LiTFSI – Lithium bis(trifluoromethanesulfonyl)imide
PVDF – Poly (vinylidene difluoride)
PEO – Polyethene oxide
PEMO – Poly(ethylene-methylene oxide)
IL– Ionic Liquid
LISCON – Lithium super-ionic conductors
CNT – Carbon Nano-Tubes
CP – Conductive Polymer
ECP – Extrinsicly Conductive Polymers
ICP – Intrinsic Conductive Polymers
PAc – Polyacetylene
PPy – Polypyrrole
PEDOT – Poly (3,4-ethylene dioxythiophene)
PPP – Poliparaphenylene
LSB – Lithium-Sulphur batteries
SCP – Supercapacitors
LEB – Leucoemeraldine
EB – Emeraldine
PE – Pernigraniline
TMD – Transition Metal Dichalcogenides

DFT – Density Functional Theory

CB – Conduction Band

VB – Valence Band

CBM – Conductive Band Minimum

VBM – Valence Band Maximum

CHP – N-cyclohexyl-2-pyrrolidone

XPS – X ray Photon Spectroscopy

CVD – Chemical Vapour Deposition

MOCVD – Metal-Organic Chemical Vapour Deposition

FCT – Faculdade de Ciências e Tecnologia

FESEM - Field Emission Scanning Electron Microscopy

PSA – Ammonium Peroxydisulfate

CSA – Camphor-10-sulfonic acid, beta

XRD – X-ray Diffraction

EDS – Energy Dispersion X-ray Spectroscopy

KJB – Ketjenblack

NMP – N-Methyl-2-Pyrrolidone

CV – Cyclic Voltammetry

WE – Working Electrode

CE – Counter Electrode

RE – Reference Electrode

EOF – End Off Life

CTC – Charge Transfer Coefficient

GDL – Gas Diffusion Layer

Simbols

CO_2 – Carbon dioxide

C – Celsius

MoS_2 – Molybdenum Disulfide

I – Current

V – Voltage

O – Oxidized species

z – Electrons

R – Reduced species

E_{cell} – Theoretical cell voltage

$E_{positive}$ – Standard potential at the positive electrode

$E_{negative}$ – Standard potential at the negative electrode

ΔG_{cell} – Gibbs Free Energy

n – Number of electrons exchanged

F – Faraday constant $96.485 \text{ C mol}^{-1}$

ΔG_{prod} – Free Energy of the products

ΔG_{react} – Free Energy of the reagents

μ_i – Chemical potential of the i species

μ_{prod} – Chemical potential of the products

μ_{react} – Chemical potential of the reagents

Σ – Summation

a – Activity

μ_i^0 – Standard chemical potential for species i

R – Gas constant

T – Temperature [K]

$\Phi_{electrode}$ – Electrostatic potential in the electrode

$\Phi_{electrolyte}$ – Electrostatic potential in the electrolyte

$\Delta\phi$ – Galvani potential

E^0 – Standard potential

H_2 – Hydrogen

H^+ – Reduced Hydrogen

i_0 – Exchange current

η – Overpotential

α – Transfer coefficient

η_{ct} – Activation polarisation

η_c – Concentration polarisation

IR – Ohmic polarisation

Q – Total charge

Q_{th} – Theoretical specific capacity

M_w – Molecular weight

Q_{dis} – Charge transferred during the discharging process

Q_{cha} – Charge transferred during the charge process

$\eta_{Coulombic}$ – Coulombic efficiency

η_{Energy} – Energy efficiency

j – Current density

A – Normal surface

Li – Lithium

S – Sulfur

S_8 – Octahedral Sulfur

Li_2S – Lithium Sulfide

0D – Zero dimension

1D – One dimension

2D – Two dimension

3D – Three dimension

M – Cation

A – Anion

R – Reduced base units of PANI

O – Oxidised base units of PANI

Γ – Brillouin point

K – Brillouin point

E_{21g} – In-plane vibration modes of the S atoms

A_{1g} – Out-of-plane vibration modes of the S atoms

ΔE_p – Peak-to-peak separation

ΔE – Voltage difference

U – External potential

i – Electrical current

b – Slope of Tafel graph

α – Charge Transfer Coefficient

Figure Index

Figure 1.1: Impact of passenger vehicles on total CO ₂ emissions in different countries (2005): [9]	2
Figure 2.1: Operational scheme of an electrochemical battery. [13]	5
Figure 2.2: Typical structure of a coin cell. [16]	7
Figure 2.3: (a) Double-layer structure and (b) the potential distribution through it. [11]	13
Figure 2.4: Effect of different types of polarisation on the voltage-current graph. [11]	15
Figure 2.5: The graph shows the number of lithium-ion batteries sold in the world (from 2000 to 2006) and the application field in which they were used. [6].....	19
Figure 2.6: Three different examples of host structures that can be used as electrode materials: 1D (a), 2D (b), 3D (c). [11].....	20
Figure 2.7: Summary diagram of the temporal evolution of lithium-ion batteries. [26]	21
Figure 2.8: Schematic diagram of a LCO battery structure. [24]	21
Figure 2.9: Possible cathodic material for Lithium-Ion batteries. [24].....	22
Figure 2.10: Spatial and temporal evolution of publications concerning lithium-sulfur batteries. [10]	24
Figure 2.11: Diagram showing the number of publications on lithium-sulfur batteries and the topics they have involved. [10].....	24
Figure 2.12: Comparison between different types of batteries in term of gravimetric and volumetric energy densities [30].....	25
Figure 2.13: Comparison between life cycle impact of Li-S and NCM batteries. [10]	26
Figure 2.14: Comparison between Li-S and Li-ion performances and characteristics. [10].....	27
Figure 2.15: Summary scheme of the advantage and disadvantage aspects of Li-ion and Li-S batteries. [10]....	28
Figure 2.16: Pie chart showing the weight distribution of the various components that make up a Li-S cell. [18]	30
Figure 2.17 : Morphology comparison of carbon materials used for the preparation of the cathodes. [18]	32
Figure 2.18: Comparison between three different types of porosity (macro, meso and micro) and their functions within the cathodes. [18]	33
Figure 2.19: Different approach to obtain carbon-sulfur composites. [29]	34
Figure 2.20 : (a)Lithium distribution by country in 2016 and, (b) by source. [37].....	36
Figure 2.21: Diagram showing the annual consumption of Lithium and the industrial sector in which it is used [34].....	37
Figure 2.22: Several pie charts (one in each year considered) which shows how Lithium consumption varies in the various industrial sectors over time [34].....	37
Figure 2.23: Schematic diagram of the operation of a Lithium-Sulfur cell and the reactions products. [15]	41
Figure 2.24: Typical voltage profile of a Li-S cell. [15]	43
Figure 2.25: Degradation mechanism in Lithium-sulphur batteries [32]	46
Figure 2.26: Voltage profile of a Li-S cell which also takes into account the transformations of the polysulphides. [4].....	47
Figure 2.27: Effects of shuttle phenomenon [32].....	47
Figure 2.28: Influence of the charge shuttle factors f_c on the charge plateaus. [3].....	48
Figure 2.29: Self-discharge phenomenon of pristine sulfur cathodes at different resting times. [3].....	49
Figure 2.30: Comparison in terms of conductivity, ability to act positively on the shuttle effect, viscosity and wettability of the electrode, between different electrolyte systems used in Li-S batteries. [29]	50
Figure 2.31 : Representation of single and double bonds that make up the backbone of extrinsic conductive polymers [41]	53
Figure 2.32: In the top: representation of the π -conjugation typical of conducting polymers. In the bottom: the same structure in the presence of defects. [40]	54

Figure 2.33 : Typical dopant elements used for CPs.	54
Figure 2.35 : Deprotonated form of PANI with reduced and oxidized units [43].....	56
Figure 2.36 : (a), (b): Representation of the three typical PANI oxidation states. [44] [46]	56
Figure 2.37 : Oxidation process of aniline under acidic conditions. [47].....	57
Figure 2.38 : Conversion reaction from emeraldine salt to emeraldine base. [47].....	58
Figure 2.39 : Different structures of protonated Emeraldine. [48]	59
Figure 2.40 : Different structures and reaction that could involve PANI.	60
Figure 2.41 : Schematic representation of the doping process by a proton acid. [44].....	60
Figure 2.42 : Schematic diagram of doping process for PANI. [48].....	61
Figure 2.43 : Bipolaronic and polaronic structures. [48].....	61
Figure 2.44 : Comparison of the properties (conductivity and density) obtainable, according to the type of acid used during the synthesis process. [47].....	62
Figure 2.45 : (a) 2H-MoS ₂ structure with trigonal prismatic coordination both from top view and side view [54]. (b) 3D representation of 2H-MoS ₂ structure. [51].....	64
Figure 2.46 : Structure comparison between the main three different MoS ₂ polymorphs. [50].....	65
Figure 2.47 : Structure comparison between the different MoS ₂ polymorphs that have been proposed for a monolayer.[50].....	66
Figure 2.48 : Electronic structure of 2H and 1T bulk MoS ₂ . [50].....	67
Figure 2.49 : Schematic representation of the "Scotch tape method". [52].....	68
Figure 2.50 : Schematic representation of MoS ₂ bulk exfoliation through a lithiation process. [51]	69
Figure 2.51 : Schematic representation of electrochemical intercalation and exfoliation process. [52].....	69
Figure 2.52 : Schematic illustration of solvent assisted exfoliation procedure. [52].....	70
Figure 2.53 : Schematic representation of hydrothermal/solvothermal methods. [52]	71
Figure 2.54 : Schematic illustration of chemical vapor deposition process. [52]	72
Figure 2.55 : Comparison in terms of achievable size, advantages and disadvantages of the various approaches that can be used to obtain MoS ₂ in the form of nanosheets. [51]	73
Figure 3.1 : Constitutive diagram of a Li-S battery. [4].....	75
Figure 3.2 : Schematic representation of quinonoid imines formation (left) and polysulfides binding energies on different materials. [58].....	76
Figure 3.3 : Examples of structures and binding energy for three different materials: carbon matrix (a), NC (b) and MoS ₂ (c) [4].....	77
Figure 3.4 : Energy profile of polysulfide reaction on MoS ₂ surface. [4].....	78
Figure 3.5 : Samples obtained during the experimental part done at FCT University of Lisbon.	79
Figure 3.6 : Schematic representation of the samples obtained and their subdivision into samples electrochemically analysed and not yet analyzed.	80
Figure 3.7 : Schematic representation of the significant steps necessary to obtain Italian PANI.	81
Figure 3.8 : Schematic representation of the significant steps necessary to obtain Portuguese PANI.	82
Figure 3.9 : Comparison between the FESEM analysis of Italian PANI (left) and Portuguese PANI (right), at 200 nm magnification.	83
Figure 3.10 : Comparison between the FESEM analysis of Italian PANI (left) and Portuguese PANI (right), at 1-2 μm magnification.	84
Figure 3.11 : Left: Comparison between the XRD analysis of Italian PANI (top) and Portuguese PANI (bottom). Right: table with the characteristic peaks of PANI in the emeraldine form.	84
Figure 3.12 : Left: Comparison between the Raman analysis of Italian PANI (top) and Portuguese PANI (bottom). Right: table with the characteristic peaks of PANI in the emeraldine form.	86
Figure 3.13 : Comparison between the FESEM analysis of MoS ₂ commercial at 200 nm magnification (left) and MoS ₂ commercial at 1μm magnification (right).	87
Figure 3.14 : (a) Correlation between the number of layers and the phonon vibration modes [49]. (b) In-plane and out-off-plane phonon modes. [67]	88
Figure 3.15 : Raman analysis of commercial MoS ₂ with characteristic peaks of the bulk form.	88

Figure 3.16: Schematic representation of the significant steps necessary to obtain Hydrothermal MoS ₂ .	89
Figure 3.17 : Comparison between the FESEM analysis of MoS ₂ hydrothermal at 200 nm magnification (left) and MoS ₂ hydrothermal at 1 μ m magnification (right).	90
Figure 3.18 : Raman analysis of hydrothermal MoS ₂ with its main peaks.	91
Figure 3.19: Schematic representation of the significant steps, and process conditions, necessary to obtain the exfoliation of commercial MoS ₂ .	92
Figure 3.20: Comparison between the FESEM analysis of commercial MoS ₂ in its bulk form (left) and exfoliated MoS ₂ (right), at 200 nm magnification.	93
Figure 3.21 : Comparison between the FESEM analysis of IN-SITU composite (with 0.3g commercial MoS ₂) at 200 nm magnification (left) and at 1 μ m magnification (right).	94
Figure 3.22 : Comparison between the FESEM analysis of IN-SITU composite (with 0.03g commercial MoS ₂) at 200 nm magnification (left) and at 1 μ m magnification (right).	95
Figure 3.23: FESEM analysis of IN-SITU composite (with 0.03g commercial MoS ₂) at 100 nm magnification.	95
Figure 3.24: Left: Raman analysis of IN-SITU composite. Right: table with the characteristic peaks of PANI in the emeraldine form.	96
Figure 3.25 : EDS images of IN-SITU composite.	97
Figure 3.26: Comparison between the FESEM analysis of EX-SITU composite (with 0.3g commercial MoS ₂ and 0.7g Italian PANI) at 200 nm magnification (left) and at 1 μ m magnification (right).	99
Figure 3.27: Comparison between the FESEM analysis of EX-SITU composite (with 0.7g commercial MoS ₂ and 0.3g Italian PANI) at 200 nm magnification (left) and at 1 μ m magnification (right).	99
Figure 3.28: Comparison between the FESEM analysis of EX-SITU composite (with 0.7g commercial MoS ₂ and 0.3g Portuguese PANI) at 200 nm magnification (left) and at 1 μ m magnification (right).	100
Figure 3.29: Left: Comparison between the Raman analysis of the three EX-SITU composites. Right: Zoom in the Raman chart to highlight the characteristic peaks of PANI in the emeraldine form.	101
Figure 3.30 : EDS images of EX-SITU composite with 0.3 g of Italian PANI and 0.7 of MoS ₂ .	101
Figure 3.31: Comparison between the FESEM analysis of Hydrothermal composite at 200 nm magnification (left) and at 1 μ m magnification (right).	103
Figure 3.32 : FESEM analysis of Hydrothermal composite at 200 nm magnification.	104
Figure 3.33 : Raman analysis of Hydrothermal composite with the characteristic peaks of PANI in the emeraldine form and that of Hydrothermal MoS ₂ .	104
Figure 4.1: Double- Layer coated on a sulfur-carbon cathode.	Errore. Il segnalibro non è definito.
Figure 4.2: Schematic representation of an assembled cell. [70]	109
Figure 4.3: Schematic example of a CV curve depicting a simple reversible reaction. [71]	110
Figure 4.4: Typical CV curve obtained from a Lithium Sulfur battery with a scan rate of 0.1mV s ⁻¹ . [71]	111
Figure 4.5: Diagrams reporting for each sample the cyclic voltammetry plot of the first five cycles.	112
Figure 4.6: Comparison of the cyclic voltammetry diagram at cycle 1 (left) and cycle 5 (right) for all the samples electrochemical analyzed.	112
Figure 4.7: Cyclic voltammetry (cycle 1) in which are highlighted the peaks related to the standard STD	113
Figure 4.8: Cyclic voltammetry (cycle 5) in which are highlighted the peaks related to the standard STD	114
Figure 4.9: Cyclic voltammetry carried out only on the active materials (MoS ₂ and PANI) in order to separate their contribution from that of sulfur.	115
Figure 4.10: Galvanostatic cycling for STD- MoS ₂ and PANI ITA with current C / 10 for cycles 1-2-3 and current C/5 for cycles 5-10-50-100.	117
Figure 4.11: Galvanostatic cycling for the EX-SITU composites containing 0.7g PANI ITA -0.3 g MoS ₂ and 0.3g PANI ITA-0.7g MoS ₂ with current C / 10 for cycles 1-2-3 and current C/5 for cycles 5-10-50-100.	118
Figure 4.12: Galvanostatic cycling for the EX-SITU composites containing 0.3g PANI PORT -0.7 g MoS ₂ and hydrothermal composite with current C / 10 for cycles 1-2-3 and current C/5 for cycles 5-10-50-100.	118
Figure 4.13: Comparative galvanostatic cycling analysis (at the same number of cycles) of all the samples analyzed. Current C / 10 for cycles 1-3 and current C/5 for cycles 5-100.	120

Figure 4.14: Comparison in terms of Specific Capacity on Cycle number between STD, PANI, MoS₂ and the two EX-SITU composites containing Italian PANI respectively at 100 (top) and 500 cycles (bottom)..... 121

Figure 4.15: Columbic efficiency curves for: STD, MoS₂ and PANI ITA 122

Figure 4.16: Columbic efficiency curves for the two EX-SITU composites with: 0.7g PANI Ita -0.3g MoS₂ (left) and 0.3g PANI ITA -0.7g MoS₂ (right) 123

Figure 4.17: Tafel plot for KJB, MoS₂ and PANI ITA..... 125

Table Index

Table 2.1: Possible structure and related properties of the cathodic materials used in Li-ion batteries. [24].....	23
Table 3.1: Reagents used for the synthesis of Italian PANI.....	81
Table 3.2: Reagents used for the synthesis of Portuguese PANI.....	82
Table 3.3: Reagents used for Hydrothermal MoS ₂ synthesis.....	89
Table 3.4: Process parameters for the microwave synthesis of hydrothermal MoS ₂	89
Table 3.5: Reagents and polymerization protocol used for IN-SITU composite synthesis.	93
Table 3.6: Element table of EDS analysis.	98
Table 3.7: Constituent elements of the three EX-SITU composite materials and their relative quantities.	98
Table 4.8: Element table of EDS analysis.	102
Table 3.9: Reagents and synthesis protocol used for the Hydrothermal composite.....	102
Table 3.10: Element table of EDS analysis.	105
Table 4.1: Solvent and binder used for the cathodic composition.	107
Table 4.2: Double-Layer composition	108
Table 4.3: Comparison between the peak values found in the literature for a Li-S battery and those experimentally obtained for the standard (STD) at cycle 1 and cycle 5	113
Table 4.4: Compositions used for the Tafel analysis	125
Table 4.5: Exchange current density for the samples analyzed	126

Bibliography

- [1] R. S. Recchi Giuseppe, *Nuove energie Le sfide per lo sviluppo dell'Occidente*, Second. Venezia, 2014.
- [2] C. Jude, "Energy as a foundation of modern life," *J. Energy Dev.*, vol. 35, pp. 33–48, 2009.
- [3] A. Manthiram, Y. Fu, S. Chung, C. Zu, and Y. Su, "Rechargeable Lithium – Sulfur Batteries," 2014, doi: 10.1021/cr500062v.
- [4] Y. Liu, C. Cui, Y. Liu, W. Liu, and J. Wei, "Application of MoS₂ in the cathode of lithium sulfur batteries," *RSC Adv.*, vol. 10, no. 13, pp. 7384–7395, 2020, doi: 10.1039/c9ra09769d.
- [5] C. Olson and F. Lenzmann, "The social and economic consequences of the fossil fuel supply chain," *MRS Energy Sustain.*, 2016, doi: 10.1557/mre.2016.7.
- [6] T. Placke, R. Kloepsch, S. Dühnen, and M. Winter, "Lithium ion, lithium metal, and alternative rechargeable battery technologies: the odyssey for high energy density," *J. Solid State Electrochem.*, vol. 21, no. 7, pp. 1939–1964, 2017, doi: 10.1007/s10008-017-3610-7.
- [7] S. S. Martin and A. Chebak, "Concept of educational renewable energy laboratory integrating wind, solar and biodiesel energies," *Int. J. Hydrogen Energy*, vol. 41, no. 45, pp. 21036–21046, 2016, doi: 10.1016/j.ijhydene.2016.06.102.
- [8] G. Tarquini, "Materiali catodici a base di zolfo per batterie Li-S ad alte prestazioni." Sapienza University, Rome, 2017.
- [9] M. Tran, D. Banister, J. D. K. Bishop, and M. D. McCulloch, "Realizing the electric-vehicle revolution," *Nat. Clim. Chang.*, vol. 2, no. 5, pp. 328–333, 2012, doi: 10.1038/nclimate1429.
- [10] G. Benveniste, H. Rallo, L. Canals Casals, A. Merino, and B. Amante, "Comparison of the state of Lithium-Sulphur and lithium-ion batteries applied to electromobility," *J. Environ. Manage.*, 2018, doi: 10.1016/j.jenvman.2018.08.008.
- [11] H. Berg and H. Berg, *The electrochemical cell*. 2015.
- [12] D. Linden and T. B. Reddy, *Handbook of batteries*, vol. 33, no. 04. 1995.
- [13] R. Fate, *Encyclopedia of Sustainability Science and Technology*. 2012.
- [14] M. Morris, "COMPARISON OF RECHARGEABLE BATTERY TECHNOLOGIES," no. March, 2017.
- [15] X. Bai, T. Li, U. Gulzar, and R. P. Zaccaria, "Comprehensive Understanding of Lithium-Sulfur Batteries : Current Status and Outlook."
- [16] L. Duan, F. Zhang, and L. Wang, "Cathode Materials for Lithium Sulfur Batteries: Design, Synthesis, and Electrochemical Performance," *Alkali-ion Batter.*, 2016, doi: 10.5772/62439.
- [17] M. Wild, "Anode – Electrolyte Interface," pp. 121–127, 2019.
- [18] H. Althues, S. Dörfler, S. Thieme, P. Strubel, and S. Kaskel, "Sulfur Cathodes 2 . 1 Cathode Design Criteria," 2019.
- [19] A. F. Hollenkamp and A. S. Best, "3. Electrolyte for Lithium – Sulfur Batteries 3 . 1 The Case

- for Better Batteries 3 . 2 Li – S Battery : Origins and Principles,” pp. 20–22, 2019.
- [20] S. Yasin, T. Ali, U. Draz, A. Shaf, and M. Ayaz, “A Parametric Performance Evaluation of Batteries in Wireless Sensor Networks,” pp. 187–196, 2019, doi: 10.1007/978-3-319-99966-1_17.
- [21] C. H. Bamford and R. G. Compton, “Electrode Kinetics: Principles and Methodology,” in *Comprehensive Chemical Kinetics*, New York: Elsevier Science Publishing B.V, 1986, p. 450.
- [22] G. Minton, “Electrochemical Theory and Physics,” *Lithium-Sulfur Batter.*, vol. 8, pp. 3–32, 2019, doi: 10.1002/9781119297895.ch1.
- [23] Z. S. S. Lundgren C.A., Xu K., Jow T.R., Allen J., *Lithium-Ion Batteries and Materials*. Springer, Berlin, Heidelberg, 2017.
- [24] C. A. Aravena Valenzuela, “Estudio y caracterización de ánodos de litio metálico,” p. 208, 2015, [Online]. Available: <http://repositorio.uchile.cl/handle/2250/132023>.
- [25] J. Yan, X. Liu, and B. Li, “Capacity fade analysis of sulfur cathodes in lithium– sulfur batteries,” *Adv. Sci.*, vol. 3, no. 12, 2016, doi: 10.1002/advs.201600101.
- [26] T. Kim, W. Song, D. Y. Son, L. K. Ono, and Y. Qi, “Lithium-ion batteries: outlook on present, future, and hybridized technologies,” *J. Mater. Chem. A*, vol. 7, no. 7, pp. 2942–2964, 2019, doi: 10.1039/C8TA10513H.
- [27] A. Yoshino, “Development of the Lithium-Ion Battery and Recent Technological Trends,” pp. 1–20, 2020.
- [28] Y. X. Yin, S. Xin, Y. G. Guo, and L. J. Wan, “Lithium-sulfur batteries: Electrochemistry, materials, and prospects,” *Angew. Chemie - Int. Ed.*, vol. 52, no. 50, pp. 13186–13200, 2013, doi: 10.1002/anie.201304762.
- [29] L. Borchardt, M. Oschatz, and S. Kaskel, “Carbon Materials for Lithium Sulfur Batteries - Ten Critical Questions,” *Chem. - A Eur. J.*, vol. 22, no. 22, pp. 7324–7351, 2016, doi: 10.1002/chem.201600040.
- [30] *Advanced Battery Materials*. 2019.
- [31] A. Rosenman, E. Markevich, G. Salitra, D. Aurbach, A. Garsuch, and F. F. Chesneau, “Review on Li-Sulfur Battery Systems: An Integral Perspective,” *Adv. Energy Mater.*, vol. 5, no. 16, pp. 1–21, 2015, doi: 10.1002/aenm.201500212.
- [32] M. Wild *et al.*, “Lithium sulfur batteries, a mechanistic review,” *Energy Environ. Sci.*, vol. 8, no. 12, pp. 3477–3494, 2015, doi: 10.1039/c5ee01388g.
- [33] A. Manthiram, Y. Fu, and Y. S. Su, “Challenges and prospects of lithium-sulfur batteries,” *Acc. Chem. Res.*, vol. 46, no. 5, pp. 1125–1134, 2013, doi: 10.1021/ar300179v.
- [34] G. Yushin, R. Dash, J. Jagiello, J. E. Fischer, and Y. Gogotsi, “Carbide-derived carbons: Effect of pore size on hydrogen uptake and heat of adsorption,” *Adv. Funct. Mater.*, vol. 16, no. 17, pp. 2288–2293, 2006, doi: 10.1002/adfm.200500830.
- [35] S. Xin *et al.*, “Smaller sulfur molecules promise better lithium’sulfur batteries,” *J. Am. Chem. Soc.*, vol. 134, no. 45, pp. 18510–18513, 2012, doi: 10.1021/ja308170k.
- [36] L. Kavanagh, J. Keohane, G. G. Cabellos, A. Lloyd, and J. Cleary, “Global lithium sources-industrial use and future in the electric vehicle industry: A review,” *Resources*, vol. 7, no. 3, 2018, doi: 10.3390/resources7030057.

- [37] W. T. S. Lenntech, “Chemical properties of lithium.” [Online]. Available: <https://www.lenntech.com/periodic/elements/li.htm>.
- [38] B. Liu, J. G. Zhang, and W. Xu, “Advancing Lithium Metal Batteries,” *Joule*, vol. 2, no. 5, pp. 833–845, 2018, doi: 10.1016/j.joule.2018.03.008.
- [39] M. Reporting, “Argus White Paper : The lithium market – the future is electric.”
- [40] R. Purkayastha, “Degradation in Lithium – Sulfur Batteries,” 2019.
- [41] L. Gireaud, “Lithium metal stripping / plating mechanisms studies : A metallurgical approach,” vol. 8, pp. 1639–1649, 2006, doi: 10.1016/j.elecom.2006.07.037.
- [42] D. Wang *et al.*, “Reversible insertion/extraction of polysulfides into/from polyaniline as an effective strategy to confine polysulfides in lithium-sulfur batteries,” *Ionics (Kiel)*, vol. 26, no. 1, pp. 191–199, 2020, doi: 10.1007/s11581-019-03209-9.
- [43] J. Garche, C. K. Dyer, P. T. Moseley, Z. Ogumi, D. A. J. Rand, and B. Scrosati, *Encyclopedia of Electrochemical Power Sources*. Newnes, 2013.
- [44] S. Walu, “6. Lithium Sulfide $6 \cdot 2 \text{Li}_2 \text{S}$ as the End Discharge Product,” 2019.
- [45] M. Wild and G. J. Offer, *Lithium-Sulfur Batteries*. John Wiley & Sons, 2019.
- [46] A. F. Hofmann, D. N. Fronczek, and W. G. Bessler, “Mechanistic modeling of polysulfide shuttle and capacity loss in lithium-sulfur batteries,” *J. Power Sources*, vol. 259, pp. 300–310, 2014, doi: 10.1016/j.jpowsour.2014.02.082.
- [47] W. Ren, W. Ma, S. Zhang, and B. Tang, “Recent advances in shuttle effect inhibition for lithium sulfur batteries,” *Energy Storage Mater.*, vol. 23, no. January, pp. 707–732, 2019, doi: 10.1016/j.ensm.2019.02.022.
- [48] A. Vizintin *et al.*, “The mechanism of Li_2S activation in lithium-sulfur batteries: Can we avoid the polysulfide formation?,” *J. Power Sources*, vol. 344, pp. 208–217, 2017, doi: 10.1016/j.jpowsour.2017.01.112.
- [49] P. Chandrasekhar and P. Chandrasekhar, “Introducing Conducting Polymers (CPs),” *Conduct. Polym. Fundam. Appl.*, pp. 159–174, 2018, doi: 10.1007/978-3-319-69378-1_27.
- [50] A. M. Grancarić *et al.*, *Conductive polymers for smart textile applications*, vol. 48, no. 3. 2018.
- [51] Y. Luo *et al.*, “Application of Polyaniline for Li-Ion Batteries, Lithium–Sulfur Batteries, and Supercapacitors,” *ChemSusChem*, vol. 12, no. 8, pp. 1591–1611, 2019, doi: 10.1002/cssc.201802186.
- [52] G. Yang *et al.*, “Nanocomposites of polyaniline and a layered inorganic acid host: Polymerization of aniline in the layers, conformation, and electrochemical studies,” *Adv. Funct. Mater.*, vol. 17, no. 3, pp. 401–412, 2007, doi: 10.1002/adfm.200500941.
- [53] S. Bhandari, *Polyaniline*. Elsevier Inc., 2018.
- [54] Y. Yao, H. Zhang, and X. Wang, “Polyaniline: an effective suppressor against diffusion and dissolution of polysulfides in Li-S battery,” *J. Solid State Electrochem.*, vol. 23, no. 8, pp. 2559–2567, 2019, doi: 10.1007/s10008-019-04340-3.
- [55] M.- Protocol, C. Cao, Y. Chen, Y. Wu, and E. Deumens, “OPAL : A Multiscale Multicenter Simulation Package Based on MPI-2 Protocol,” *Int. J. Quantum Chem.*, vol. 111, no. 2008, pp. 4020–4029, 2011, doi: 10.1002/qua.

- [56] J. Stejskal *et al.*, *Conducting Polymers: Polyaniline*, no. October 2017. 2015.
- [57] M. Zagórska, I. Kulszewicz-Bajer, A. Proń, P. Barta, F. Cacialli, and R. H. Friend, “Influence of polymerization conditions on the properties of poly(4,4'-dialkyl-2,2'-bithiophenes),” *Synth. Met.*, vol. 101, no. 1, p. 142, 1999, doi: 10.1016/S0379-6779(98)01426-X.
- [58] S. Santhosh and A. A. Madhavan, “A review on the structure, properties and characterization of 2D Molybdenum Disulfide,” *2019 Adv. Sci. Eng. Technol. Int. Conf. ASET 2019*, pp. 1–5, 2019, doi: 10.1109/ICASET.2019.8714360.
- [59] W. Zhao *et al.*, “Metastable MoS₂: Crystal Structure, Electronic Band Structure, Synthetic Approach and Intriguing Physical Properties,” *Chem. - A Eur. J.*, vol. 24, no. 60, pp. 15942–15954, 2018, doi: 10.1002/chem.201801018.
- [60] X. Wang, W. Xing, X. Feng, L. Song, and Y. Hu, “MoS₂/Polymer Nanocomposites: Preparation, Properties, and Applications,” *Polym. Rev.*, vol. 57, no. 3, pp. 440–466, 2017, doi: 10.1080/15583724.2017.1309662.
- [61] X. L. Li, T. C. Li, S. Huang, J. Zhang, M. E. Pam, and H. Y. Yang, “Controllable Synthesis of Two-Dimensional Molybdenum Disulfide (MoS₂) for Energy-Storage Applications,” *ChemSusChem*, vol. 13, no. 6, pp. 1379–1391, 2020, doi: 10.1002/cssc.201902706.
- [62] D. Mombrú, M. Romero, R. Faccio, and A. W. Mombrú, “Polyaniline intercalated with MoS₂ nanosheets: structural, electric and thermoelectric properties,” *J. Mater. Sci. Mater. Electron.*, vol. 29, no. 20, pp. 17445–17453, 2018, doi: 10.1007/s10854-018-9844-z.
- [63] M. Chhowalla, H. S. Shin, G. Eda, L. J. Li, K. P. Loh, and H. Zhang, “The chemistry of two-dimensional layered transition metal dichalcogenide nanosheets,” *Nat. Chem.*, vol. 5, no. 4, pp. 263–275, 2013, doi: 10.1038/nchem.1589.
- [64] Y. Cao *et al.*, “Two-Dimensional MoS₂ for Li–S Batteries: Structural Design and Electronic Modulation,” *ChemSusChem*, vol. 13, no. 6, pp. 1392–1408, 2020, doi: 10.1002/cssc.201902688.
- [65] L. Tan, X. Li, Z. Wang, H. Guo, and J. Wang, “Lightweight Reduced Graphene Oxide @ MoS₂ Interlayer as Polysulfide Barrier for High-Performance Lithium-Sulfur Batteries,” 2018, doi: 10.1021/acsami.7b18645.
- [66] D. Liu *et al.*, “Catalytic Effects in Lithium–Sulfur Batteries: Promoted Sulfur Transformation and Reduced Shuttle Effect,” *Adv. Sci.*, vol. 5, no. 1, 2018, doi: 10.1002/advs.201700270.
- [67] X. Hong, Y. Liu, Y. Li, X. Wang, J. Fu, and X. Wang, “Application progress of polyaniline, polypyrrole and polythiophene in lithium-sulfur batteries,” *Polymers (Basel)*, vol. 12, no. 2, 2020, doi: 10.3390/polym12020331.
- [68] Q. Zhang, X. Zhang, M. Li, J. Liu, and Y. Wu, “Sulfur-deficient MoS_{2-x} promoted lithium polysulfides conversion in lithium-sulfur battery: A first-principles study,” *Appl. Surf. Sci.*, vol. 487, no. April, pp. 452–463, 2019, doi: 10.1016/j.apsusc.2019.05.138.
- [69] J. Stejskal, A. Riede, D. Hlavatá, J. Prokeš, M. Helmstedt, and P. Holler, “The effect of polymerization temperature on molecular weight, crystallinity, and electrical conductivity of polyaniline,” *Synth. Met.*, vol. 96, no. 1, pp. 55–61, 1998, doi: 10.1016/s0379-6779(98)00064-2.
- [70] S. Ebnesajjad, *Surface and Material Characterization Techniques*. 2014.
- [71] C. Cullity and B. D. Morris, *Elements of X-Ray diffraction*. Massachusetts: ADDISON-WESLEY PUBLISHING COMPANY, Inc., 1956.

- [72] L. Ren *et al.*, “Three-Dimensional Tubular MoS₂/PANI Hybrid Electrode for High Rate Performance Supercapacitor,” *ACS Appl. Mater. Interfaces*, vol. 7, no. 51, pp. 28294–28302, 2015, doi: 10.1021/acsami.5b08474.
- [73] R. S. Das and Y. K. Agrawal, “Raman spectroscopy: Recent advancements, techniques and applications,” *Vib. Spectrosc.*, vol. 57, no. 2, pp. 163–176, 2011, doi: 10.1016/j.vibspec.2011.08.003.
- [74] R. Mažeikiene, V. Tomkute, Z. Kuodis, G. Niaura, and A. Malinauskas, “Raman spectroelectrochemical study of polyaniline and sulfonated polyaniline in solutions of different pH,” *Vib. Spectrosc.*, vol. 44, no. 2, pp. 201–208, 2007, doi: 10.1016/j.vibspec.2006.09.005.
- [75] W. Wang, F. Yang, C. Chen, L. Zhang, Y. Qin, and M. Knez, “Tuning the Conductivity of Polyaniline through Doping by Means of Single Precursor Vapor Phase Infiltration,” *Adv. Mater. Interfaces*, vol. 4, no. 4, 2017, doi: 10.1002/admi.201600806.
- [76] M. I. Boyer *et al.*, “Vibrational analysis of polyaniline: A model compound approach,” *J. Phys. Chem. B*, vol. 102, no. 38, pp. 7382–7392, 1998, doi: 10.1021/jp972652o.
- [77] H. Taghinejad *et al.*, “Nonlinear Raman Shift Induced by Exciton-to-Trion Transformation in Suspended Trilayer MoS₂,” 2015, [Online]. Available: <http://arxiv.org/abs/1502.00593>.
- [78] A. Molina-Sánchez and L. Wirtz, “Phonons in single-layer and few-layer MoS₂ and WS₂,” *Phys. Rev. B - Condens. Matter Mater. Phys.*, vol. 84, no. 15, pp. 1–8, 2011, doi: 10.1103/PhysRevB.84.155413.
- [79] H. Song, A. Tang, G. Xu, L. Liu, M. Yin, and Y. Pan, “One-step convenient hydrothermal synthesis of MoS₂/RGO as a high-performance anode for sodium-ion batteries,” *Int. J. Electrochem. Sci.*, vol. 13, no. 5, pp. 4720–4730, 2018, doi: 10.20964/2018.05.29.
- [80] L. Della Seta, “Catodi per batterie litio-zolfo preparati con leganti polimerici.”
- [81] E. Talaie, P. Bonnick, X. Sun, Q. Pang, X. Liang, and L. F. Nazar, “Methods and protocols for electrochemical energy storage materials research,” *Chem. Mater.*, vol. 29, no. 1, pp. 90–105, 2017, doi: 10.1021/acs.chemmater.6b02726.
- [82] X. Huang *et al.*, “Cyclic Voltammetry in Lithium – Sulfur Batteries — Challenges and Opportunities,” vol. 1801001, pp. 1–13, 2019, doi: 10.1002/ente.201801001.
- [83] L. Khalafi, *Cyclic Voltammetry*, vol. 196, no. Cv. 2014.
- [84] N. Elgrishi, K. J. Rountree, B. D. McCarthy, E. S. Rountree, T. T. Eisenhart, and J. L. Dempsey, “A Practical Beginner’s Guide to Cyclic Voltammetry,” *J. Chem. Educ.*, vol. 95, no. 2, pp. 197–206, 2018, doi: 10.1021/acs.jchemed.7b00361.
- [85] N. Elgrishi, K. J. Rountree, B. D. McCarthy, E. S. Rountree, T. T. Eisenhart, and J. L. Dempsey, “A Practical Beginner’s Guide to Cyclic Voltammetry,” *J. Chem. Educ.*, 2018, doi: 10.1021/acs.jchemed.7b00361.
- [86] C. Core, *7 Battery usage and degradation*. 2019.
- [87] Z. A. Ghazi *et al.*, “MoS₂/Celgard Separator as Efficient Polysulfide Barrier for Long-Life Lithium–Sulfur Batteries,” *Adv. Mater.*, vol. 29, no. 21, pp. 1–6, 2017, doi: 10.1002/adma.201606817.
- [88] S. Yang, J. Zhang, T. Tan, Y. Zhao, N. Liu, and H. Li, “A 3D MoS₂/graphene microsphere coated separator for excellent performance Li-S batteries,” *Materials (Basel)*, vol. 11, no. 10, pp. 1–13, 2018, doi: 10.3390/ma11102064.

- [89] Y. H. Fang and Z. P. Liu, “Tafel kinetics of electrocatalytic reactions: From experiment to first-principles,” *ACS Catal.*, vol. 4, no. 12, pp. 4364–4376, 2014, doi: 10.1021/cs501312v.
- [90] Q. Pang, C. Y. Kwok, D. Kundu, X. Liang, and L. F. Nazar, “Lightweight Metallic MgB₂ Mediates Polysulfide Redox and Promises High-Energy-Density Lithium-Sulfur Batteries,” *Joule*, vol. 3, no. 1, pp. 136–148, 2019, doi: 10.1016/j.joule.2018.09.024.

Appendix: Instruments and Operation Conditions

- *CENTRIFUGE*: Bench Top Model REMI Centrifuge (NEYA 8 Model); rpm = 4500, Time = 15 min
- *BALANCE*: Sartorius Analytical Scale, Model ENTRIS 224i-1S
- *HOT PLATE*: Thermo Fisher Hot Plate Stirrer 10x10, Time = 15 min; Temperature = 80°C
- *STIRRER*: Thermo Fisher Scientific 50094596 Cimarec i Poly 15 Stirrer
- *SONICATOR*: Sonics sonicator vibracell model VCX 130 PB; Time = 9h, Power = 300W, Tape = small, Type of sonication = discontinuos
- *VACUUM OVEN*: Büchi Glass oven B-585 at 40°C for 4h in vacuum
- *OVEN*: Nabertherm 30-30000°C Muffle furnace L 3/12, Temperature = 60°C, Time = 24h
- *MICROWAVE*: CEM Corporation Microwave Synthesizer Discover 2.0; Temperature = 200°C, Time = 60 min, Pressure = 280 Pa, Power = 100 W, Stirring = off, Pre-stirring = off
- *FESEM*: (Zeiss Auriga CrossBeam system); EHT = 5.00kV, Aperture size = 30.00 μm , Signal A = InLens
- *EDS* for elemental analysis: Oxford XMax 150
- *XRD*: (PANalytical Xpert PRO MRD), Source of X-rays is Cu K-alpha: wavelength = 1.540598 Å
- *RAMAN*: inVia confocal Raman microscope; Laser wavelength = 532 nm, Exposure time = 5 sec, Power = 1% (of max power), Number of accusations = 5 for each
- *CICLIC VOLTAMMETRY*: CH Instruments 660D model. Scan rate = 0.1 MV s⁻¹ in a potential range = 1.6 - 2.8 V
- *GALVANOSTATIC CYCLING*: Arbin 32-channel battery tester (software Arbin's MIT Pro®). 3 cycles at C / 10, the rest at C / 5. Potential range = 1.8 – 2.6 V
- *CULOMBIC EFFICIENCY*: Arbin 32-channel battery tester (software Arbin's MIT Pro®)
- *TAFEL*: Potential scan rate = 10⁻⁴ V s⁻¹ in a potential range from 2.75 to 2.95 V. To decide the potential range, an OCV (Open Circuit Voltage) measurement was previously done. The result of OCV test found was around 2.8V
- *GLOVE-BOX*: model UNIlab plus di MBraun®
- *ATOMATIC FILM APPLICATOR*: with Doctor Blade (thickenss = 50- 225 μm)

Acknowledgments

At the end of this work, I think it is right to take a few minutes to thank all people who made it possible or who, with its presence, made it more pleasant.

I would like, therefore, to thank Professor Silvia Bodoardo for allowing me to carry out this research and for having enthusiastically followed its progress. Thanks also for reminding me and showing the strength and energy that women can invest in their work.

I would also like to thank Professor Luis Pereira for welcoming me to FCT University and for providing full availability of tools and laboratories to carry out my research at best. During the whole period spent in Portugal, the opportunity to carry out analyzes has never been lacking, despite the numerous research work in progress.

A dutiful thanks go to Daniele, who despite my English, read and corrected my whole thesis, providing valid support for its writing.

Special thanks to Sumita, for the great help, for the constant availability and above all for her friendship. She made my stay in Lisbon fruitful and pleasant.

Finally, a huge and probably insufficient thanks to my parents, to my brother and Isac, for the patience, encouragement and everything that involved being close to me on this journey.